Precursor Synthesis and Chemical Vapour Deposition of Transition Metal Nitrides and Carbonitrides

A thesis presented to the University of London in partial fulfilment of the requirements for the Degree of Doctor of Philosophy.

Stephen E. Potts

Supervised by Dr. C. J. Carmalt

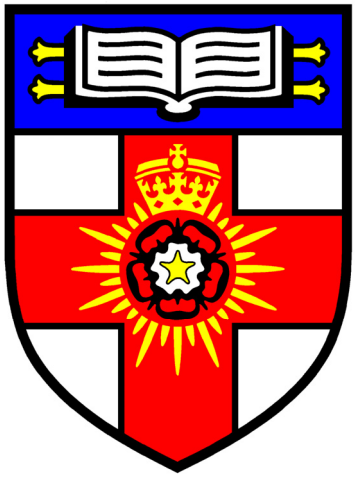

Submitted for examination 14th October 2008

Examined 2nd December 2008

I, Stephen E. Potts, confirm that the work presented in this thesis is my own. Where information has been derived from other sources, I confirm that this has been indicated in the thesis.

Abstract

This thesis is concerned with the chemical vapour deposition (CVD) of tungsten and zirconium nitride and carbonitride thin films. $[W(\mu\text{-}N^tBu)(N^tBu)Cl_2(H_2N^tBu)]_2$, $[W(N^tBu)_2Cl_2(TMEDA)]$ (TMEDA = *N*,*N*,*N'*,*N'*-tetramethylethylenediamine) and $[W(N^tBu)_2Cl_2(py)_2]$ (py = pyridine) have been investigated as potential precursors. Additionally, two novel precursors, $[W(N^tBu)_2Cl\{N(SiMe_3)_2\}]$ and $[W(N^tBu)_2(\eta^5\text{-}Cp')(\eta^1\text{-}Cp')]$ (Cp' = methylcyclopentadienyl), have been synthesised *via* metathesis reactions of $[W(N^tBu)_2Cl_2(py)_2]$ with the appropriate lithium or sodium amide salt. The attempted synthesis of $[W(N^tBu)_2Cl\{N(H)NMe_2\}]$ by lithium salt metathesis was unsuccessful due to polymerisation.

Cyclopentadienyl-based precursors to zirconium carbonitride have been investigated, including $[ZrCp_2(NMe_2)_2]$, $[ZrCp'_2(NMe_2)_2]$ and four novel compounds: $[ZrCp_2(\eta^2\text{-}MeNCH_2CH_2NMe)]$, $[ZrCp'_2(NEt_2)_2]$, $[ZrCp'\{(^iPrN)_2CNMe_2\}_2Cl]$ and $[ZrCp'_2\{(^iPrN)_2CNMe_2\}Cl]$ (Cp = η^5-cyclopentadienyl, Cp' = η^5-methylcyclopentadienyl). The compounds were synthesised *via* sodium or lithium metathesis reactions. All compounds synthesised were characterised by NMR, mass spectrometry, elemental analysis and IR, and their decomposition was investigated by thermogravimetric analysis (TGA). The molecular structures of $[ZrCp'\{(^iPrN)_2CNMe_2\}_2Cl]$ and $[ZrCp'_2\{(^iPrN)_2CNMe_2\}Cl]$ were determined by single crystal X-ray diffraction.

Thin films of tungsten carbonitride, zirconium carbide and zirconium carbonitride were deposited by low pressure CVD (LPCVD) at 550-600 °C and 0.1 Torr using the aforementioned precursors. In addition, aerosol-assisted CVD (AACVD) of $[W(\mu\text{-}N^tBu)(N^tBu)Cl_2(H_2N^tBu)]_2$ in toluene was investigated as a comparison. All films deposited *via* CVD were characterised using wavelength dispersive X-ray spectroscopy (WDX), glancing-angle XRD, UV/Vis spectroscopy (for reflectance and transmission measurements) and their morphology and thickness were investigated using SEM imaging. Plasma-enhanced atomic layer deposition (PEALD) using $[ZrCp_2(NMe_2)_2]$ and $[ZrCp_2(\eta^2\text{-}MeNCH_2CH_2NMe)]$ was studied with the view to

depositing stoichiometric ZrN. It showed these precursors to be insufficiently volatile for the ALD system as the growth rates were low. The ALD progress was analysed using *in situ* ellipsometry and mass spectrometry.

Acknowledgements

I would like to take this opportunity to thank all of the people who made the smooth running of this project possible.

First, and foremost, I would like to thank my supervisor, Dr. Claire J. Carmalt, for all her encouragement, support and advice and for getting me through both my Ph.D. and my M.Sci. projects. Also, thanks go to Prof. Ivan Parkin and Dr. Chris Blackman for their advice and help with CVD and particular thanks go to Dr. Andrea Sella for all his general lab advice and the loan of various pieces of glassware.

I am grateful to SAFC Hitech Ltd. for sponsoring this project and to Dr. Hywel Davies for providing the necessary link between there and UCL. I would also like to thank everyone at SAFC Hitech Ltd. for making me feel welcome when I visited.

I am extremely grateful to Dr. Erwin Kessels at the Eindhoven University of Technology for allowing me to visit and run ALD using two of my compounds and to his student, Noémi Leick, for running the samples during and after my visit.

At UCL, I would like to thank Jill Maxwell for running elemental analysis samples, Dr. Lisa Harris for running mass spectrometry samples, Dr. Abil Aleiv and Dave Butler for NMR advice and assistance, Dr. Steve Firth for TGA advice and training, Kevin Reeves for assistance and helpful advice concerning SEM and WDX, Dr. Geoff Hyett for XRD advice and Dr. David Pugh for running and solving my crystal structures.

I would particularly like to acknowledge Dr. Siama Basharat for all her support in the lab, even when she was busy, especially now I know how she felt! I would also like to thank Caroline Knapp and Tegan Thomas for making the research group pleasant and for assisting me with housekeeping. Thanks also go to the rest of my year group: Paolo Melgari, Kristopher Page and Naima Narband for being good friends over the past four years. Dr. Luke Thomas, Rosie Coates, Luanne Thomas, Mathew Waugh, Dr. Clara Piccirillo, Dr. Daniel Stone, Dr. Nicolas Boscher, Sujata Kundu, Dr. Russell Binions, John Kilmartin, Dr. Dina Solanki, Dr. Jalpa Patel, Dr. Uzma Qureshi, Dr. Rob

Palgrave, Dr. Dorothy Farrell, Andreas Kafizas and Emily MacCready are all thanked for their camaraderie and friendship.

Finally, I would like to thank my parents primarily for financial support and UCL Department of Chemistry for taking me on as a transfer student during my undergraduate degree. Had that not happened, I probably wouldn't be writing this.

Contents

List of Figures, Schemes and Tables

Chapter 1: Introduction 20

Chapter 3: Chemical Vapour Deposition of Tungsten Carbonitride 91

Chapter 4: Synthesis of Zirconium Carbonitride Precursors 109

List of Abbreviations

AACVD	Aerosol-assisted chemical vapour deposition
ALD	Atomic layer deposition
APCVD	Atmospheric pressure chemical vapour deposition
Cp	Cyclopentadienyl (ligand), $-C_5H_5$
Cp'	Methylcyclopentadienyl (ligand), $-C_5H_4(CH_3)$
CVD	Chemical vapour deposition
Cy^{hex}	Cyclohexyl group, $-C_6H_{11}$
DCM	Dichloromethane
Et	Ethyl group, $-CH_2CH_3$
fcc	Face-centred cubic crystal lattice
FT-IR spectroscopy	Fourier transform infrared spectroscopy
m	Medium
s	Strong
sh	Shoulder (peak)
w	Weak
vs	Very strong
vw	Very weak
hcp	Hexagonal close-packed crystal lattice
hex	Simple hexagonal crystal lattice
^{i}Pr	Isopropyl group, $-CH(CH_3)_2$
LPCVD	Low pressure chemical vapour deposition
Me	Methyl group, $-CH_3$
Mes	2,4,6-trimethylphenyl (mesityl) group
MOCVD	Metal-organic chemical vapour deposition
mmp	1-methoxy-2-methylpropan-2-olate, $-OC(CH_3)_2CH_2OCH_3$
^{n}Bu	*Neo*-butyl, $-CH_2CH_2CH_2CH_3$
NMR spectroscopy	Nuclear magnetic resonance spectroscopy
$^{13}C\{^{1}H\}$-NMR	Proton-decoupled carbon-13 NMR

COSY	2D correlation NMR spectroscopy
d	Doublet (peak)
^{1}H-NMR	Proton NMR
m	Multiplet (indistinct)
NOESY	Nuclear Overhauser 2D NMR spectroscopy
quart.	Quartet (peak)
s	Singlet (peak)
sept.	Septet (peak)
t	Triplet (peak)
orth	Orthorhombic crystal lattice
PEALD	Plasma-enhanced atomic layer deposition
Ph	Phenyl group, $–C_6H_5$
PVD	Physical vapour deposition
py	Pyridine
SEM	Scanning electron microscopy
^{t}Bu	*Tert*-butyl, $–C(CH_3)_3$
TGA	Thermogravimetric analysis
THF	Tetrahydrofuran
TMEDA	*N*,*N*,*N'*,*N'*-tetramethylethylenediamine
WDX	Wavelength Dispersion by X-Rays
xs	Excess

1

Introduction

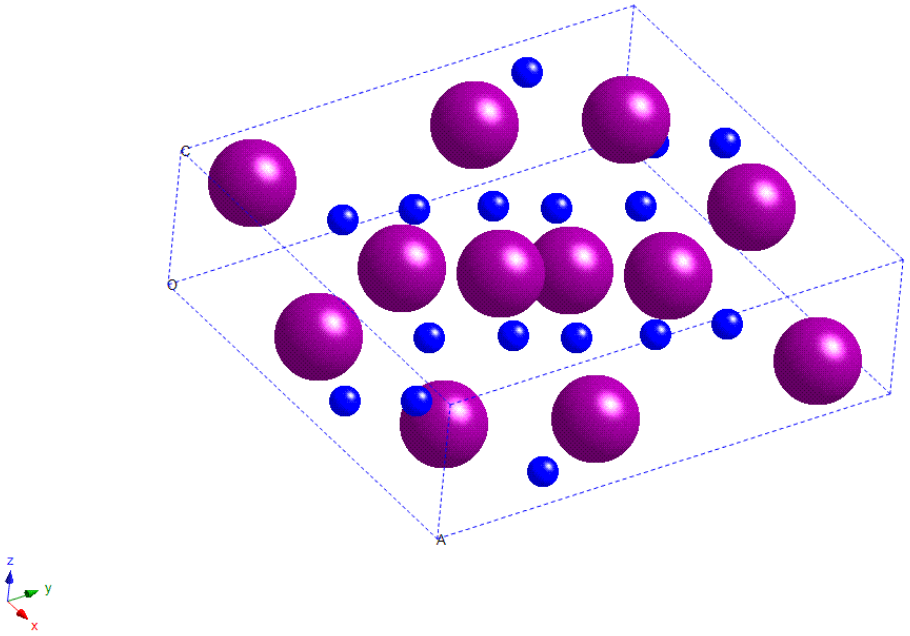

Figure 1.0 Unit cell of orthorhombic Zr_3N_4.[1] Purple spheres = zirconium, blue spheres = nitrogen.

1.1. Introduction

Electronic devices and gadgets are essential to modern life, but over time demand for more functionality and smaller devices is ever increasing. In order to achieve these requirements, circuitry must be significantly reduced in size, which consequently means that the barrier layer between interconnects must be smaller and more reliable.[9-12] Barrier layers will be described in Section 1.4.3. Currently, TiN is the material of choice for barrier layers where aluminium interconnects are concerned, but TaN[13-15] and WN_x[9,16-19] are more suited to copper and are more effective at higher working temperatures. Particular advantages of WN_x (over TaN, for example) are that deposited copper is more adhesive to it and it is still an effective diffusion barrier at temperatures up to 750 °C.[10,20,21] Tungsten or zirconium carbonitride, MN_xC_y, is equally suitable as a barrier layer, if not preferable, as the conductivity is higher than that of the pure nitride.[14]

Barrier layers can be deposited by one of three methods: physical vapour deposition (PVD), chemical vapour deposition (CVD) or atomic layer deposition (ALD). As such, this work is concerned with the synthesis of precursors to tungsten carbonitride and zirconium carbonitride, and subsequent CVD using these precursors.

1.2. Background

There are four categories of nitride and carbide:[2]

- Covalent: such as BN or SiC,
- Ionic (salt-like): which are formed from metals in groups 1-3, such as Na_3N or Ca_2C_2,
- Interstitial: formed by early transition metals (groups 4-6), see Section 1.2,
- Intermediate: formed by metals in groups 7 and 8, where the bonding lies somewhere between covalent and ionic, although the interstices are too small to accommodate carbon or nitrogen atoms without severely distorting the lattice.

As tungsten and zirconium form interstitial nitrides and carbides, these will be examined in more detail.

1.3. Interstitial Nitrides, Carbides and Carbonitrides

Interstitial nitrides and carbides comprise a close-packed lattice of the host metal with the anions resting, as the name implies, in the interstices.[3,5] The metal lattice is often different from that of the pure metal. In order for an interstitial material to form, the non-metal/metal ratio of the atomic radii must not exceed 0.59. This is because, for example, in a face-centred cubic structure the non-metal atoms must be able to fill the octahedral holes (the tetrahedral holes being too small). The maximum non-metal/metal ratio for this is 0.59. The atomic radii and ratios for the elements in question are shown in **Table 1.1**. This shows that zirconium and tungsten nitride and carbide all obey this rule.

Table 1.1 Atomic radii of selected elements and their ratios.[2-5]

Element	Atomic Radius/Å	N/M	C/M
W	1.394	0.53	0.56
Zr	1.597	0.46	0.49
N	0.74	-	-
C	0.78	-	-

The interstitial structure allows for many different stoichiometric phases as the quantity of nitrogen or carbon can be easily varied, however, the nitrogen/carbon is usually ordered throughout the lattice. As such, metal nitrides and carbides readily form solid solutions with each other to form carbonitrides.

The bonding in such interstitial materials is largely metallic although there are some degrees of ionic bonding and covalent bonding as a series of σ and π *p-d* interactions between the metal and anion. The metallic bonding results in the interstitial

nitrides and carbides essentially behaving as metals, as they exhibit low resistivity and high thermal conductivity. Their melting points are high (>1800 °C, with the exception of tungsten nitrides, see Section 1.3.1) and generally those of carbides are higher than nitrides. As such, they are considered refractory.[2,4] Where interstitial nitrides differ from metals is that they are hard and have high mechanical strength, similar to ceramic materials. In general, carbonitrides will exhibit intermediate properties to those of pure nitrides and carbides.

1.3.1. Tungsten Nitrides and Carbides

Tungsten nitride is a conductive material, which has a metallic gold or grey-brown sheen, whereas tungsten carbide is metallic grey. Selected properties are summarised in **Table 1.2**.

Table 1.2 Selected properties of tungsten nitride and tungsten carbide.[3,5-8]

Property	**Tungsten Nitride**			**Tungsten Carbide**		
Formula	WN		W_2N	WC	W_2C	WC_{1-x}
Crystal lattice	hex	fcc	fcc	hex	hcp	fcc
a/Å	2.89	4.15	4.13	2.91	3.00	4.22
Melting point/°C	See below, **Eq. 1.1**			2870	2730	*
Electrical resistivity/μΩ.cm (20 °C)	200-400				17-22	

* Unstable below 1530 °C, presumed intermediate to WC and W_2C.

Tungsten nitride has two main compositions: stoichiometric WN, which can either be hexagonal (δ-WN, **Figure 1.1**) or face-centred cubic (NaCl structure), and face-centred cubic β-W_2N. The resistivity of tungsten nitride is relatively low at 200-400 μΩ.cm, which makes it suitably conductive for its use as a barrier layer.

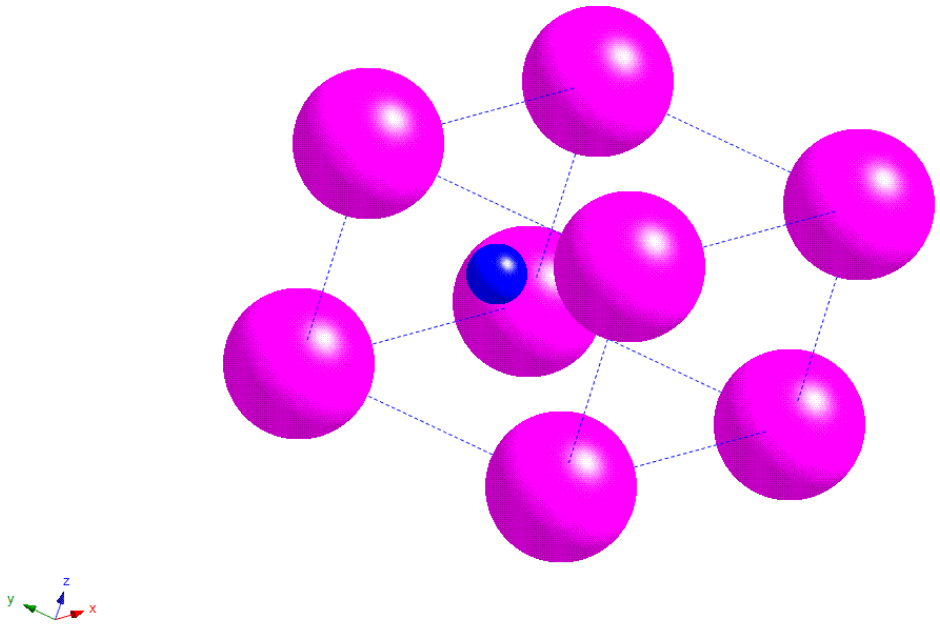

Figure 1.1 Unit cell of hexagonal δ-WN.[22] Magenta spheres = tungsten, blue sphere = nitrogen.

Of all the compounds discussed in this thesis, tungsten nitride is perhaps one which may not be considered refractory. A feature required to make a substance refractory is to have a melting point higher than 1800 °C.[4] The melting point of pure WN is difficult to ascertain as it decomposes *via* the loss of gaseous nitrogen at around 600 °C to form W_2N, which decomposes further at approximately 800 °C to metallic tungsten and nitrogen gas (**Eq. 1.1**).[23]

$$2\ WN \rightarrow W_2N + \tfrac{1}{2}\ N_2 \qquad \sim 600\ ^\circ C \qquad \textbf{(1.1a)}$$

$$W_2N \rightarrow 2\ W + \tfrac{1}{2}\ N_2 \qquad \sim 800\ ^\circ C \qquad \textbf{(1.1b)}$$

This is also evident when considering the resistivity, as the more nitrogen rich the tungsten nitride, the higher the resistivity (therefore the lower the conductivity). A

study by Lin *et al.* described an inverse relation between resistivity and annealing temperature (under vacuum),[18] where higher annealing temperatures promoted the loss of molecular nitrogen. This reduced the nitrogen within the tungsten nitride lattice which reduced the degree of covalent bonding and increased the metallic bonding, thereby making the resulting material more electrically conductive.

Tungsten carbide is more stable to decomposition than its relative nitride although it has a similar range of stoichiometries: δ-WC, which has a simple hexagonal crystal structure and β-W_2C, which is hexagonal close-packed (**Figure 1.2**). W_2C is less stable than stoichiometric WC, as it decomposes at ~1300 °C (**Eq. 1.2**).[8]

$$W_2C \rightarrow WC + W \qquad \textbf{(1.2)}$$

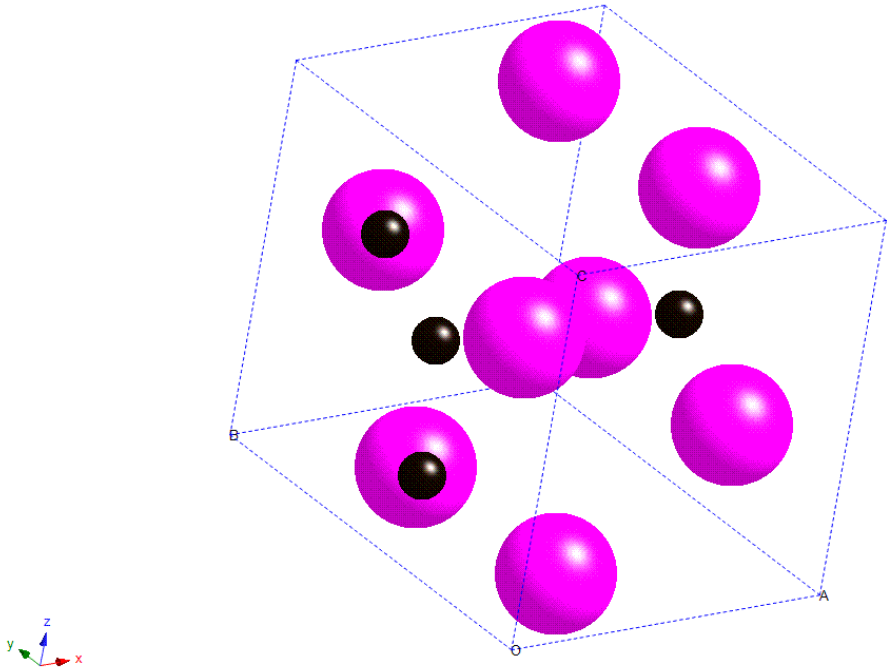

Figure 1.2 Unit cell of hexagonal close-packed W_2C.[24] Magenta spheres = tungsten, black spheres = carbon.

However, there is a third composition of intermediate stoichiometries, face-centred cubic γ-WC_{1-x},[8] where x = 0.35-0.42 ($WC_{0.58}$-$WC_{0.65}$).[25] It is only stable above 1530 °C, but tungsten carbide in general is believed to adopt this structure at lower temperatures when in solution with W_2N.[26,27] The resistivity of tungsten carbide is lower than that of tungsten nitride despite having generally larger lattice parameters. This may be due to the larger atomic radius of carbon allowing greater orbital overlap for the fluid movement of electrons throughout the system. These attributes might make tungsten carbide seem more suitable than tungsten nitride as a barrier layer, but tungsten carbide is less chemically resistant, being attacked by acids at high temperatures.[8]

1.3.2. Zirconium Nitrides and Carbides

Zirconium nitride is golden in colour, whereas the carbide is metallic grey. Nitrogen-rich Zr_3N_4 is transparent and yellow, with no metallic lustre. Selected properties are summarised in **Table 1.3**.

Table 1.3 Selected properties of zirconium nitride and zirconium carbide.[2,3,5-7]

Property	**Zirconium Nitride**			**Zirconium Carbide**
Formula	ZrN	Zr_3N_4		ZrC_x (x = 0.55-0.99)
Crystal lattice	fcc	fcc	orth	fcc
a/Å	4.57	6.74	9.73	4.69 (x = 1)
Melting point/°C	2980	See below, **Eq. 1.3**		3420
Electrical resistivity/μΩ.cm (20 °C)	17-22	>1000		35-55

The main phase, stoichiometric ZrN adopts a face-centred cubic structure (**Figure 1.3**). It is stable and melts at 2980 °C so it is considered a refractory nitride.[7]

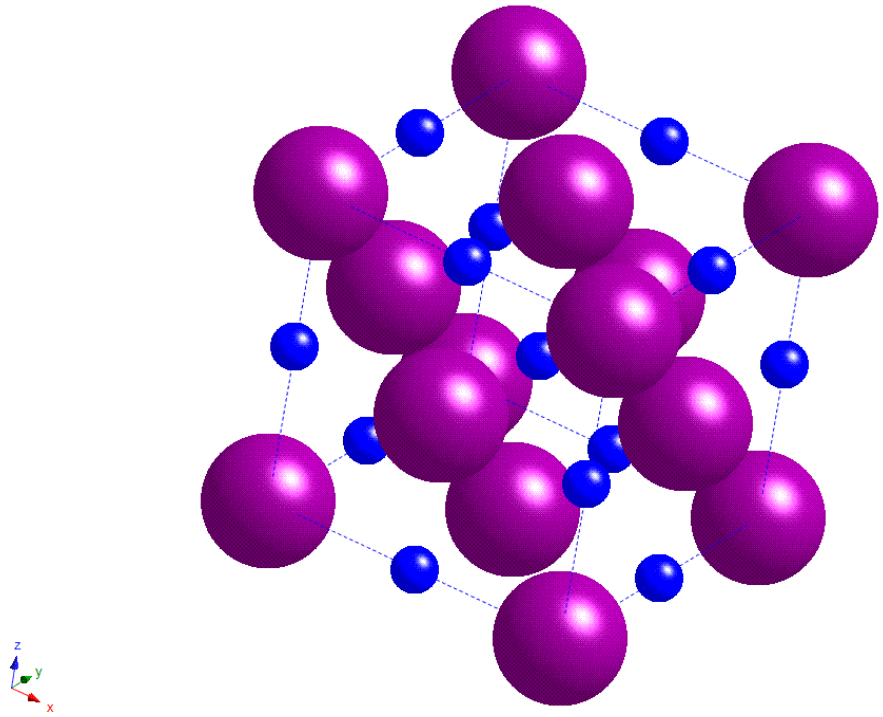

Figure 1.3 The rock salt face-centred cubic unit cell of ZrN.[28] Purple spheres = zirconium, blue spheres = nitrogen. W_2N also adopts this structure.

The other main form of zirconium nitride is nitrogen-rich Zr_3N_4, which can occur in both face-centred cubic (c-Zr_3N_4) and orthorhombic (o-Zr_3N_4) phases.[15] In c-Zr_3N_4, the stoichiometry is achieved by zirconium vacancies,[29] which has the effect of altering the band structure so that there is an optical band gap of 2.2 eV.[30,31] It is for this reason that Zr_3N_4 has no metallic lustre and a high resistivity, in excess of 1000 μΩ.cm at 20 °C. This phase of zirconium nitride is also metastable, and it decomposes to ZrN and nitrogen at temperatures above 800 °C (**Eq. 1.3**),[12] reducing the zirconium from the +4 to the +3 state.

$$Zr_3N_4 \rightarrow 3\ ZrN + \tfrac{1}{2}\ N_2 \qquad \textbf{(1.3)}$$

In general, zirconium nitride is chemically resistant, only being attacked by acids at high temperatures or undergoing oxidation in air at 800 °C.[7]

Zirconium carbide adopts only the face-centred cubic structure, although the stoichiometries vary widely: ZrC_x (x = 0.55-0.99). It has a similar conductivity to the nitride but it shows less resistance to chemical attack, as it is dissolved by cold acids (such as nitric acid or a mixture of phosphoric and sulphuric acids) and will easily form a solid solution with zirconium nitride or zirconium oxide as the lattices are similar.[6] It is also sensitive to gases: like zirconium nitride it undergoes oxidation in air at 800 °C but, unlike zirconium nitride, it reacts readily with halogens.

1.4. Applications of Transition Metal Nitrides and Carbides

The main uses of transition metal nitrides and carbides arise from their hardness, stability at high temperatures (carbides) and high conductivity (low resistivity).[32] Generally, these applications require the material to be deposited as a thin film coating. Deposition methods are described in Section 1.5.

1.4.1. Hard and Corrosion Resistant Coatings

The high hardness of materials such as TiN, ZrN and WC has lead to their use as coatings for machinery and drill bits,[32,33] TiN and ZrN are particularly favoured for steel tools as they adhere well to it. This allows the films to be deposited by PVD, which ordinarily would result in poorly-adhesive films and does not require high deposition temperatures.[34] This consequently prevents distortion of the steel and requires less energy. The chemical resistance of the films also prevents corrosion, greatly enhancing the working life of the machinery.

1.4.2. Decoration

Metal nitrides, in particular titanium and zirconium nitrides, have an aesthetic application as decorative coatings.[35] As they are gold in colour, they provide a suitable alternative to gold coatings. Thin films of TiN and ZrN are also more abrasion and scratch resistant than gold, so the provide a longer-lasting, scratch-free finish.

1.4.3. Barrier Layers

A barrier layer prevents diffusion of two materials, thereby avoiding a change in their properties. In modern electronics, the use of integrated circuits is on the increase and these need to be ever smaller and reliable to cope with demand.[9-11] The integrated circuits comprise semiconducting components, usually based on silicon, and copper or aluminium linkages. A problem arises at the interconnects, as copper (or aluminium) can diffuse into the silicon and form copper silicide (Cu_3Si),[36] which alters the semiconducting properties of the component and therefore changes the output of the circuit. To overcome this, a thin conducting barrier layer is deposited between the two materials. This layer cannot be a pure metal as it may form an alloy with the copper, therefore, transition metal nitrides and carbonitrides are materials of choice for this application,[11,14,27,37-42] as the interstitial nitrogen or carbon atoms effectively block the prominent diffusion sites (the octahedral holes) while maintaining a high electrical conductivity. Ideally, the films need to be epitaxial or amorphous, as polycrystalline films provide fast diffusion routes *via* the grain boundaries. Also, very thin layers with good conformal coverage are required, therefore low pressure CVD or ALD are the deposition methods of choice.

1.5. Methods of Thin Film Deposition

Nowadays, there is a great variety of thin film deposition techniques. The choice will depend on the properties of the desired film. This also affects the choice of precursor or source. Currently, the three most popular methods of thin film deposition are chemical vapour deposition, atomic layer deposition and physical vapour deposition.

1.5.1. Chemical Vapour Deposition (CVD)

Chemical vapour deposition, commonly abbreviated to CVD, involves the formation of a thin film on a heated substrate from reagents (precursors) in the gas phase. The films have different properties to those of the substrate and are chemically bound to it, making them very adhesive.[34] The precursors can either be single-source, where all the desired film components are in one molecule, or dual-source, where more than one molecule is employed (see Section 1.6 for a more detailed explanation).

1.5.1.1. Fundamentals of CVD

The important steps of the CVD process are outlined in **Figure 1.4**.

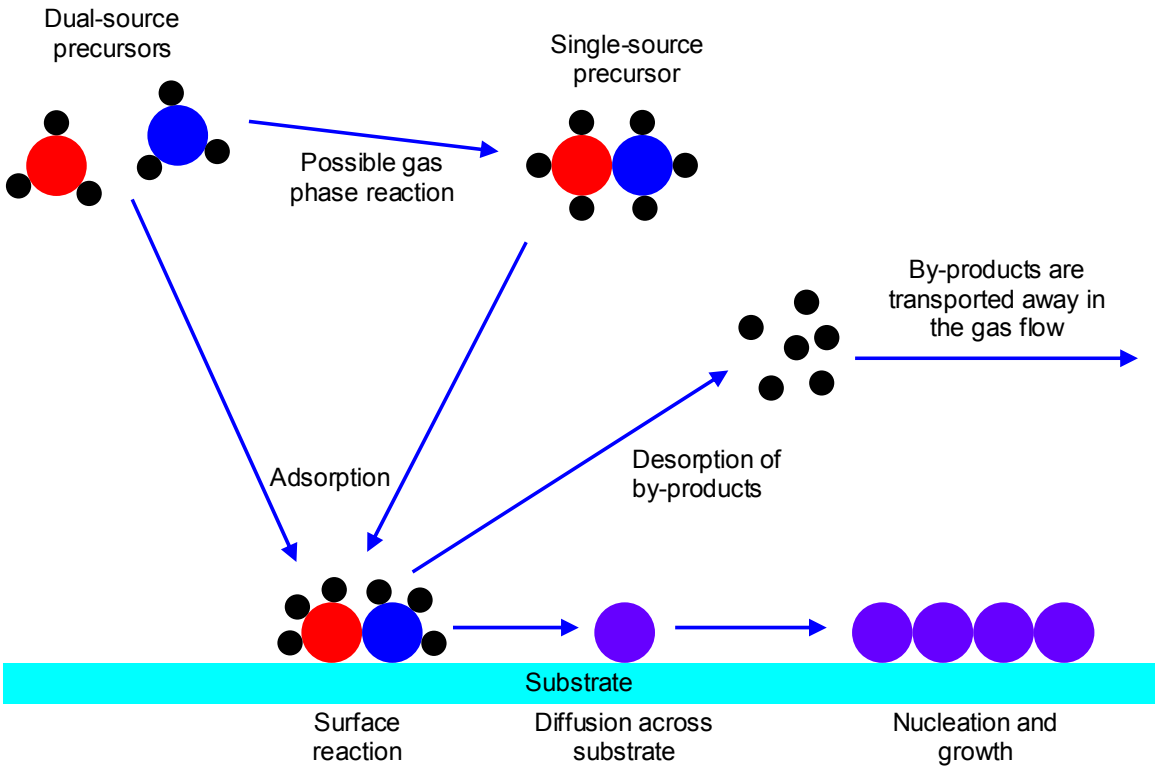

Figure 1.4 Stages of the CVD process.

Firstly, the precursors are transported to the reaction chamber in the gas phase. This is achieved either by sublimation or evaporation of the precursors by heating them, introducing them to a vacuum or by bubbling an inert carrier gas through them. They are then carried to the reaction chamber either by the inert gas flow or in a vacuum. Once reaching the surface, the precursor will adsorb and any unrequired ligands will dissociate due to the heat of the substrate and the resulting by-products desorb from the substrate and are carried away in the gas flow or vacuum. The remaining atoms, or substrate defects, act as nucleation points to which further atoms migrate, forming clusters of the desired material. The resulting island of material continues to grow, forming the film over time.

There are three main types of film growth:

- Epitaxial growth: the lattice of the film is matched to that of the substrate. A subset of this is preferred orientation, where the lattice of the film is not matched to the substrate but is preferentially perpendicular or parallel to the substrate surface.
- Polycrystalline growth: the film contains micro-crystalline grains whose lattice orientations are randomly aligned.
- Amorphous growth: no crystallinity.

A factor other than the type of growth is the deposition mechanism, which affects the physical structure of the films. The three most prominent mechanisms are outlined in **Figure 1.5**.

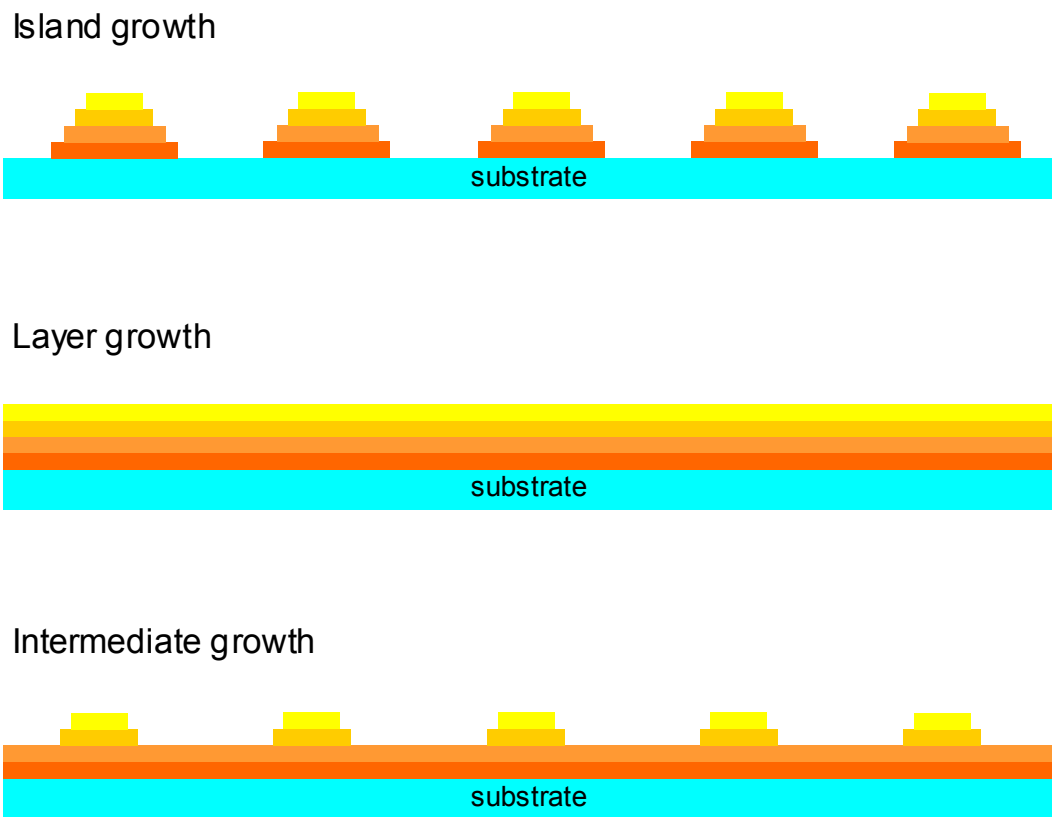

Figure 1.5 Common film growth mechanisms in CVD.

Island growth occurs when there are stronger interactions between the atoms in the film than between the film and the substrate, and is the most prominent due to the

aforementioned cluster formation. Layered islands of the desired material grow and eventually combine to form a continuous film. If, however, the atom-substrate interactions are stronger, uniform layer growth occurs. It is possible to have a combination of the two, resulting in intermediate growth.

1.5.1.2. Types of CVD

There is an increasing variety of CVD techniques, which can be tailored to specific applications, such as liquid-injection CVD, laser-enhanced CVD or plasma-enhanced CVD. However, the three most common types are described below.

1.5.1.2.1. Low Pressure Chemical Vapour Deposition (LPCVD)

By far the most common form of CVD, low pressure CVD, as its name implies operates at pressures of 1 mTorr or lower. Generally, the precursors are heated such that they sublime/evaporate so they can then be drawn to the reaction chamber by the ambient vacuum. The precursors can either be single- or dual-source (as gas bleeds can be introduced), and air-sensitive compounds are not affected. The use of a vacuum means the system has to be robust and larger apparatus would require longer times to reach the desired pressure. As such, LPCVD is relatively expensive and generally used to coat small areas, which does not require large apparatus. The films deposited by this process are generally adhesive and exhibit good step coverage. These features make LPCVD ideal for the microelectronics industry.

1.5.1.2.2. Atmospheric Pressure Chemical Vapour Deposition (APCVD)

Operating between 1 mTorr and atmospheric pressure, APCVD is suited both to small- and large-scale depositions as there are no equipment size restrictions. As such, it is a popular choice for on-line deposition processes.[43,44] Single-source precursors are not generally suitably volatile for this procedure and, while not necessarily open to air, there is a high possibility of contamination if single-source precursors are used, despite the use of an inert purge gas, so APCVD is a dual-source method. The precursors are carried through the system *via* a flow of inert gas and give highly adhesive and conformal films.

1.5.1.2.3. Aerosol-Assisted Chemical Vapour Deposition (AACVD)

AACVD involves the generation of an aerosol of the precursor in solution, which is then carried to the reaction chamber in an inert carrier gas. The clear advantage of this method is that the volatility of the precursor is not a concern, which allows a range of precursors not previously thought ideal for CVD to be used. However, the precursors must be suitably soluble in the chosen solvent. A standing wave is passed through the precursor solution using a piezo-electric crystal, which creates a mist. When in the reaction chamber, the solvent evaporates and is carried out in the exhaust, leaving the precursor in the gas phase to react with the substrate. However, the solvent can play a role in contamination of the final film.[45] A typical AACVD set up is shown in **Figure 1.6**.

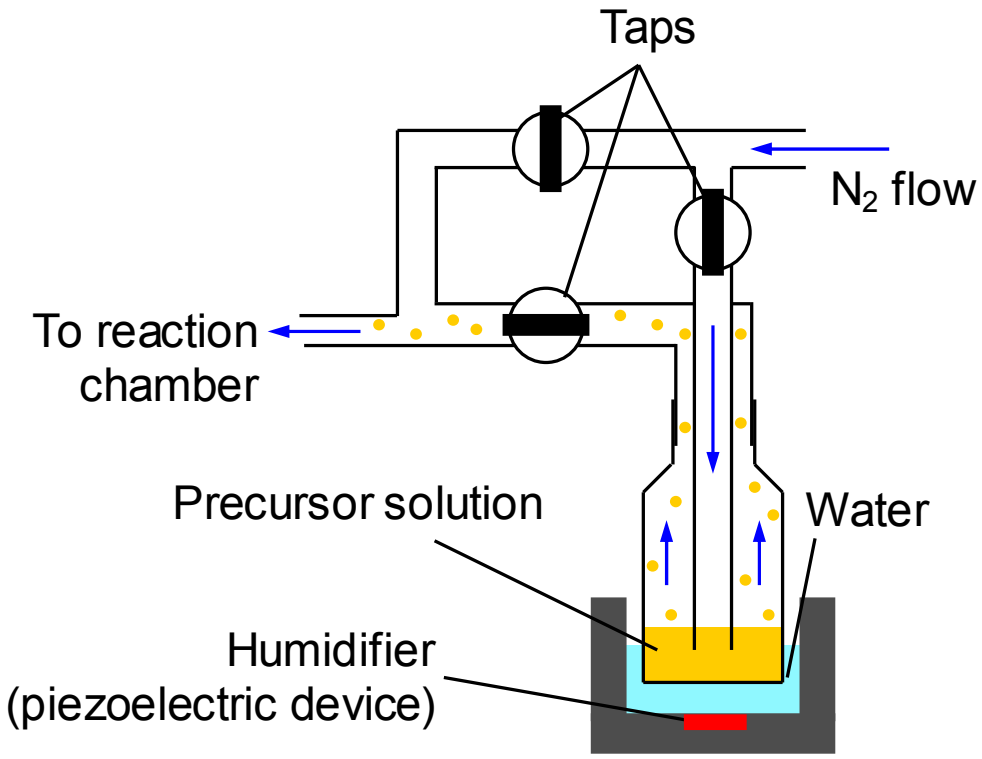

Figure 1.6 A schematic example of how an aerosol is created in AACVD.

A related method is liquid injection CVD, where a solution of the precursor is injected at a set rate into a hot zone, which vaporises the solution prior to carrying it to

the reaction chamber under vacuum or *via* an inert carrier gas.[46,47] A clear advantage of both AACVD and liquid injection CVD is that thermal decomposition of relatively involatile precursors is avoided as the solution is at room temperature before it enters the system, as opposed to APCVD and LPCVD bubblers, where the precursor is heated. However, an advantage of liquid injection CVD over AACVD in that lower pressures can be used, which is beneficial for nitride and carbide systems.

1.5.2. Atomic Layer Deposition (ALD)

Atomic layer deposition (ALD) is essentially a form of CVD where two or more precursors are introduced into the system on an alternating basis, the chemical reactions of which are self-limiting.[9] While CVD can be carried out over long or continuous deposition times, ALD is carried out in cycles. A typical ALD cycle is described in **Figure 1.7**. The key difference between CVD and ALD is that the growth kinetics of CVD are controlled by thermal decomposition of the precursors, whereas ALD involves exchange reactions between the precursors and the substrate surface. This means that lower substrate temperatures can be employed (no higher than 400 °C) and greater control over the stoichiometry and thickness of the films can be achieved. In particular, ultrathin films can be deposited, which is particularly important as electronic devices continually become smaller. Disadvantages are that growth rates are comparatively lower than in CVD and that it is limited to dual-source precursors.

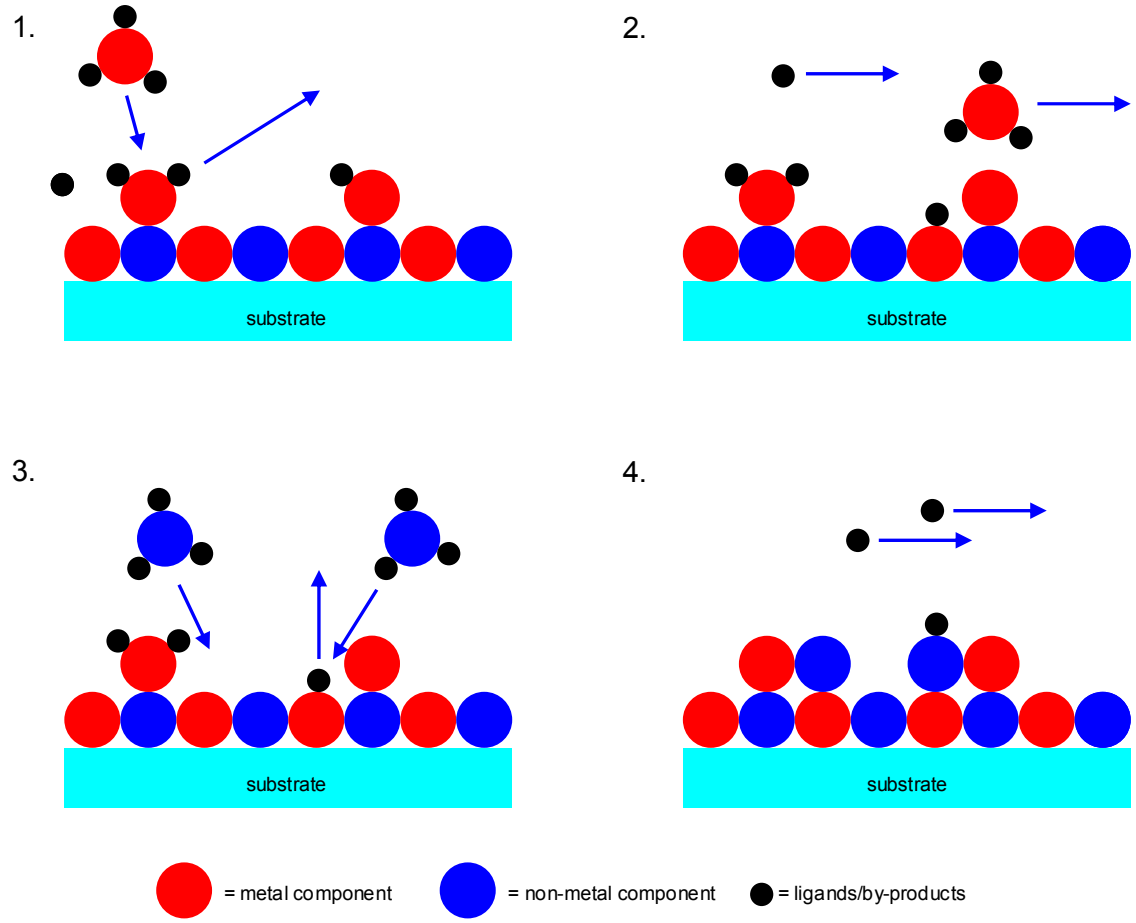

Figure 1.7 A typical ALD cycle. 1. Introduction of first (metal) precursor and desorption of by-products. 2. Purge of inert gas to remove unreacted precursor and by-products. 3. Introduction of second (non-metal) precursor and further desorption of by-products. 4. Second purge.

The ALD cycles are set up so that the system is purged with an inert gas between the introduction of each precursor, ensuring by-products and unreacted precursor molecules are removed from the system, resulting in purer films. The ultrathin film is gradually formed over a series of cycles. The cycles also allow the progress of the deposition to be monitored by *in situ* analytical techniques such as ellipsometry and mass spectrometry of the reactants and by-products.[48-50] This is particularly useful when tuning the deposition conditions during the gradual build-up of the film.

1.5.3. Physical Vapour Deposition (PVD)

Perhaps the main distinction between physical vapour deposition (PVD) and CVD is that the former requires the material components as either atoms or ions, whereas the latter requires molecular precursors.[34] As such, the starting materials are referred to as the source, rather than as precursors. The system is such that the source atoms or ions are aimed directly at the substrate, making PVD a line of sight technique. This puts PVD at a disadvantage when compared with CVD or ALD, as poor step coverage results because the source material only travels in straight lines. Another disadvantage of PVD is that the films are formed *via* condensation rather than chemical reaction and, as a result, are generally poorly adhesive and mechanically weak compared to those formed by CVD.

The most straightforward method is evaporation, where the source (in this case the bulk starting material) is heated to above its boiling point under pressures lower than approximately 5×10^{-6} Torr. The heating methods vary, typically being resistance heaters, lasers or electron beams. The gaseous source atoms or ions are then transported to the substrate, where they condense and deposit the film. Where the substrate is crystalline, a crystalline film may result, in which case the PVD process is referred to as molecular beam epitaxy (MBE).[51]

Another popular method of PVD is sputtering, where the source is bombarded with a plasma (typically argon) under very low pressures. This releases atoms and ions of the source material, which are subsequently drawn to the substrate under vacuum. However, ion plating is also rising in popularity; where an already-deposited film is bombarded with atoms or ions of another substance with a view to changing the properties of the film.[40,52] Sol-gel dip coating methods are also well known, where a liquid precursor is placed on a substrate by dipping and converted to a thin film *via* a gel by heating it in a furnace. However, this is unsuitable for metal nitrides and carbides.

1.6. Precursors

The choice of deposition method is inevitably linked with the choice of precursors. The components of the desired film can either be provided by two or more precursors (dual-source precursors) or can be contained in one molecule (single-source precursors).

1.6.1. Dual-Source Precursors

Dual source precursors can generally be obtained from commercial sources and their minimal ligands result in fewer impurities in the films. They exhibit high deposition rates, although this can result in more film defects.

For metal nitride films, the typical combination of precursors is the reaction of the metal halide with ammonia (**Eq. 1.4**), which provides the nitrogen source. (For carbides, methane could be used.)

$$MCl_{2n}\,(g) \;+\; n\,NH_3\,(g) \;\rightarrow\; MN\,(s) \;+\; 2n\,HCl\,(g) \;+\; N_2\,(g) \qquad \textbf{(1.4)}$$

Examples of this method include the ALD of WF_6 and ammonia, onto Si{100} substrates, at temperatures between 300-400 °C (below which the reaction was not self-limiting).[53,54] This afforded amorphous thin films of both cubic W_2N and tungsten metal although the HF by-product reacted with the glass in the ALD reactor. Lee and Yong have since investigated the potential of $W(CO)_6$ as the tungsten source for metal-organic CVD (MOCVD) of tungsten nitride, the rationale being that the W–C bond is weak so fewer carbide and oxide impurities would result and lower temperatures than those required for WF_6 could be used.[11] MOCVD of $W(CO)_6$ and ammonia on SiO_2/Si or HF-rinsed Si substrates between 250-500 °C afforded W_xN (x = 2-3.5) thin films 15 nm thick. The metal halide route is not just restricted to ammonia, as MN (M = Nb, Ta) thin films were deposited by APCVD from MCl_5 and $HN(SiMe_3)_2$.[55] The facile loss of volatile Me_3SiCl being a potential driving force for the formation of the metal nitride.

The reaction of $ZrCl_4$ and ammonia is known for bulk synthesis[12] but not for CVD or ALD due to its low volatility. Another popular reactant with ammonia for metal nitrides are homoleptic metal amide compounds, such as $[M(NR_2)_n]$ (R = Me, Et; n = 4, M = Ti, Zr; n = 5, M = Nb, Ta).[13,34] Decomposition studies of $[Ti(NMe_2)_4]$ with ammonia have been reported, which suggest that the nitrogen in the remaining film comes entirely from the ammonia rather than the dimethylamido ligands in the $[Ti(NMe_2)_4]$ (**Scheme 1.1**).[56] It is effectively a transamination process.

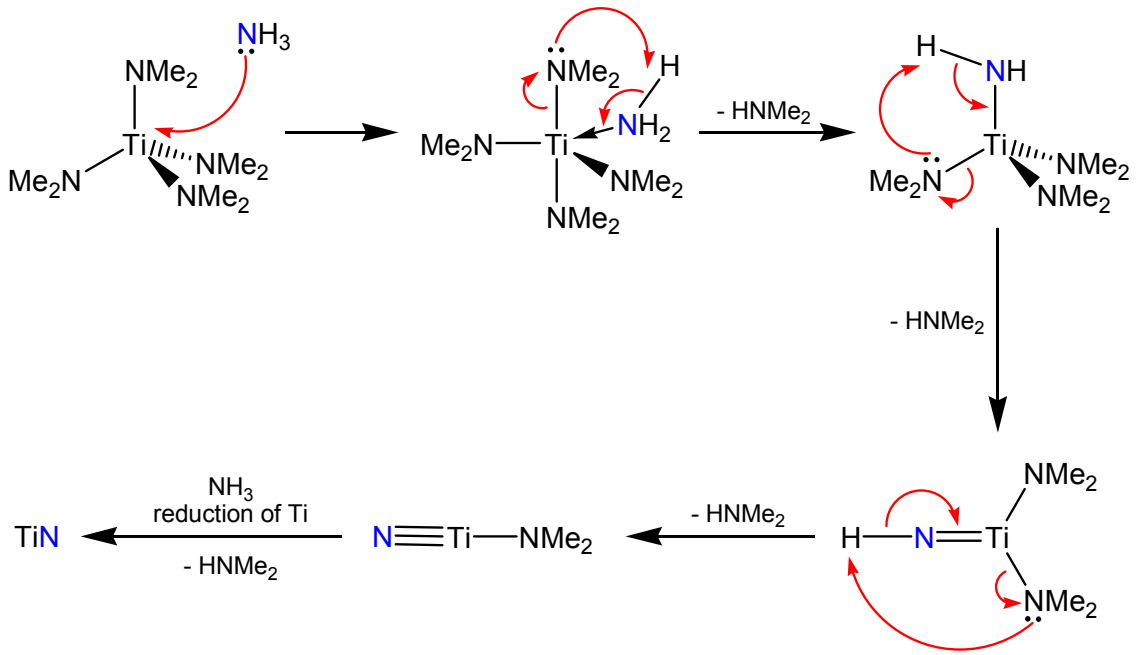

Scheme 1.1 Mechanism of the dual-source CVD of TiN from $[Ti(NMe_2)_4]$ and ammonia.

This mechanism opens up the potential for $[Ti(NMe_2)_4]$ as a dual-source precursor to a variety of TiX_n thin fims (X = chalcogenide, pnictide). For example, TiS_2 films have been deposited using $[Ti(NMe_2)_4]$ and thiols.[57]

1.6.2. Single-Source Precursors

The idea behind single-source precursors is that all the components of the desired thin film are contained in a single molecule. For tungsten nitride, for example, an ideal precursor should contain at least one pre-formed W–N bond, as this should theoretically lower the energy required for film formation, and hence lower the deposition temperature.[58] This, however, is less relevant to ALD, where the precursor needs to stay intact until it is bound to the surface.[9] Another benefit is that pre-reaction is limited as there only one precursor in the system. Single-source precursors are generally less volatile than dual-source precursors, and they air- and moisture-sensitive, leading to a reduced shelf-life.

The ligands bound to the metal centre and moieties bound to the nitrogen should be labile so they can leave the molecule at low temperatures and avoid contamination of the film. An example of this is β-hydrogen elimination (**Figure 1.8**), which is prevalent in alkyl groups, such as ethyl, isopropyl and *tert*-butyl, as they all contain β-hydrogen atoms.

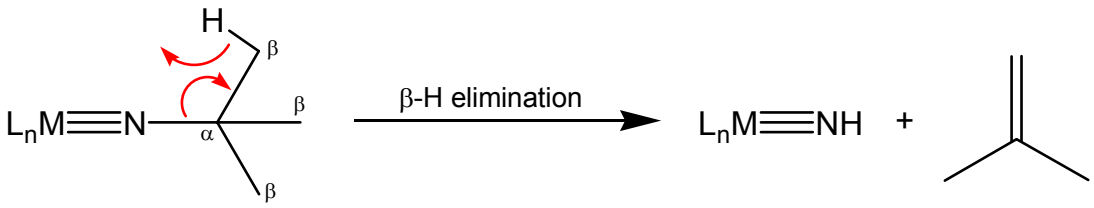

Figure 1.8 An example of β-hydrogen elimination, as shown in a *tert*-butylimido ligand.

This suggests that smaller ligands would be preferable as fewer undesired atoms per precursor molecule would be present, reducing the possibility of impurities in the resulting films, which can be problematic where single-source precursors are concerned. Further benefits of single-source precursors are avoidance of the need to use toxic and/or pyrophoric precursors (for example WF_6), single molecules are easier to purify and pre-reactions in the CVD apparatus are limited.[59]

One advantage of single-source precursors that may not be directly relevant for those to transition metal nitride thin films is the retention of stoichiometry.[60] As, with single-source CVD of transition metal nitrides, the M:N ratio tends to be greater than 1,[13,61] so the nitrogen in the precursor must be maximised. Ideally, an all-nitrogen coordination sphere around the metal centre is required so as to limit the incorporation of impurities, such as carbon, in the resulting film. However, for more precise stoichiometries and subtle stoichiometry changes, dual-source precursors are more suitable as the quantities entering the system may be precisely tuned.

1.6.2.1. Ligands for Nitride and Carbonitride Thin Films

To achieve the best film possible, the ligands must be selected with care. Below are descriptions of selected ligands, which should prove suitable for transition metal nitride thin films. For electron counting in this work, the ionic model is used.

1.6.2.1.1. Amido Ligands

Probably the simplest method of achieving a metal-nitrogen bond is *via* a datively bound amine molecule to the metal centre. However, the simplest direct bond is achieved through an amido group (NR_2^-), which binds primarily through an M–N σ bond. Amido ligands show promise as metal nitride precursors as they can undergo synergic bonding with transition metal centres, exhibiting a degree *pπ-dπ* back-donation strengthening the M–N bond.[62] **Scheme 1.2** shows how the resonance occurs, with form **A** being the generally accepted trigonal pyramidal shape of the amido ligand with an sp^3 hybridised nitrogen and **B** being trigonal planar with an sp^2 hybridised nitrogen.

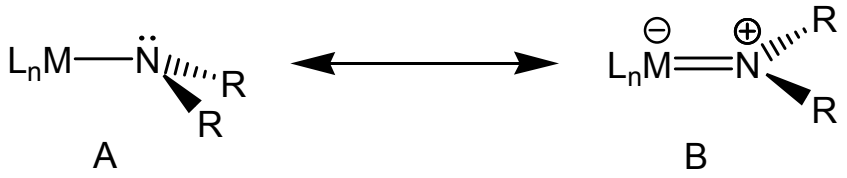

Scheme 1.2 Resonance forms of the amido ligand.

It is theoretically possible for a complete resonance form (**B**) to occur, but for this to happen, the metal centre would need to have a vacant *d*-orbital of appropriate symmetry. This is, of course, dependant on the other ligands on the metal centre and generally amido ligands tend to remain largely sp^3 hybridised (form **A**).[63] For this reason, the amido group is considered to be a 2-electron donor.

In most cases, amido compounds are synthesised *via* lithium metathesis reactions (**Eq. 1.5**):

$$MCl_n + n\,LiNR_2 \rightarrow [M(NR_2)_n] + n\,LiCl \qquad \textbf{(1.5)}$$

However, other methods include transamination (**Eq. 1.6**), which relies on the leaving group being highly volatile, such as $HNMe_2$;[63] and hydrochloride salt elimination (**Eq. 1.7**).

$$[M(NR_2)_n] + \text{excess } HNR'_2 \rightarrow [M(NR_2)_{n-x}(NR'_2)_x] + x\ HNR_2 \quad \textbf{(1.6)}$$

$$[MCl_n] + 2n\ HNR_2 \rightarrow [M(NR_2)_n] + n\ HNR_2.HCl \quad \textbf{(1.7)}$$

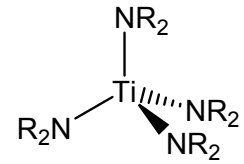

1.1

$NR_2 = NMe_2, N^nPr_2, N^iBu_2, NC_5H_{10}$

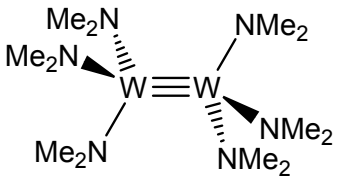

1.2

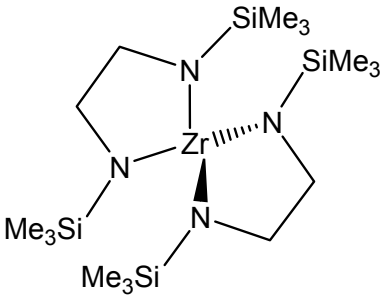

1.3

Figure 1.9 Selected examples of compounds containing amido ligands.

The amido ligand is ubiquitous in inorganic chemistry[63] (see **Figure 1.9**) and known examples of homoleptic transition metal amides, generally synthesised by the metathesis route, include $[Ti(NR_2)_4]$ (**1.1**, NR_2 = NMe_2, N^nPr_2, N^iBu_2, NC_5H_{10}),[64] $[Zr(NR_2)_4]$ (R = Me, Et),[64] $[W(NMe_2)_6]$[65] and $[W_2(NMe_2)_6]$ (**1.2**).[66] There are also some chelating amido compounds known, such as $[Zr\{\eta^2\text{-}(Me_3Si)NCH_2CH_2N(SiMe_3)\}_2]$ (**1.3**),[67] which was synthesised by transamination. However, amido ligands tend to

appear with a variety of other ligands, some of which will be mentioned later in this chapter.

1.6.2.1.2. Imido Ligands

Although amido ligands might be the obvious starting point to achieve an all-nitrogen coordination sphere, they are still generally quite labile and so ligands with a stronger M–N bond are desirable. A solution is to have imido (NR^{2-}) ligands on the metal centre, as the bond order of the M=N bond is >1, therefore reducing the lability of the ligand. However, as with the amido ligand, it is overly simplistic to view the N=R as a simple 'double bond' as the lone pair on the nitrogen atom can undergo *p*π-*d*π donation to the metal *d*-orbitals of the same symmetry (**Scheme 1.3**).[68]

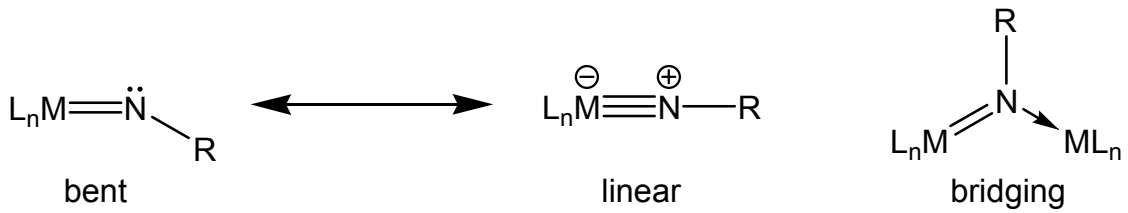

Scheme 1.3 Resonance forms of the imido ligand and its bridging capability.

The *p*π-*d*π donation plays a much more important role in the stability of the imido ligand when compared to the amido ligand. Where the nitrogen lone pair does not interact with the metal centre, the ligand will be bent (sp^2 hybridised, considered to be a 4-electron donor), although this is seldom the case. More often than not, there is a contribution from the lone pair so the ligand will generally take the linear (*sp* hybridised, a 6-electron donor) form or a combination of the two forms. The shape of the imido ligand is most obvious from crystal structures, and the M–N–R bond angle is often close to 180°.[69]

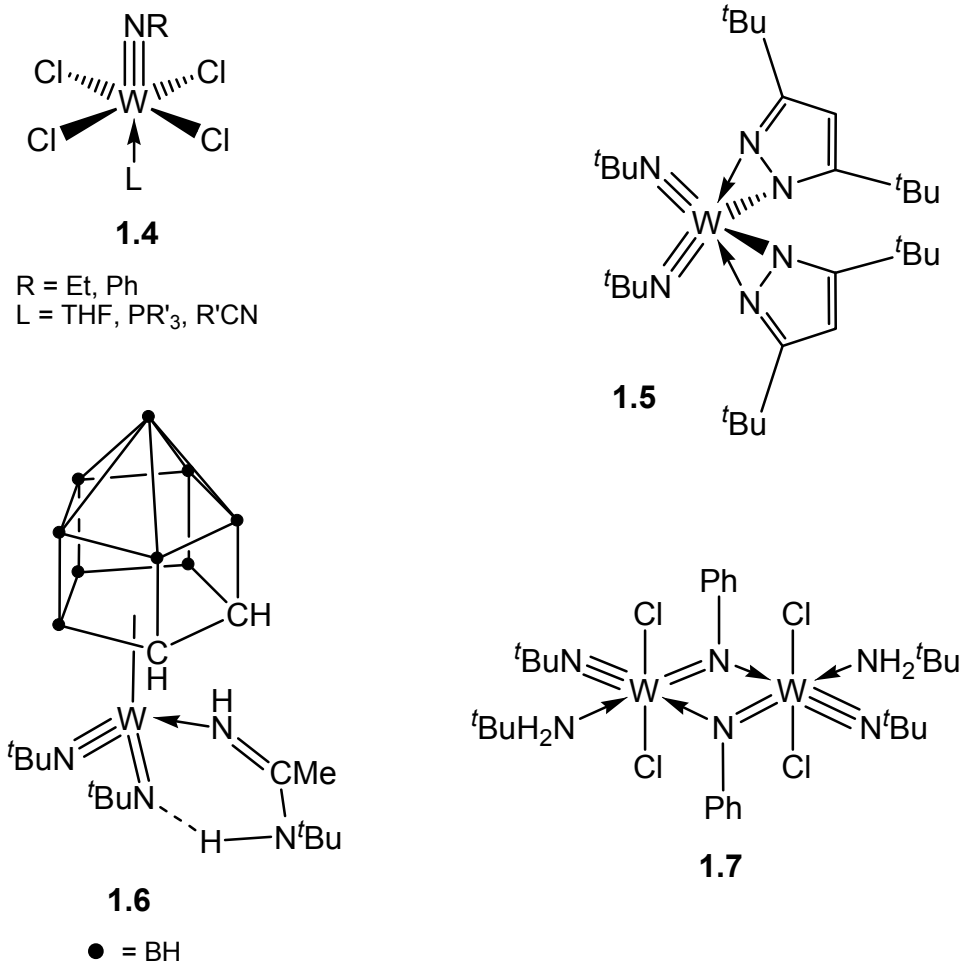

Figure 1.10 Selected examples of compounds containing imido ligands.

Examples are numerous (**Figure 1.10**), and include $[W(NR)Cl_4(L)]$ (**1.4**, R = Et, Ph; L = various Lewis bases, e.g. THF, PR'$_3$, R'CN),[70] $[W(N^tBu)_2(NH^tBu)_2]$[71] and $[(^tBuN)_2W(\eta^2\text{-}^tBu_2pz)_2]$ (**1.5**, $^tBu_2pz$ = 3,5-bis(*tert*-butyl)pyrazoyl).[72] However, where the metal is saturated with π-bonds, the imido ligand will take the bent form, such as in $[W(NMes)_2(\eta^5\text{-Cp})(\eta^1\text{-Cp})]$ (Mes = 2,4,6-trimethylphenyl, Cp = cyclopentadienyl)[73] and $[W(N^tBu)_2\{N(H)=C(Me)NH^tBu\}(C_2B_9H_{11})]$ (**1.6**),[74] the latter being a particularly good example of the availability of the lone pair on the imido nitrogen, which exhibits a hydrogen-bond with the proton on the $[=C(Me)NH^tBu]$ moiety. Indeed, other examples of imido complexes contain bridging imido ligands (**Scheme 1.3**) include $[Ti(\mu\text{-}N^tBu)(\eta^5\text{-Cp})Cl]_2$[75] and $[W(\mu\text{-NPh})(N^tBu)Cl_2(H_2N^tBu)]_2$ (**1.7**),[76] where the ligand

is still essentially a 6-electron donor, but over two metal centres. In terms of CVD, this ligand may be especially effective if the R group itself is labile, such as ethyl, isopropyl or *tert*-butyl, which readily decompose by β-hydrogen elimination mechanisms.

1.6.2.1.3. Hydrazido Ligands

Derived from hydrazine, hydrazido ligands comprise two subgroups: monoanionic hydrazido(1-), $(N\{R'\}NR_2)^-$ (**Scheme 1.4**), and dianionic hydrazido(2-), $(NNR_2)^{2-}$ (**Scheme 1.5**).[68] Depending on the mode of binding, they can be 2-, 4- or 6-electron donors.

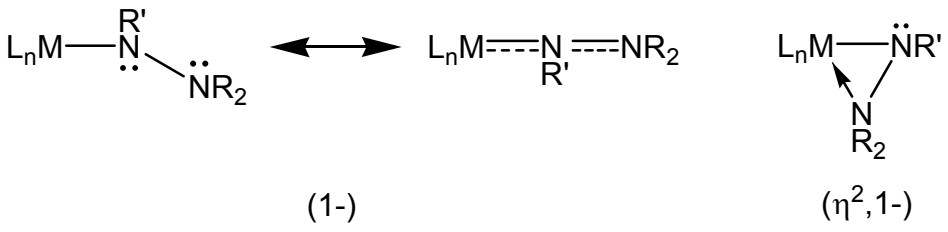

Scheme 1.4 Binding modes of hydrazido(1-) ligands.

Hydrazido(1-) ligands can essentially be considered as amido ligands bearing an NR_2 substituent. As such, their behaviour is comparable to that of amido ligands in the sense that they can undergo a degree of π-donation to the metal centre. However, the lone pair on the NR_2 moiety can also contribute to the π-system in the hydrazido(1-) ligand, which results in a linear structure, although, for metal centres with low coordination numbers, the NR_2 will chelate *via* the lone pair (η^2, 1-).

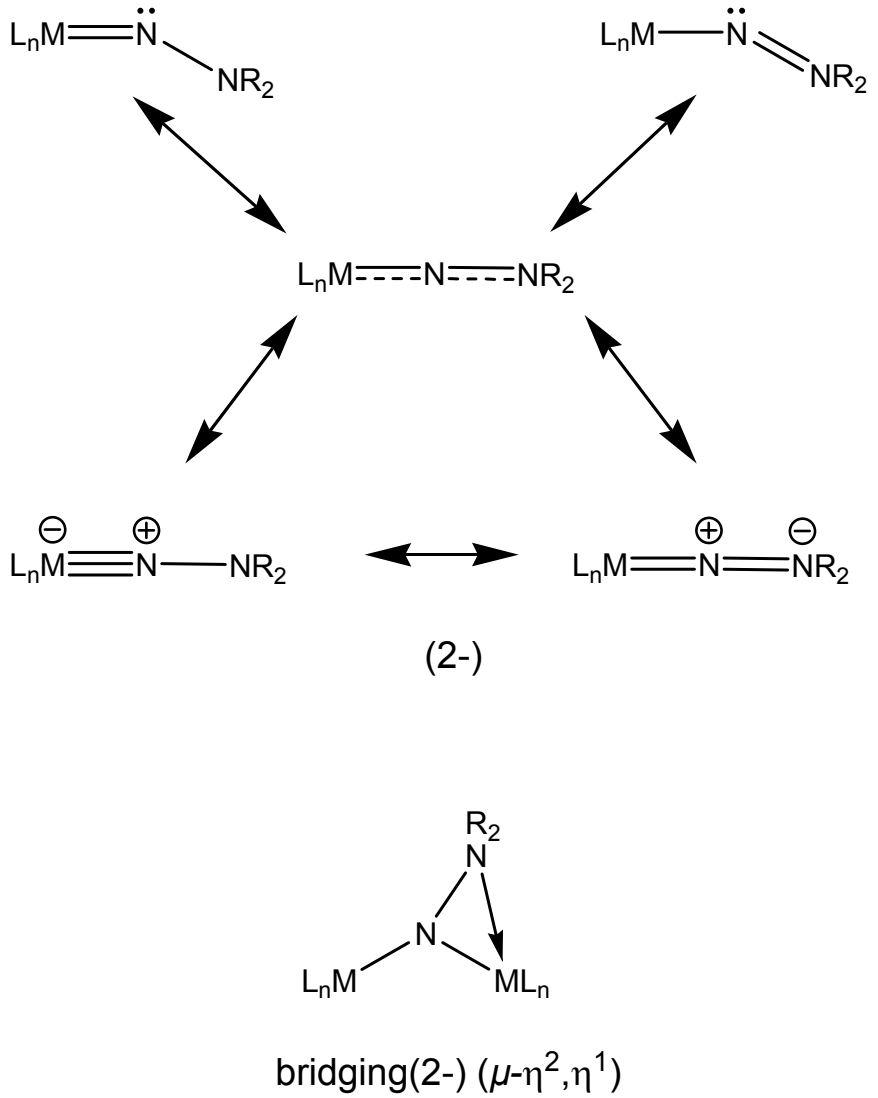

Scheme 1.5 Binding modes of hydrazido(2-) ligands.

Hydrazido(2-) ligands behave in a similar manner to imido groups although π delocalisation occurs over the M–N–N region. For this reason, they tend to be linear, or close to linear, in geometry. They can also bridge two metal centres, with the lone pair of the NR_2 substituent chelating to one of them.

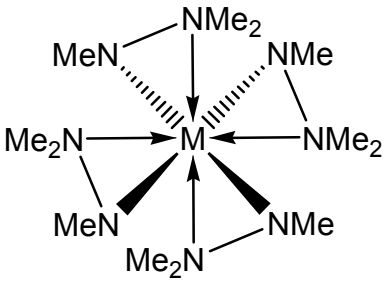

1.8

M = Zr, Hf

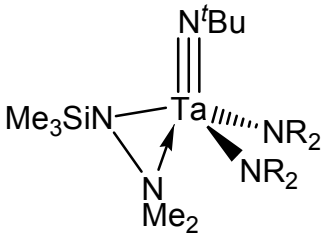

1.9

NR_2 = NMe_2, NEtMe, NEt_2

Figure 1.11 Selected examples of compounds containing hydrazido(1-) ligands.

The syntheses of hydrazido compounds (two of which are shown in **Figure 1.11**) are similar to amido and imido complexes, for example, $[M\{\eta^2\text{-}N(Me)NMe_2\}_4]$ (**1.8**, M = Zr, Hf)[77] is formed by the metathesis reaction of $[MCl_4]$ and four equivalents of $[Li\{N(Me)NMe_2\}]$, whereas $[W(N^tBu)_2\{\eta^2\text{-}N(SiMe_3)NMe_2\}X]$ (X = Cl, Br)[78] can be synthesised from $[W(N^tBu)_2Cl_2(py)_2]$ (py = pyridine) either by metathesis with a Grignard reagent, $[Mg\{N(SiMe_3)NMe_2\}X]$, or via hydrochloride salt elimination from the direct reaction with the hydrazine, $H(Me_3Si)NNMe_2$ (X = Cl only). Transamination is also a viable route, exemplified by the synthesis of $[Ta(N^tBu)\{\eta^2\text{-}N(SiMe_3)NMe_2\}(NR_2)_2]$ (**1.9**) from $[Ta(N^tBu)(NR_2)_3]$ (NR_2 = NMe_2, NEtMe, NEt_2), although the reactions took days to complete and required a large excess of the hydrazine.[79]

In contrast, hydrazido(2-) ligands (examples are shown in **Figure 1.12**) are generally not formed by salt metathesis reactions, rather by hydrochloride salt elimination or transamination. For example, $[W(=NNR_2)Cl_4]$ (**1.10**, NR_2 = NMe_2, NHPh, NMePh, NPh_2) was synthesised by George *et al.* by the reaction of WCl_6 with the hydrochloride salts of various hydrazine derivatives (except for NR_2 = NMe_2, where only the hydrazine was used).[80]

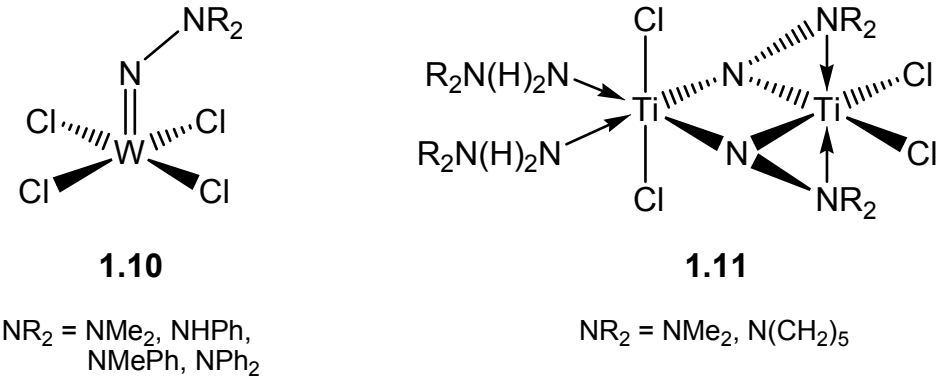

Figure 1.12 Selected examples of compounds containing hydrazido(2-) ligands.

$[Ti(NMe_2)_2Cl_2]$ undergoes a transamination reaction with *N*,*N*-diphenylhydrazine to give $[Ti(=NNPh_2)Cl_2(NHMe_2)_2]$, as described by Mountford *et al.*[81] Incidentally, their work also features bridging hydrazido(2-) ligands (**Figure 1.12**), as featured in the asymmetric dimer $[Ti_2(\mu\text{-}\eta^2,\eta^1\text{-}NNR_2)_2Cl_4(H_2NNR_2)_2]$ (**1.11**, NR_2 = NMe_2, $N(CH_2)_5$), which was formed *via* hydrochloride salt elimination between $TiCl_4$ and the related *N*,*N*-disubstituted hydrazine. In this case, it is interesting to see two hydrazine molecules behaving as amine ligands.

1.6.2.1.4. Guanidinate Ligands

Based on neutral guanidine, anionic dihapto guanidinate(1-), $((RN)_2NCR'_2)^-$, and guanidinate(2-), $((RN)_2NCR')^{2-}$, ligands, can stabilise a large variety of metals and oxidation states.[82] Guanidinate(1-) ligands in particular exhibit more electronic flexibility than imido or hydrazido ligands as there is the possibility of delocalisation over the carbon centre between the three nitrogen atoms. As such, there are two canonical forms (**Scheme 1.6**) making guanidinato ligands 6-electron donors.

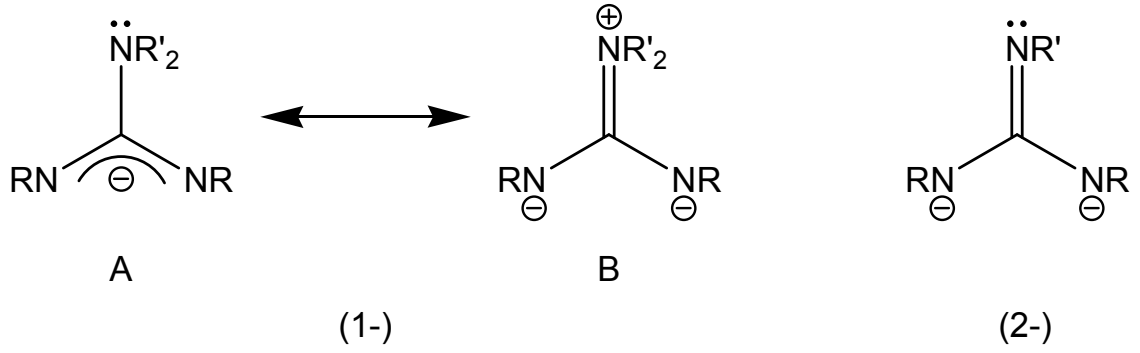

Scheme 1.6 Guanidinate(1-) and (2-) ligands.

Where the metal centre is electron rich, resonance form **A** prevails, in which all N–C bond lengths are similar and the ligand essentially behaves as an amidinate bearing an NR'$_2$ substituent. In this form, the uncoordinated N–C bond is significantly longer. This is generally the preferred structure in the majority of guanidinate compounds. However, if the metal centre is electron deficient there will be a greater contribution from form **B**, which behaves as a guanidinate(2-) ligand. This results in the shortening of the uncoordinated N–C bond and the geometry of the NR'$_2$ moiety becoming more planar. An example of this is [Ti{η^2-(PhN)$_2$CNEt$_2$}$_2$Cl$_2$] (**1.12**, **Figure 1.13**),[83] where the C–NEt$_2$ bond is statistically similar to the N–Ph bonds, indicating a significant contribution from form **B**.

In terms of synthesis, there are three known routes to metal guanidinate complexes: salt metathesis reactions with metal chloride complexes (**Eq. 1.8**), insertion of carbodiimides into M–NR$_2$ bonds (**Eq. 1.9**) and proton transfer, which is related to transamination, whereby a metal alkyl is treated with a substituted guanidine (**Eq. 1.10**).

$$[ML_nCl_x] + x\,[Li\{(RN)_2CNR'_2\}] \rightarrow [ML_n\{\eta^2\text{-}(RN)_2CNR'_2\}_x] + x\,LiCl \qquad \textbf{(1.8)}$$

$$[M(NR'_2)_n] + x\,RN{=}C{=}NR \rightarrow [M(NR'_2)_{n-x}\{\eta^2\text{-}(RN)_2CNR'_2\}_x] \qquad \textbf{(1.9)}$$

$$[M(CH_2Ph)_n] + x\,(RHN)_2C{=}NR \rightarrow [M(CH_2Ph)_{n-x}\{\eta^2\text{-}(RN)_2CNHR\}_x] + x\,MePh \qquad \textbf{(1.10)}$$

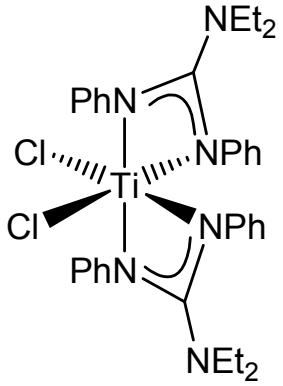

1.12

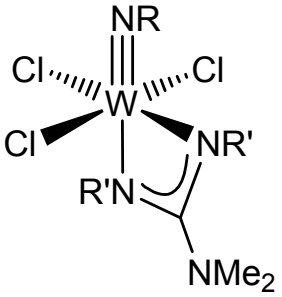

1.13

R = ^{i}Pr, Ph, Cy^{hex}
R' = ^{i}Pr, ^{t}Bu, SiMe$_3$

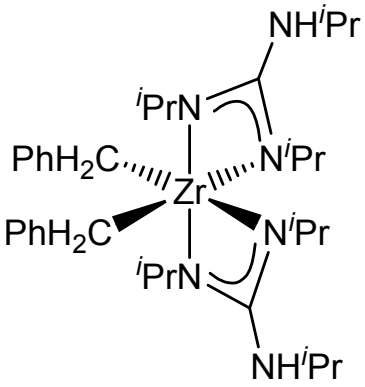

1.14

Figure 1.13 Selected examples of compounds containing guanidinate ligands.

The most widespread method is the metathesis reaction whereby a carbodiimide is treated with a lithium amide salt to form a lithium guanidinate salt, which is subsequently reacted with a transition metal chloride. Examples include $[W(NR)\{\eta^2\text{-}(R'N)_2CNMe_2\}Cl_3]$ (**1.13**, R = ^{i}Pr, Ph, Cy^{hex}; R' = ^{i}Pr, ^{t}Bu, SiMe$_3$),[84] $[ZrCl_2\{\eta^2\text{-}(RN)_2CNR'_2\}_2]$ (R = ^{i}Pr, Cy^{hex}; NR'$_2$ = N^{i}Pr$_2$, N(CH$_2$)$_5$)[85] and the closely related $[MCl_2\{\eta^2\text{-}(RN)_2CN(SiMe_3)_2\}_2]$ (M = Zr, Hf; R = ^{i}Pr, Cy^{hex}),[86] which resulted from the reaction of the metal chloride and respective lithium guanidinate salts. However, the reaction of $[ZrCl_2(NMe_2)_2(THF)_2]$ with diisopropylcarbodiimide also readily forms $[ZrCl_2\{\eta^2\text{-}(^{i}PrN)_2CNMe_2\}_2]$,[87] although with more sterically demanding ligands, this isn't generally a good route. Probably the least known route is proton transfer, an example of which was reported by Richeson *et al.*,[88] where $[Zr(CH_2Ph)_4]$

was treated with two equivalents of (^{i}PrHN)$_2$CN^{i}Pr, which gave [Zr(CH$_2$Ph)$_2${η^2-(^{i}PrN)$_2$CN(H)^{i}Pr}$_2$] (**1.14**) *via* the loss of two toluene molecules.

1.6.2.1.5. Cyclopentadienyl Ligands and Analogues

Although they do not contain nitrogen, cyclopentadienyl ligands, $C_5H_5^-$ or Cp^-, and alkyl-substituted derivatives may be promising spectator ligands for metal nitride precursors, as they stabilise the metal centre that they are bound to and potentially leave the precursors as an intact molecule in CVD or ALD apparatus. They are considered to be covalent when bound to transition metals and are versatile as they can bind to the metal centre in both a σ and π fashion (**Scheme 1.7**), and are generally formed by metathesis reactions of [ML$_n$Cl$_x$] and M'Cp (M' = Li, Na, K, Tl).

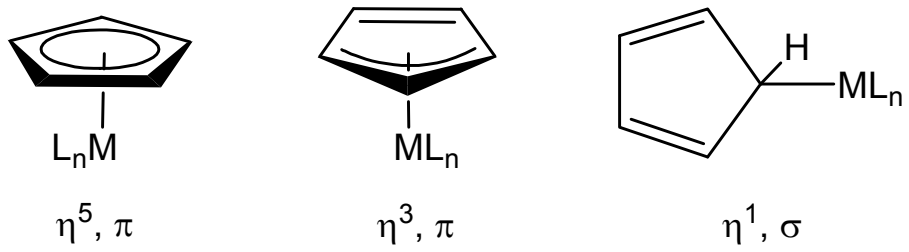

Scheme 1.7 Binding modes of cyclopentadienyl ligands.

The most common binding mode in organometallic chemistry is pentahapto, η^5,[67,75,89-96] where the ring sits over the metal such that all the carbon atoms are approximately equidistant from it, as in ferrocene.[97] It can be thought of as if each carbon were binding to the metal, hence the pentahapto label. This is described as π bonding as it is essentially the six electrons in the delocalised π system of the cyclopentadienyl that bind to three lobes of the metal *d* orbitals of the same symmetry, making η^5-Cp^- a 6-electron donor.

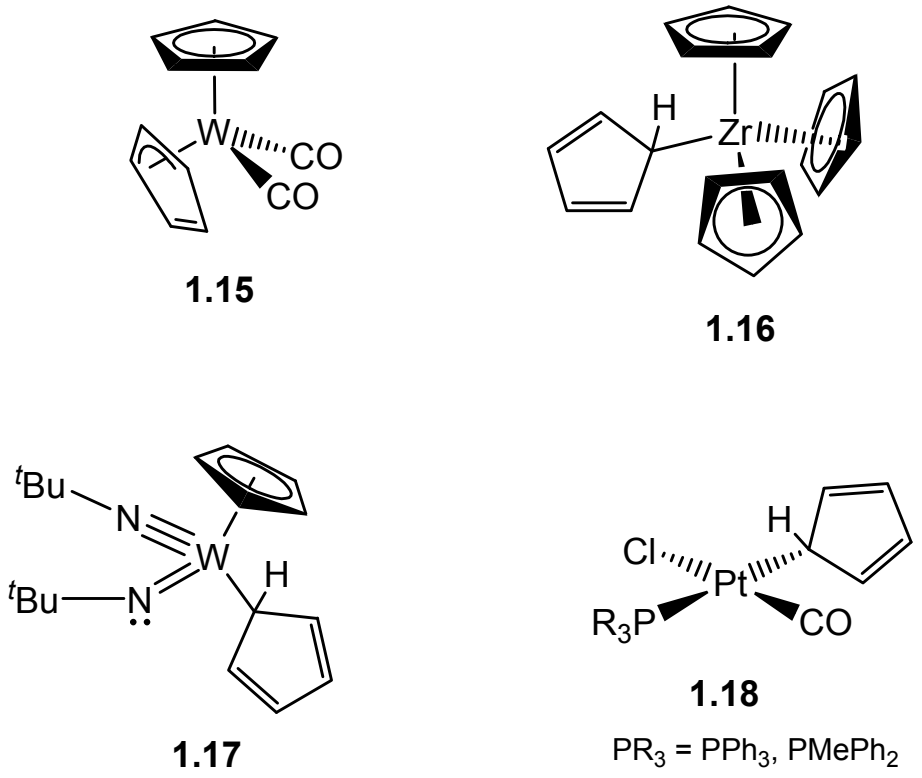

1.15 **1.16**

1.17 **1.18**

Figure 1.14 Selected examples of compounds containing cyclopentadienyl ligands.

Trihapto, η^3, binding can also occur if the metal centre is either saturated with π-electrons or the complex will exceed the 18 electron rule. In this case it can be considered similar to an η^3-allyl ligand and is a 4-electron donor, although this is not widely observed, the only example being $[W(CO)_2(\eta^5\text{-Cp})(\eta^3\text{-Cp})]$ (**1.15**, **Figure 1.14**) as reported by Huttner *et al.*[98] The monohapto form can also occur, in which the cyclopentadienyl ligand binds *via* a conventional σ bond. For example, in $[Zr(\eta^5\text{-Cp})_3(\eta^1\text{-Cp})]$ (**1.16**)[99] and $[W(N^tBu)_2(\eta^5\text{-Cp})(\eta^1\text{-Cp})]$ (**1.17**),[73] the metal centres are sterically crowded and saturated with π-electrons, whereas in $[Fe(CO)_2(\eta^5\text{-Cp})(\eta^1\text{-Cp})]$,[100] the monohapto configuration is required for the complex to obey the 18 electron rule, or, in the case of $[Pt(\eta^1\text{-Cp})(CO)Cl(PR_3)]$ (**1.18**, $PR_3 = PPh_3$, $PMePh_2$),[101] the 16 electron rule.

1.6.2.2. Examples of Tungsten-Based Precursors

There have been a number of attempts to deposit thin films of tungsten nitride using single-source precursors by CVD. However, to deposit tungsten nitride *via* ALD requires a co-reactant. This section gives a brief overview of attempts at tungsten nitride deposition.

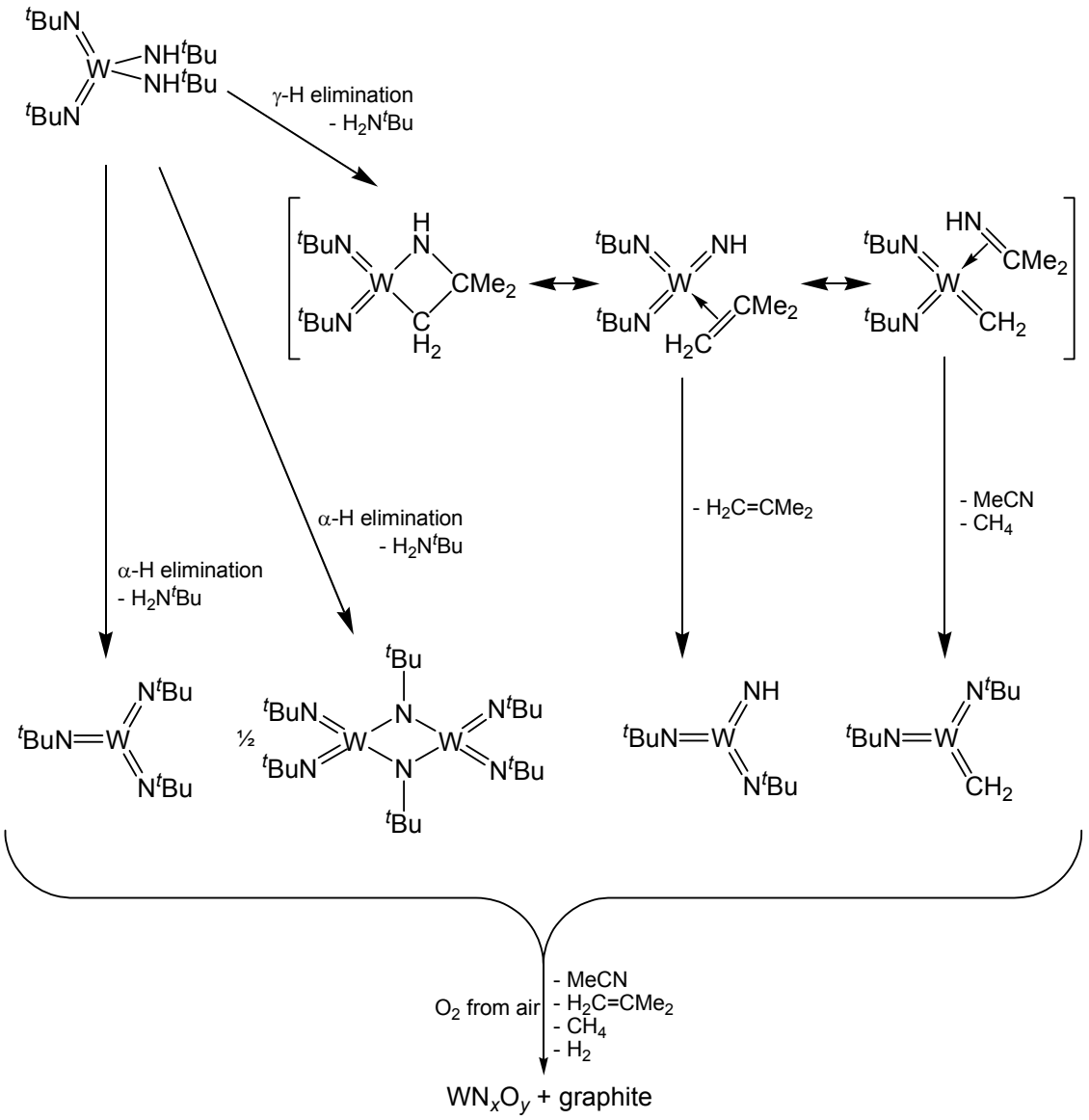

Scheme 1.8 Proposed decomposition pathway for $[W(N^tBu)_2(NH^tBu)_2]$, adapted from references.[102,103] Assignments of α- and γ- are with respect to the nitrogen atoms in the *tert*-butylimido ligand.

The compound $[W(N^tBu)_2(NH^tBu)_2]$, which was readily synthesised from the reaction of WCl_6 and excess H_2N^tBu,[71] was one of the most obvious candidates for CVD. Kinetic and mechanistic studies of $[W(N^tBu)_2(NH^tBu)_2]$ were undertaken to see how it might decompose in a CVD reactor (**Scheme 1.8**).[102,103] This was investigated using synchrotron X-ray spectroscopy. The suggested decomposition pathway comprised a series of possible hydride abstractions to from triimido or diimido-carbene tungsten(VI) intermediates, which would then decompose further to form tungsten nitride with graphite, the latter being a result of by-product decomposition. The product was calculated to have the composition $WN_{1.5}O_{0.1}$.

In comparison, $[W(N^tBu)_2(NH^tBu)_2]$ has been employed as a LPCVD precursor to tungsten nitride over the temperature range 500-600 °C.[104] The films were polycrystalline (face-centred cubic), contained low concentrations of carbon and showed excellent step coverage. It was noted that, at a deposition temperature of 500 °C, the film was nitrogen-rich, approximating to $WN_{1.8}$. However, at temperatures above 550 °C, the composition was a more uniform $WN_{0.7}$.

In contrast to the all-nitrogen coordination sphere of $[W(N^tBu)_2(NH^tBu)_2]$, McElwee-White *et al.* investigated derivatives of $[W(NR)Cl_4(R'CN)]$ as precursors to tungsten nitride thin films.[10,26,45,105-107] Initial studies were focussed on the potential of $[W(N^iPr)Cl_4(MeCN)]$ as a tungsten nitride precursor for AACVD. AACVD was necessary as the precursors of this form have low vapour pressures, making them unsuitable for solid-source delivery. $[W(N^iPr)Cl_4(MeCN)]$ was dissolved in benzonitrile, nebulised and passed through a cold-wall reactor *via* dihydrogen carrier gas.[10] The substrate was p-type boron-doped Si{100} and the WN_x films were deposited over a temperature range 450-700 °C. Below 500 °C, the films were amorphous and above 500 °C, they were polycrystalline, but the crystallinity increased with temperature. This suggested that films deposited below 500 °C are ideal as barrier layers in circuitry as copper can leach through the grain boundaries in polycrystalline materials. The W/N ratio ranged from 6-18 and increased with increasing temperature, although powder X-ray diffraction (XRD) patterns showed that β-W_2N was present, suggesting that there were localised areas of W_2N in a tungsten film. Other aspects of the film composition included carbon contamination, which increased with temperature and the absence of chlorine in the film, which was attributed to the presence of the

hydrogen in the carrier gas. Oxygen contamination occurred after deposition *via* absorption from the air and the oxygen levels were highest in the films deposited below 500 °C, indicating that the amorphous films must be porous (the opposite of what is required for a barrier layer).

An analogous study using [W(NPh)Cl_4(PhCN)] was carried out so as to compare it to the previous study.[26] The results were very similar, although the nitrogen and carbon content of films deposited from [W(NPh)Cl_4(PhCN)] was lower than those deposited from [W(N^{i}Pr)Cl_4(MeCN)], especially at higher temperatures. In order to reduce carbon contamination, AACVD using [W(N^{i}Pr)Cl_4(MeCN)] was repeated with 1,2-dichlorobenzene as the solvent rather than benzonitrile,[45] affording films with lower carbon concentrations than the initial study. This suggested that the decomposition of the solvent was a significant source of carbon, rather than the precursor. However, the W/N ratio was still too high for W_2N, so the affect of ammonia as a carrier gas was investigated.[105] Again, using [W(N^{i}Pr)Cl_4(MeCN)] as the precursor, AACVD was run with an ammonia concentration of 0.1%. It was noted that the nitrogen content of the films was higher (10-30 at.%) when ammonia was present in the carrier gas than ammonia was absent (2-10 at.%). Carbon levels were lower (10-40 at.% with ammonia, 10-48 at.% without), but not significantly so, and there was only a marked decrease in oxygen levels in films deposited below 500 °C (the amorphous films).

Although the addition of ammonia had a desirable outcome on the deposited films, a further comparative study was carried out without ammonia on [W(NC_3H_5)Cl_4(RCN)] (R = Me, Ph).[106] Again, films deposited below 500 °C were amorphous and above 500 °C, polycrystalline. No chlorine was detected in the films but there was carbon and oxygen contamination. Overall, films deposited at 450-600 °C from [W(NC_3H_5)Cl_4(RCN)] had a slightly higher carbon content (6-38 at.%) than those deposited from [W(N^{i}Pr)Cl_4(MeCN)] (13-48 at.%), which was far higher than films from [W(NPh)Cl_4(PhCN)] (4-20 at.%). The nitrogen content was similar to that of films from [W(N^{i}Pr)Cl_4(MeCN)], suggesting that the N–Ph bond strength is higher than N–^{i}Pr and N–C_3H_5, which accounts for the lower nitrogen content in films from [W(NPh)Cl_4(PhCN)]. Therefore, the compounds containing isopropyl- or allylimido groups are better precursors as less nitrogen deposition resulted in the films, due to their weaker R–N bond strength and the lability of the alkyl moiety. However, the group

considered [W(N^{i}Pr)Cl$_4$(MeCN)] to be preferable to [W(NC$_3$H$_5$)Cl$_4$(RCN)] as, at the lowest deposition temperature, deposition of [W(N^{i}Pr)Cl$_4$(MeCN)] affords a higher nitrogen content.

McElwee-White *et al.* described the synthesis of [W(NR)Cl$_3${η^2-(R'N)$_2$CNMe$_2$}] (**1.13**) and [W(NR)Cl$_3${η^2-(R'N)$_2$CMe}] (R = ^{i}Pr, Cy^{hex}, Ph; R' = ^{i}Pr, ^{t}Bu, SiMe$_3$) with a view to using these compounds as CVD precursors to tungsten carbonitride.[84] However, at the time of writing, the CVD of these guanidinate and amidinate complexes has not been reported. However, Fischer *et al.* have employed [W(N^{t}Bu)$_2$(R){η^2-(^{i}PrN)$_2$CNMe$_2$}] (R = NMe$_2$, H) in an LPCVD process with a dinitrogen bleed gas to deposit amorphous WN$_x$C$_y$ thin films onto Si{100}. The substrate temperatures ranged 500-800 °C, with film crystallinity increasing with temperature. Where ammonia was used as a co-reactant, the carbon contamination was significantly lower in films deposited from both precursors, and the crystalline grains increased in size.

Atomic layer deposition is becoming increasingly popular as a deposition method to metal nitride thin films, exemplified by Gordon *et al.*, who used [W(N^{t}Bu)$_2$(NMe$_2$)$_2$] as a precursor with excess ammonia, depositing onto various substrates, including silicon, glass, quartz, gold, stainless steel and copper.[23,38] The precursor was vaporised and carried through the ALD apparatus *via* dinitrogen gas. Ammonia was introduced into the system in each cycle, affording highly conformal, amorphous WN films 500 nm thick at notably low temperatures 250-350 °C. However, on annealing for 30 minutes at 725 °C and higher, the films were converted to polycrystalline tungsten metal. A more recent study by Gordon's group attempted to recreate the conditions in microcircuitry.[39] Again, ALD of [W(N^{t}Bu)$_2$(NMe$_2$)$_2$] and ammonia was employed to deposit WN on silica and UV-ozone-treated Si$_3$N$_4$ at 380 °C. Copper and cobalt were deposited on the resultant amorphous film, affording highly adhesive structures, five times more adhesive than current circuit interconnects.

Winter *et al.* investigated the potential of a similar compound, [W(N^{t}Bu)$_2$(η^2-^{t}Bu$_2$pz)$_2$] (^{t}Bu$_2$pz = 3,5-bis(*tert*-butyl)pyrazoyl) as an ALD precursor to test its suitability as a precursor to tungsten nitride.[72] In the presence of ammonia, films of tungsten carbonitride, W$_{1.0}$N$_{1.7}$C$_{1.5}$, were deposited over the temperature range 400-450 °C. The only possible source of carbon was the ligands, suggesting that pyrazolate

ligands may not be suitable for high purity WN films. However, more recently, Winter *et al.* have carried out ALD studies on $[W_2(NMe_2)_6]$ with ammonia at substrate temperatures 150-250 °C.[108] The benefit of $[W_2(NMe_2)_6]$, originally synthesised by Chisholm *et al.*,[66] is that the tungsten atoms are already in the +3 oxidation state, so no reduction is required to form stoichiometric WN. The films were not as nitrogen rich or carbon contaminated as those formed from $[W(N^tBu)_2(\eta^2\text{-}^tBu_2pz)_2]$, being of composition $WN_{0.74\text{-}0.82}C_{0.13\text{-}0.33}$, and they were amorphous. Annealing under nitrogen did not improve the crystallinity significantly. X-ray photoelectron spectroscopy (XPS) data showed the carbon to be carbidic as opposed to graphitic. There was some oxygen and hydrogen contamination, which was attributed to the air sensitive nature of the films. To overcome this, a 50 nm layer of aluminium nitride was deposited over the film, from trimethyl aluminium and ammonia, while it was still in the ALD reactor, which had the desired effect.

1.6.2.3. Examples of Zirconium-Based CVD Precursors

There are not many examples of precursors for the CVD of zirconium nitride as physical vapour deposition techniques, such as the cathodic arc technique,[109] are used. However, there have been some attempts, the first focussing on homoleptic amido compounds. APCVD of $[Zr(NEt_2)_4]$ and ammonia, onto a variety of substrates, was attempted in the presence of helium.[31,110] Over the temperature range 200-450 °C, crystalline, transparent films of Zr_3N_4 were deposited. These were insulating and had an optical band gap of approximately 2.2 eV. However, in order to obtain better step coverage and generally have more control over the uniformity of the films, ALD of $[Zr(NR_2)_4]$ (NR_2 = NMe_2, NEtMe, NEt_2) onto silicon, glass and quartz was studied.[111] It was found that the ammonia reacted most effectively with $[Zr(NMe_2)_4]$, as the resultant films contained significantly low levels of oxygen contamination. The films were amorphous as the substrate temperatures were low (150-250 °C), although not suitable as barrier layers as they were insulating.

There are some known examples of precursors which, at first glance, may seem ideal for the deposition of zirconium nitride as they possess an all-nitrogen coordination sphere. Examples include $[Zr\{\eta^2\text{-}N(Me)NMe_2\}_4]$, which was used to deposit amorphous $ZrO_{1.5\text{-}1.8}$ by LPCVD.[112] $[Zr(NEtMe)_2\{\eta^2\text{-}(^iPrN)_2CNEtMe\}_2]$ has also been

tested as a precursor to ZrO_2 over the temperature range 350-600 °C onto silicon substrates.[113] Both of these precursors afforded high-quality zirconium oxide with negligible nitrogen and carbon contamination. Therefore, it could be feasible that replacement of the oxygen co-reactant with ammonia could result in zirconium nitride thin films, although ALD might be preferable as the stoichiometry of the film could be more rigidly controlled.

1.6.3. Summary of Dual- and Single-Source Precursors

To summarise, the choice of precursor and technique affect the composition of the final film. The potential advantages of single-source over dual-source precursors are that they are generally less toxic and have a lower tendency to undergo gas-phase pre-reactions. This lower reactivity may indeed lead provide a route to materials that are difficult to grow using dual-source techniques. Owing to the pre-formed metal–non-metal bonds (for example, pre-formed W–N bonds in a precursor to WN), single-source precursors also potentially lower the temperature required for film growth as fewer bonds need to be broken. However, dual-source precursors are preferable to single-source when the reactant ratio needs to be tuned so as to obtain specific stoichiometries, whereas single-source precursors only offer fixed stoichiometries. Additionally, due to the presence of one or more metal centres, single-source precursors generally tend to exhibit lower vapour pressures.

1.7. Aims

The aims of this work are to synthesise a range of tungsten and zirconium complexes, which contain some nitrogen-based ligands. These compounds will then be investigated as precursors for the CVD and ALD of tungsten and zirconium nitride and carbonitride thin films.

1.8. References

1. T. Bredow, M. Lerch, *Z. Anorg. Allg. Chem.*, 2004, **630**, 2262-2266.
2. H. O. Pierson, *Handbook of Refractory Carbides and Nitrides. 2: The Refractory Carbides*. 1996: William Andrew Publishing. 8-16.

3. H. O. Pierson, *Handbook of Refractory Carbides and Nitrides. 3: Interstitial Carbides: Structure and Composition*. 1996: William Andrew Publishing. 17-54.
4. H. O. Pierson, *Handbook of Refractory Carbides and Nitrides. 9: The Refractory Nitrides*. 1996: William Andrew Publishing. 156-162.
5. H. O. Pierson, *Handbook of Refractory Carbides and Nitrides. 10: Interstitial Nitrides: Structure and Composition*. 1996: William Andrew Publishing. 163-180.
6. H. O. Pierson, *Handbook of Refractory Carbides and Nitrides. 4: Carbides of Group IV*. 1996: William Andrew Publishing. 55-80.
7. H. O. Pierson, *Handbook of Refractory Carbides and Nitrides. 11: Interstitial Nitrides: Properties and General Characteristics*. 1996: William Andrew Publishing. 181-208.
8. H. O. Pierson, *Handbook of Refractory Carbides and Nitrides. 6: The Carbides of Group VI*. 1996: William Andrew Publishing. 100-117.
9. H. Kim, *J. Vac. Sci. Technol. B*, 2003, **21**, 2231-2261.
10. L. McElwee-White, O. J. Bchir, S. W. Johnston, A. C. Cuadra, T. J. Anderson, C. G. Ortiz, B. C. Brooks, D. H. Powell, *J. Cryst. Growth*, 2003, **249**, 262-274.
11. K. Yong, B. H. Lee, *J. Electrochem. Soc.*, 2004, **151**, C594-C597.
12. M. Lerch, E. Füglein, J. Wrba, *Z. Anorg. Allg. Chem.*, 1996, **622**, 367-372.
13. C. H. Winter, *Aldrichimica Acta*, 2000, **33**, 3-12.
14. H. Volders, Z. Tökei, H. Bender, B. Brijs, R. Caluwaerts, L. Carbonell, T. Conard, C. Drijbrooms, A. Franquet, S. Garaud, I. Hoflijk, A. Moussa, F. Sinapi, Y. Travaly, D. Vanhaeren, G. Vereecke, C. Zhao, W.-M. Li, H. Sprey, A. M. Jonas, *Microelectron. Eng.*, 2007, **84**, 2460-2465.
15. M. Chhowalla, H. Emrah Unalan, *Nat. Mater.*, 2005, **4**, 317-322.
16. H. T. Chiu, S. H. Chuang, *J. Mater. Res.*, 1993, **8**, 1353-1360.
17. A. Zerr, G. Miehe, R. Riedel, *Nat. Mater.*, 2003, **2**, 185-189.
18. J. Lin, T. Suzuki, A. Tsukune, M. Yamada, *J. Vac. Sci. Technol. A*, 1999, **17**, 936-938.
19. J.-C. Parlebas, H. M. Benia, M. Guemmaz, A. Mosser, G. Schmerber, *Appl. Surf. Sci.*, 2002, **200**, 231-238.
20. P. J. Pokela, C. K. Kwok, E. Kolawa, S. Raud, M. A. Nicolet, *Appl. Surf. Sci.*, 1991, **53**, 364-372.

21. M. Yashima, K. Nakamura, *Mater. Sci. Eng., B*, 2008, **148**, 69-72.
22. N. Schönberg, *Acta Chem. Scand.*, 1954, 204-207.
23. R. G. Gordon, J. S. Becker, S. Suh, S. Wang, *Chem. Mater.*, 2003, **15**, 2969-2976.
24. K. Yvon, H. Nowotny, P. Benesovsky, *Monatsh. Chem.*, 1968, **99**, 726-729.
25. A. S. Kurlov, A. I. Gusev, *Inorg. Mater.*, 2006, **42**, 121-127.
26. L. McElwee-White, O. J. Bchir, K. M. Green, M. S. Hlad, T. J. Anderson, B. C. Brooks, C. B. Wilder, D. H. Powell, *J. Organomet. Chem.*, 2003, **684**, 338-350.
27. K.-B. Kim, S.-H. Kim, S. S. Oh, H.-M. Kim, D.-H. Kang, W.-M. Li, S. Haukka, M. Tuominen, *J. Electrochem. Soc.*, 2004, **151**, C272-C282.
28. A. N. Christensen, *Acta Chem. Scand. A*, 1975, **29**, 563-568.
29. A. L. Ivanovskii, N. I. Medvedeva, S. V. Okatov, *Inorg. Mater.*, 2001, **37**, 459-465.
30. P. Prieto, L. Galán, J. M. Sanz, *Phys. Rev. B*, 1993, **47**, 1613-1615.
31. R. G. Gordon, D. M. Hoffman, R. Fix, *Chem. Mater.*, 1991, **3**, 1138-1148.
32. H. O. Pierson, *Handbook of Refractory Carbides and Nitrides. 16: Applications of Refractory Carbides and Nitrides*. 1996: William Andrew Publishing. 309-326.
33. F. Liu, Y. Meng, Z. Ren, X. Shu, *Plasma Sci. Technol.*, 2008, **10**, 170-175.
34. H. O. Pierson, *Handbook of Chemical Vapour Deposition (CVD)*. 2nd ed. 1999: William Andrew Publishing.
35. B. Mishra, W. Grant, S. Niyomsoan, D. L. Olson, *Thin Solid Films*, 2002, **415**, 187-194.
36. M. O. Aboelfotoh, B. G. Svensson, *Semicond. Sci. Technol.*, 1991, **6**, 647-652.
37. S. J. Wang, S. C. Sun, H. Y. Tasi, *Thin Solid Films*, 2001, **394**, 180-188.
38. R. G. Gordon, J. S. Becker, *Appl. Phys. Lett.*, 2003, **82**, 2239-2241.
39. R. G. Gordon, D. B. Farmer, Z. Li, Y. Lin, J. Vlassak, *Electrochem. Solid-State Lett.*, 2005, **8**, G182-G185.
40. S. Berg, R. Buchta, H.-O. Blom, P. Norström, S. Nygren, M. Östling, C. S. Petersson, P. Wiklund, *J. Vac. Sci. Technol. A*, 1984, **2**, 281-283.
41. M. H. Tsai, S. C. Sun, C. P. Lee, H. T. Chiu, C. E. Tsai, S. H. Chuang, S. C. Wu, *Thin Solid Films*, 1995, **270**, 531-536.
42. S. C. Sun, H. Y. Tsai, S. J. Wang, *J. Electrochem. Soc.*, 2000, **147**, 2766-2772.
43. T. Oshani, M. Hirata, *Thin Solid Films*, 2003, **442**, 44-47.

44. I. P. Parkin, T. Manning, *Polyhedron*, 2004, **23**, 3087–3095.
45. L. McElwee-White, O. J. Bchir, K. M. Green, M. S. Hlad, T. J. Anderson, B. C. Brooks, *J. Cryst. Growth*, 2004, **261**, 280-288.
46. M. J. Crosbie, P. J. Wright, D. J. Williams, P. A. Lane, J. Jones, A. C. Jones, T. J. Leedham, P. O'Brien, H. O. Davies, *J. Phys. IV*, 1999, **9**, 935-942.
47. A. C. Jones, R. O'Kane, J. Gaskell, P. R. Chaulker, K. Black, M. Werner, P. Taechakumput, S. Taylor, P. N. Heys, R. Odedra, *Chem. Vap. Deposition*, 2007, **13**, 609-617.
48. W. M. M. Kessels, S. B. S. Heil, E. Langereis, M. C. M. van de Sanden, *J. Appl. Phys.*, 2006, **100**, 023534.
49. W. M. M. Kessels, H. C. M. Knoops, E. Langereis, A. J. M. Mackus, F. Roozeboom, M. C. M. van de Sanden, *J. Appl. Phys.*, 2007, **102**, 083517.
50. W. M. M. Kessels, R. Engeln, S. B. S. Heil, P. Kudlacek, E. Langereis, M. C. M. van de Sanden, *Appl. Phys. Lett.*, 2006, **89**, 131505.
51. H. Yanagi, S. Mashiko, T. Mikami, H. Tada, T. Terui, *J. Appl. Phys.*, 1997, **81**, 7306-7312.
52. J. Brücker, T. Mäntylä, *Surf. Coat. Technol.*, 1993, **59**, 166-170.
53. S. M. George, S. J. Ferro, J. W. Klaus, *Appl. Surf. Sci.*, 2000, **162-163**, 479-491.
54. S. M. George, S. J. Ferro, J. W. Klaus, *J. Electrochem. Soc.*, 2000, **147**, 1175-1181.
55. C. J. Carmalt, J. E. Bleau, A. C. Newport, S. A. O'Neill, I. P. Parkin, *J. Mater. Chem.*, 2004, **14**, 3333-3336.
56. B. H. Weiller, *J. Am. Chem. Soc.*, 1996, **118**, 4975-4983.
57. C. J. Carmalt, I. P. Parkin, E. S. Peters, *J. Mater. Chem.*, 2004, **14**, 3474–3477.
58. A. C. Jones, *Chem. Soc. Rev.*, 1997, 101-110.
59. P. O'Brien, N. L. Pickett, *The Chemical Record*, 2001, **1**, 467-479.
60. L. McElwee-White, *Dalton Trans.*, 2006, 5327-5333.
61. D. M. Hoffman, *Polyhedron*, 1994, **13**, 1169-1179.
62. W. L. Jolly, R. A. Andersen, D. B. Beach, *Inorg. Chem.*, 1985, **24**, 4741-4743.
63. M. F. Lappert, P. P. Power, A. R. Sanger, R. C. Srivastava, *Metal and Metalloid Amides: Syntheses, Structures, and Physical and Chemical Properties*. 1980: Ellis Horwood Ltd.

64. D. C. Bradley, I. M. Thomas, *J. Chem. Soc.*, 1960, **765**, 3857-3861.
65. M. H. Chisholm, D. C. Bradley, M. W. Extine, *Inorg. Chem.*, 1977, **16**, 1791-1794.
66. M. H. Chisholm, F. A. Cotton, M. W. Extine, B. R. Stults, *J. Am. Chem. Soc.*, 1976, **98**, 4477-4485.
67. M. S. Eisen, H. Mack, *J. Organomet. Chem.*, 1996, **525**, 81-87.
68. W. A. Nugent, J. M. Mayer, *Metal-Ligand Multiple Bonds*. 1988: John Wiley & Sons, Inc.
69. W. A. Nugent, B. L. Haymore, *Coord. Chem. Rev.*, 1980, **31**, 123-175.
70. D. B. Bradley, M. B. Hursthouse, R. J. Errington, A. J. Nielson, R. L. Short, *Polyhedron*, 1983, **2**, 843-847.
71. W. A. Nugent, R. L. Harlow, *Inorg. Chem.*, 1980, **19**, 777-779.
72. C. H. Winter, O. M. El-Kadri, M. J. Heeg, *Dalton Trans.*, 2006, **16**, 1943-1953.
73. J. Sundermeyer, K. Peters, U. Radius, H.-G. von Schnering, *Eur. J. Inorg. Chem.*, 2001, 1617-1623.
74. A. K. Hughes, A. S. Batsanov, A. E. Goeta, J. A. K. Howard, A. L. Johnson, K. Wade, *J. Chem. Soc., Dalton Trans.*, 2001, 1210-1217.
75. P. Mountford, S. C. Dunn, D. A. Robson, *J. Chem. Soc., Dalton Trans.*, 1997, 293-304.
76. A. J. Nielson, *Polyhedron*, 1987, **6**, 1657-1667.
77. D. M. Hoffman, J.-S. M. Lehn, *Inorg. Chim. Acta*, 2003, **345**, 327-332.
78. J. Sundermeyer, D. Gaess, K. Harms, M. Pokoj, W. Stolz, *Inorg. Chem.*, 2007, **46**, 6688-6701.
79. R. A. Fischer, A. Baunemann, Y. Kim, M. Winter, *Dalton Trans.*, 2006, 121-128.
80. T. A. George, J. R. D. Debord, J. D. Niemoth-Anderson, C. R. Ross, II, J. J. Stezowski, *Polyhedron*, 1996, **15**, 4031-4040.
81. P. Mountford, A. R. Cowley, J. C. Green, N. Hazari, T. B. Parsons, *Inorg. Chem.*, 2005, **44**, 8442-8458.
82. P. J. Bailey, S. Pace, *Coord. Chem. Rev.*, 2001, **214**, 91-141.
83. P. J. Bailey, K. J. Grant, L. A. Mitchell, S. Pace, A. Parkin, S. Parsons, *J. Chem. Soc., Dalton Trans.*, 2000, 1887-1891.

84. L. McElwee-White, K. A. Abboud, L. L. Reitfort, C. B. Wilder, *Inorg. Chem.*, 2006, **45**, 263-268.
85. Q. Shen, X.-A. Pang, H.-T. Sheng, J.-F. Wang, Y.-M. Yoa, Y. Zhang, *Chin. J. Chem.*, 2005, **23**, 1193-1197.
86. D. S. Richeson, D. Wood, G. P. A. Yap, *Inorg. Chem.*, 1999, **38**, 5788-5794.
87. R. G. Bergman, J. Arnold, A. P. Duncan, S. M. Mullins, *Organometallics*, 2001, **20**, 1808-1819.
88. D. S. Richeson, P. Bazinet, D. Wood, G. P. A. Yap, *Inorg. Chem.*, 2003, **42**, 6225-6229.
89. S. R. Stobart, A. Bonny, A. D. McMaster, *Inorg. Chem.*, 1978, **17**, 935-938.
90. M. L. H. Green, J. A. McCleverty, L. Pratt, G. Wilkinson, *J. Chem. Soc.*, 1961, 4854-4859.
91. R. R. Schrock, T. E. Glassman, M. G. Vale, *J. Am. Chem. Soc.*, 1992, **114**, 8098-8109.
92. C. H. Brubaker, Jr., B.-H. Chang, H.-S. Tung, *Inorg. Chim. Acta*, 1981, **51**, 143-148.
93. M. Gómez, A. Castro, M. V. Galakhov, F. Sánchez, *J. Organomet. Chem.*, 1999, **580**, 161-168.
94. B. S. Garg, V. K. Jain, V. Kumar, *Inorg. Chim. Acta*, 1978, **26**, 197-200.
95. J. H. Teuben, A. K. Hughes, A. Meetsma, *Organometallics*, 1993, **12**, 1936-1945.
96. T. Cuenca, G. Ciruelo, R. Gómez, P. Gómez-Sal, A. Martín, *J. Chem. Soc., Dalton Trans.*, 2001, 1657-1663.
97. G. Wilkinson, M. Rosenblum, M. C. Whiting, R. B. Woodward, *J. Am. Chem. Soc.*, 1952, **74**, 2125-2126.
98. G. Huttner, V. Bejenke, L. G. Bell, H. H. Brintzinger, P. Friedrich, D. Neugebauer, *J. Organomet. Chem.*, 1978, **145**, 329-333.
99. J. L. Atwood, R. D. Rogers, R. Vann Bynum, *J. Am. Chem. Soc.*, 1978, **100**, 5238-5239.
100. J. A. Labinger, *J. Organomet. Chem.*, 1977, **136**, C31-C36.
101. R. J. Cross, L. J. Farrugia, K. E. A. Kuma, *J. Organomet. Chem.*, 1994, **471**, 273-276.
102. R. G. Nuzzo, H.-T. Chiu, E. L. Crane, *J. Phys. Chem. B*, 2001, **105**, 3549-3556.

103. Y.-W. Yang, H.-T. Chiu, Y.-F. Lin, J. Wang, J.-B. Wu, *Surface Science*, 2006, **600**, 743-754.
104. M. H. Tsai, H. T. Chiu, S. H. Chuang, S. C. Sun, *Appl. Phys. Lett.*, 1996, **68**, 1412-1414.
105. L. McElwee-White, O. J. Bchir, K. C. Kim, T. J. Anderson, V. Craciun, B. C. Brooks, *J. Electrochem. Soc.*, 2004, **151**, G697-G703.
106. L. McElwee-White, O. J. Bchir, K. M. Green, H. M. Ajmera, E. A. Zapp, T. J. Anderson, B. C. Brooks, L. L. Reitfort, D. H. Powell, K. A. Abboud, *J. Am. Chem. Soc.*, 2005, **127**, 7825-7833.
107. L. McElwee-White, T. J. Anderson, I. Ghiviriga, Y. S. Kim, L. L. Reitfort, Y. S. Won, *J. Am. Chem. Soc.*, 2006, **128**, 13781-13788.
108. C. H. Winter, C. L. Dezelah IV, O. M. El-Kadri, K. Kukli, K. Arstila, R. J. Baird, J. Lu, L. Niinstö, *J. Mater. Chem.*, 2007, **17**, 1109-1116.
109. A. Devia, Y. C. Arango, D. F. Arias, *Appl. Surf. Sci.*, 2006, **253**, 1683-1690.
110. D. M. Hoffman, R. G. Gordon, R. M. Fix, *J. Am. Chem. Soc.*, 1990, **112**, 7833-7835.
111. R. G. Gordon, J. S. Becker, E. Kim, *Chem. Mater.*, 2004, **16**, 3497-3501.
112. D. M. Hoffman, S. Javed, J.-S. M. Lehn, *Chem. Vap. Deposition*, 2006, **12**, 280-284.
113. R. Fischer, A. Devi, R. Bhakta, A. Milanov, M. Hellwig, D. Barreca, E. Tondello, R. Thomas, P. Ehrhart, M. Winter, *Dalton Trans.*, 2007, 1671-1676.

2

Synthesis of Tungsten Carbonitride Precursors

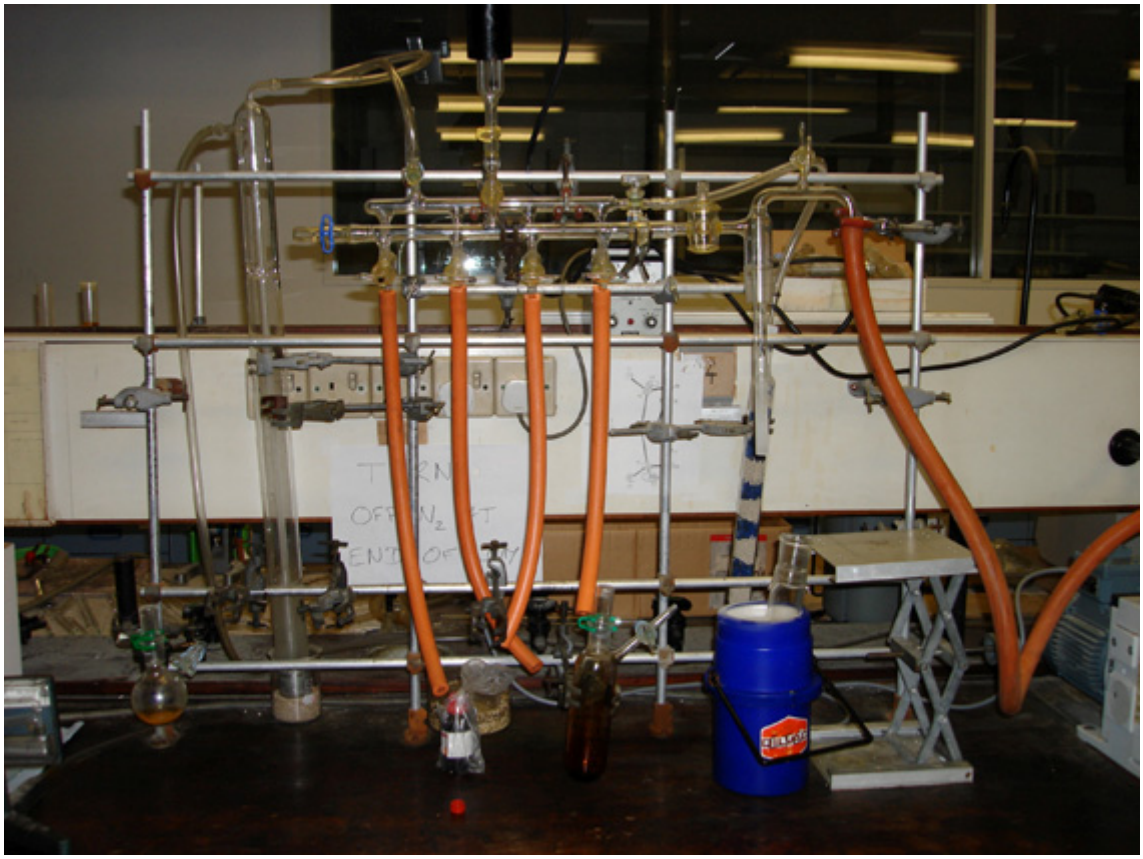

Figure 2.0 Schlenk apparatus with vacuum and nitrogen lines.

2.1. Introduction

This chapter describes the synthesis of a selection of tungsten imido compounds, including $[W(\mu\text{-}N^tBu)(N^tBu)Cl_2(H_2N^tBu)]_2$ (**2.1**), $[W(N^tBu)_2Cl_2(TMEDA)]$ (**2.2**, TMEDA = *N*,*N*,*N'*,*N'*-tetramethylethylenediamine), $[W(N^tBu)_2Cl_2(py)_2]$ (**2.3**, py = pyridine), $[W(N^tBu)_2Cl\{N(SiMe_3)_2\}]$ (**2.4**), $[W(N^tBu)_2Cl\{N(H)NMe_2\}]$ (**2.5**) and $[W(N^tBu)_2(\eta^5\text{-}Cp')(\eta^1\text{-}Cp')]$ (**2.6**, Cp' = methylcyclopentadienyl), which are potential LPCVD and AACVD precursors. Although some of the compounds have been described previously,[1-3] generally as intermediates in a reaction sequence, their thermal properties have not been investigated, nor have they been used as precursors for the chemical vapour deposition of tungsten carbonitride.

2.2. Experimental

2.2.1. General Procedures

All reactions were performed under a dry, oxygen-free nitrogen atmosphere using standard Schlenk techniques and an Mbraun Unilab glove box. Nitrogen (99.99%) was obtained from BOC and used as supplied. All solvents were stored in alumina columns and dried with anhydrous engineering equipment, such that the water concentration was 5-10 ppm. All reagents were procured from Sigma Aldrich, except for WCl_6, which was purchased from Strem. Amines were degassed and stored over 3 Å molecular sieves under nitrogen. All other compounds were used without further purification.

2.2.2. Physical Measurements

Microanalytical data were obtained at University College London (UCL). NMR spectra were recorded on Bruker AMX400, AMX500 or ADVANCE III 600 spectrometers, referenced to C_6D_6 distilled over benzophenone or dried and degassed $CDCl_3$. ^1H and $^{13}C\{^1H\}$ chemical shifts are reported relative to $SiMe_4$ (δ = 0.00 ppm). FT-IR spectra were recorded on a Perkin Elmer Spectrum RX I instrument, over the range 4000-400 cm^{-1}. Mass spectra were recorded on a Micromass ZABSE instrument. Thermogravimetric analysis (TGA) was performed

on a Netzsh STA 449C instrument. The TGA was carried out in aluminium pans at atmospheric pressure, under a flow of helium gas. The rate of heating was 10 °C min^{-1}. Vapour pressure measurements were carried out at SAFC Hitech Ltd. on custom-built apparatus.

2.2.3. Synthesis of Starting Materials

2.2.3.1. Synthesis of [Li{N(H)NMe$_2$}]

^{n}BuLi (41.5 cm^3, 1.6 M in hexane, 66.40 mmol) was added dropwise to a stirred colourless solution of H_2NNMe_2 (5.1 cm^3, 4.03 g, 67.12 mmol) in hexane (120 cm^3), which was cooled to -78 °C. The colourless solution was stirred for 18 h, after which time the hexane and excess H_2NNMe_2 was removed under vacuum, giving a white powder (yield = 4.44 g, 94%). **Anal. Calc.** for $C_2H_7N_2Li$: C, 36.38; H, 10.69; N, 42.42%. **Found:** C, 36.51; H, 10.93; N, 41.29%. **^{1}H NMR** δ/ppm (C_6D_6, 600 MHz): 1.21 (s, 1H, N(*H*)NMe_2), 2.48 (s, 6H, N(CH_3)$_2$). **^{13}C{^{1}H} NMR** δ/ppm (C_6D_6, 600 MHz): 56.4 (N(CH_3)$_2$). **FT-IR** and **mass spectrometry** data are not available due to the highly air-sensitive nature of this compound.

2.2.3.2. Synthesis of [NaCp'(THF)]

A solution of freshly cracked methylcyclopentadiene (42.0 cm^3, 33.39 g, 0.42 mol) in THF (50 cm^3) was added dropwise to a stirred white suspension of sodium hydride (10.00 g, 0.42 mol) in THF (500 cm^3). Once the addition was complete the solution was stirred until no more hydrogen evolved. The turbid pink solution was allowed to settle overnight and was then filtered. The maroon filtrate was reduced to dryness under vacuum and the resulting pink solid was washed with a minimum amount of hexane (*ca.* 10 cm^3) and dried under vacuum giving a beige solid (yield = 50.05 g, 68%). **Anal. Calc.** for C_6H_7Na: C, 70.58; H, 6.91%. **Calc.** for $C_{10}H_{15}ONa$: C, 68.94; H, 8.68%. **Found** ($C_{10}H_{15}ONa$): C, 68.31; H, 8.25%. **^{1}H NMR** δ/ppm (C_6D_6, 400 MHz): 1.29 (br s, 4H, CH_2CH_2O (THF)), 2.26 (s, 3H, $C_5H_4(CH_3)$), 3.34 (br s, 4H, CH_2CH_2O (THF)), 5.57 (s, 4H, C_5H_4Me). **^{13}C{^{1}H} NMR** δ/ppm (C_6D_6, 400 MHz): 14.7 ($C_5H_4(CH_3)$), 25.5 (CH_2CH_2O (THF)), 67.8 (CH_2CH_2O (THF)), 102.1 (3-C_5H_4Me), 103.7 (2-C_5H_4Me),

114.7 (1-C_5H_4Me). **FT-IR** and **mass spectrometry** data are not available due to the highly air-sensitive nature of this compound.

2.2.4. Precursor Synthesis

2.2.4.1. Synthesis of $[W(\mu\text{-}N^tBu)(N^tBu)Cl_2(H_2N^tBu)]_2$ (2.1)

A solution of $HN^tBu(SiMe_3)$ (29.0 cm^3, 0.15 mol) in toluene (33.0 cm^3) was added dropwise to a purple suspension of WCl_6 (15.00 g, 37.82 mmol) in toluene (150 cm^3) over a period of approximately 5 minutes. The suspension was stirred for 18 h, after which time the colour was maroon. The suspension was filtered through celite and the amber filtrate was reduced to dryness under vacuum, leaving a sticky brown solid. Hexane (*ca.* 25 cm^3) was added with stirring and the resulting suspension was cooled to -20 °C for 18 h. The dark brown supernatant solution was removed by filtration and the yellow residue was rinsed with 3 × 10 cm^3 portions of hexane. The product was dried under vacuum, affording a green-yellow powder (yield = 9.51 g, 53%). **Anal. Calc.** for $C_{12}H_{29}N_3Cl_2W$: C, 30.66; H, 6.22; N, 8.94%. **Found:** C, 30.81; H, 6.34; N, 8.51%. **^{1}H NMR** δ/ppm (500 MHz, C_6D_6): 1.11 (s, 18H, $H_2NC(CH_3)_3$), 1.45 (s, 36H, $NC(CH_3)_3$), 2.65 (s, br, 2H, NH_2 (H-bound)), 4.78 (s, br, 2H, NH_2). **^{13}C{^{1}H} NMR** δ/ppm (500 MHz, C_6D_6): 31.0 ($H_2NC(CH_3)_3$), 31.5 ($=NC(CH_3)_3$), 52.5 (H_2NCMe_3), 68.3 ($=NCMe_3$). **FT-IR** cm^{-1} (KBr disc, nujol): 3294 w (N–H stretch), 3177 w (N–H stretch), 3100, w (N–H stretch), 2924 vs (C–H stretch), 2854 s (C–H stretch), 1564 m (N–H bend), 1460 br m (C–CH_3 bend), 1403 w, 1379 m (C–CH_3 bend), 1357 sh w, 1262 br m, 1238 br m, 1209 br m, 1180 br m, 1096 vbr m, 1023 br m, 892 w, 803 m, 750 w, 605 w, 478 w. **Mass Spec.** *m/z* (CI+, methane): 71 $[^tBuN]H^+$, 88, 104, 128, 145, 149, 186, 229, 254 $[WCl_2]H^+$, 341, 381 $[W(N^tBu)Cl_2(NCMe_2)]H^+$, 471 $[W(N^tBu)_2Cl_2(H_2N^tBu)]H^+$, 484 $[W(N^tBu)_2(N)Cl_2(H_2N^tBu)]H^+$, 509 $[W(N^tBu)_2Cl_2(H_3N^tBuCl)]H^+$, 667, 722 $[W_2(\mu\text{-}N^tBu)_2Cl_4(N^tBu)]H^+$, 789, 848, 940 $[M]H^+$. **TGA:** mass loss 63% (calc. WN, 58%; W_2N, 59%) at 590 °C.

2.2.4.2. Synthesis of $[W(N^tBu)_2Cl_2(TMEDA)]$ (2.2)

$[W(\mu\text{-}N^tBu)(N^tBu)Cl_2(H_2N^tBu)]_2$ (4.00 g, 4.25 mmol) was suspended in diethyl

ether (100 cm^3) and stirred until all the solid had dissolved. TMEDA (3.5 cm^3, 2.71 g, 23.34 mmol) was added to the stirred amber solution. The solution was stirred for 18 h, by which time the colour had turned pale green. The solution was filtered and the solvent and excess TMEDA were removed under vacuum, giving a pale green sticky solid (yield = 3.89 g, 89%). **Anal. Calc.** for $C_{14}H_{34}N_4Cl_2W$: C, 32.77; H, 6.68; N, 10.92%. **Found:** C, 33.03; H, 6.85; N, 10.78%. **^{1}H NMR** δ/ppm (500 MHz, C_6D_6): 1.45 (s, 18H, NC(CH_3)$_3$), 2.06 (s, 4H, CH_2N(CH_3)$_2$), 2.60 (s, 12H, CH_2N(CH_3)$_2$). **^{13}C{^{1}H} NMR** δ/ppm (500 MHz, C_6D_6): 31.7 (=NC(CH_3)$_3$), 51.0 (CH_2N(CH_3)$_2$), 57.4 (CH_2N(CH_3)$_2$), 67.5 (=NCMe$_3$). **FT-IR** cm^{-1} (KBr disc, nujol): 2924 s (C–H stretch), 2854 s (C–H stretch), 1465 br m (C–CH_3 bend), 1456 br m (C–CH_3 bend), 1379 m (C–CH_3 bend), 1356 m, 1209 br m, 1150 w, 1140 br w, 1118 w, 1103 w, 1067 w, 1018 br m, 954 m, 926 w, 799 br m, 774 sh w, 666 w, 591 br w, 477 w, 428 sh s, 422 vs, 416 vs, 410 sh s. **Mass Spec.** *m/z* (CI+, methane): 58 [^{t}Bu]H$^+$, 72 [^{t}BuN]H$^+$, 115 [TMEDA - 2 H]H$^+$, 116 [TMEDA - H]H$^+$, 117 [TMEDA]H$^+$, 118, 174, 235, 499 [M - Me]H$^+$. **TGA:** mass loss 51% (calc. WN, 61%; W_2N, 63%) at 590 °C.

2.2.4.3. Synthesis of [W(N^{t}Bu)$_2$Cl$_2$(py)$_2$] (2.3)

[W(μ-N^{t}Bu)(N^{t}Bu)Cl$_2$(H$_2$N^{t}Bu)]$_2$ (3.00 g, 3.19 mmol) was suspended in diethyl ether (100 cm^3) and stirred until all the solid had dissolved. Pyridine (1.6 cm^3, 1.56 g, 19.78 mmol) was added to the stirred amber solution. The solution was stirred for 18 h, by which time the colour had turned dark green. The solution was filtered and the solvent was removed under vacuum, giving a dark green sticky solid (yield = 3.47 g, 98%). **Anal. Calc.** for $C_{18}H_{28}N_4Cl_2W$: C, 38.94; H, 5.08; N, 10.09%. Found: C, 38.21; H, 5.17; N, 10.97%. **^{1}H NMR** δ/ppm (500 MHz, C_6D_6): 1.53 (s, 18H, NC(CH_3)$_3$), 6.52 (m, 4H, *m*-py), 6.86 (m, 2H, *p*-py), 9.11 (m, 4H, *o*-py). **^{13}C{^{1}H} NMR** δ/ppm (500 MHz, C_6D_6): 31.5 (=NC(CH_3)$_3$), 67.9 (=NCMe$_3$), 123.4 (*m*-py), 137.1 (*p*-py), 152.2 (*o*-py). **FT-IR** cm^{-1} (KBr disc, nujol): 2924 vs (C–H stretch), 2854 s (C–H stretch), 1638 vw, 1604 m, 1488 m, 1447 m (C–CH_3 bend), 1378 w (C–CH_3 bend), 1355 m, 1286 m, 1247 m, 1222 m, 1154 w, 1072 m, 1040 m, 1008 m, 801 w, 763 m, 703 m, 666 vw, 628 w, 598 vw, 478 sh m, 433 vs, 420 vs, 410 vs.

Mass Spec. *m/z* (CI+, methane): 80 $[py]H^+$, 88, 159, 186, 287, 324, 339, 397 $[W(N^tBu)_2Cl_2]H^+$, 460, x, 541 $[M - Me]H^+$, 725, 740. **TGA:** mass loss 67% (calc. WN, 64%; W_2N, 66%) at 590 °C.

2.2.4.4. Synthesis of $[W(N^tBu)_2Cl\{N(SiMe_3)_2\}]$ (2.4)

A Schlenk flask was charged with $[W(N^tBu)_2Cl_2(py)_2]$ (2.00 g, 3.60 mmol) and $NaN(SiMe_3)_2$ (0.67 g, 3.65 mmol). Cooled THF (80 cm^3, -78 °C) was added to the solids with stirring. The pale yellow suspension was allowed to warm to room temperature and was subsequently heated under reflux for 18 h with stirring. After the solution had cooled to room temperature, the THF was removed under vacuum and the brown semi-solid was suspended in hexane (*ca.* 40 cm^3). The NaCl was allowed to settle before the pale orange solution was filtered. The filtrate was reduced to dryness under vacuum, giving a dark orange oil (yield = 0.56 g, 29%). **^{1}H NMR** δ/ppm (500 MHz, C_6D_6): 0.39 (s, 18H, $N\{Si(CH_3)_3\}_2$), 1.36 (s, 18H, $NC(CH_3)_3$). **$^{13}C\{^1H\}$** NMR δ/ppm (500 MHz, C_6D_6): 5.4 ($N\{Si(CH_3)_3\}_2$), 33.0 ($NC(CH_3)_3$), 67.9 ($NC(CH_3)_3$). **FT-IR** cm^{-1} (KBr disc, neat): 3173 vw (N–H stretch), 2971 vs (C–H stretch), 2925 s (C–H stretch), 2899 s (C–H stretch), 2107 m, 1610 w, 1473 sh w, 1452 br m ($C–CH_3$ bend), 1386 w, 1358 s ($C–CH_3$ bend), 1249 vs, 1233 vs, 124 vs, 1144 m, 1099 br m, 1025 br, m, 949 br, m, 865 vbr s, 803 sh s, 722 m, 675 m, 620 w, 584 w, 554 w, 630 w, 472 w, 436 sh m, 428 s, 424 s, 420 s, 416 s, 404 sh m. **Mass Spec.** *m/z* (CI+, methane): 109 $[Me_3SiCl]H^+$, 146 $[HN(SiMe_3)(SiMe_2)]H^+$, 162 $[HN(SiMe_3)_2]H^+$, 306 $[W(N^tBu)NCl]H^+$, 327 $[W(N^tBu)_2]H^+$, 341, 362 $[W(N^tBu)_2Cl]H^+$, 378 $[W(N^tBu)N_2Cl]H^+$, 397, 419 $[M - SiMe_3 - 2\ Me]H^+$, 434 $[M - SiMe_3 - Me]H^+$, 448 $[M - 5\ Me]H^+$ or $[M - SiMe_3]H^+$, 463 $[M - 4\ Me]H^+$, 478 $[M - 3\ Me]H^+$, 486 $[M - Cl]H^+$, 493 $[M - 2\ Me]H^+$, 508 $[M - Me]H^+$, 522 $[M]H^+$, 562. Theoretical mass $[M]H^+$ = 522.17239, measured mass $[M]H^+$ = 522.17384 (error, 2.78 ppm). **TGA:** mass loss 74% (calc. WN, 62%; W_2N, 63%) at 590 °C.

2.2.4.5. Attempted Synthesis of $[W(N^tBu)_2Cl\{N(H)NMe_2\}]$ (2.5)

A colourless solution of $Li(H)NNMe_2$ (0.30 g, 4.50 mmol) in diethyl ether (50 cm^3) was added dropwise to a cooled (-78 °C) solution of $[W(N^tBu)_2Cl_2(py)_2]$ (2.50 g, 4.50 mmol) in diethyl ether (100 cm^3) with stirring. The green solution was allowed to warm

to room temperature and was stirred for 18 h. After this time, the solution was removed under vacuum and the orange-brown solid was dissolved in hexane (150 cm^3). The LiCl was allowed to settle and the dark orange solution was filtered. The filtrate was reduced to dryness under vacuum affording a dark orange solid (yield = 1.02 g, 54%). Attempted sublimation at 130 °C, 5 × 10^{-2} Torr, only served to remove residual pyridine. **Anal. Calc.** for $C_{10}H_{25}N_4ClW$: C, 28.55; H, 5.99; N, 13.32%. Found: C, 28.50; H, 5.68; N, 12.16%. **^{1}H NMR** δ/ppm (500 MHz, C_6D_6): 1.50 (v br). **^{13}C{^{1}H} NMR** δ/ppm (500 MHz, C_6D_6): 33.0 (br). **FT-IR** cm^{-1} (KBr disc, nujol): 2923 vs (C–H stretch), 2854 s (C–H stretch), 1606 w, 1456 m, 1356 m, 1261 m, 1215 m, 1095 w, 1021 w, 861 vw, 803 m, 698 vw, 667 vw, 430 s, 423 vs, 407 m. **Mass Spec.** *m/z* (CI+, methane): 109, 121, 137, 139, 152, 164, 178, 191, 205, 224, 261, 279, 287, 329, 352, 391, 400, 410 $[M - Me]H^+$, 419 $[M - H]H^+$, 420 $[M]H^+$, 432 $[M + Cl]H^+$, 464, 480, 492, 508, 534, 550, 564, 607.

2.2.4.6. Synthesis of [W(N^{t}Bu)$_2$(η^5-Cp')(η^1-Cp')] (2.6)

A pink solution of [NaCp'(THF)] (1.98 g, 11.35 mmol) in THF (60 cm^3) was added slowly to a cooled (-78 °C) solution of $[W(N^tBu)_2Cl_2(py)_2]$ (3.00 g, 5.40 mmol) in diethyl ether (60 cm^3) with stirring. The brown solution was allowed to warm to room temperature and was then heated under reflux for 1 h. The solution was allowed to stir at room temperature for a further 18 h. The solvents were removed under vacuum and the brown oily solid was dissolved in hexane (120 cm^3). Once the NaCl had settled, the pale yellow solution was filtered and the filtrate reduced to dryness under vacuum, giving a dark yellow oil (yield = 1.39 g, 53%). **^{1}H NMR** δ/ppm (400 MHz, $CDCl_3$, +50 °C): 1.34 (s, 36H, NC(CH_3)$_3$), 2.22 (s, 12H, $C_5H_4(CH_3)$), 5.51 (s, v br, 16H, 2,3-C_5H_4Me); (+20 °C): 1.33 (s, 36H, NC(CH_3)$_3$), 2.17 (s, br, 6H, η^5-$C_5H_4(CH_3)$), 2.26 (s, br, 6H, η^1-$C_5H_4(CH_3)$), 5.41 (m, 8H, η^5-2,3-C_5H_4Me) 6.26 (s, v br, 8H, η^1-2,3-C_5H_4Me); (-50 °C) 1.36 (d, $^3J_{HH}$ = 1.20 Hz, 9H, ≡NC(CH_3)$_3$), 1.37 (d, $^3J_{HH}$ = 1.20 Hz, 9H, ≡NC(CH_3)$_3$), 1.40 (d, $^3J_{HH}$ = 1.20 Hz, 9H, =NC(CH_3)$_3$), 1.42 (d, $^3J_{HH}$ = 1.20 Hz, 9H, =NC(CH_3)$_3$), 2.21 (s, 3H, η^5-$C_5H_4(CH_3)$), 2.24 (s, 3H, η^5-$C_5H_4(CH_3)$), 2.28 (s, 3H, η^1-3-$C_5H_4(CH_3)$), 2.38 (s, 3H, η^1-2-$C_5H_4(CH_3)$), 4.40 (s, 1H, η^1-3-C_5H_4Me, WC*H*CHCMe), 4.48 (s, 1H, η^1-2-C_5H_4Me, WC*H*CMe), 5.34 (s, 1H, η^5-C_5H_4Me), 5.37 (s, 1H, η^5-C_5H_4Me), 5.46 (s, 2H, η^5-C_5H_4Me), 5.50 (s, 1H, η^5-C_5H_4Me), 5.55 (s, 3H,

η^5-C_5H_4Me), 6.33 (m, 2H, η^1-C_5H_4Me), 6.37 (m, 2H, η^1-C_5H_4Me), 6.54 (m, 1H, η^1-C_5H_4Me), 6.73 (s, br, 1H, η^1-C_5H_4Me). Please see section 2.3.2 for more detailed peak assignments. **$^{13}C\{^1H\}$** NMR δ/ppm (400 MHz, $CDCl_3$, +20 °C): 15.3 ($C_5H_4(CH_3)$), 32.2 ($NC(CH_3)_3$), 66.5 ($NCMe_3$), 106.2 (br, 2,3-C_5H_4Me), 119.6 (1-C_5H_4Me). **FT-IR** cm^{-1} (KBr disc, neat): 3085 m (aromatic C–H stretch), 3053 m (aromatic C–H stretch), 2965 vs (C–H stretch), 2921 vs (C–H strectch), 2860 s (C–H stretch), 2728 vw, 2565 vw, 1613 br vw (C=C stretch), 1578 w, 1500 sh m, 1453 s (CH_3 bend), 1376 m (CH_3 bend), 1354 s, 1284 vs, 1242 vs, 1212 s, 1137 sh m, 1097 m, 1024 s, 985 sh m, 967 sh w, 936 vw, 872 br s, 797 vs, 723 s, 622 vw, 593 m, 573 w, 543 w, 471 m, 420 s, 408 s. **Mass Spec.** *m/z* (CI+, methane): 81 $[Cp'H]H^+$, 333 [M - Cp' - ^{t}Bu - Me]H^+, 349 [M - Cp' - ^{t}Bu]H^+, 390 [M - Cp' - Me]H^+, 405 [M - Cp']H^+, 427 [M - ^{t}Bu]H^+, 469 [M - Me]H^+, 485 [M]H^+. Theoretical mass [M]H^+ = 485.21531, measured mass [M]H^+ = 485.21600 (error, 1.42 ppm). **TGA:** mass loss 86% (calc. WN, 59%; W_2N, 61%) at 590 °C.

2.3. Results and Discussion

2.3.1. Synthesis of Precursors

The syntheses of $[W(\mu\text{-}N^tBu)(N^tBu)Cl_2(H_2N^tBu)]_2$ (**2.1**),[1] $[W(N^tBu)_2Cl_2(TMEDA)]$ (**2.2**)[2] and $[W(N^tBu)_2Cl_2(py)_2]$ (**2.3**),[1,3] were carried out by modified literature procedures, as described in the experimental section and **Scheme 2.1**. The spectroscopic data for compounds **2.1-2.3** were as expected, according to their respective papers. For compound **2.1**, it was interesting to note the two peaks at 2.65 and 4.78 ppm, which account for the four NH_2 protons, two of which undergo a weak hydrogen-bonding interaction with a chloride ligand on the opposite tungsten centre. It is assumed that the bond order of the *tert*-butyl imido ligands is closer to 3, as the bent form only occurs in π-saturated compounds. As such, the bond order will be drawn as 3 in this work, unless it is known to be 2.

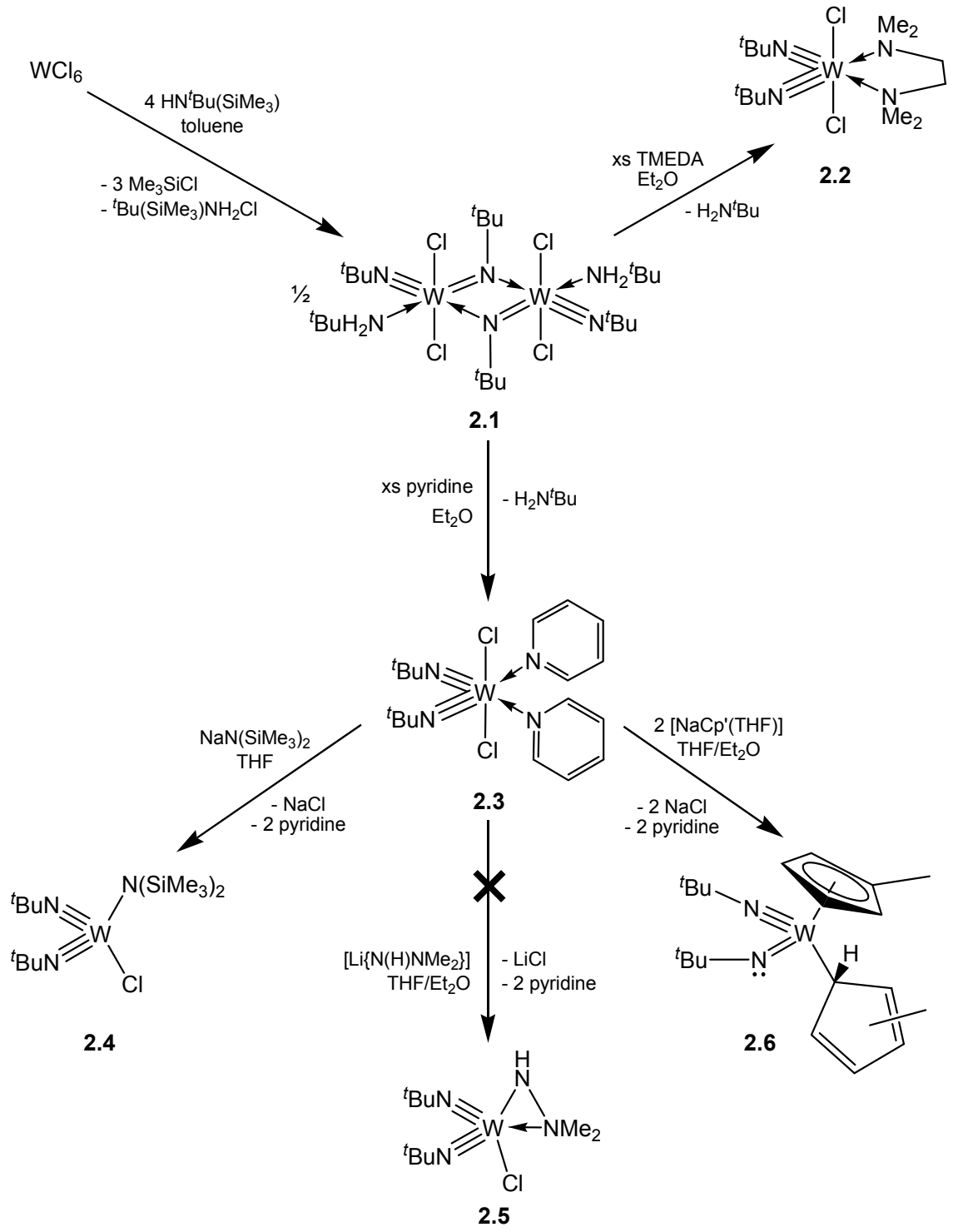

Scheme 2.1 Synthetic routes to compounds **2.1-2.6**.

$[W(N^tBu)_2Cl\{N(SiMe_3)_2\}]$ (**2.4**) was synthesised as a dark orange oil *via* the reaction of one equivalent of sodium bis(trimethylsilyl)amide with compound **2.3**.

Attempts were made to displace both chloride ligands from **2.3** by using two and four equivalents of $NaN(SiMe_3)_2$, but these were unsuccessful, as the ^tBu and $SiMe_3$ peaks in the proton NMR spectra (1.36 and 0.39 ppm respectively) consistently integrated to 18 protons each. This suggested that only one chloride had been displaced on each attempt, although, this might not pose a problem for CVD in terms of decomposition, as there is the possibility for the facile loss of a Me_3SiCl molecule when sufficiently heated. To confirm this, high resolution mass spectrometry was run on the oil. The mass of the most abundant peak in the parent ion cluster, $[M]H^+$, was measured to be *m/z* = 522.17384 (calculated *m/z* = 522.17239). The spectrum (**Figure 2.1**) shows successive losses of methyl groups from the parent ion peak, in addition to a higher peak at *m/z* = 562, which could account for the disubstituted compound, albeit as a minor product. These are likely to originate from the $SiMe_3$ moieties, as the most abundant peaks at *m/z* 419 and 434 can be assigned to the loss of $SiMe_3$ in addition to two and one methyl groups respectively. Unfortunately, X-ray quality crystals of **2.4** could not be grown, despite numerous attempts with a variety of solvents.

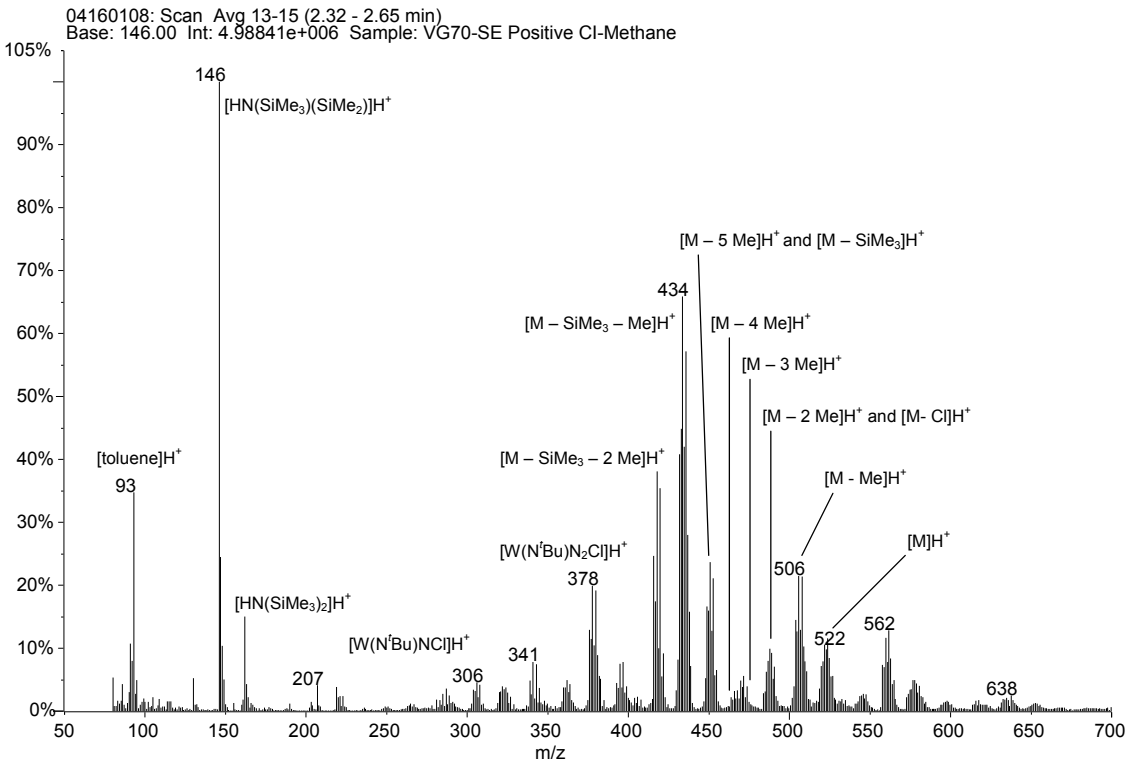

Figure 2.1 The CI+ mass spectrum of $[W(N^tBu)_2Cl\{N(SiMe_3)_2\}]$ (**2.4**), run in toluene.

A similar metathesis technique to that used for the preparation of compound **2.4** was adopted for the attempted synthesis of $[W(N^tBu)_2Cl\{N(H)NMe_2\}]$ (**2.5**). However, the reaction between $[W(N^tBu)_2Cl_2(py)_2]$ (**2.3**) and one or two equivalents of $[Li\{N(H)NMe_2\}]$ (synthesised from the reaction of one equivalent of ^{n}BuLi and *N*,*N*-dimethylhydrazine) did not afford a single isolable product. Initial reactions using two equivalents of $[Li\{N(H)NMe_2\}]$ gave a bright orange powder, which was contaminated with a significant quantity of the lithium salt. Dissolving the product in dichloromethane to remove the excess salt and subsequent filtering and drying afforded a dark orange glassy material. The elemental analysis suggested that only one chloride substitution had taken place, although the percentage nitrogen was lower than that calculated for **2.5**, possibly due to tungsten nitride formation during the procedure. The proton NMR spectrum was not particularly insightful as only a large broad peak at ~1.50 ppm was present. There was a collection of sharper peaks protruding from this, which could represent the *tert*-butyl or dimethylamido moieties, so these could not be integrated. There was no obvious N–H peak, although there was a very weak N–H stretch in the FT-IR spectrum at 3173 cm^{-1}. The mass spectrum showed a significant number of intense peaks at a greater *m/z* to the molecular ion peak. The broad peak in the proton NMR spectrum did not change on heating or cooling of the NMR solution, suggesting that more than just a straightforward metathesis reaction had occurred. Attempted sublimation of compound **2.5** at 5×10^{-2} Torr at 75-130 °C only served to remove residual pyridine and did not improve the analytical results and attempts to crystallise **2.5** from a variety of solvents have so far proved unsuccessful.

Sundermeyer *et al.* reported a very similar complex $[W(N^tBu)_2Cl\{N(SiMe_3)NMe_2\}]$, with a view to its use as a volatile CVD precursor.[4] Both metathesis using a Grignard reagent and direct reaction with the hydrazine gave the desired compound. It would seem that the blocking of the NH site with a trimethylsilyl moiety is the key to this reaction working, as a bare proton is still likely to be reactive. The broad peak in the NMR spectrum of **2.5** could suggest that the hydrazine is either reducing the tungsten to tungsten(V), rendering it paramagnetic. Another possibility is that polymerisation is readily occurring despite the dilute conditions, which would account for the lack of sublimation occurring and the extra

peaks in the mass spectrum. With this uncertainty in mind, it was decided not to use **2.5** in the TGA and CVD studies.

Attempts at transamination reactions using commercially available $[W(N^tBu)_2(NMe_2)_2]$ and ethylenediamine derivatives, such as $R(H)NCH_2CH_2N(H)R$ (R = Me, ^{i}Pr) were attempted with a view to making more volatile complexes. Synthesis of $[W(N^tBu)_2(\eta^2\text{-}RNCH_2CH_2NR)]$ (R = Me, ^{i}Pr) in hexane yielded dark orange powders, which decomposed within a week in the glove box to form dark brown solids. The NMR spectra of these compounds showed only a broad peak at ~1.5 ppm with many sharp peaks in that region that may have resulted from *tert*-butyl moieties. This may have been due to polymerisation although reducing the concentration of the reaction solutions gave the same results. The reaction of compound **2.3** with $[Li_2(MeNCH_2CH_2NMe)]$ to form $[W(N^tBu)_2(\eta^2\text{-}MeNCH_2CH_2NMe)]$ was also attempted to see if metathesis improved the analytical quality of the product. Unfortunately this was not the case as the NMR results were the same. The low stability of these products may be due to the fact that they are all 16-electron complexes with little steric hindrance to prevent nucleophilic attack.

With this in mind, further transamination reactions using donor functionalised amines, $R(H)NCH_2CH_2NMe_2$ (R = Me, Et), were carried out so see if the NMe_2 moiety would chelate and stabilise the tungsten centre (**Figure 2.2**). It was also hoped that these ligands would help prevent polymerisation as they only have one reactive proton. However, the NMR spectra only showed peaks corresponding to the starting materials, with no evidence that the di- or mono-substituted products had formed.

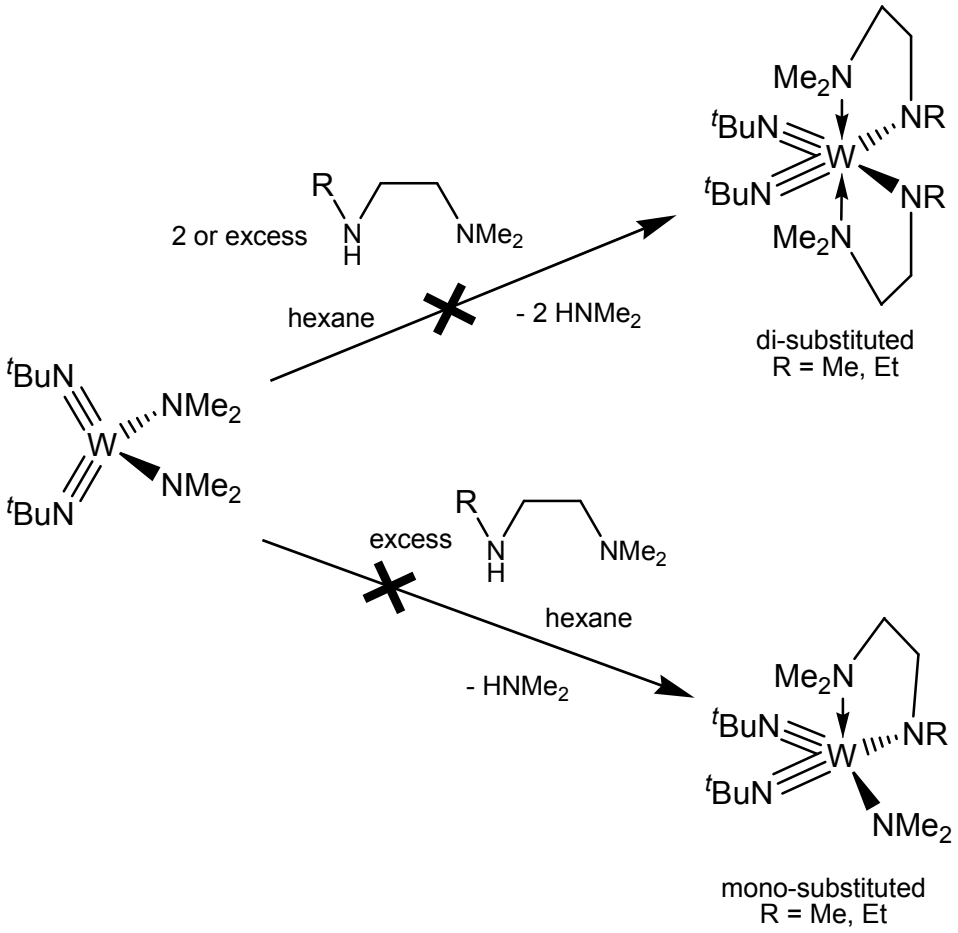

Scheme 2.2 Attempted transamination reactions of donor-functionalised amines with $[W(N^tBu)_2(NMe_2)_2]$.

The synthesis of $[W(N^tBu)_2(\eta^5\text{-Cp'})(\eta^1\text{-Cp'})]$ (**2.6**) was adapted from that of $[W(N^tBu)_2(\eta^5\text{-Cp})(\eta^1\text{-Cp})]$, which was first reported by Sundermeyer *et al.* They described what was essentially a two step process, involving the synthesis of $[W(N^tBu)_2(\eta^5\text{-Cp})Cl]$[5] from **2.3** and NaCp, and the subsequent reaction with a further equivalent of NaCp in dimethoxyethane,[6] affording $[W(N^tBu)_2(\eta^5\text{-Cp})(\eta^1\text{-Cp})]$ as a yellow oil. In this work, $[W(N^tBu)_2(\eta^5\text{-Cp'})(\eta^1\text{-Cp'})]$ (**2.6**) was synthesised directly from compound **2.3** and two equivalents of [NaCp'(THF)], giving a dark yellow oil. The methyl-substituted cyclopentadienyl ligand was selected with a view to increasing the volatility of the compound. The room temperature NMR confirmed the presence of **2.6** and is discussed in Section 2.3.2. The high resolution CI-mass spectrometry showed

a clear molecular ion peak, $[M]H^+$, at *m/z* = 485.21600 (calculated 485.21531), in addition to peaks corresponding to the losses of methyl, *tert*-butyl and methylcyclopentadiene. The facile loss of these groups would indeed be beneficial for the formation of tungsten nitride.

2.3.2. NMR Studies of [W(N^{t}Bu)$_2$(η^5-Cp')(η^1-Cp')] (2.6)

Compound **2.6** is a direct analogue of [W(N^{t}Bu)$_2$(η^5-Cp)(η^1-Cp)] (**1.17**), which was reported by Sundermeyer *et al.* in 2001.[6] They proposed that one cyclopentadienyl ligand was π-bound in an η^5 fashion, which, with the two *tert*-butylimido ligands, saturated the metal centre. Therefore, the second cyclopentadienyl ligand was σ-bound in an η^1-mode. As such, the room-temperature proton NMR spectrum showed both Cp environments as broad singlets. Warming the solution up caused them to merge into one environment and cooling the solution resolved the η^1-Cp into a multiplet.

For this study, the methylcyclopentadienyl ligand was employed with a view to increasing the volatility of the precursor. In a similar manner, the room temperature (20 °C) proton NMR spectrum of **2.6** was seemingly simple, in that there were two distinct η^5- and η^1-Cp' environments, and two corresponding methyl groups in the region of 2.1-2.3 ppm. Variable temperature NMR studies were carried out on compound **2.6** (**Figure 2.2**).

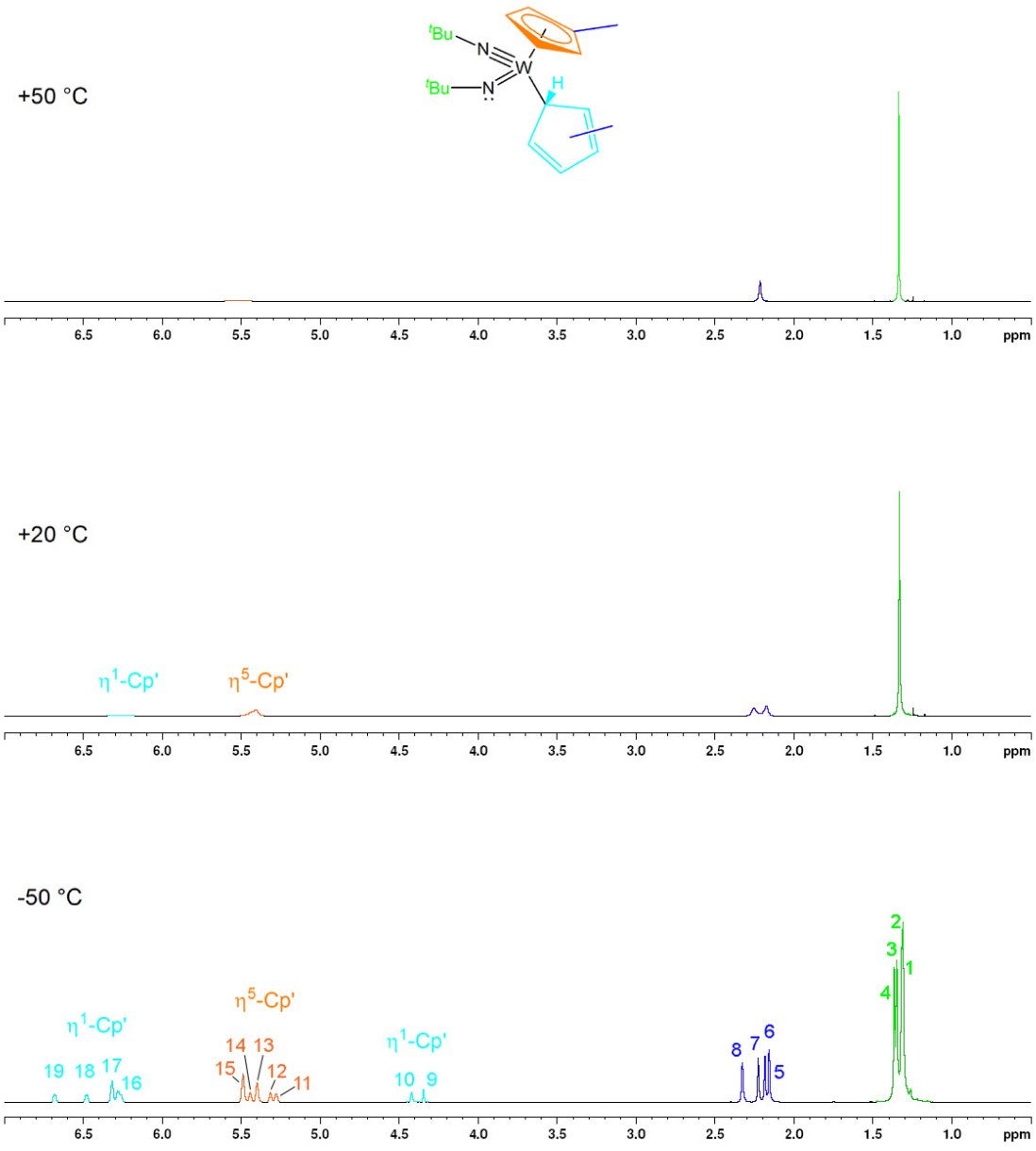

Figure 2.2 Stacked ^{1}H-NMR spectra of [W(N^{t}Bu)$_2$(η^5-Cp')(η^1-Cp')] (**2.6**) in $CDCl_3$. The peaks at -50 °C are numbered for ease of discussion.

At +50 °C, the two Cp' environments had merged into one, thereby suggesting that the two different binding modes were in exchange with each other. Cooling to -50 °C resulted in a greater resolution of the two different Cp' ligands, and clearly the addition of a methyl group on the cyclopentadiene ring had complicated the system. One of the initial uncertainties was the position of the methyl group on the η^1-Cp' ring.

There are three possibilities (**Figure 2.3**): the 1-position, where the methyl group is on the carbon bound to the tungsten; the 2-position, where the tungsten is one carbon atom along, and the 3-position, where it is two carbon atoms along.

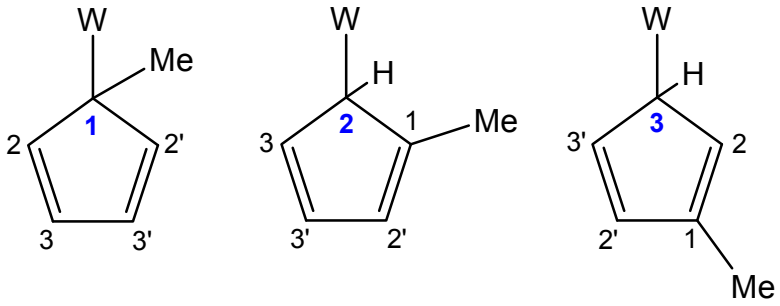

Figure 2.3 Three possible isomers of η^1-Cp' ligands.

The fact that there are four methyl peaks, each integrating to three protons, suggest that there are two isomers, i.e. two η^5-Cp' and two η^1-Cp' environments. It is likely that the methyl moiety only occupies the 3- (**2.6a**) or the 2-position (**2.6b**) because (a) the 1-position would be thermodynamically unfavourable as space that close to the tungsten centre would be restricted by the η^5-Cp' ligand, and (b) there are two peaks at 4.40 and 4.48 ppm, which integrate to one proton each. These are shifted upfield from the other η^1-Cp' protons due to their close proximity to the tungsten centre, which also accounts for the small tungsten satellite peaks either side, resulting from weak $^2J_{HW}$ coupling. These peaks also have a similar chemical shift to that assigned by Sundermeyer *et al.*[6] This consequently helps with the assignment of the remaining Cp' peaks, as the cluster in the region of 6.2-6.7 ppm integrates to six protons, therefore comprising the remainder of the aromatic η^1-Cp' protons, and the cluster at 5.2-5.6 ppm integrates to eight protons, which are those on the η^5-Cp' ring.

So as to fully assign the protons to each isomer, a COSY spectrum (**Figure 2.4**) was run at -50 °C. The couplings are summarised in **Table 2.1**.

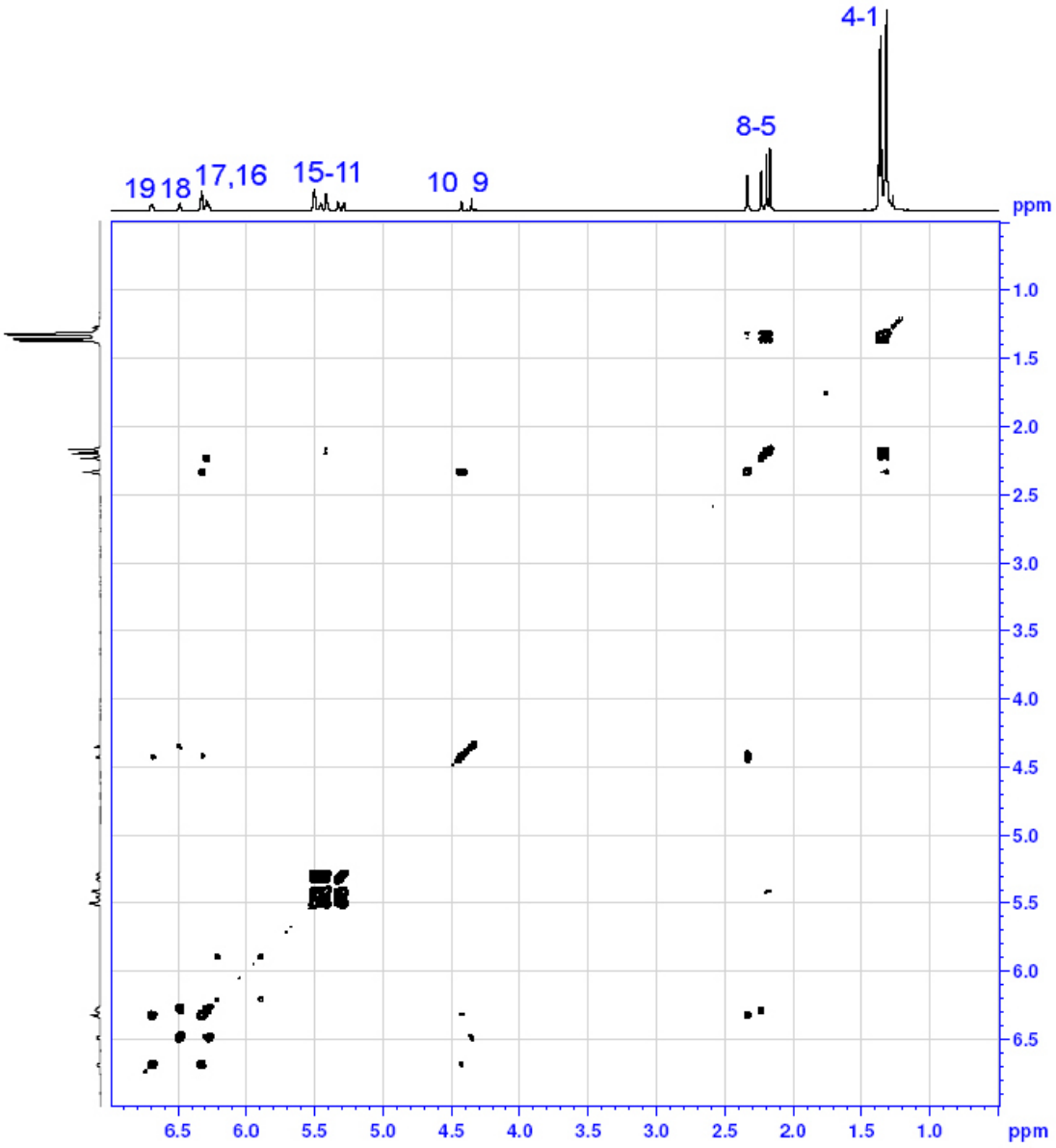

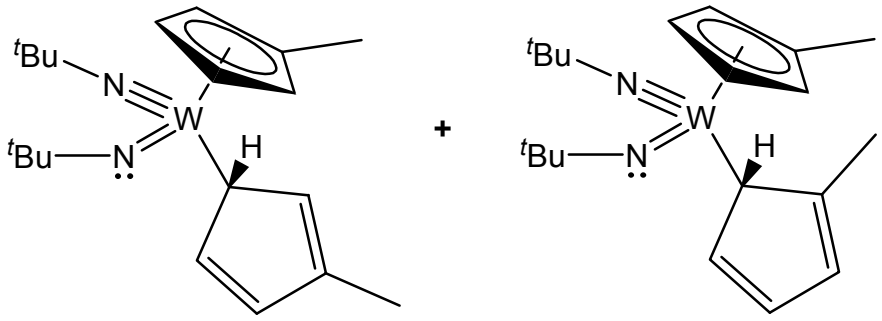

2.6a **2.6b**

Figure 2.4 COSY spectrum of compound 2.6 at -50 °C.

Table 2.1 Summary of coupling of peaks in the COSY spectrum of compound **2.6**.

Peak	Environment	Integral	Coupled To
5	η^5-$C_5H_4CH_3$	3	12, 13
6	η^5-$C_5H_4CH_3$	3	13, 14
7	η^1-$C_5H_4CH_3$	3	16
8	η^1-$C_5H_4CH_3$	3	10, 17
9	η^1-3-C_5H_4Me	1	18
10	η^1-2-C_5H_4Me	1	8, 17, 19
11	η^5-C_5H_4Me	1	13, 14, 15
12	η^5-C_5H_4Me	1	5, 13, 14, 15
13	η^5-C_5H_4Me	2	5, 6, 11, 12, 14, 15
14	η^5-C_5H_4Me	1	5, 6, 11, 12, 13, 15
15	η^5-C_5H_4Me	3	11, 12, 13, 14
16	η^1-C_5H_4Me	2	7, 18
17	η^1-C_5H_4Me	2	8, 10, 19
18	η^1-C_5H_4Me	1	9, 16
19	η^1-C_5H_4Me	1	10, 17

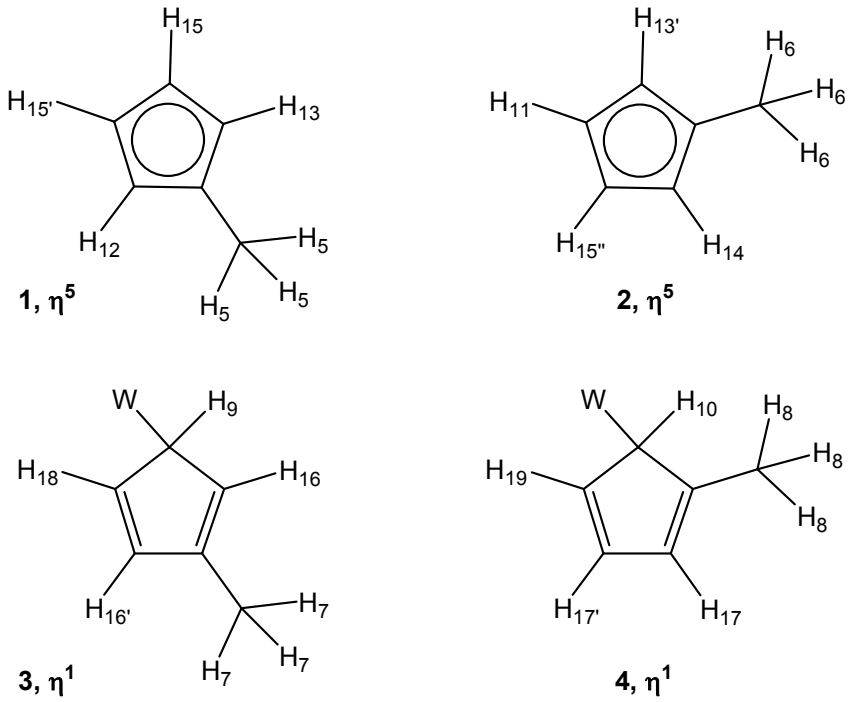

Figure 2.5 Proton assignments for compound **2.6**.

Based on the couplings, and assuming there are four different Cp' environments, it is possible to assign the protons on each of the rings, as shown in **Figure 2.5**. For example, peak 15 accounts for three protons and is coupling to peaks 11-14. The fact that peaks 11-15 are not coupling to peaks 9 or 10 means that they are all in an η^5-Cp' environment (ring **1**). Peaks 12 and 13 are undergoing $^4J_{HH}$ coupling to the peak 5, which suggests they occupy the 2 and 2' positions on the ring with two protons from peak 15 occupying the 3 and 3' positions. Peak 13 is also coupling to peak 6, so this must account for the methyl group on ring **2** and the remaining proton 13, which is adjacent to it in the 2 position. The 2' position is occupied by the proton associated with peak 14 as this is also coupling to peak 6. The remaining proton from peak 15 and peak 11 therefore occupy the 3' and 3 positions respectively.

For the η^1-Cp' environments, peak 9 (ring **3**) is coupled to peak 18, so this must be adjacent to it. Peak 18 is also coupled to 16, the latter showing an interaction with peak 7. Although there is no coupling visible on the COSY spectrum between peaks 9 and 16, the only possible positions for these protons are 2 and 2'. Finally, for ring **4**, peak 10 shows an interaction with the remaining methyl peak (8) and peaks 17 and 19. Therefore, the proton associated with peak 19 is adjacent to that of peak 10, with the protons associated with 17 occupying the remaining spaces.

Although the protons were assigned to their respective rings, it was still unclear as to which η^5-Cp' ring was associated with which η^1-Cp' *via* a common tungsten centre. Sundermeyer *et al*. proposed a [σ,π] hapticity exchange mechanism for $[W(N^tBu)_2(\eta^5\text{-Cp})(\eta^1\text{-Cp})]$,[6] whereby the rings can convert reversibly between η^5- and η^1- binding modes *via* an η^3- (allyl) intermediate. This also made a metallotropic [1,3] exchange possible, which involves the effective rotation of the η^1-bound ring by two carbon atoms. It was facilitated by the electronic flexibility of the ^{t}BuN^{2-} ligands, as the remaining 6-electron donor converts to the bent 4-electron donor form so as to prevent the electron count of the complex exceeding 18. This mechanism was adapted for $[W(N^tBu)_2(\eta^5\text{-Cp'})(\eta^1\text{-Cp'})]$ (**2.6**) and is shown in **Scheme 2.3**. It is clear that the addition of the methyl group complicates the mechanism, especially as the methyl-bearing carbon of the η^1-Cp' ligand cannot be bound to the tungsten centre, as shown by the proton NMR spectra, although the [1,3] exchange could account for interconversion between the 2- and 3-isomers.

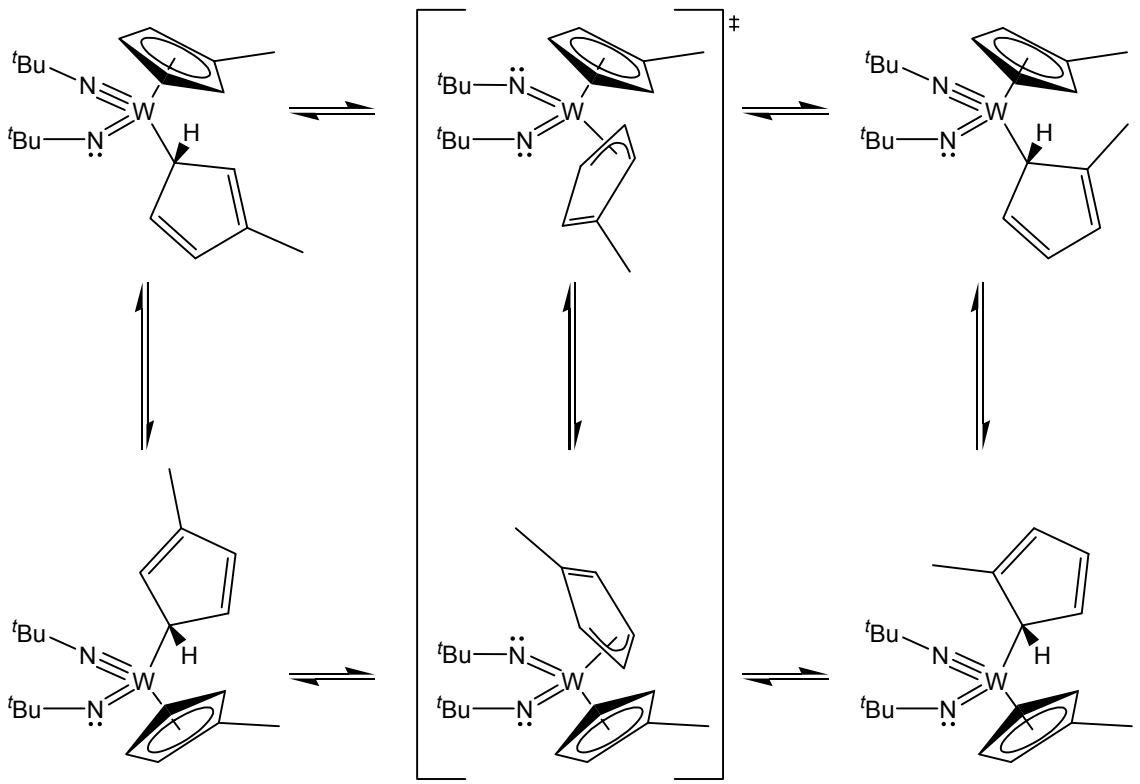

Scheme 2.3 Proposed [σ,π] and [1,3] exchange mechanisms for compound **2.6**. Adapted from reference.[6]

Another possible mechanism for rotation of the η^1-Cp' rings in compound **2.6** is [1,2] metallotropic migration, as described by Cotton *et al.* when discussing the NMR spectra of $[Fe(CO)_2(\eta^5\text{-Cp})(\eta^1\text{-Cp})]$.[7] Shown in **Scheme 2.4**, this mechanism provides a more direct route between the 3- and 2-isomers (**a** and **b** respectively).

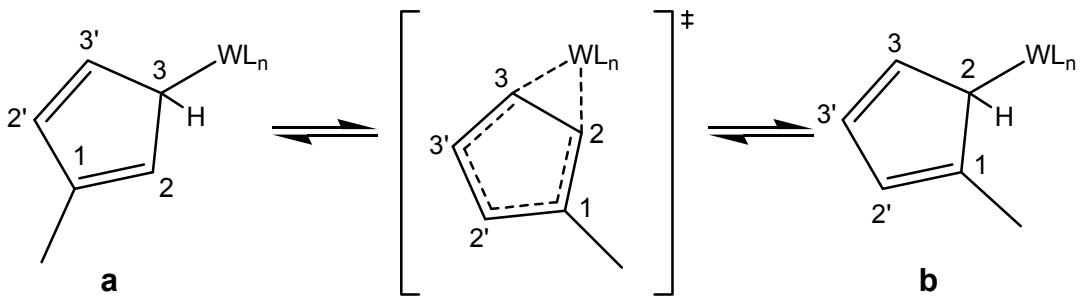

Scheme 2.4 Proposed [1,2] metallotropic exchange mechanism for compound **2.6**. Adapted from reference.[6]

With respect to form **a**, the [1,2] metallotropic rearrangement would show the preferred broadening of the protons in positions 2 and 3'. However, in the proton NMR spectrum of compound **2.6**, no preferential broadening is observed, suggesting that a mixture of [σ,π], [1,2] and [1,3] rearrangements are taking place. The NOESY spectrum (**Figure 2.6**) did not show which of the [1,2] or [1,3] rearrangements were prevalent as, with the [σ,π] hapticity changes, all of the Cp' ligands are exchanging with each other.

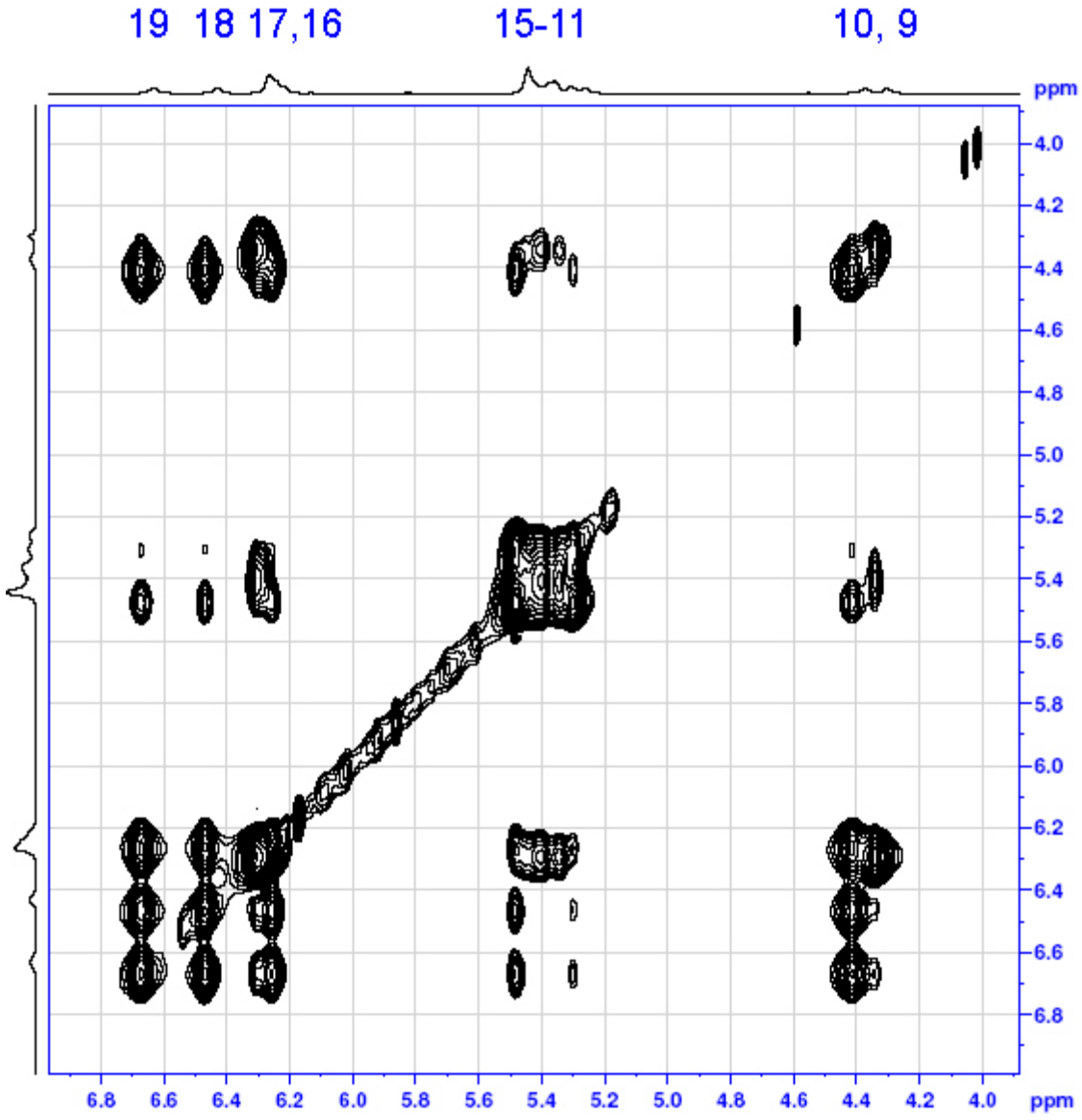

Figure 2.6 NOESY spectrum of compound **2.6**, focussing on the aromatic/olefinic Cp' protons.

2.3.3. Decomposition Studies

Decomposition studies on compounds **2.1-2.4** and **2.6** were carried out by thermogravimetric analysis (TGA). The results are summarised in **Figure 2.7** and **Table 2.2**. The curves showed that the compounds start to decompose between 100 and 200 °C. Generally, the decompositions were clean with clear stepped mass losses, which can be attributed to the loss of certain moieties. Compound **2.4** had a notably shallower curve, which suggests that its decomposition is more gradual, so at first glance it may not be suitable as a CVD precursor.

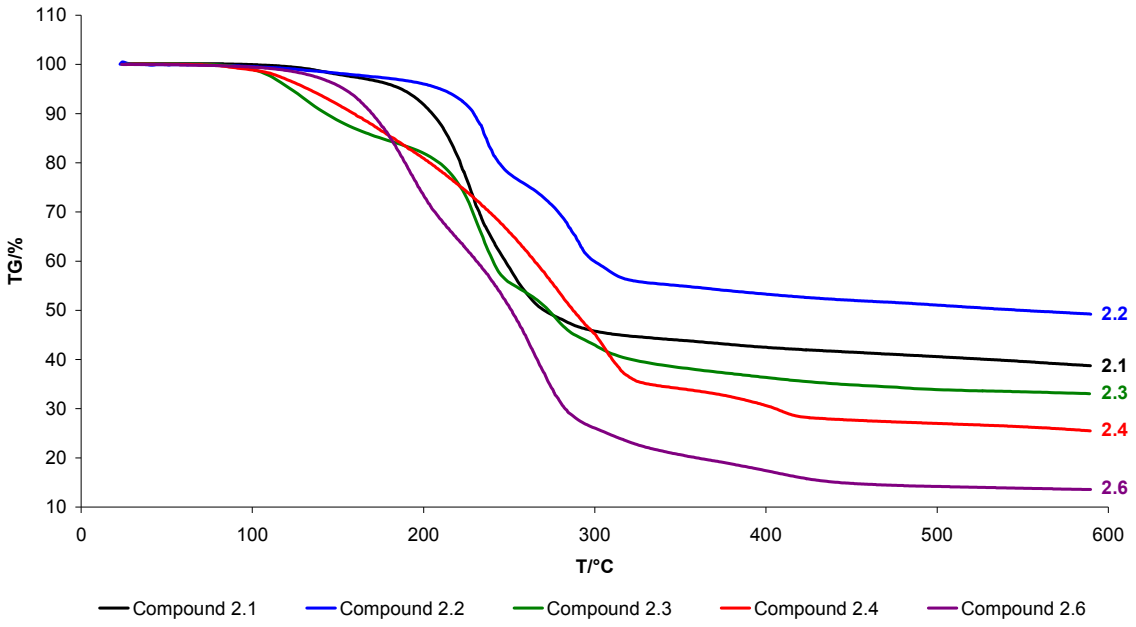

Figure 2.7 TGA plots for compounds **2.1-2.4** and **2.6**.

It is evident that, in some cases, the decomposition occurs in stages such that the TGA curve shows stepped mass losses rather than one overall loss. It is particularly evident with compounds **2.2**, **2.3** and **2.6**. From this, it is possible to propose a decomposition mechanism. For example, for $[W(N^tBu)_2Cl_2(py)_2]$ (**2.3**) there are three steps during the decomposition, although there is some overlap between them. From these, it is possible to estimate how the 64% calculated mass loss is accounted for (**Scheme 2.5**). The first step is likely to be the loss of the pyridine ligands as the first

mass loss is a shallow curve, suggesting a more gradual loss. This also accounts for the most abundant peak in the mass spectrum of **2.3** being $[W(N^tBu)_2Cl_2]H^+$. Then isobutene may be lost *via* a β-hydrogen elimination mechanism, leaving the imido nitrogens protonated. These protons could then facilitate the loss of the chloride ligands through elimination of HCl, which would account for the final step, leaving nitrogen-rich tungsten nitride, WN_2. This would gradually decompose to WN (and perhaps further to W_2N) *via* the gradual loss of molecular nitrogen. It is likely that the related compounds decompose in a similar manner.

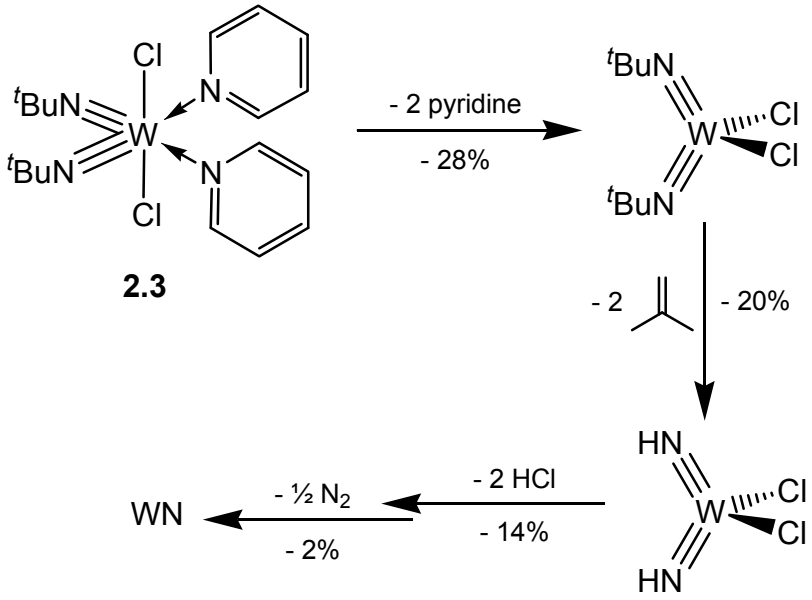

Scheme 2.5 Proposed decomposition pathway for $[W(N^tBu)_2Cl_2(py)_2]$ (**2.3**).

It is possible that the first two steps could be reversed, with the loss of isobutene occurring first. However, the overlap of the mass losses makes this difficult to ascertain.

Table 2.2 TGA Data for compounds **2.1-2.4** and **2.6**.

Compound	Observed Mass Loss at 590 °C (%)	Calc. Mass Loss for WN (%)	Calc. Mass Loss for W_2N (%)
2.1	63	58	59
2.2	51	61	63
2.3	67	64	66
2.4	74	62	63
2.6	86	59	61

All compounds showed a substantial mass loss by 590 °C. However, for compounds **2.1** **2.3**, **2.4** and **2.6**, the overall mass loss was greater than those calculated for WN and W_2N. The likely reason for this is sublimation or evaporation prior to decomposition, resulting in a greater mass loss than expected. This was most evident for $[W(N^tBu)_2Cl\{N(SiMe_3)_2\}]$ (**2.4**) and particularly $[W(N^tBu)_2(\eta^5\text{-Cp'})(\eta^1\text{-Cp'})]$ (**2.6**), which are both oils, and consequently it is expected that they would be more volatile than solid compounds. In comparison, the mass losses for **2.1** and **2.3** are within 5% of the calculated mass losses. The anomaly of the group of compounds is **2.2**, whose mass loss was lower than expected. This suggests that a substantial amount of the ligands remain, as it doesn't decompose as fully as the other compounds. The TMEDA ligand is most likely to be the cause of this, taking into consideration that compounds **2.1-2.3** have a $[W(N^tBu)_2Cl_2]$ fragment in common. Therefore, with the possible exception of compound **2.2**, the TGA data suggests that all the tungsten imido compounds are promising candidates for CVD.

2.3.4. Vapour Pressure Studies

An important property of a CVD precursor is its volatility, as it needs to remain stable in the gas phase until it has reached the substrate. Vapour pressure studies were run on compounds **2.1-2.3** at SAFC Hitech Ltd., and the results are summarised in **Figure 2.8**.

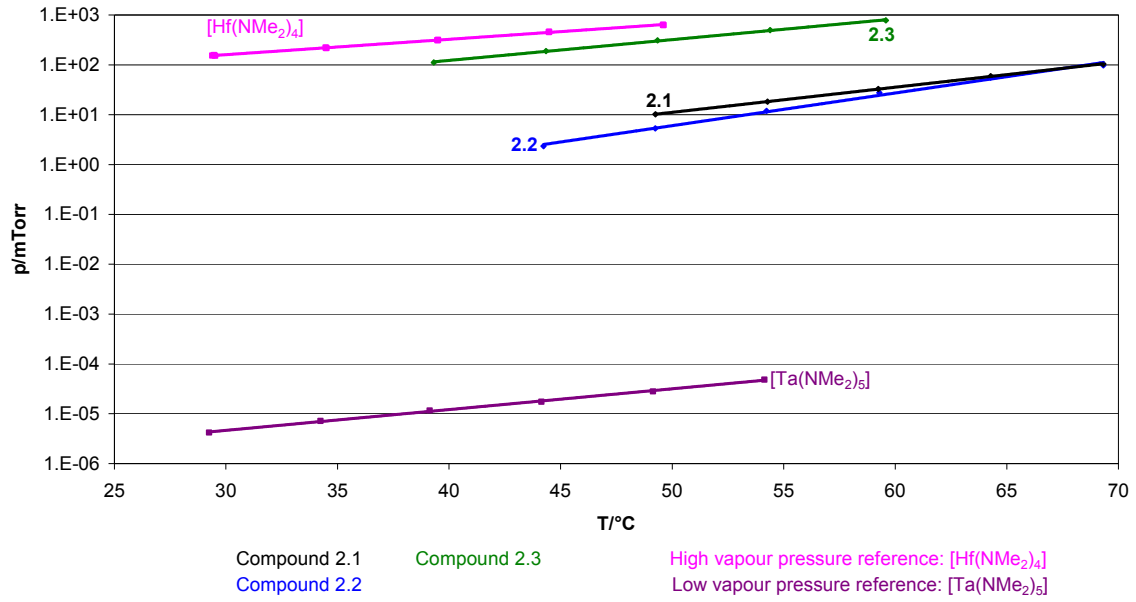

Figure 2.8 Vapour pressure lines for compounds **2.1-2.3** as compared to the high pressure industry standard, $[Hf(NMe_2)_4]$, and the low pressure industry standard, $[Ta(NMe_2)_5]$.

The industry standard compounds, $[Hf(NMe_2)_4]$ and $[Ta(NMe_2)_5]$ (SAFC Hitech Ltd.), provide a useful comparison to ascertain as to how suitable compounds may be as precursors for CVD. $[Hf(NMe_2)_4]$ exhibits a considerably high vapour pressure of just under 1 Torr at 50 °C, whereas the vapour pressure of $[Ta(NMe_2)_5]$ is negligible at under 0.1 μTorr. It is interesting to note, that despite its low vapour pressure, $[Ta(NMe_2)_5]$ has been successfully employed as a precursor to tantalum carbonitride and highly pure tantalum oxide thin films by plasma-enhanced ALD.[8]

The vapour pressures of $[W(\mu\text{-}N^tBu)(N^tBu)Cl_2(H_2N^tBu)]_2$ (**2.1**) and $[W(N^tBu)_2Cl_2(TMEDA)]$ (**2.2**) at 50 °C are comparable, being 10 mTorr and 5 mTorr respectively. These vapour pressures are significantly higher than that of $[Ta(NMe_2)_5]$, suggesting that **2.1** and **2.2** should be suitably volatile for use in a CVD reactor. Most surprising is the seemingly high pressure of $[W(N^tBu)_2Cl_2(py)_2]$ (**2.3**), which was approximately 300 mTorr at 50 °C; almost comparable to that of $[Hf(NMe_2)_4]$. Using the vapour pressure data alone, it is not certain as to whether the seemingly high vapour pressure of **2.3** is due to the compound itself or the loss of pyridine ligands during the heating process. However, as the vapour pressure of pyridine is approximately 20 Torr

at 25 °C,[9] it seems highly unlikely to be related to pyridine alone because the vapour pressure of **2.3** at 25 °C is approximately 29 mTorr.

2.4. Conclusions

$[W(\mu\text{-}N^tBu)(N^tBu)Cl_2(H_2N^tBu)]_2$ (**2.1**), $[W(N^tBu)_2Cl_2(TMEDA)]$ (**2.2**), $[W(N^tBu)_2Cl_2(py)_2]$ (**2.3**), $[W(N^tBu)_2Cl\{N(SiMe_3)_2\}]$ (**2.4**) and $[W(N^tBu)_2(\eta^5\text{-Cp'})(\eta^1\text{-Cp'})]$ (**2.6**) were synthesised in good yields. The synthesis of $[W(N^tBu)_2Cl\{N(H)NMe_2\}]$ (**2.5**) was complicated due to the reactivity of the NH portion of the *N,N'*-dimethylhydrazido ligand, which resulted in polymerisation. Variable temperature, COSY and NOESY NMR spectra of compound **2.6** suggested that exchange was occurring between the η^5- and η^1-Cp' environments as well as two potential exchange mechanisms within the η^1-Cp' alone. This lead to the conclusion that there were both 2-η^1-Cp' and 3-η^1-Cp' isomers of **2.6**.

Compounds **2.1-2.4** and **2.6** decomposed cleanly. The mass losses of **2.1** and **2.3** approximated to those expected for tungsten carbonitride but those of **2.4** and **2.6** were greater than expected, as they are oils and consequently more volatile. The mass loss of compound **2.2** was lower than expected, suggesting that it does not decompose as fully by 550 °C. The clean decomposition of compounds **2.1**-**2.4** and **2.6** suggests that they may be suitable precursors to tungsten carbonitride. However, compounds **2.2** and **2.6** may lead to a large amount of carbon in the resultant films. The measured vapour pressures of **2.1-2.3** were all greater than 1 mTorr at 50 °C. The vapour pressure of **2.3** was somewhat higher and close to that of $[Hf(NMe_2)_4]$ (the SAFC Hitech Ltd. high pressure standard). This is not necessarily due to the dissociation of pyridine, as the resultant vapour pressure would be two orders of magnitude higher. These high vapour pressures means **2.1-2.4** are promising as precursors.

2.5. References

1. R. G. Gordon, J. S. Becker, S. Suh, S. Wang, *Chem. Mater.*, 2003, **15**, 2969-2976.
2. A. J. Nielson, *Polyhedron*, 1987, **6**, 1657-1667.
3. R. A. Fischer, A. Baunemann, D. Rische, M. Winter, *Inorg. Chem.*, 2006, **45**, 269-277.

4. J. Sundermeyer, D. Gaess, K. Harms, M. Pokoj, W. Stolz, *Inorg. Chem.*, 2007, **46**, 6688-6701.
5. J. Sundermeyer, *Chem. Ber.*, 1991, **124**, 1977-1979.
6. J. Sundermeyer, K. Peters, U. Radius, H.-G. von Schnering, *Eur. J. Inorg. Chem.*, 2001, 1617-1623.
7. F. A. Cotton, M. J. Bennett, Jr., A. Davidson, J. W. Faller, S. J. Lippard, S. M. Morehouse, *J. Am. Chem. Soc.*, 1966, **88**, 4371-4376.
8. H. Kim, W. J. Maeng, S.-J. Park, *J. Vac. Sci. Technol. B*, 2006, **24**, 2276-2281.
9. R. A. Pandey, K. V. Padoley, A. S. Rajvaidya, T. V. Subbarao, *Bioresour. Technol.*, 2006, **97**, 1225-1236.

3

Chemical Vapour Deposition of Tungsten Carbonitride

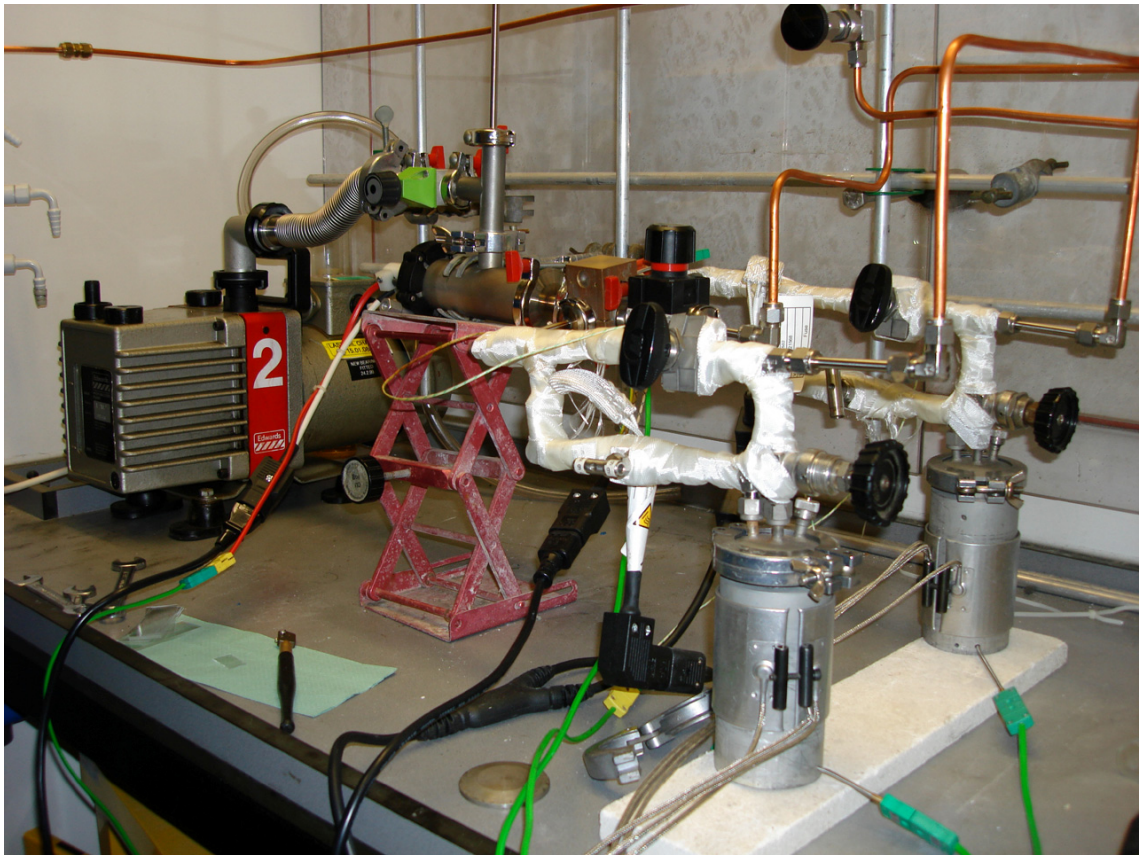

Figure 3.0 The LPCVD rig used for deposition of tungsten carbonitride films.

3.1. Introduction

This chapter examines the low pressure CVD (LPCVD) of tungsten carbonitride thin films using $[W(\mu\text{-}N^tBu)(N^tBu)Cl_2(H_2N^tBu)]_2$ (**2.1**), $[W(N^tBu)_2Cl_2(TMEDA)]$ (**2.2**, TMEDA = *N*,*N*,*N'*,*N'*-tetramethylethylenediamine), $[W(N^tBu)_2Cl_2(py)_2]$ (**2.3**, py = pyridine) and $[W(N^tBu)_2Cl\{N(SiMe_3)_2\}]$ (**2.4**) using nitrogen and ammonia as bleed gases. The LPCVD of $[W(N^tBu)_2(\eta^5\text{-Cp'})(\eta^1\text{-Cp'})]$ (**2.6**, Cp' = methylcyclopentadienyl) using a vapour-draw and the aerosol-assisted CVD of $[W(\mu\text{-}N^tBu)(N^tBu)Cl_2(H_2N^tBu)]_2$ (**2.1**) are also discussed.

3.2. Experimental

3.2.1. General Procedures

Nitrogen (99.99%) and ammonia were obtained from BOC and used as supplied. To obtain a standing wave for AACVD, a Vicks VE5520E Humidifier was used, which was purchased from Argos.

3.2.2. Physical Measurements

X-ray diffraction (XRD) was carried out on a Bruker AXS D8 Discover machine using monochromatic Cu-Kα radiation (λ_1 = 1.54 Å). WDX was performed on a Philips XL30ESEM machine. Scanning electron microscope (SEM) images were obtained on a JSM-6301F Scanning Microscope Field Emission machine. UV-Vis spectra were recorded in the range 300-2500 nm using a Helios double beam instrument.

3.2.3. Low Pressure Chemical Vapour Deposition

3.2.3.1. LPCVD with Bleed Gases

Coatings were obtained on borosilicate glass (2 cm × 3 cm) using a custom-made cold wall LPCVD reactor (**Figure 3.1**) from 250 mg of precursor. The deposition section of the reactor comprised a graphite block angled at approximately 30° such that the precursor flow was aimed directly at the substrate thereon. The sublimation section comprised an airtight stainless steel bubbler, which could be loaded in the glove box.

The graphite block was heated using a Whatlow Firerod cartridge heater, controlled with Pt-Rh thermocouples. The exhaust was attached to a vacuum *via* a liquid nitrogen trap.

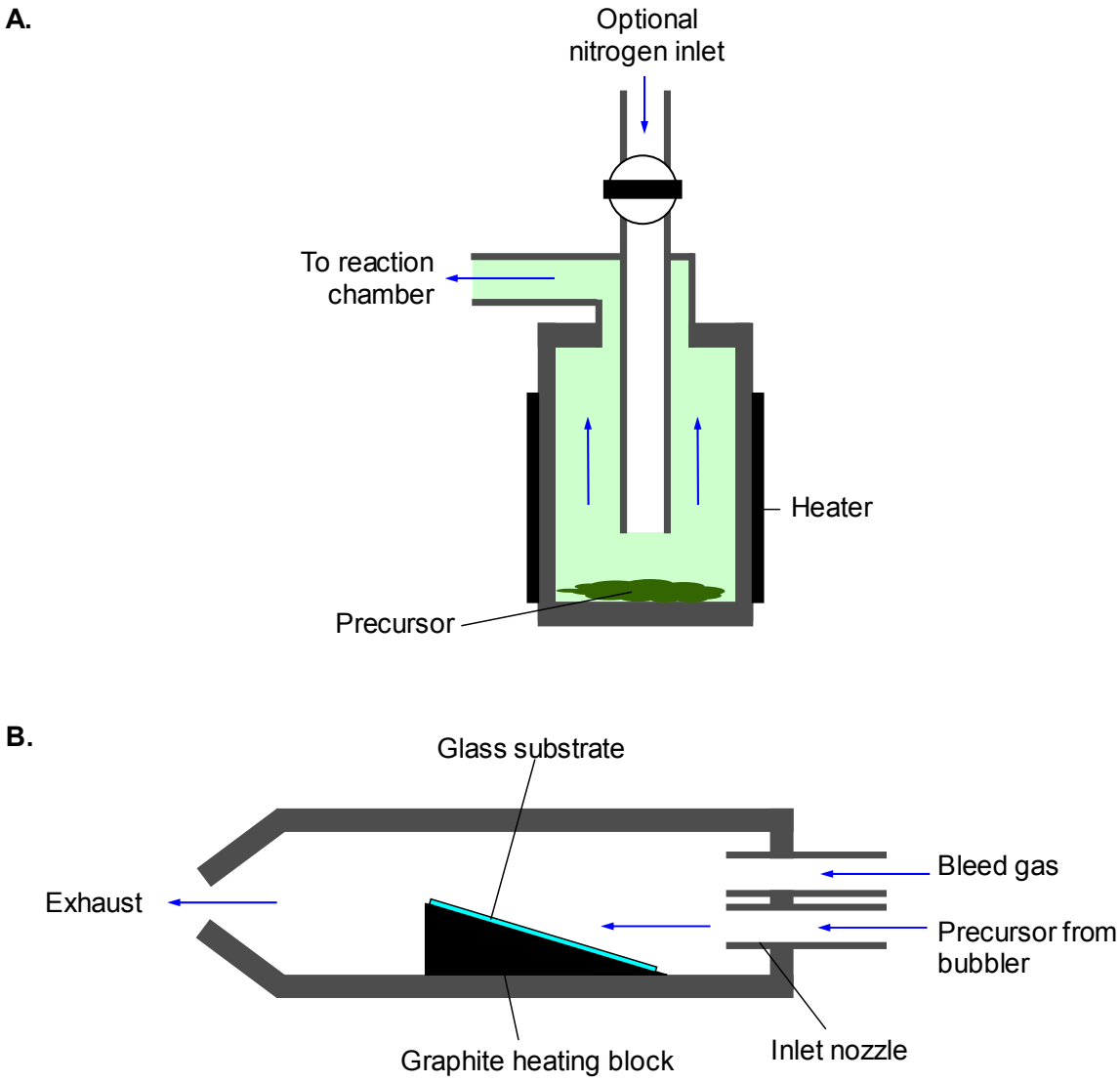

Figure 3.1 Schematic diagram of the LPCVD apparatus. (A) The precursor bubbler and (B) the reaction chamber.

The pressure was monitored using a Pirani gauge and the base pressure was typically 0.1 Torr. A gas bleed was attached to the inlet of the reaction chamber, through which

nitrogen or ammonia was passed. The inlet partial pressures were ~0.1 Torr for both nitrogen and ammonia. Prior to use, the apparatus was evacuated then filled with nitrogen three times, then evacuated to the appropriate pressure once the desired sublimation (typically 70-90 °C depending on the precursor) and substrate (550 °C) temperatures had been reached. A nitrogen carrier flow (0.1 Torr partial pressure) was used to transport the precursor to the chamber, which was also opened to the bleed gas, and the deposition was run for approximately 1 h.

3.2.3.2. LPCVD with a Vapour-Draw

Coatings were obtained on six borosilicate glass slides (75 mm × 12 mm × 1 mm) per run. In the glove box, the precursor (250 mg) was placed in a small sample vial at the end of a quartz tube 60 cm long and 1.5 cm in diameter. The glass slides were placed along the tube end-to-end and the end was sealed with a Schlenk tap fitting, which was attached to a vacuum line after removal from the glove box. The tube was placed in a tube furnace such that the precursor was not directly in contact with the heater (**Figure 3.2**). The furnace was allowed to reach 600 °C before the tube was opened to vacuum (typically 50 mTorr) and left to run for 1 h or until the precursor had all sublimed, whichever was sooner.

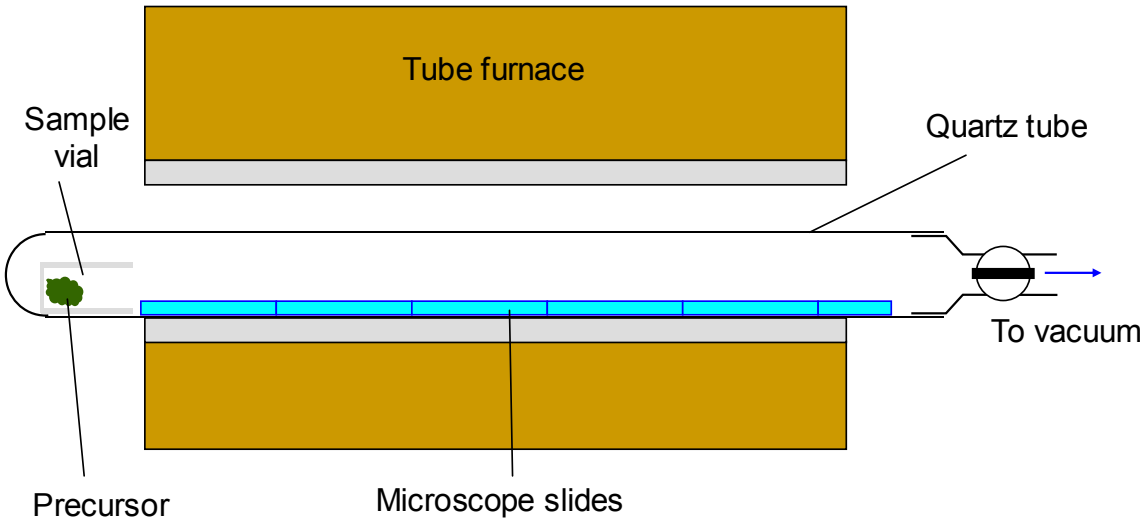

Figure 3.2 Schematic diagram of the vapour-draw LPCVD apparatus.

3.2.4. Aerosol-Assisted Chemical Vapour Deposition

Coatings were obtained on SiCO coated glass substrates supplied by Pilkington Glass. AACVD experiments were conducted on 150 mm × 45 mm × 3 mm pieces of glass using a horizontal bed cold wall CVD reactor (**Figure 3.3**).

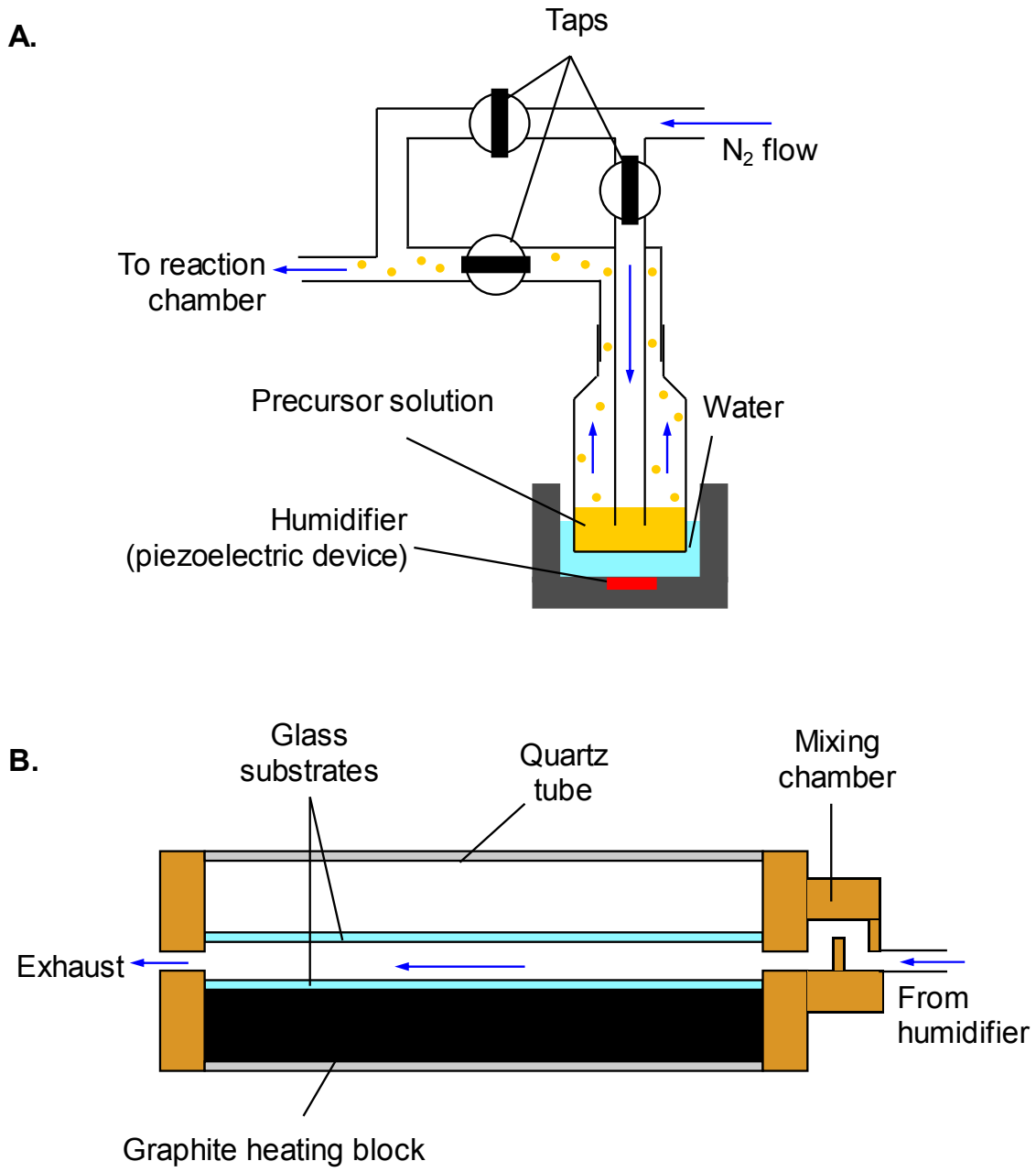

Figure 3.3 AACVD apparatus. (A) The humidifier and bypass valve and (B) the deposition chamber.

The glass substrates were cleaned prior to use by washing with propan-2-ol and then dried, first in air, then at 150 °C in an oven to reduce the moisture levels. The substrate mount comprised a graphite block containing a Whatman cartridge heater, the temperature of which was monitored by a Pt–Rh thermocouple. The design of the rig is such that the vapour was passed between two glass plates. The bottom plate was in direct contact with the graphite block, whereas the top plate was suspended above the gas flow with no direct heating. The temperature of the top plate was typically 50 °C lower than that of the bottom plate.

The bubbler comprised a flat-bottomed glass Schlenk flask attached to a two-way valve such that the gas flow could be diverted away from the bubbler. The flask was charged with *ca.* 500 mg of the relevant precursor in 20 cm^3 toluene and placed over a piezo-electric device to obtain a mist of the precursor solution. Nitrogen gas was passed through the mist and carried it over the substrate plates. The gas flow was 1 L min^{-1} and was regulated using a calibrated flow meter. The exhaust from the reactor was vented directly into a fume cupboard.

3.3. Results and Discussion

3.3.1. Low Pressure CVD Using Bis(imido)chloro Tungsten Compounds

LPCVD of $[W(\mu\text{-}N^tBu)(N^tBu)Cl_2(H_2N^tBu)]_2$ (**2.1**), $[W(N^tBu)_2Cl_2(TMEDA)]$ (**2.2**, TMEDA = *N*,*N*,*N'*,*N'*-tetramethylethylenediamine), $[W(N^tBu)_2Cl_2(py)_2]$ (**2.3**, py = pyridine) and $[W(N^tBu)_2Cl\{N(SiMe_3)_2\}]$ (**2.4**) at 550 °C with a nitrogen or ammonia bleed gas resulted in grey mirror-like films. They were not removed by tissue or Scotch tape tests and were not scratched by brass or steel styluses, showing the films to be adhesive and hard, as expected of tungsten carbonitride.[1,2] Ammonia is known to affect the amount of nitrogen in films by altering the reaction mechanism.[3-5] A comparison of nitrogen and ammonia as bleed gases is made in this chapter.

3.3.1.1. Composition of Films

All films were analysed by wavelength dispersive X-ray spectroscopy (WDX) and they were generally shown to be nitrogen-rich. The average composition results are shown in **Table 3.1**.

Table 3.1 Compositions of films from compounds **2.1-2.4** as found by WDX. The compositions are the average values for at least three runs.

Compound	Composition	
	Nitrogen bleed	**Ammonia bleed**
2.1	$WN_{1.18\pm0.12}C_{0.22\pm0.05}$	$WN_{1.32\pm0.11}C_{0.23\pm0.05}$
2.2	$WN_{0.95\pm0.11}C_{0.87\pm0.12}$	$WN_{1.13\pm0.10}C_{0.27\pm0.08}$
2.3	$WN_{1.35\pm0.10}C_{0.29\pm0.06}$	$WN_{1.23\pm0.10}C_{0.20\pm0.05}$
2.4	$WN_{1.12\pm0.14}C_{0.20\pm0.05}$	$WN_{1.20\pm0.10}C_{0.24\pm0.07}$

W:N ratio varied over the range 1.12-1.35, with W:C ratios not exceeding 0.3. The exception was the film deposited from compound **2.2**, where the W:N ratio was less than 0.95; significantly lower than in the other films. Also in this case, the W:C ratio was higher (0.87). This is not unexpected as the TGA data (Section 2.3.3) shows a lower mass loss than expected for WN or W_2N, implying that the ligands in compound **2.2** will contribute significantly more to carbon contamination than in compounds **2.1**, **2.3** and **2.4**. These compositions are directly comparable to those reported by Chui *et al.*, who deposited WN_xC_y *via* LPCVD from $[W(N^tBu)_2(NH^tBu)_2]$.[6] The compositions of the films varied, where the values of x varied from 0.7 (650 °C) to 1.8 (450 °C) and y < 0.2. The typical film compositions reported here are intermediate of these values, as these films were deposited at the intermediate temperature of 550 °C.

Substitution of the nitrogen bleed for ammonia resulted in moderately more nitrogen incorporation relative to the tungsten for compounds **2.1**, **2.2** and **2.4**, although this increase was not apparent for compound **2.3**, where the nitrogen content was reduced slightly when compared to the same compound in nitrogen. Generally, the carbon content was unaffected, with the exception of compound **2.2**, for which the carbon content was significantly reduced. The overall composition of this film was more comparable to the other films than that deposited with nitrogen. In all cases (nitrogen and ammonia) the chlorine content was less than 1 at.%, which is comparable with the ambient chlorine in the glass. With nitrogen as the bleed gas, the oxygen content of the films was approximately 20-25 at.% although this was reduced to 5 at.% on average with ammonia. The Si:O ratio for the glass was measured and this was

accounted for when looking at the oxygen content of the films. Therefore, the oxygen values should only be considered as approximate due to the oxygen content of the glass.

It is apparent that the presence of ammonia affects the reaction mechanism for **2.2**. Compounds **2.1-2.3** all have a $[W(N^tBu)_2Cl_2]$ fragment in common, and compound **2.4** is similar with a $[W(N^tBu)_2Cl]$ fragment, so it is possible that some of the ammonia is undergoing transamination with the amine ligands (**Eq. 3.1**).

$$[W(N^tBu)_2Cl_2(L)_n] \; + \; 2\,NH_3 \; \rightarrow \; [W(N^tBu)_2Cl_2(NH_3)_2] \; + \; n\,L \qquad \textbf{(3.1)}$$

This would explain the increase in nitrogen and reduction in carbon contents in the films formed from $[W(N^tBu)_2Cl_2(TMEDA)]$ (**2.2**). As mentioned before, the TGA curve of **2.2** showed a lower mass loss than expected for WN, suggesting that the TMEDA ligand is more tightly bound to the tungsten centre than, for example, the pyridine is in compound **2.3**. The result was that a significant amount of carbon resulted in the films from the TMEDA. Replacement of TMEDA with ammonia in the CVD apparatus showed a marked reduction in carbon content, comparable to the other compounds.

With $[W(\mu\text{-}N^tBu)(N^tBu)Cl_2(H_2N^tBu)]_2$ (**2.1**), there was no significant difference between the uses of nitrogen and ammonia bleed gases because the *tert*-butylamine ligand is very similar to ammonia in structure. The *tert*-butylamine is also sufficiently volatile to be carried out in the CVD exhaust rather than contaminating the film, however, the ^{t}Bu moiety may also be lost as isobutene under the high temperatures, leaving ammonia. It is perhaps less clear as to how this mechanism might occur with $[W(N^tBu)_2Cl_2(py)_2]$ (**2.3**), although the mass spectrum of **2.3** suggests that the pyridine ligands are readily lost, leaving the $[W(N^tBu)_2Cl_2]$ fragment to react with the ammonia. However, this does not explain how the nitrogen content was reduced, albeit not significantly.

The reaction of ammonia with $[W(N^tBu)_2Cl\{N(SiMe_3)_2\}]$ (**2.4**) is not as clear cut. The nitrogen content was increased slightly but there was no significant difference between the runs with nitrogen and ammonia, although a higher pressure of ammonia may have reduced the carbon content significantly. The design of the compound was

such that the facile loss of a Me_3SiCl molecule could occur when heated, followed by the loss of Me_3SiH. It is possible that transamination with ammonia does occur, whereby a $HN(SiMe_3)_2$ is lost, which might give similar results as compound **2.4** in nitrogen.

3.3.1.2. X-Ray Diffraction Studies

The glancing angle X-ray powder diffraction patterns of all the films showed peaks corresponding to the {111}, {200} and {220} planes of face-centred cubic β-WN_xC_y,[7,8] which is essentially a solid solution of β-W_2N and cubic WC_{1-x}. An example pattern is shown in **Figure 3.4**.

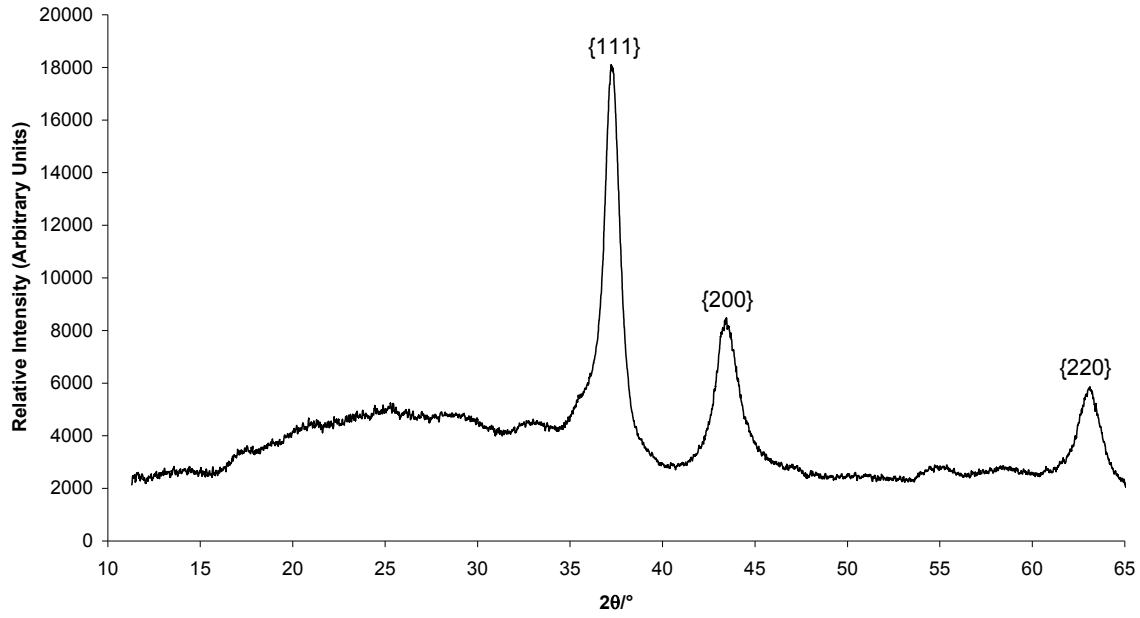

Figure 3.4 XRD pattern for the film deposited by $[W(\mu\text{-}N^tBu)(N^tBu)Cl_2(H_2N^tBu)]_2$ (**2.1**) with a nitrogen bleed.

There were no peaks present due to WO_x, WN, WC, tungsten or graphite, although the ratios obtained from WDX suggest that amorphous WN_x (or related phases) may be present in addition to the β-WN_xC_y crystalline component. The XRD patterns were broad due to the polycrystallinity of the films, which complicated the indexing process. As such, no direct comparison can be made between the XRD patterns of each film in

this case. However, the *a* values were in the range 4.13-4.15 Å, which lies between the lattice parameters values of W_2N (*a* = 4.12 Å)[9] and WC_{1-x} (a = 4.22-4.29 Å, depending on the carbon composition).[10]

3.3.1.3. Optical Properties

Reflection-transmission measurements of the films showed them to be generally non-transmitting throughout the spectrum although, where they were sufficiently thin, it was apparent that they were more transparent to infra-red light. The thicker films were highly reflective of any light although the thinner examples showed a fluctuation in reflection due to constructive interference during the measurements. An example is shown in **Figure 3.5**, where there is a false maximum at ~1000 nm and a false minimum at ~1500 nm.

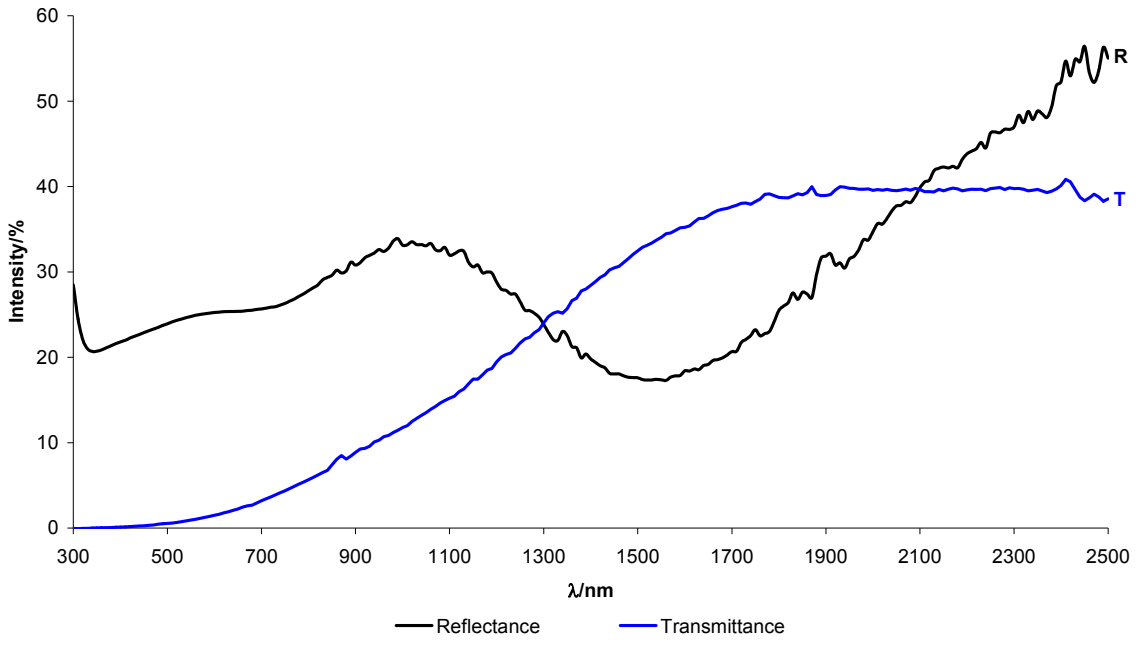

Figure 3.5 Reflectance-transmittance plots, referenced to the glass substrate, taken from a film deposited from $[W(N^tBu)_2Cl\{N(SiMe_3)_2\}]$ (**2.4**) with a nitrogen bleed.

3.3.1.4. Scanning Electron Microscopy

Scanning electron microscope (SEM) images of the films show concentric nodules approximately 100 nm in diameter (**Figure 3.6**). Smaller nodules, approximately 10 nm in diameter, were observed on the main structural features. The thicker exhibited larger nodules, for example, the nodules formed from compound **2.2** (B) were 200 nm in diameter in some cases, when compared to the film deposited from **2.4** (D), where the nodules were a more uniform 50-70 nm. This is consistent with the island growth mechanism and similar to WN_x, WC_y or WN_xC_y reported in the literature.[6,11,12]

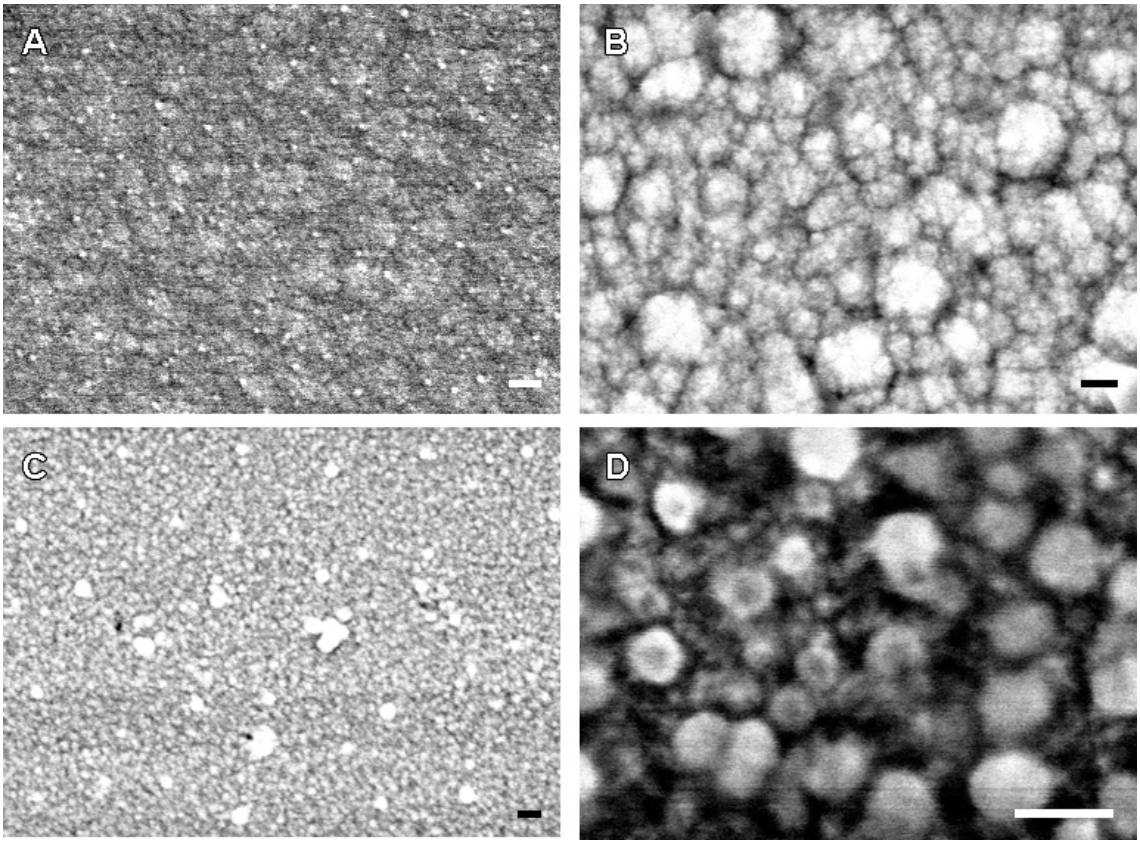

Figure 3.6 SEM images of films deposited with a nitrogen bleed gas. A = **2.1**, × 70,000; B = **2.2**, × 50,000; C = **2.3**, × 35,000; D = **2.4**, × 150,000. Bars = 100 nm.

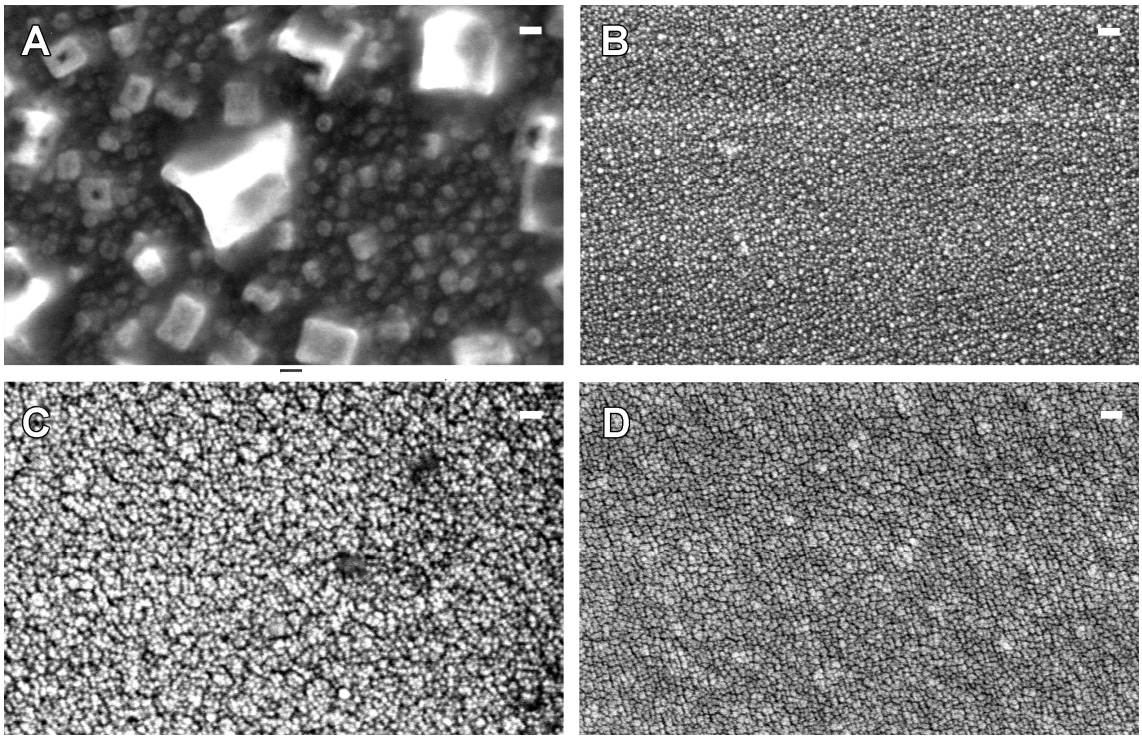

Figure 3.7 SEM images of films deposited with an ammonia bleed gas. A = **2.1**, × 45,000; B = **2.2**, × 40,000; C = **2.3**, × 45,000; D = **2.4**, × 40,000. Bars = 100 nm.

Where ammonia was used, generally the nodules were smaller (typically 20-40 nm in diameter, see **Figure 3.7**) than those observed with nitrogen, suggesting that ammonia affects the island growth mechanism by increasing the number of "islands", resulting in smaller nodules but more of them. The exception was with compound **2.1**, where cubic crystal-like structures were observed on top of larger nodules (~65 nm) although this was not observed with the other precursors. It is likely that the transamination occurring has a less significant effect on compound **2.1**, perhaps because the substitution of *tert*-butylamine for ammonia does not significantly change the shape or volatility of the compound. This corresponds to similar film compositions as described by the WDX data.

Side-on SEM images showed the films to be 120-650 nm thick, an example of which is shown in **Figure 3.8**. This also shows that, despite the nodules being smaller, some of the films are remarkably thick and uniform.

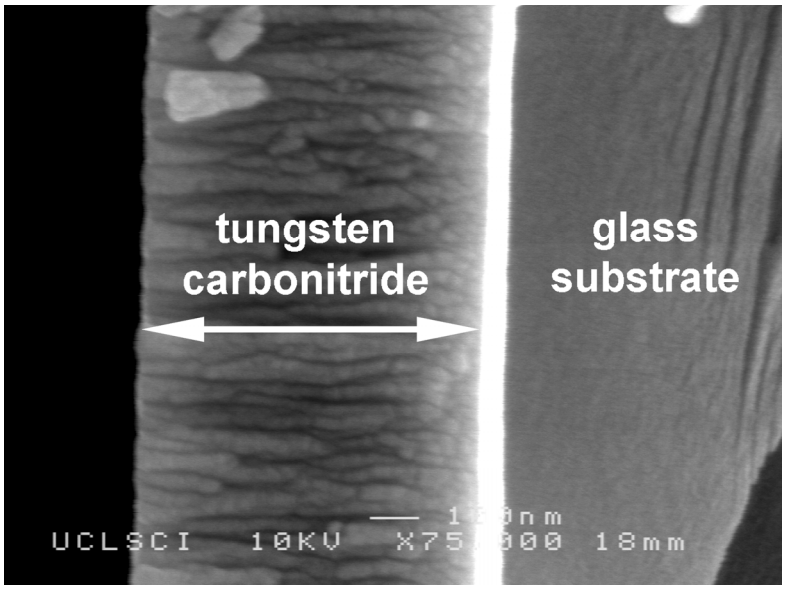

Figure 3.8 Side-on SEM image of the film deposited from $[W(N^tBu)_2Cl_2(py)_2]$ (**2.3**) and ammonia.

3.3.2. Aerosol-Assisted CVD Using $[W(\mu\text{-}N^tBu)(N^tBu)Cl_2(H_2N^tBu)]_2$ (2.1)

As described in section 3.3.1, compounds **2.1-2.4** are suitable as both single- and dual-source (with ammonia) precursors to tungsten carbonitride thin films *via* LPCVD. Aerosol-assisted (AA)CVD of $[W(\mu\text{-}N^tBu)(N^tBu)Cl_2(H_2N^tBu)]_2$ (**2.1**) was carried out in order to see how the effects of solvent in the AACVD process might affect the composition and morphologies of the films. The AACVD apparatus was set up such that there were two substrates, described as the top plate and bottom plate (refer to **Figure 3.3** for a diagram of the set up). The bottom plate was in direct contact with the graphite heating block, whereas the top plate was above, such that the gas flow travelled between the two glass plates. This resulted in a temperature difference; the top plate typically being 50-75 °C lower in temperature than the main substrate (the bottom plate).

The AACVD of **2.1** at 550 °C afforded a thick silver-black film on the bottom plate and a thin yellow ochre coloured film on the top plate. The films deposited were uniform and covered the substrate completely. The films were hard as they were not scratched by brass or steel styluses. They were not removed by tissues or Scotch tape, showing them to be adherent. There were no peaks present in the XRD patterns, suggesting that the films were amorphous, which is common in AACVD.[13]

WDX measurements suggested that tungsten carbonitride of average formula $WN_{0.41\pm0.21}C_{0.26\pm0.04}$ was formed on the bottom plate (where the substrate was directly heated), which was nitrogen-deficient compared to the films from the LPCVD of **2.1**. However, a tungsten film containing no nitrogen was present on the top plate (which was heated indirectly), although this film showed considerable chlorine contamination (14 at.%), whereas none was observed on the bottom plate. The carbon content was 3-4 at.% and the oxygen content varied from 4-28 at.%. It is unclear whether the oxygen was incorporated during the AACVD process, or afterwards on exposure to air.

SEM images of the films (**Figure 3.9**), showed island growth morphology on the bottom plate with nodules 300 nm in diameter, which is comparable to the films deposited by LPCVD, except that the nodules are larger in this case. The chlorine-rich film on the top plate comprised rod-like structures, approximately 200 nm in length and 70 nm in diameter.

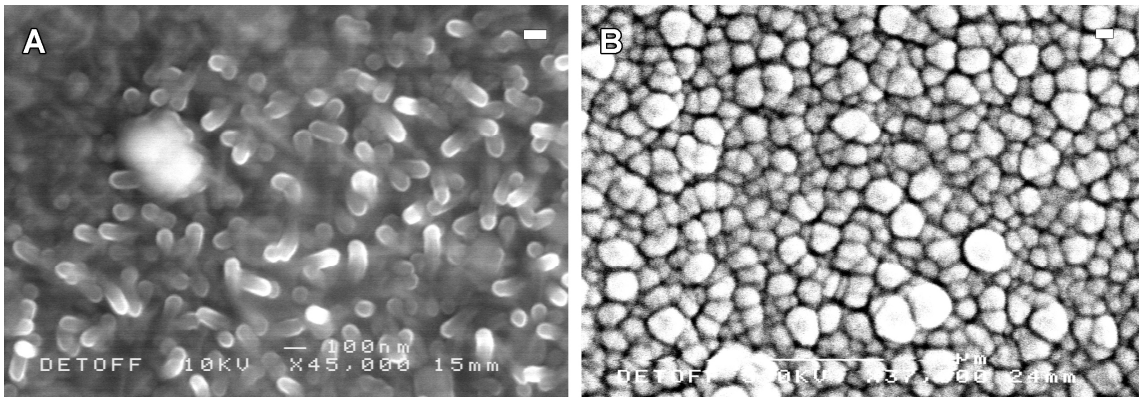

Figure 3.9 SEM images of the films resulting from the AACVD of $[W(\mu\text{-}N^tBu)(N^tBu)Cl_2(H_2N^tBu)]_2$ (**2.1**). A = top plate, × 45,000; B = bottom plate; × 37,000. Bars in top right = 100 nm.

3.3.3. LPCVD Using $[W(N^tBu)_2(\eta^5\text{-Cp'})(\eta^1\text{-Cp'})]$ (2.6)

LPCVD of compound **2.6** at 600 °C using a vapour-draw technique (as described in **Figure 3.2**) in a tube furnace afforded grey films with a metallic lustre that were very reflective. Black flakes were observed, which could be removed by wiping with a tissue, which was assumed to be deposits of amorphous graphite. The remaining film

could be scratched with brass and steel styluses, and it was not adhesive as it could be removed by Scotch tape.

The XRD pattern (**Figure 3.10**) showed one broad peak, which accounted for graphite, suggesting that the tungsten carbonitride was largely amorphous by this deposition method. However, it is possible that there are {111} and {200} peaks of β-WN_xC_y, although the graphite peak obscures them. The {220} peak is not visible due to the low concentration of polycrystalline tungsten carbonitride.

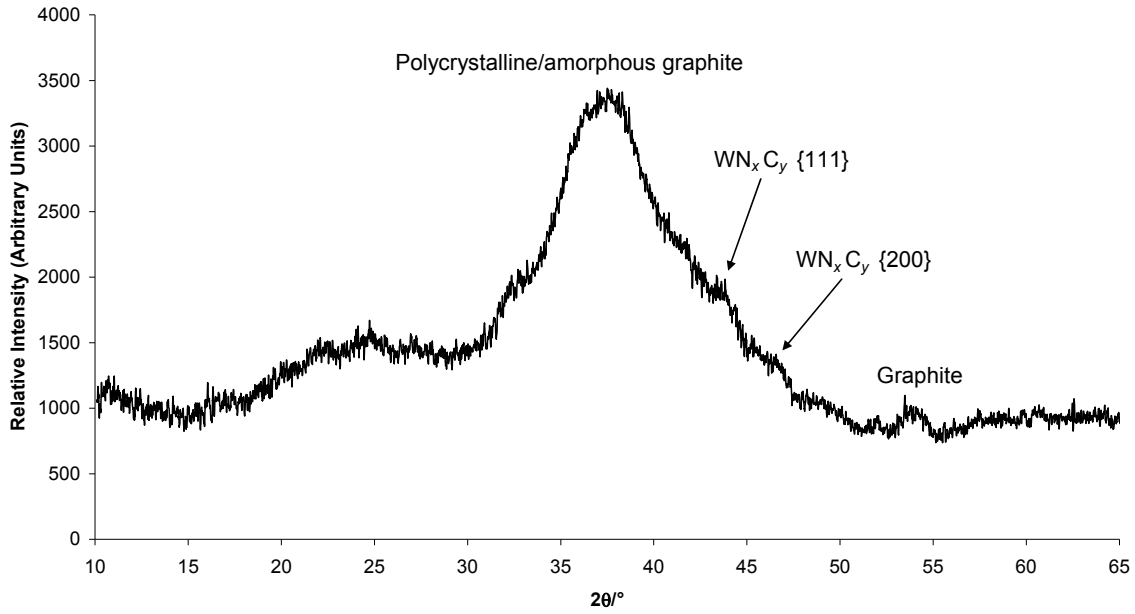

Figure 3.10 XRD pattern of the film deposited by the LPCVD of [W(N^{t}Bu)$_2$(η^5-Cp')(η^1-Cp')] (**2.6**).

WDX showed the average composition to be $WN_{1.02\pm0.40}C_{2.70\pm0.53}$, although a degree of the carbon can be attributed to the graphite. It is regions of graphite that might disrupt the tungsten carbonitride lattice, which results in a reduction of their hardness. In places, the nitrogen was a low as 13 at.% ($WN_{0.63}$) or as high as 27 at.% ($WN_{1.42}$), although carbon levels varied inversely to nitrogen. It is unsurprising that the nitrogen levels are lower than those reported for compounds **2.1-2.4**, as the higher substrate temperatures result in loss of molecular nitrogen.[6] In all films, the oxygen content was lower than 6 at.%.

The films showed a transmittance of ~40% throughout the spectrum until approximately 500 nm. An example is shown in **Figure 3.11**. They were generally reflective to infra-red light, becoming less so in the visible and ultraviolet wavelengths.

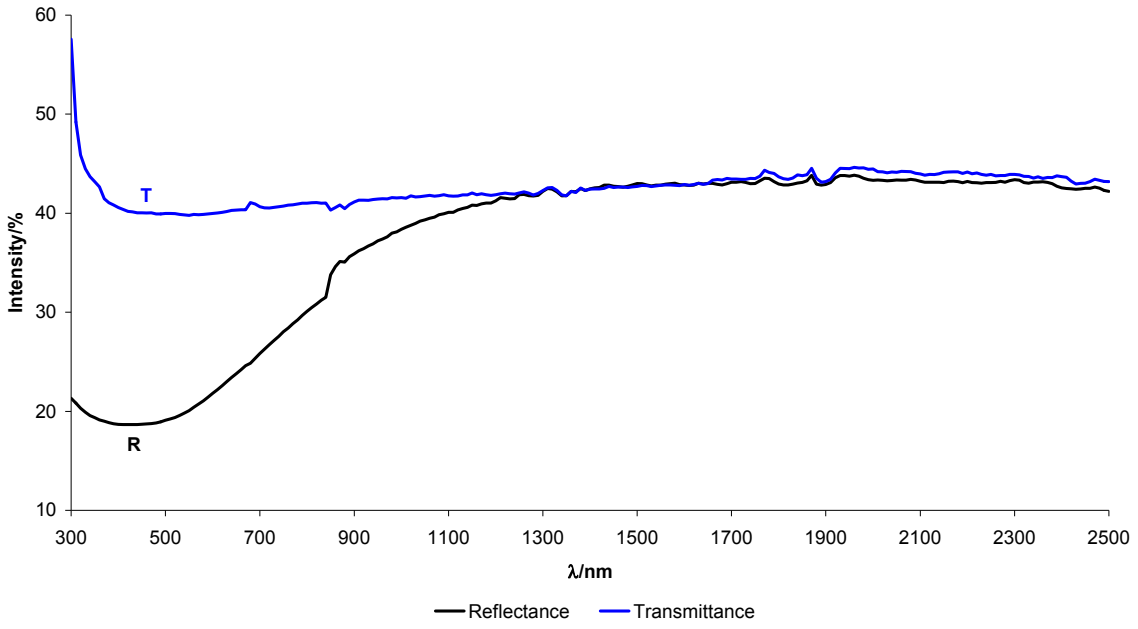

Figure 3.11 Reflectance-transmittance plots, referenced to the glass substrate, taken from a film deposited from [W(N^{t}Bu)$_2$(η^5-Cp')(η^1-Cp')] (**2.6**).

SEM images (**Figure 3.12**) of the films showed an island growth mechanism, similar to that seen with compounds **2.1-2.4**. However, cracks are visible due to the vapour-draw LPCVD method. With this in mind, the islands are estimated to be approximately 10-20 nm in diameter. Side-on SEM images showed the films to be 100-300 nm thick.

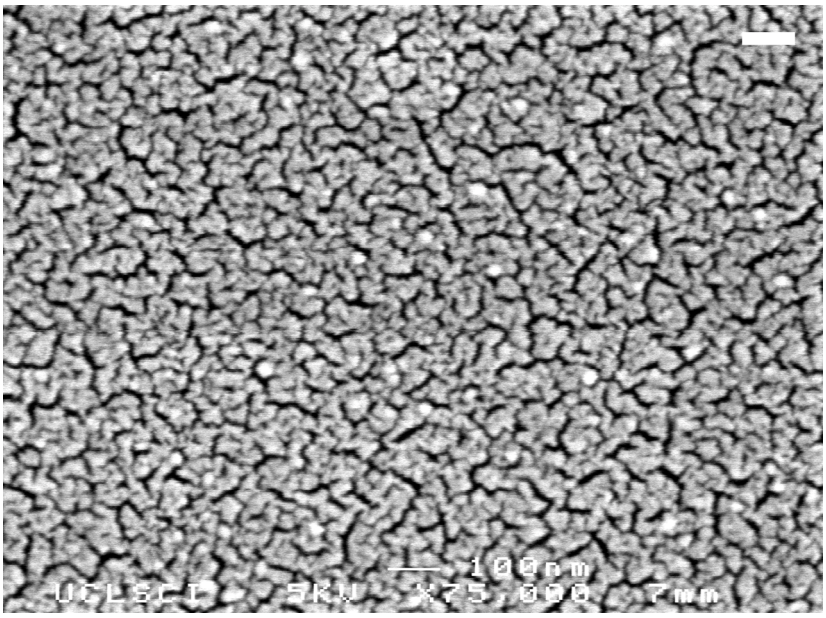

Figure 3.12 SEM image of the film deposited by [W(N^{t}Bu)$_2$(η^5-Cp')(η^1-Cp')] (**2.6**). × 75,000, bar = 100 nm.

3.4. Conclusions

Low pressure CVD (LPCVD) of compounds **2.1-2.4** onto glass substrates at 550 °C afforded highly reflective and adhesive films of polycrystalline tungsten carbonitride, which were generally nitrogen-rich. The use of ammonia as opposed to nitrogen did not affect the nitrogen levels in the films significantly, although it did reduce oxygen levels. Chlorine was notably absent from these films. Aerosol-assisted CVD (AACVD) of compound **2.1** in toluene gave reflective, amorphous films of average composition $WN_{0.41\pm0.21}C_{0.26\pm0.04}$, with negligible chlorine contamination. LPCVD of compound **2.6** onto glass at 600 °C using a vapour-draw afforded shiny grey non-adhesive films of carbon-rich tungsten carbonitride and graphite.

3.5. References

1. H. O. Pierson, *Handbook of Refractory Carbides and Nitrides. 3: Interstitial Carbides: Structure and Composition*. 1996: William Andrew Publishing. 17-54.
2. H. O. Pierson, *Handbook of Refractory Carbides and Nitrides. 11: Interstitial Nitrides: Properties and General Characteristics*. 1996: William Andrew Publishing. 181-208.

3. B. H. Weiller, *J. Am. Chem. Soc.*, 1996, **118**, 4975-4983.
4. L. McElwee-White, O. J. Bchir, K. C. Kim, T. J. Anderson, V. Craciun, B. C. Brooks, *J. Electrochem. Soc.*, 2004, **151**, G697-G703.
5. R. A. Fischer, E. Maile, *Chem. Vap. Deposition*, 2005, **11**, 409-414.
6. H. T. Chiu, S. H. Chuang, *J. Mater. Res.*, 1993, **8**, 1353-1360.
7. L. McElwee-White, O. J. Bchir, K. M. Green, M. S. Hlad, T. J. Anderson, B. C. Brooks, C. B. Wilder, D. H. Powell, *J. Organomet. Chem.*, 2003, **684**, 338-350.
8. K. Yong, S. Jeon, *Nanotechnology*, 2007, **18**, 245602.
9. M. D. Lyutaya, *Powder Metall. Met. Ceram.*, 1979, **18**, 190-196.
10. A. S. Kurlov, A. I. Gusev, *Inorg. Mater.*, 2006, **42**, 121-127.
11. K.-B. Kim, S.-H. Kim, S. S. Oh, H.-M. Kim, D.-H. Kang, W.-M. Li, S. Haukka, M. Tuominen, *J. Electrochem. Soc.*, 2004, **151**, C272-C282.
12. H. Volders, Z. Tökei, H. Bender, B. Brijs, R. Caluwaerts, L. Carbonell, T. Conard, C. Drijbrooms, A. Franquet, S. Garaud, I. Hoflijk, A. Moussa, F. Sinapi, Y. Travaly, D. Vanhaeren, G. Vereecke, C. Zhao, W.-M. Li, H. Sprey, A. M. Jonas, *Microelectron. Eng.*, 2007, **84**, 2460-2465.
13. C. J. Carmalt, I. P. Parkin, E. S. Peters, *J. Mater. Chem.*, 2004, **14**, 3474–3477.

4

Synthesis of Zirconium Carbonitride Precursors

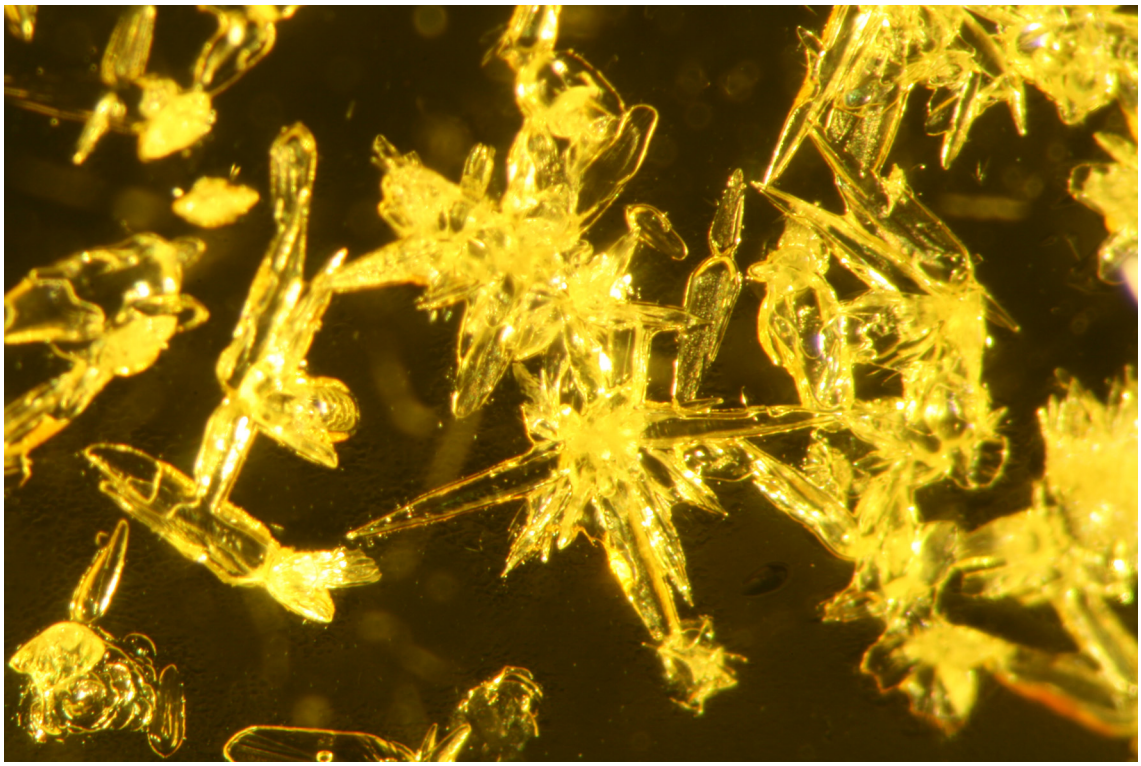

Figure 4.0 Sublimed crystals of $[ZrCp_2(NMe_2)_2]$ (**4.1**) taken using a digital camera microscope.

4.1. Introduction

This chapter examines and compares the synthesis of a selection of zirconium cyclopentadienyl compounds, $[ZrCp_2(NMe_2)_2]$ (**4.1**), $[ZrCp_2(\eta^2\text{-}MeNCH_2CH_2NMe)]$ (**4.2**), $[ZrCp'_2(NMe_2)_2]$ (**4.3**), $[ZrCp'_2(NEt_2)_2]$ (**4.4**), $[ZrCp'\{\eta^2\text{-}(^i PrN)_2CNMe_2\}_2Cl]$ (**4.5**) and $[ZrCp'_2\{\eta^2\text{-}(^i PrN)_2CNMe_2\}Cl]$ (**4.6**) (Cp = η^5-cyclopentadienyl, Cp' = η^5-methylcyclopentadienyl); as potential LPCVD and ALD precursors. Although compounds **4.1** and **4.3** have been reported previously,[1] they have not been employed as precursors to zirconium carbonitride. Compounds **4.2** and **4.4-4.6** are reported here for the first time. The rationale behind the use of cyclopentadienyl compounds as precursors is that the Cp and Cp' ligands should stabilise the metal centre, thereby improving the shelf-life of the precursor, but they should also leave the molecule intact in a CVD reactor. Liquid injection CVD and ALD of HfO_2 using $[HfCp'_2(Me)(OR)]$ (R = ^{i}Pr, $CMe_2(CH_2OMe)$) has been reported,[2] which shows that cyclopentadienyl compounds have been successful as precursors.

4.2. Experimental

4.2.1. General Procedures

All reactions were performed under a dry, oxygen-free nitrogen atmosphere using standard Schlenk techniques and an Mbraun Unilab glove box. Nitrogen (99.99%) was obtained from BOC and used as supplied. All solvents were stored in alumina columns and dried with anhydrous engineering equipment, such that the water concentration was 5-10 ppm. All reagents were procured from Sigma Aldrich, except for $ZrCl_4$, $[ZrCl_4(THF)_2]$ and zirconocene dichloride, which were purchased from Strem. $[Zr(NMe_2)_4]$ and $[Zr(NEt_2)_4]$ were kindly donated by SAFC Hitech Ltd. $[ZrCl_2(NR_2)_2(THF)_2]$ (R = Me, Et)[3] and $[ZrCl_2\{\eta^2\text{-}(^i PrN)_2CNMe_2\}_2]$[4] were prepared by published procedures. [NaCp'(THF)] was prepared as described in Chapter 2. *N*,*N*'-dimethylethylenediamine was degassed and stored over 3 Å molecular sieves under nitrogen. All other compounds were used without further purification.

4.2.2. Physical Measurements

Microanalytical data were obtained at University College London (UCL). NMR spectra were recorded on Bruker AMX500 or ADVANCE III 600 spectrometers, referenced to C_6D_6 distilled over benzophenone or dried and degassed deuterated dimethyl sulphoxide (DMSO-d_6). ^{1}H and $^{13}C\{^{1}H\}$ chemical shifts are reported relative to $SiMe_4$ ($\delta = 0.00$ ppm). FT-IR spectra were recorded on a Perkin Elmer Spectrum RX I instrument, over the range 4000-400 cm^{-1}. Mass spectra were recorded on a Micromass ZABSE instrument. Thermogravimetric analysis (TGA) was performed on a Netzsh STA 449C instrument. The TGA was carried out in aluminium pans at atmospheric pressure, under a flow of helium gas. The rate of heating was 10 °C min^{-1}. Vapour pressure measurements were carried out at SAFC Hitech Ltd. on custom-built apparatus. For crystal structures, geometric and intensity data was obtained on Bruker SMART APEX CCD diffractometer using graphite-monochromated Mo-Kα radiation ($\lambda_1 = 0.71073$ Å) at 150(2) K.

4.2.3. Synthesis of Starting Materials

4.2.3.1. Synthesis of $[Li_2(MeNCH_2CH_2NMe)]$

^{n}BuLi (59.0 cm^3, 1.6 M in hexane, 94.40 mmol) was diluted with hexane (40 cm^3). This was added dropwise to a stirred colourless solution of *N*,*N*'-dimethylethylenediamine (5.0 cm^3, 4.10 g, 46.51 mmol) in hexane (60 cm^3), which was cooled to -78 °C. A white precipitate formed after about 30 s. The mixture was stirred for 4 h, after which time it was cooled to -20 °C for 18 h. The supernatant solution was decanted off and the precipitate was dried under vacuum, affording a white powder (yield = 4.38 g, 94 %). **Anal. Calc.** for $C_4H_{10}N_2Li_2$: C, 48.03; H, 10.08; N, 28.01%. **Found:** C, 48.69; H, 10.66; N, 27.18%. **^{1}H NMR** δ/ppm (DMSO-d_6, 600 MHz): 2.21 (s, 6H, NCH_3), 2.48 (s, 4H, CH_2NMe). **$^{13}C\{^{1}H\}$ NMR** δ/ppm (DMSO-d_6, 600 MHz): 36.1 (NCH_3), 50.9 (CH_2NMe). **FT-IR** and **mass spectrometry** data are not available due to the highly air-sensitive nature of this compound.

4.2.3.2. Synthesis of [ZrCp'$_2$Cl$_2$]

A pink solution of [NaCp'(THF)] (18.50 g, 0.11 mol) in THF (160 cm^3) was added slowly to a stirred suspension of [$ZrCl_4(THF)_2$] (20.00 g, 53.02 mmol) in THF (160 cm^3), which was cooled to -78 °C. The mixture was allowed to warm to room temperature, after which time it was heated under reflux for 18 h. After cooling, the clear orange solution was filtered off and the pale orange residue was dried under vacuum. The residue was then sublimed at 180 °C, 0.1 Torr, affording a pale orange powder (yield = 10.23 g, 60%). **Anal. Calc.** for $C_{12}H_{14}Cl_2Zr$: C, 44.99; H, 4.40%. **Found:** C, 44.31; H, 4.37%. **^{1}H NMR** δ/ppm (C_6D_6, 600 MHz): 2.10 (s, 6H, $C_5H_4(CH_3)$), 5.66 (m, 4H, 3-C_5H_4Me) 5.78 (s, 4H, 2-C_5H_4Me). **^{13}C{^{1}H} NMR** δ/ppm (C_6D_6, 600 MHz): 15.52 ($C_5H_4CH_3$), 112.0 (3-C_5H_4Me), 117.5 (2-C_5H_4Me), 129.9 (1-C_5H_4Me). **FT-IR** cm^{-1} (KBr disc, nujol): 3103 w (aromatic C–H stretch), 2963 vs (C–H stretch) 2891 vs (C–H stretch), 2846 vs (C–H stretch), 1630 w (aromatic C=C stretch), 1464 s, 1378 s, 1260 w, 1154 w, 1089 m, 1016 w, 952 w, 722 w, 665 w, 439 m, 423 m, 413 s, 410 s, 406 m. **Mass Spec.** m/z (CI+, methane): 283 $[M - Cl]H^+$, 318 $[M]H^+$, 604 $[M_2 - Cl]H^+$.

4.2.4. Precursor Synthesis

4.2.4.1. Synthesis of [ZrCp$_2$(NMe$_2$)$_2$] (4.1)

A Schlenk flask was charged with zirconocene dichloride (10.00 g, 34.21 mmol) and lithium dimethylamide (4.36 g, 85.25 mmol). Hexane (400 cm^3) was cooled to -78 °C and was then added slowly to the reagents with stirring. The pale yellow mixture was allowed to warm to room temperature and was then heated under reflux for 18 h. The yellow mixture was allowed to cool and settle and the amber solution was filtered off. This was then reduced to dryness under vacuum to give a crude amber product. The product was then sublimed onto a cold finger at 85 °C at 0.1 Torr affording a canary yellow powder (yield = 5.37 g, 51%). **Anal. Calc.** for $C_{14}H_{22}N_2Zr$: C, 54.32; H, 7.16; N, 9.05%. **Found:** C, 52.39; H, 7.13; N, 9.40%. **^{1}H NMR** δ/ppm (C_6D_6, 500 MHz): 2.83 (s, 12H, $N(CH_3)_2$), 5.85 (s, 10H, C_5H_5). **^{13}C{^{1}H} NMR** δ/ppm (C_6D_6, 500 MHz): 49.3 ($N(CH_3)_2$), 109.8 (C_5H_5). **FT-IR** cm^{-1} (KBr disc, nujol): 3087 w (aromatic C–H stretch), 2941 s (C–H stretch), 2924 vs (C–H stretch), 2854 s (C–H stretch), 2810 sh w

(C–H stretch), 2759 w (C–H stretch), 1592 br w (C=C stretch), 1458 sh m, 1456 m, 1444 sh m, 1378 m, 1262 m, 1230 w, 1116 m, 1093 m, 1057 m, 1015 s, 939 m, 793 s, 738 sh m, 651 w, 635 w, 528 w, 425 s, 410 s. **Mass Spec.** *m/z* (CI+, methane): 265 [M - NMe_2]H^+, 309 [M]H^+. **TGA:** mass loss 67% (calc. ZrN, 67%; Zr_3N_4, 65%) at 590 °C.

4.2.4.2. Synthesis of [$ZrCp_2(\eta^2$-$MeNCH_2CH_2NMe)$] (4.2)

A Schlenk flask was charged with zirconocene dichloride (10.00 g, 34.21 mmol) and [$Li_2(MeNCH_2CH_2NMe)$] (3.76 g, 37.56 mmol). Hexane (400 cm^3) was cooled to -78 °C and was then added slowly to the reagents with stirring. The pale pink mixture was allowed to warm to room temperature and was then heated under reflux for 18 h. The deep red mixture was allowed to cool and settle and the red solution was filtered off. This was then reduced to dryness under vacuum to give a deep red glassy solid (yield = 6.01 g, 57%). **Anal. Calc.** for $C_{14}H_{20}N_2Zr$: C, 54.67; H, 6.55; N, 9.11%. **Found:** C, 53.49; H, 6.47; N, 7.36%. **^{1}H NMR** δ/ppm (C_6D_6, 600 MHz): 2.50 (s, 6H, NCH_3), 3.24 (s, 4H, CH_2NMe), 6.03 (s, 10H, C_5H_5). **^{13}C{^{1}H} NMR** δ/ppm (C_6D_6, 600 MHz): 43.9 (NCH_3), 60.0 (CH_2NMe), 111.8 (C_5H_5). **FT-IR** cm^{-1} (KBr disc, nujol): 3085 w (aromatic C–H stretch), 2941 s (C–H stretch), 2923 s (C–H stretch), 2854 s (C–H stretch), 2756 w (C–H stretch), 1600 br w (C=C stretch), 1456 m, 1378 m, 1261 m, 1152 sh w, 1090 m, 1918 m, 937 w, 932 w, 861 w, 797 s, 733 sh w, 630 w, 427 vs, 408 s. **Mass Spec.** *m/z* (CI+, methane): 220 [M - $MeNCH_2CH_2NMe$]H^+, 241 [M - Cp]H^+, 255, 263 [M - CH_2NMe]H^+, 305 [M - H]H^+, 306 [M]H^+. **TGA:** mass loss 70% (calc. ZrN, 66%; Zr_3N_4, 64%) at 590 °C.

4.2.4.3. Synthesis of [$ZrCp'_2(NMe_2)_2$] (4.3)

A pink solution of [NaCp'(THF)] (4.90 g, 28.13 mmol) in THF (100 cm^3) was added dropwise to a stirred solution of [$ZrCl_2(NMe_2)_2(THF)_2$] (5.00 g, 12.67 mmol) in diethyl ether (100 cm^3), which was cooled to -78 °C. The turbid amber mixture was stirred for 18 h and was then heated under reflux for 1 h with stirring. The THF and diethyl ether were then removed under vacuum and the pale yellow solid was resuspended in hexane (100 cm^3). The NaCl was allowed to settle out and then the yellow solution was filtered. The filtrate was reduced to dryness under vacuum affording a yellow solid (yield = 3.75 g, 88%). **Anal. Calc.** for $C_{16}H_{26}N_2Zr$: C, 56.92; H, 7.76; N, 8.30%.

Found: C, 56.48; H, 7.74; N, 8.79%. **^{1}H NMR** δ/ppm (C_6D_6, 500 MHz): 1.96 (s, 6H, $C_5H_4(CH_3)$), 2.84 (s, 12H, $N(CH_3)_2$), 5.77 (m, 8H, C_5H_4Me). **$^{13}C\{^1H\}$ NMR** δ/ppm (C_6D_6, 500 MHz): 14.6 ($C_5H_4(CH_3)$), 49.2 ($N(CH_3)_2$), 108.7 (3-C_5H_4Me), 112.1 (2-C_5H_4Me), 121.0 (1-C_5H_4Me). **FT-IR** cm^{-1} (KBr disc, nujol): 3074 w (aromatic C–H stretch), 2942 s (C–H stretch), 2924 vs (C–H stretch), 2854 s (C–H stretch), 2759 (C–H stretch), 1578 br w (C=C stretch), 1496 w, 1461 m, 1420 w, 1377 m, 1262 m, 1232 w, 1095 br m, 1022 m, 938 w, 849 sh w, 793 m, 727 m, 646 w, 618 w, 422 vs, 408 vs. **Mass Spec.** m/z (CI+, methane): 257 [M - Cp']H$^+$, 291 [M - NMe_2]H$^+$, 336 [M]H$^+$. **TGA:** mass loss 63% (calc. ZrN, 69%; Zr_3N_4, 67%) at 590 °C.

4.2.4.4. Synthesis of [ZrCp'$_2$(NEt$_2$)$_2$] (4.4)

A pink solution of [NaCp'(THF)] (2.87 g, 13.62 mmol) in THF (60 cm^3) was added dropwise to a stirred pale orange solution of [$ZrCl_2(NEt_2)_2(THF)_2$] (3.00 g, 6.66 mmol) in THF (60 cm^3), which was cooled to -78 °C. The dark orange mixture was stirred for 18 h and was then heated under reflux for 1 h with stirring. The THF was then removed under vacuum and the dark orange oil was resuspended in hexane (120 cm^3). The NaCl was allowed to settle out and then the yellow solution was filtered. The filtrate was reduced to dryness under vacuum affording a yellow solid (yield = 1.81 g, 69%). **Anal. Calc.** for $C_{20}H_{34}N_2Zr$: C, 61.01; H, 8.70; N, 7.12%. **Found:** C, 59.21; H, 8.58; N, 7.81%. **^{1}H NMR** δ/ppm (C_6D_6, 600 MHz): 0.98 (t, $^3J_{HH}$ = 6.96 Hz, 12H, $N(CH_2CH_3)_2$), 2.04 (s, 6H, $C_5H_4(CH_3)$), 3.24 (q, $^3J_{HH}$ = 6.92 Hz, 8H, $N(CH_2Me)_2$), 5.73 (m, 4H, 3-C_5H_4Me) 5.85 (s, 4H, 2-C_5H_4Me). **$^{13}C\{^1H\}$ NMR** δ/ppm (C_6D_6, 600 MHz): 15.2 ($C_5H_4CH_3$ and $N(CH_2CH_3)_2$), 48.0 ($N(CH_2Me)_2$), 108.0 (3-C_5H_4Me), 113.0 (2-C_5H_4Me), 119.6 (1-C_5H_4Me). **FT-IR** cm^{-1} (KBr disc, nujol): 3078 br w (aromatic C–H stretch), 2941 s (C–H stretch), 2925 vs (C–H stretch), 2854 s (C–H stretch), 1590 br w (C=C stretch), 1478 w, 1460 m, 1377 m, 1261 m, 1178 sh w, 1138 sh w, 1094 br m, 1036 br m, 935 w, 856 sh w, 788 s, 728 s, 645 w, 566 w, 436 s, 418, vs, 410 s, 405 s. **Mass Spec.** m/z (CI+, methane): 283, 311 [M - Cp'H]H$^+$, 318, 321 [M - NEt_2]H$^+$, 331, 392 [M - H]H$^+$, 393 [M]H$^+$, 394 [M + H]H$^+$. **TGA:** mass loss 42% (calc. ZrN, 74%; Zr_3N_4, 72%) at 590 °C.

4.2.4.5. Synthesis of [ZrCp'{η^2-(^{i}PrN)$_2$CNMe$_2$}$_2$Cl] (4.5)

A pink solution of [NaCp'(THF)] (1.57 g, 9.01 mmol) in THF (100 cm^3) was added slowly to a stirred colourless solution of [ZrCl$_2${η^2-(^{i}PrN)$_2$CNMe$_2$}$_2$] (3.50 g, 9.01 mmol) in diethyl ether (100 cm^3), which was cooled to -78 °C. The solution was stirred for 18 h at room temperature before the solution was reduced to dryness under vacuum. The resulting yellow oil was resuspended in hexane (200 cm^3) and the NaCl was allowed to settle. The yellow solution was filtered off and reduced until small amounts of solid material were observed. This was then cooled to -20 °C overnight, affording pale orange X-ray quality crystals (yield = 2.94 g, 60%). The crystals were only stable at 10 °C and below. Above this temperature the product was a glassy orange-yellow solid. **Anal. Calc.** for $C_{24}H_{47}N_6ClZr$: C, 52.76; H, 8.67; N, 15.38%. **Found:** C, 52.77; H, 8.66; N, 16.01%. **^{1}H NMR** δ/ppm (C_6D_6, 600 MHz): 1.04 (d, $^3J_{HH}$ = 5.70 Hz, 3H, NCH(C*H*$_3$)), 1.18 (d, $^3J_{HH}$ = 5.82 Hz, 3H, NCH(C*H*$_3$)), 1.24 (d, $^3J_{HH}$ = 5.64 Hz, 3H, NCH(C*H*$_3$)), 1.33 (m, 9H, NCH(C*H*$_3$)), 1.41 (d, $^3J_{HH}$ = 6.12 Hz, 3H, NCH(C*H*$_3$)), 1.48 (d, $^3J_{HH}$ = 5.64 Hz, 3H, NCH(C*H*$_3$)), 2.40 (s, 12H, CN(C*H*$_3$)$_2$), 2.54 (s, 3H, C$_5$H$_4$(C*H*$_3$)), 3.57 (m, 1H, NC*H*Me$_2$), 3.71 (m, 2H, NC*H*Me$_2$), 3.97 (m, 1H, NC*H*Me$_2$), 6.22 (m, 2H, 3-C$_5$*H*$_4$Me) 6.39 (br s, 2H, 2-C$_5$*H*$_4$Me). **^{13}C{^{1}H} NMR** δ/ppm (C_6D_6, 600 MHz): 16.6 (C$_5$H$_4$*C*H$_3$), 23.9 (NCH(*C*H$_3$)), 24.4 (NCH(*C*H$_3$)), 24.6 (NCH(*C*H$_3$)), 25.4 (NCH(*C*H$_3$)), 25.7 (NCH(*C*H$_3$)), 40.2 (N(*C*H$_3$)$_2$), 47.0 (N*C*HMe$_2$), 47.5 (N*C*HMe$_2$), 48.3 (N*C*HMe$_2$), 49.1 (N*C*HMe$_2$), 111.3 (3-*C*$_5$H$_4$Me), 111.6 (3-*C*$_5$H$_4$Me), 113.3 (2-*C*$_5$H$_4$Me), 113.5 (2-*C*$_5$H$_4$Me), 115.6 (1-*C*$_5$H$_4$Me), 164.5 ((^{i}PrN)$_2$*C*NMe$_2$), 171.4 ((^{i}PrN)$_2$*C*NMe$_2$). **FT-IR** cm^{-1} (KBr disc, nujol): 3096 w (aromatic C–H stretch), 2987 s (C–H stretch), 2976 s (C–H stretch), 2930 m (C–H stretch), 2869 m (C–H stretch), 2794 m, 1632 w (C=C stretch), 1546 br s, 1480 br vs, 1404 vs, 1360 br vs, 1262 m, 1193 vs, 1169 s, 1129 s, 1053 vs, 980 m, 940 w, 846 m, 790 vs, 739 m, 727 m, 694 w, 612 w, 540 w, 435 s, 428 s, 422 m, 416 s, 403 s. **Mass Spec.** m/z (CI+, methane): 172 [H(^{i}PrN)$_2$CNMe$_2$]H$^+$, 511 [M - Cl]H$^+$, 514 [M - 2 Me]H$^+$, 545 [M]H$^+$. **TGA:** mass loss 74% (calc. ZrN, 81%; Zr_3N_4, 80%) at 590 °C.

4.2.4.6. Synthesis of [ZrCp'$_2${η^2-(^{i}PrN)$_2$CNMe$_2$}Cl] (4.6)

A colourless solution of diisopropyl carbodiimide (2.45 cm^3, 2.00 g, 15.85 mmol) in THF (100 cm^3) was added slowly to a stirred slurry of $LiNMe_2$ (0.80 g, 15.68 mmol) in THF (100 cm^3), which was cooled to 0 °C. Once all the $LiNMe_2$ had dissolved, the solution was stirred for 2 h at room temperature. After this time, the pale yellow solution was added slowly to a stirred orange solution of [ZrCp'$_2$Cl$_2$] (5.00 g, 15.61 mmol) in THF (300 cm^3), which was cooled to -78 °C. The turbid orange mixture was then stirred for 18 h at room temperature, after which the solvent was removed under vacuum and the resulting pale orange-yellow solid was dissolved in hexane (300 cm^3). The yellow solution was filtered and the filtrate reduced to dryness under vacuum, giving an orange-beige solid (yield = 4.69 g, 66%). X-ray quality crystals were grown from a solution of the compound (*ca.* 0.25 g) in hexane (30 cm^3) kept at -20 °C for approximately one week. **Anal. Calc.** for $C_{21}H_{34}N_3ClZr$: C, 55.41; H, 7.53; N, 9.23%. **Found:** C, 55.12; H, 7.45; N, 10.21%. **^{1}H NMR** δ/ppm (C_6D_6, 600 MHz): 1.19 (d, $^3J_{HH}$ = 6.72 Hz, 6H, NCH(CH_3)$_2$) 1.48 (d, $^3J_{HH}$ = 6.66 Hz, 6H, NCH(CH_3)$_2$), 2.21 (s, 6H, CN(CH_3)$_2$), 2.24 (s, 6H, C$_5$H$_4$(CH_3)), 2.97 (sept., $^3J_{HH}$ = 6.72 Hz, 1H, NC*H*Me$_2$), 3.43 (sept., $^3J_{HH}$ = 6.66 Hz, 1H, NC*H*Me$_2$), 5.56 (m, 2H, 3-C$_5$*H*$_4$Me), 5.64 (m, 2H, 2-C$_5$*H*$_4$Me), 5.78 (m, 2H, 3-C$_5$*H*$_4$Me), 5.88 (m, 2H, 2-C$_5$*H*$_4$Me). **^{13}C{^{1}H} NMR** δ/ppm (C_6D_6, 600 MHz): 15.8 (C$_5$H$_4$(*C*H$_3$)), 24.3 (NCH(*C*H$_3$)$_2$), 24.6 (NCH(*C*H$_3$)$_2$), 40.9 (CN(*C*H$_3$)$_2$), 48.1 (N*C*HMe$_2$), 48.9 (N*C*HMe$_2$), 105.9 (3-*C*$_5$H$_4$Me), 109.5 (2-*C*$_5$H$_4$Me), 115.2 (3-*C*$_5$H$_4$Me), 116.9 (2-*C*$_5$H$_4$Me), 123.4 (1-*C*$_5$H$_4$Me), 165.8 ((^{i}PrN)$_2$*C*NMe$_2$). **FT-IR** cm^{-1} (KBr disc, nujol): 3100 w (aromatic C–H stretch), 2925 vs (C–H stretch), 2854 s (C–H stretch), 2790 (C–H stretch), 1621 br w (C=C stretch), 1527 m, 1487 m, 1460 m, 1411 m, 1377 m, 1354 m, 1272 sh w, 1262 m, 1197 m, 1157 w, 1124 m, 1059 m, 1043 m, 974 w, 931 vw, 867 w, 801 s, 725 w, 418 vs, 405 m. **Mass Spec.** m/z (CI+, methane): 172 [H(^{i}PrN)$_2$CNMe$_2$]H$^+$, 419 [M - Cl]H$^+$, 454 [M]H$^+$, 505, 549, 587. **TGA:** mass loss 84.5% (calc. ZrN, 77%; Zr_3N_4, 76%) at 590 °C.

4.3. Results and Discussion

4.3.1. Synthesis of Precursors

Zirconocene bis(dimethylamide), $[ZrCp_2(NMe_2)_2]$ (**4.1**), was synthesised in good yields *via* a lithium metathesis reaction between zirconocene dichloride and lithium dimethylamide, as initially reported by Lappert in 1968.[1] Compound **4.2**, $[ZrCp_2(\eta^2\text{-}MeNCH_2CH_2NMe)]$, was synthesised using the same metathesis principle. *N,N'*-dimethylethylenediamine was treated with two equivalents of *n*-butyl lithium to give the dilithium salt, which was then heated under reflux with zirconocene dichloride to give **4.2** as a deep red glassy solid. The syntheses of compounds **4.1** and **4.2** are summarised in **Scheme 4.1**.

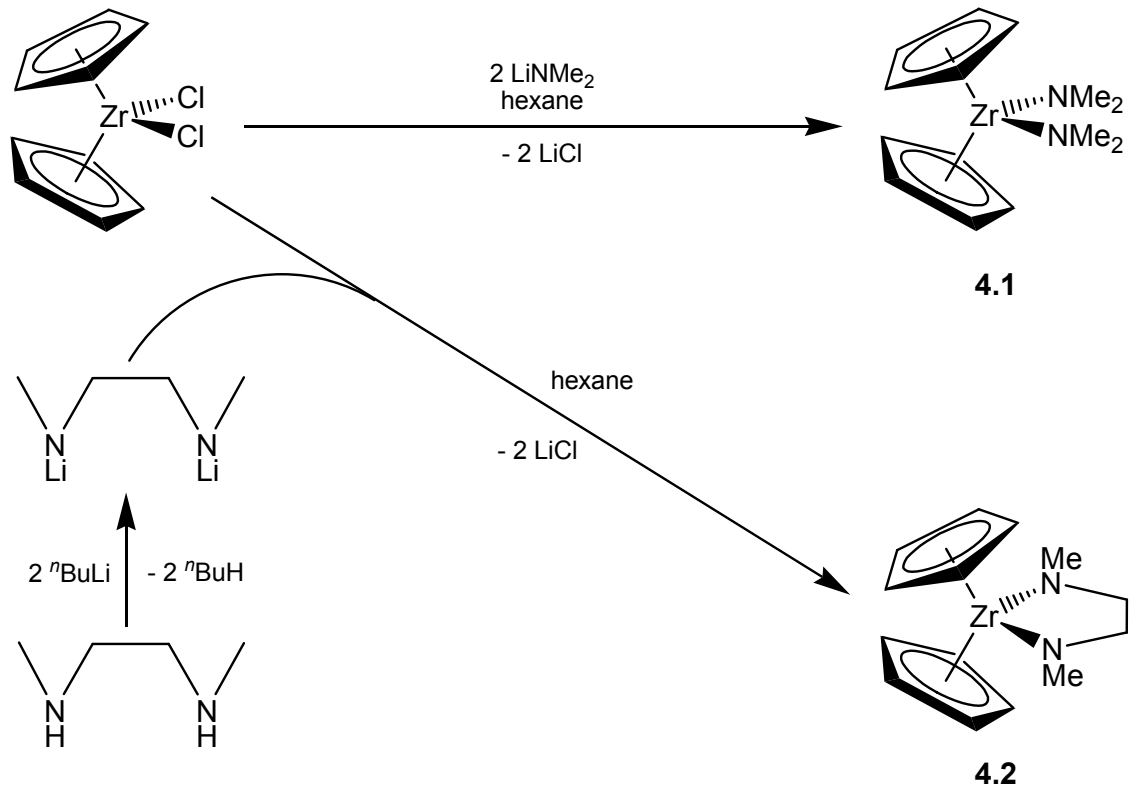

Scheme 4.1 Synthetic routes to compounds **4.1** and **4.2**.

The proton NMR of **4.2** spectrum showed a singlet at 6.03 ppm integrated to ten protons, assigned to the cyclopentadienyl ligands, and 2.50 and 3.24 ppm, assigned to

the methyl group and the CH_2CH_2 backbone of the ligand respectively. Purification of this compound was problematic, as some unreacted [$Li_2(MeNCH_2CH_2NMe)$] would frequently be drawn through the filter (which either comprised a filter cannula sealed with glass paper or celite over a glass frit). The lithium salt was also sufficiently volatile to be sublimed with compound **4.2**. Therefore, for analytical purposes, the product was filtered twice in an attempt to reduce this contamination.

Methylcyclopentadienyl molecules might prove more effective as ligands for CVD precursors as the methyl group should disrupt the packing in the solid, rendering it more volatile than cyclopentadienyl analogues. Lappert's paper mentioned the methylcyclopentadienyl analogue of **4.1**, [$ZrCp'_2(NMe_2)_2$] (**4.3**),[1] which was also synthesised by a metathesis route, although it was described as "a reddish-brown, waxy solid" rather than a yellow powder. An alternative synthesis was attempted in this work whereby [$ZrCl_2(NMe_2)(THF)_2$] was synthesised *via* the Schlenk equilibrium between $ZrCl_4$ and [$Zr(NMe_2)_4$] as described by Kempe *et al*. (**Eq. 4.1**).[3]

$$ZrCl_4 + [Zr(NMe_2)_4] + 4\ THF \rightleftharpoons 2\ [ZrCl_2(NMe_2)(THF)_2] \qquad \textbf{(4.1)}$$

This was then treated with two equivalents of sodium methylcyclopentadienide and heated under reflux for one hour, affording [$ZrCp'_2(NMe_2)_2$] (**4.3**) as a yellow powder. The elemental analysis was in close agreement with the proposed formula and peaks at 1.96 and 5.77 ppm in the proton NMR spectrum account for the methyl substituent on the cyclopentadienyl rings and the aromatic protons respectively. The peak corresponding to NMe_2 ligand was at 2.84 ppm. In the mass spectrum, the parent ion peak was the most intense at *m/z* = 336, although there were peaks at *m/z* = 257 and 291, accounting for the loss of a methylcyclopentadienyl ligand and a dimethylamido ligand respectively. Compound **4.4**, [$ZrCp'_2(NEt_2)_2$], was synthesised as a yellow powder in an analogous fashion by the reaction of [$ZrCl_2(NEt_2)(THF)_2$] with two equivalents of sodium methylcyclopentadienide. The NMR spectra were comparable to those of **4.3**, with a triplet at 0.98 ppm and a quartet at 3.24 ppm corresponding to the NCH_2CH_3 and NCH_2CH_3 protons respectively on the NEt_2 moieties. The peaks at 2.04

ppm, corresponding to the methyl substituent on the cyclopentadienyl rings, is comparable to that for compound **4.3**, but in case of **4.4** the aromatic protons are resolved into two peaks at 5.73 and 5.85 ppm. The syntheses of compounds **4.3-4.5** are summarised in **Scheme 4.2**.

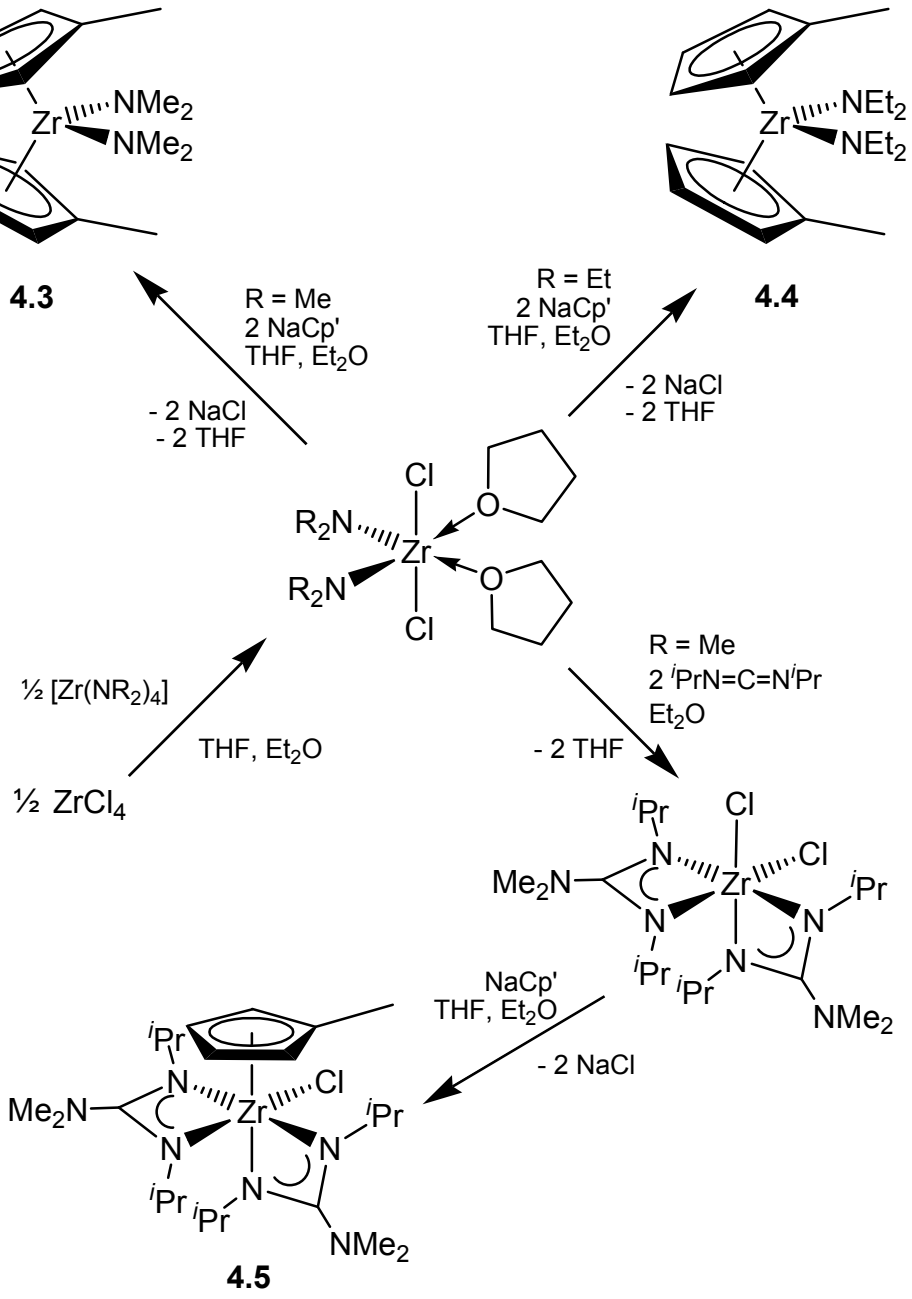

Scheme 4.2 Synthetic routes to compounds **4.3-4.5**.

In order to increase the nitrogen in the coordination sphere, use of hydrazido or guanidinate ligands was the next step. However, reactions of zirconocene dichloride with [Li{N(H)NMe$_2$}] did not yield an isolable product. The NMR spectra showed only a broad noisy peak at ~1.5 ppm in addition to multiple peaks in the range of 5-6 ppm, suggesting that, again, the proton in the ligand was leading to polymerisation. Hence, hydrazido ligands were not investigated further.

Guanidinate ligands proved more successful. A useful bis(guanidinato) synthetic intermediate, [ZrCl$_2${η^2-(^{i}PrN)$_2$CNMe$_2$}$_2$], was reported by Bergman *et al.*,[4] which was synthesised by the insertion of diisopropyl carbodiimide into the dimethylamido moieties of [ZrCl$_2$(NMe$_2$)$_2$(THF)$_2$] (**Scheme 4.2**). Initial treatments of [ZrCl$_2${η^2-(^{i}PrN)$_2$CNMe$_2$}$_2$] with two equivalents of sodium methylcyclopentadienide yielded only the mono-substituted product as a glassy orange solid, which formed a yellow powder when ground. It was not expected that two pentahapto methylcyclopentadienyl ligands would result, due to the consequent π-electron overcrowding of the metal centre, although perhaps one might have bound in a monohapto, σ fashion. The fact that no second substitution has taken place must therefore be the result of the steric crowding at the metal centre. In subsequent reactions, only one equivalent of sodium methylcyclopentadienide was used (**Scheme 4.2**).

The fact that only one substitution had occurred is confirmed by the elemental analysis and mass spectral data for **4.5**, the latter showing a peak at *m/z* = 545 and smaller peaks at 511 and 514, accounting for the loss of a chloride ligand and two methyl groups respectively. More interesting, however, was the proton NMR (**Figure 4.1**).

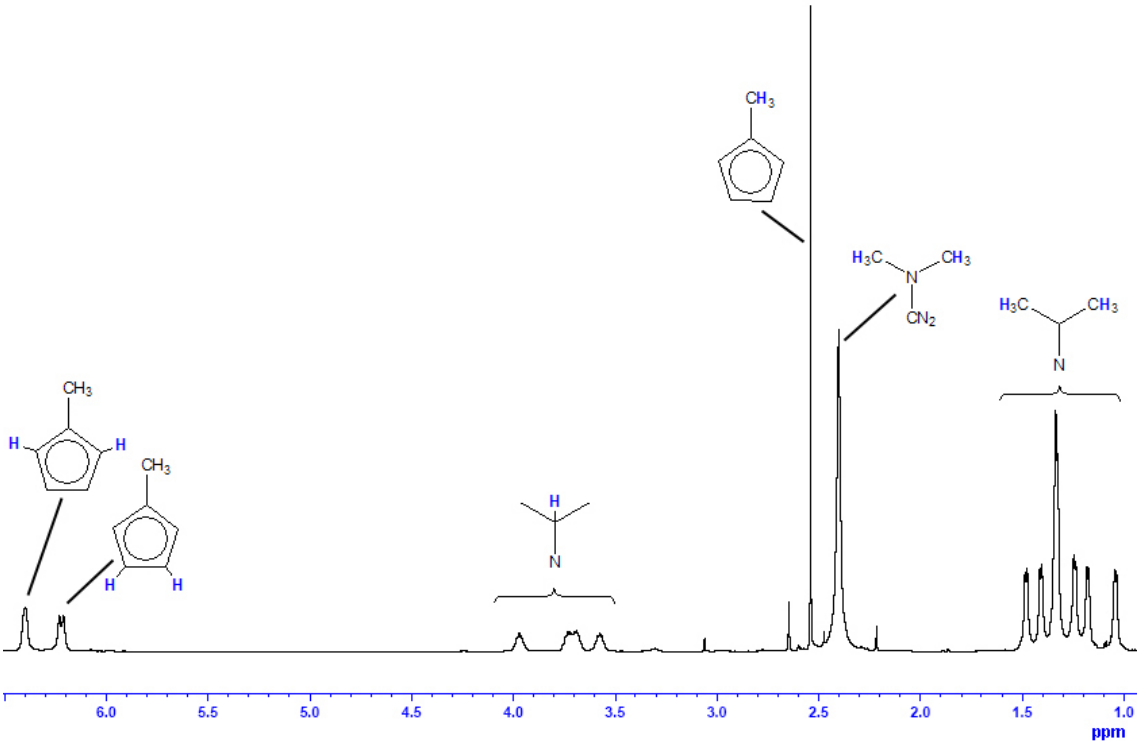

Figure 4.1 ^{1}H NMR spectrum of [ZrCp'{η^2-(^{i}PrN)$_2$CNMe$_2$}$_2$Cl] (**4.5**) in C_6D_6. Integrals omitted for clarity.

From the proton NMR, it is evident that there are six different methyl environments, suggesting that all but three NCH*Me*$_2$ moieties are inequivalent. It is likely that they are diastereotopic as **4.5** is a highly asymmetric molecule. In fact, all the isopropyl groups are inequivalent as there are four peaks between 3.5 and 4.0 ppm, which appear to be unresolved septets, accounting for the NC*H*Me$_2$ moiety. The methyl protons on the NMe$_2$ groups are not diastereotopic as those moieties are free to rotate, but it results in a broad peak. For the methylcyclopentadienyl ligand, the protons in the 2- and 3-positions are resolved, and are assigned to the peaks at 6.39 and 6.22 ppm respectively, as suggested by Stobart *et al*. for bis(methylcyclopentadienyl) compounds of germanium, tin and lead.[5] The only additional features on the carbon NMR are those of the quaternary carbon on the methylcyclopentadienyl group at 115.6 ppm, and the carbon atoms associated with the two CN_3 units of the guanidinate ligands, at 164.5 and 171.5 ppm.

X-ray quality crystals of [ZrCp'{η^2-(^{i}PrN)$_2$CNMe$_2$}$_2$Cl] (**4.5**) were grown from hexane, but these only remained crystalline at temperatures below 10 °C. An X-ray

crystallographic study at low temperatures resulted in the structure shown in **Figure 4.2**. Selected bond lengths and angles are given in **Table 4.1**.

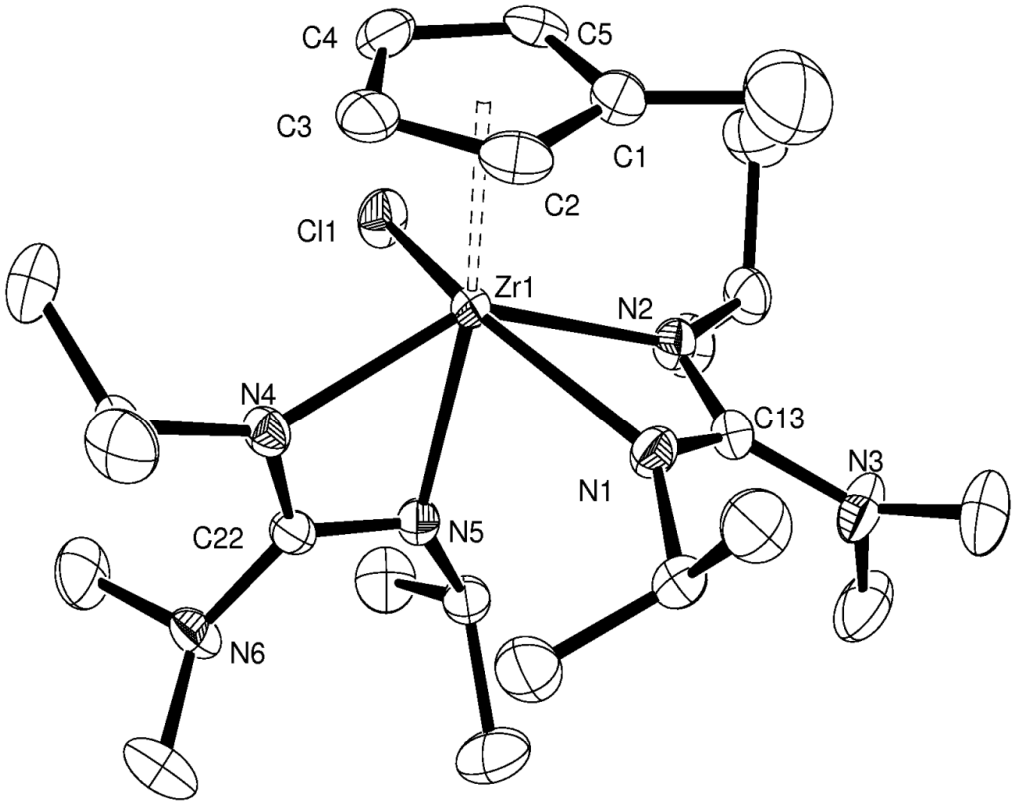

Figure 4.2 ORTEP plot of [ZrCp'{η^2-(^{i}PrN)$_2$CNMe$_2$}$_2$Cl] (**4.5**) with 50% probability ellipsoids. Hydrogen atoms have been omitted for clarity.

The structure of [ZrCp'{η^2-(^{i}PrN)$_2$CNMe$_2$}$_2$Cl] (**4.5**) exhibits a distorted octahedral geometry due to the steric constraints of the guanidinate ligand (**Figure 4.2**). This is shown by the non-linear angles of *trans*-ligands subtending the zirconium centre, for example, N(2)–Zr(1)–N(4) and N(1)–Zr(1)–Cl(1) are 140.07(10) and 143.52(7)° respectively. The Zr–C (Cp') bonds average approximately 2.573(3) Å, which are comparable to other substituted cyclopentadienyl ligands in the literature, although they are certainly at the longer end of the scale when compared to those reported.[6-8] As such, the methylcyclopentadienyl ligand can be considered to be bound in an η^5 mode.

Table 4.1 Selected bond lengths and angles for compound **4.5**.

Bond	Length (Å)	Bond	Length (Å)
Zr(1)–C(1)	2.583(3)	Zr(1)–N(4)	2.237(3)
Zr(1)–C(2)	2.563(4)	Zr(1)–N(5)	2.273(3)
Zr(1)–C(3)	2.560(3)	C(13)–N(1)	1.330(4)
Zr(1)–C(4)	2.586(3)	C(13)–N(2)	1.331(4)
Zr(1)–C(5)	2.575(3)	C(13)–N(3)	1.408(4)
Zr(1)–Cl(1)	2.4961(9)	C(22)–N(4)	1.299(4)
Zr(1)–N(1)	2.287(2)	C(22)–N(5)	1.356(4)
Zr(1)–N(2)	2.260(2)	C(22)–N(6)	1.421(4)
Bonds	Angle (°)	Bonds	Angle (°)
N(1)–Zr(1)–N(2)	58.38(10)	N(1)–C(13)–N(3)	124.4(3)
N(1)–Zr(1)–N(4)	103.53(10)	N(2)–C(13)–N(3)	122.7(3)
N(1)–Zr(1)–N(5)	81.11(9)	C(13)–N(3)–C(14)	120.0(3)
N(2)–Zr(1)–N(4)	140.07(10)	C(13)–N(3)–C(15)	122.1(3)
N(2)–Zr(1)–N(5)	82.36(9)	C(14)–N(3)–C(15)	116.1(3)
N(4)–Zr(1)–N(5)	58.66(9)	N(4)–C(22)–N(5)	112.6(3)
N(1)–Zr(1)–Cl(1)	143.52(7)	N(4)–C(22)–N(6)	125.5(3)
N(2)–Zr(1)–Cl(1)	87.50(7)	N(5)–C(22)–N(6)	121.9(3)
N(4)–Zr(1)–Cl(1)	94.70(8)	C(22)–N(6)–C(23)	116.8(3)
N(5)–Zr(1)–Cl(1)	81.93(7)	C(22)–N(6)–C(24)	117.4(3)
N(1)–C(13)–N(2)	112.9(3)	C(23)–N(6)–C(24)	115.2(3)

The Cp' ring appears to be somewhat distorted as the C(2) and C(3) carbons are closest to the zirconium centre whereas C(1) and C(4) are furthest, with a difference of approximately 0.025(3) Å. C(5) lies at a distance between the two extremes, suggesting that the ring is slightly puckered. However, the internal C–C angles lie in the range 106.9-108.9°, which are the values expected for the internal angles of a pentagon, suggesting that the Cp' ring is close to planar. The Zr–N (bound guanidinate) bond lengths lie in the range 2.23-2.29 Å, which is similar to those in other sterically crowded guanidinate complexes in the literature.[9-12] On closer inspection, it is clear that the two

guanidinate ligands are inequivalent, which agrees with the NMR spectra of **4.5**. The guanidinate nitrogen, N(5) has the longest Zr–N bond length (2.273(3) Å) as this is being affected by the π-donation of the Cp' ring *trans* to it. In contrast, Zr(1)–N(4), on the same ligand, is the shortest Zr–N distance in the molecule at 2.237(3) Å. This leads to the clear difference in N^{i}Pr environments in the proton and carbon NMR spectra. The other guanidinate ligand (N(1)–C(13)–N(2)) has more symmetry, although Zr(1)–N(1) is the slightly longer of the two Zr–N bonds as it lies *trans* to the chloride ligand, although the difference between the Zr–N distances in this ligand is not as significant as previously mentioned.

Another factor to consider is the extent to which each guanidinate ligand contributes electronically to the zirconium centre. As mentioned in Chapter 1, guanidinate ligands can be either 4- or 6-electron donors, depending on the level of π-electron delocalisation over the CN_3 unit.[13] If one were to count the electrons in compound **4.5** assuming 6 from each guanidinate, 6 from Cp'$^{-}$ and 2 from the chloride ligand; the total would be 20. It is likely that one of the guanidinate ligands is only acting as a 4-electon donor. A comparison of the unbound guanidinate nitrogen atoms, N(3) and N(6) indicates that this might be the case. The angles between N(3) and its three surrounding carbon atoms, C(13-15) are 120.0(3)°, 122.1(3)° and 116.1(3)° respectively, suggesting that N(3) is sp^2 hybridised and is taking part in the π-donation to the zirconium centre, despite the C(13)–N(3) distance being significantly longer than the other C–N distances in the ligand. With respect to N(6) and C(22-24), the angles are 116.8(3)°, 117.4(3)° and 115.2(3)°, which implies the N(6) environment is less planar with more sp^3 hybrid character, although there is still some contribution to the π-system. With this in mind, the two guanidinate ligands could be considered as 6- and 4-electron donors respectively, allowing compound **4.5** to obey the 18-electron rule, but it is likely to be a situation intermediate to this.

As described in Section 1.6.2.1.4, the most common method of introducing a guanidinate ligand onto metal centres is by lithium metathesis. As such, [ZrCp'$_2${η^2-(^{i}PrN)$_2$CNMe$_2$}Cl] (**4.6**) was synthesised as described in **Scheme 4.3**.

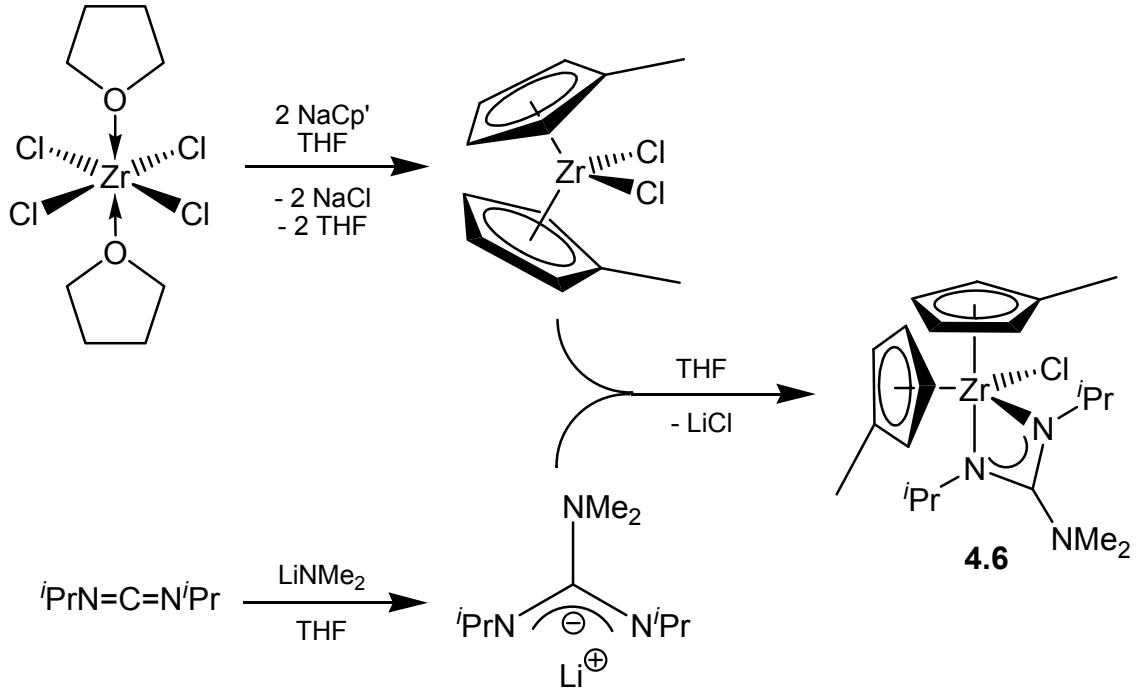

Scheme 4.3 Synthetic route to $[ZrCp'_2\{\eta^2\text{-}(^iPrN)_2CNMe_2\}Cl]$ (**4.6**).

Bis(methylcyclopentadienyl)zirconium dichloride was synthesised by the reaction of two equivalents of sodium methylcyclopentadienide and $[ZrCl_4(THF)_2]$. The resulting $[ZrCp'_2Cl_2]$ was purified by sublimation. Inferences from the mass spectrum of this compound suggest that it may be dimeric, as a peak at *m/z* = 604 could account for the dimeric species $[ZrCp'_2Cl_2]_2$ having lost a chloride ligand. The lithium guanidinate salt was prepared *in situ* by the insertion of lithium dimethylamide into diisopropyl carbodiimide. Initial reactions involved the treatment of $[ZrCp'_2Cl_2]$ with two equivalents of the lithium guanidinate salt, although the elemental analysis and NMR spectra showed that only one chloride displacement had occurred. This is unsurprising, as the addition of two guanidinate ligands would result in the complex exceeding 18 valence electrons. Subsequent reactions were carried out with only one equivalent of the lithium guanidinate salt, affording a beige powder in a good yield.

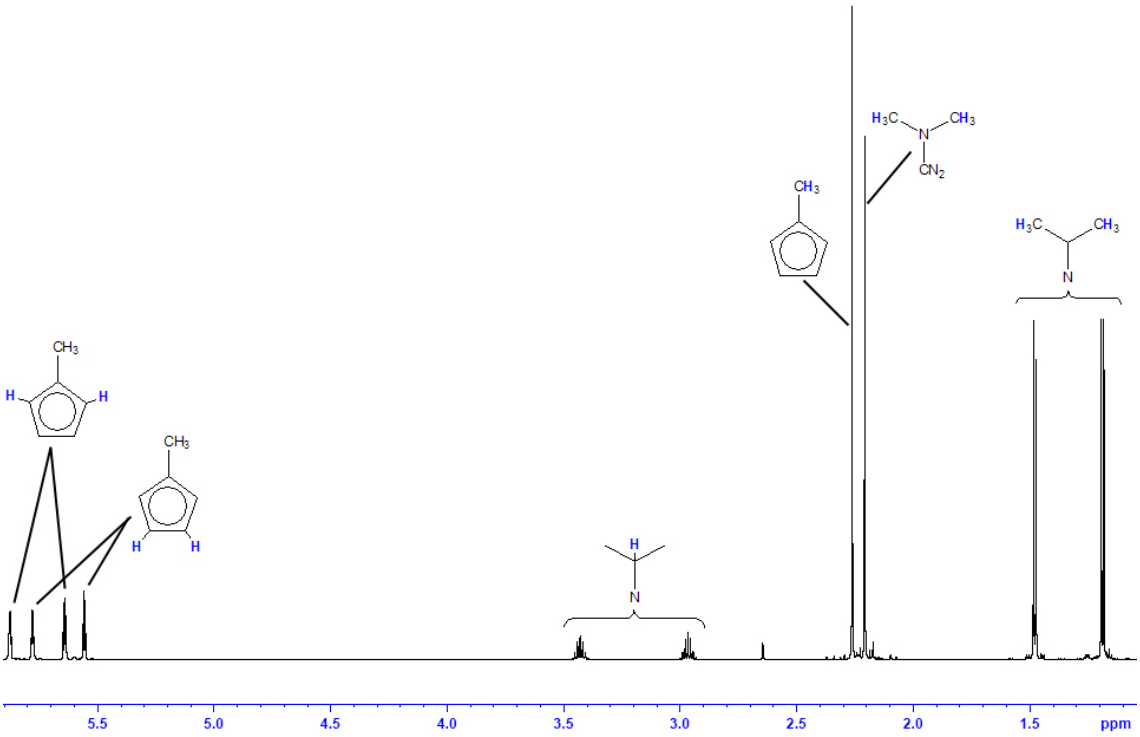

Figure 4.3 ^{1}H NMR spectrum of [ZrCp'$_2${η^2-(^{i}PrN)$_2$CNMe$_2$}Cl] (**4.6**) in C_6D_6. Integrals omitted for clarity.

The proton NMR spectrum of **4.6** (**Figure 4.3**) showed two different isopropyl (methyl) environments, which suggests that the isopropyl groups are not diastereotopic, and that they are freer to rotate than those in compound **4.5**. This is likely to be due to less steric hindrance within the molecule. The methyl groups in the methylcyclopentadienyl ligand and on the NMe_2 moiety on the guanidinate ligand were assigned to the peaks at 2.24 and 2.21 ppm respectively. The assignment was more complicated as, in this case, both peaks integrate to six protons each, they are sharp (the NMe_2 peak of compound **4.5** was somewhat broader) and they are further upfield than those in the spectrum of **4.5**. However, based on the fact that the $C_5H_4CH_3$ peak was downfield of the NMe_2 peak for compound **4.5**, it was assumed that this would also be the case for compound **4.6**. It is also notable that the aromatic protons at 5.5-6 ppm suggest that the two methylcyclopentadiene ligands are inequivalent, for example, in this five-coordinate complex, one Cp' may be axial and one equatorial. It is possible that the peak for their methyl substituents just happen to occur at the same frequency, resulting in one peak.

The mass spectrum of compound **4.6** (**Figure 4.4**) showed the molecular ion peak at *m/z* = 454, although the most intense peak occurred at *m/z* = 419, which accounts for the loss of the chloride ligand, which is promising as any chloride contamination in resulting films could potentially be reduced.

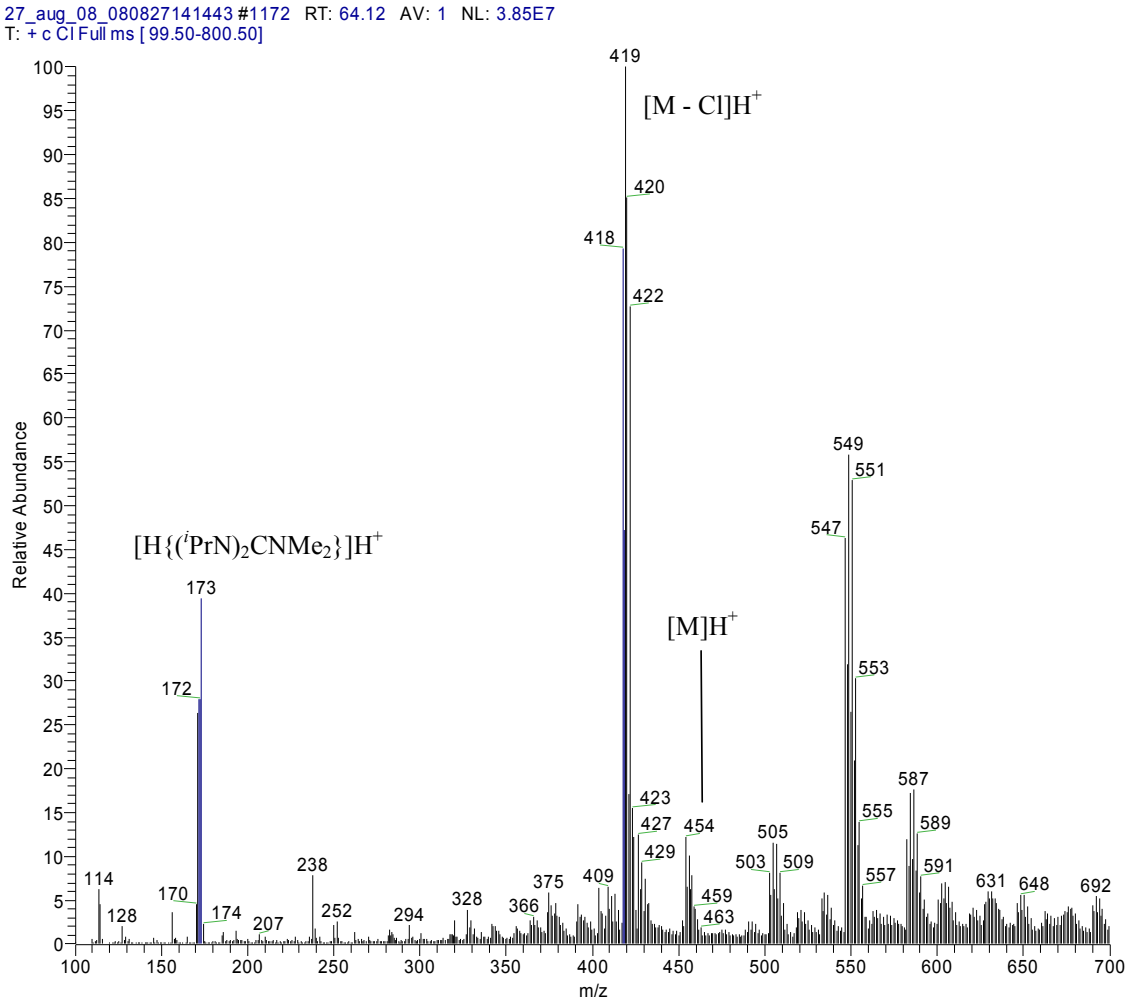

Figure 4.4 The CI+ mass spectrum of [ZrCp'$_2${η^2-(^{i}PrN)$_2$CNMe$_2$}Cl] (**4.6**), run in toluene.

What is unclear, however, is the presence of three higher peaks at *m/z* = 505, 549 and 587 respectively. The peak at *m/z* = 587 could account for the disubstituted compound [ZrCp'$_2${η^2-(^{i}PrN)$_2$CNMe$_2$}$_2$] minus a proton, although the more prominent peak at *m/z* = 549 would represent the loss of a chlorine from this, which would not be possible.

More likely there could be dimerisation and/or recombination occurring in the mass spectrometer, as the NMR spectra and elemental analysis results are more concurrent with the structure of $[ZrCp'_2\{\eta^2\text{-}(^i PrN)_2CNMe_2\}Cl]$ (**4.6**).

X-ray quality crystals of $[ZrCp'_2\{\eta^2\text{-}(^i PrN)_2CNMe_2\}Cl]$ (**4.6**) were grown from hexane. A single crystal X-ray study resulted in the structure shown in **Figure 4.5**. Selected bond lengths and angles are shown in **Table 4.2**.

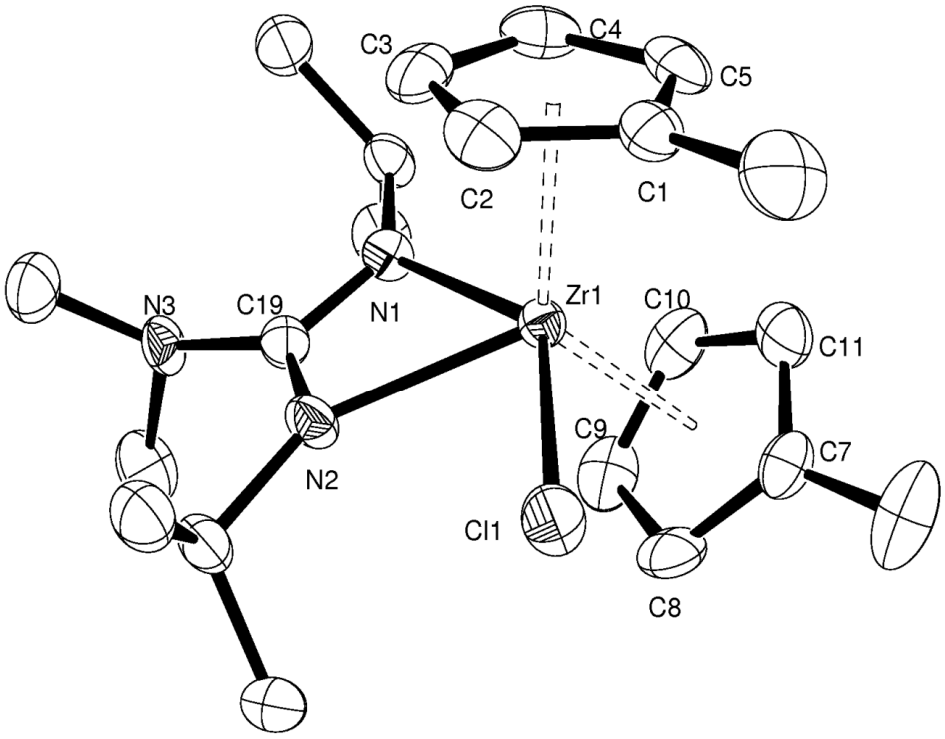

Figure 4.5 ORTEP plot of $[ZrCp'_2\{\eta^2\text{-}(^i PrN)_2CNMe_2\}Cl]$ (**4.6**) with 50% probability ellipsoids. Hydrogen atoms have been omitted for clarity.

The structure of $[ZrCp'_2\{\eta^2\text{-}(^i PrN)_2CNMe_2\}Cl]$ (**4.6**) is a distorted trigonal bipyramid, again due to the constraints of the guanidinate ligand (**Figure 4.5**). On examination of the Zr–C distances of the Cp' rings it is apparent that they are both tilted, whereby the carbon bearing the methyl substituent is furthest from the zirconium centre. The ring comprising C(7-11) shows the least variation in Zr–C distances, the shortest being

2.510(3) Å and the longest being 2.579(3) Å. The latter is comparable to the Cp' ring in compound **4.5**, and the former is similar to M–Cp bond distances in the literature.[6-8]

Table 4.2 Selected bond lengths and angles for compound **4.6**.

Bond	Length (Å)	Bond	Length (Å)
Zr(1)–C(1)	2.598(3)	Zr(1)–C(10)	2.510(3)
Zr(1)–C(2)	2.522(3)	Zr(1)–C(11)	2.556(3)
Zr(1)–C(3)	2.511(3)	Zr(1)–Cl(1)	2.5542(3)
Zr(1)–C(4)	2.523(3)	Zr(1)–N(1)	2.298(3)
Zr(1)–C(5)	2.571(3)	Zr(1)–N(2)	2.274(3)
Zr(1)–C(7)	2.579(3)	C(19)–N(1)	1.311(4)
Zr(1)–C(8)	2.550(3)	C(19)–N(2)	1.331(4)
Zr(1)–C(9)	2.518(3)	C(19)–N(3)	1.422(4)
Bonds	Angle (°)	Bonds	Angle (°)
N(1)–Zr(1)–N(2)	57.17(9)	N(2)–C(19)–N(3)	127.0(3)
N(1)–Zr(1)–Cl(1)	139.05(7)	C(19)–N(3)–C(20)	116.6(3)
N(2)–Zr(1)–Cl(1)	81.88(7)	C(19)–N(3)–C(21)	116.6(3)
N(1)–C(19)–N(2)	111.7(3)	C(20)–N(3)–C(21)	114.5(3)
N(1)–C(19)–N(3)	121.3(3)		

In the Cp' ring comprising C(1-5), the differences are more marked, the longest Zr–C distance being 2.598(3) Å and the shortest 2.511(3) Å. It was unclear as to whether the longest Zr–C distance suggested that this Cp' ligand was bound in an η^3 fashion, similar to an allyl group. The distances in compound **4.6** were compared to those in $[W(CO)_2(\eta^5\text{-Cp})(\eta^3\text{-Cp})]$, as described by Huttner *et al.*,[14] who reported a W–C (unbound) distance of 2.98(2) Å. This is significantly longer than Zr(1)–C(1) and therefore it is assumed that both Cp' rings are bound in an η^5 fashion.

Again, analysis of the interatomic distances in the guanidinate ligand suggest that there is some contribution to the π-system from the NMe_2 moiety, although this is not so significant as the C(19)–N(3) distance is significantly longer than C(19)–N(1,2). It is interesting to note the asymmetry of the guanidinate ligand in this case, as C(19)–

N(1) and C(19)–N(2) differ by 0.020(4) Å. This accounts for the two distinct isopropyl environments in the NMR spectra.

4.3.2. Decomposition Studies

As with the tungsten precursors, decomposition studies on compounds **4.1-4.6** were carried out by thermogravimetric analysis (TGA), the results of which are summarised in **Figure 4.6** and **Table 4.3**. The four bis(amido)bis(cyclopentadienyl)zirconium compounds (**4.1-4.4**) do not start to decompose significantly until approximately 250 °C. The compounds containing guanidinate ligands (**4.5** and **4.6**) begin to decompose at approximately 150-200 °C, although there is a degree of sublimation from each of them starting around 100 °C, which is encouraging for a CVD precursor.

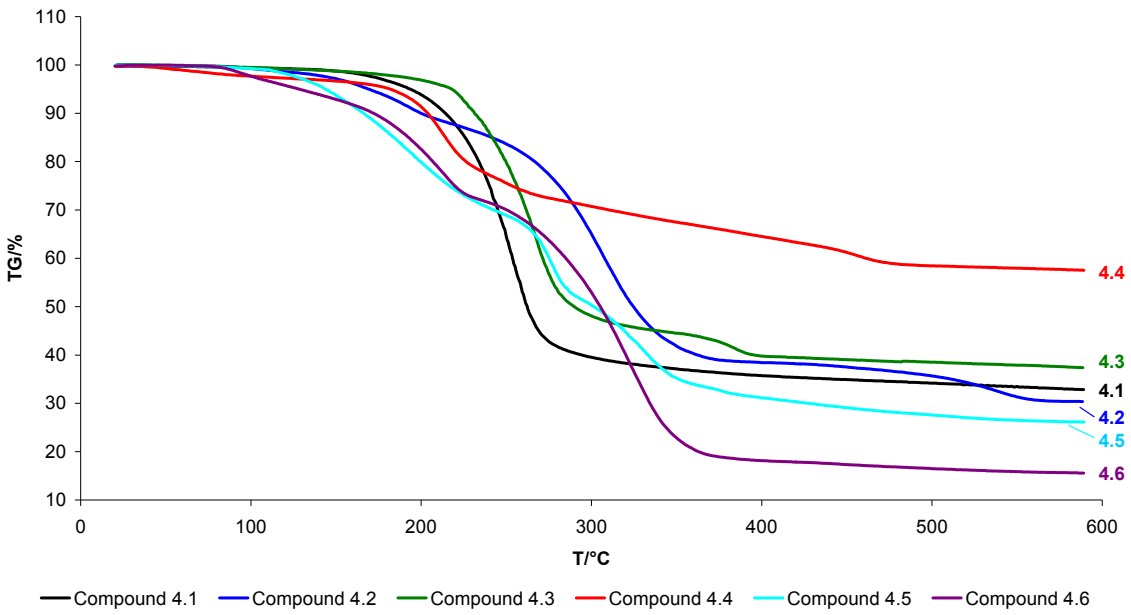

Figure 4.6 TGA plots for compounds **4.1-4.6**.

For compounds **4.1** and **4.3**, the decomposition is relatively clean, in one major step. Although this does not give any direct indication as to how they might decompose, their mass losses suggest that the compounds are decomposing to leave either ZrN or ZrC.

Table 4.3 TGA Data for compounds **4.1-4.6**.

Compound	Observed Mass Loss at 590 °C (%)	Calc. Mass Loss for ZrN (%)	Calc. Mass Loss for Zr_3N_4 (%)
4.1	67	67	65
4.2	70	66	64
4.3	63	69	67
4.4	42	74	72
4.5	74	81	80
4.6	85	77	76

The remaining compounds show distinct steps, which can be attributed to the loss of specific ligands. For example, compound **4.2** shows an initial mass loss of 9%, accounting for the two methyl groups on the *N,N'*-dimethylethylenediamide ligand. This is followed by a large drop of approximately 45%, which approximates to the loss of both cyclopentadienyl groups. The remaining loss therefore accounts for the decomposition of the remaining NCH_2CH_2N moiety. Compound **4.4** is perhaps the most distinct in that the mass loss is not as great as expected. The overall mass loss of 42% is concurrent with the loss of the two NEt_2 ligands, leaving the remains of the methylcyclopentadienyl ligands bound to the zirconium. It is perhaps not surprising that the amido ligands leave first, particularly in the case of $[MCp'_2(L)_2]$ compounds, as the methyl substituent can donate a proton to the other ligands (L), as suggested by Rossetto *et al*.[15] and as described in **Scheme 4.4**. However, the residual mass suggests that compound **4.4** does not decompose beyond $[Zr(H_2C{=}C_5H_4)_2]$.

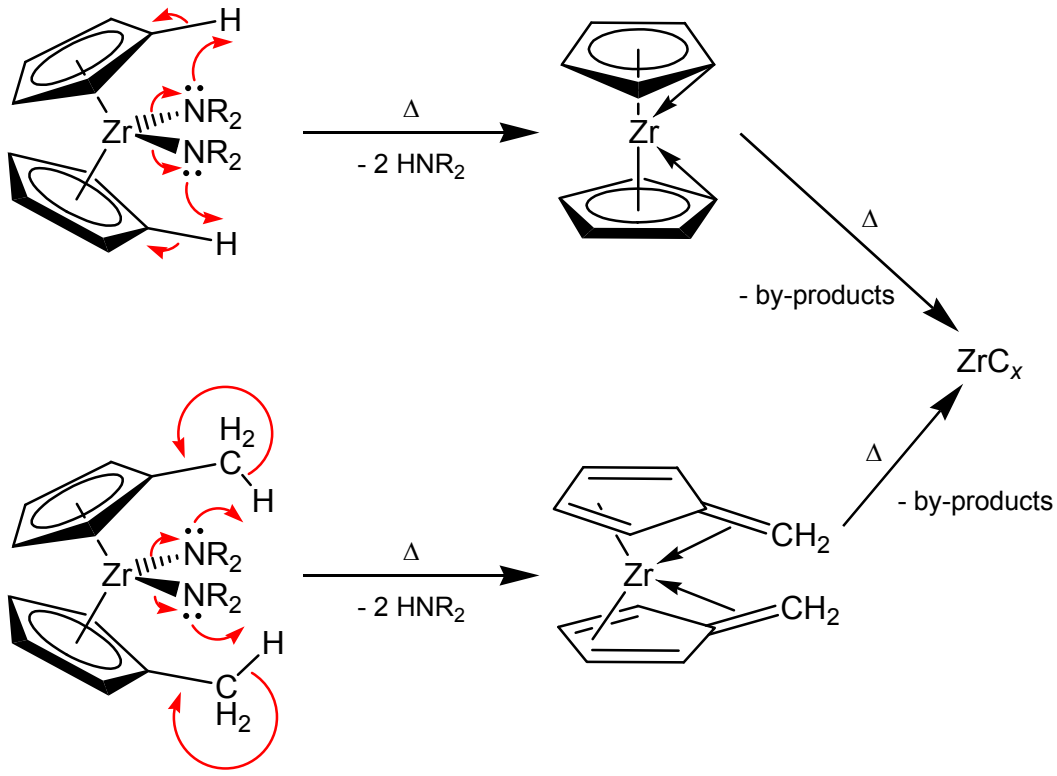

Scheme 4.4 Possible decomposition pathways for $[ZrCp_2(NR_2)_2]$ and $[ZrCp'_2(NR_2)_2]$ compounds, based on similar mechanisms for $[ZrCp_2(Me)_2]$ and $[ZrCp'_2(Me)_2]$ discussed in the literature.[15]

It is difficult to say whether this mechanism applies for compound **4.3** as there are no obvious steps in the TGA plot, although it is likely as $HNMe_2$ is a suitably volatile by-product.[16] However, this does not explain fully the large residual mass of **4.4** when compared to **4.3**.

Compounds **4.5** and **4.6** also exhibit steps in their TGA curves. The more complex is the curve of $[ZrCp'\{\eta^2\text{-}(^i PrN)_2CNMe_2\}_2Cl]$ (**4.5**), in which there are three steps. The mass loss is slightly lower than expected, suggesting incomplete decomposition. The proposed decomposition pathway is given in **Scheme 4.5**. It is likely that the initial mass loss of approximately 30% results from the loss of complete guanidinate ligand and the second loss of ~20% could be the loss of the protonated Cp' ligand (Cp'H) and the simultaneous loss of one of the isopropyl groups as propene. Then, the loss of the second remaining isopropyl group could facilitate the loss of the chloride ligand as HCl. The final gradual loss could then be attributed to the loss of

methyl groups to obtain an overall mass loss of 73%. This is comparable to the observed mass loss of 74% (**Table 4.3**), although the assignment of mass losses is, to a degree, subjective due to the overlap of the steps.

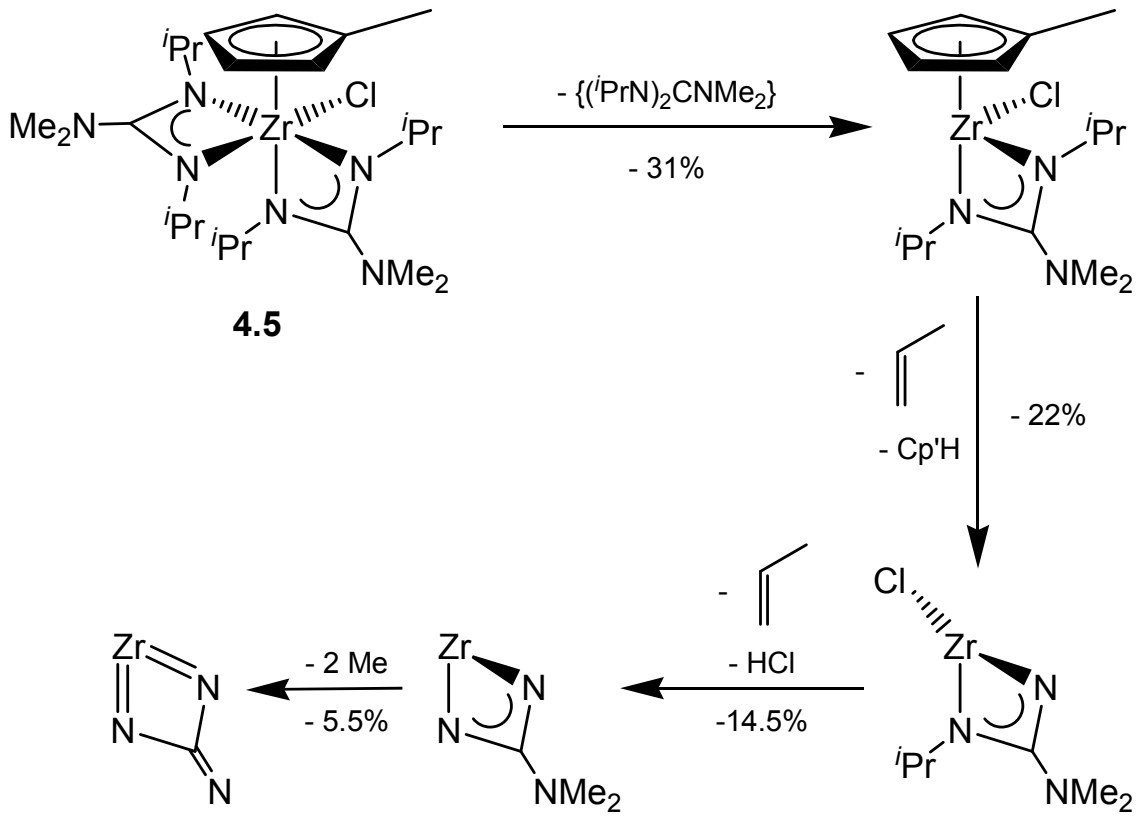

Scheme 4.5 Proposed decomposition pathway for [ZrCp'{η^2-(^{i}PrN)$_2$CNMe$_2$}$_2$Cl] (**4.5**).

When compared to compound **4.5**, [ZrCp'$_2${η^2-(^{i}PrN)$_2$CNMe$_2$}Cl] (**4.6**) has a more simple TGA curve of two steps. The mass loss (85%) is significantly greater than expected for ZrN/ZrC (77%) and even for complete decomposition to zirconium metal (80%). This is due to sublimation of the sample at lower temperatures to an extent that the residual mass is affected, which is visible by the initial shallow curve over the temperature range 80-140 °C (**Figure 4.6**). However, this suggests that compound **4.6** is highly volatile, which is beneficial for CVD but not for accurate assignment of mass losses. As compound **4.6** is structurally similar to compounds **4.1-4.4** (in essence it is

[ZrCp'$_2$(L)$_2$]) it might be expected to decompose in a similar manner. With reference to the mass spectrum of **4.6** (**Figure 4.4**), it is a possibility that the chloride ligand is the first to dissociate, followed by the guanidinate ligand. However, this is unclear from the TGA. Guanidinate ligands display more electronic flexibility than amido ligands and so could potentially compete with the methylcyclopentadienyl ligands to remain bound to the zirconium. Therefore, it is unclear which leaves the compound first. However, compound **4.6** does decompose sufficiently to suggest it might, at best, deposit zirconium carbonitride.

4.3.3. Vapour Pressure Studies

As for compounds **2.1-2.3**, vapour pressure studies were run on compounds **4.1-4.3** at SAFC Hitech Ltd., which is summarised in **Figure 4.7**.

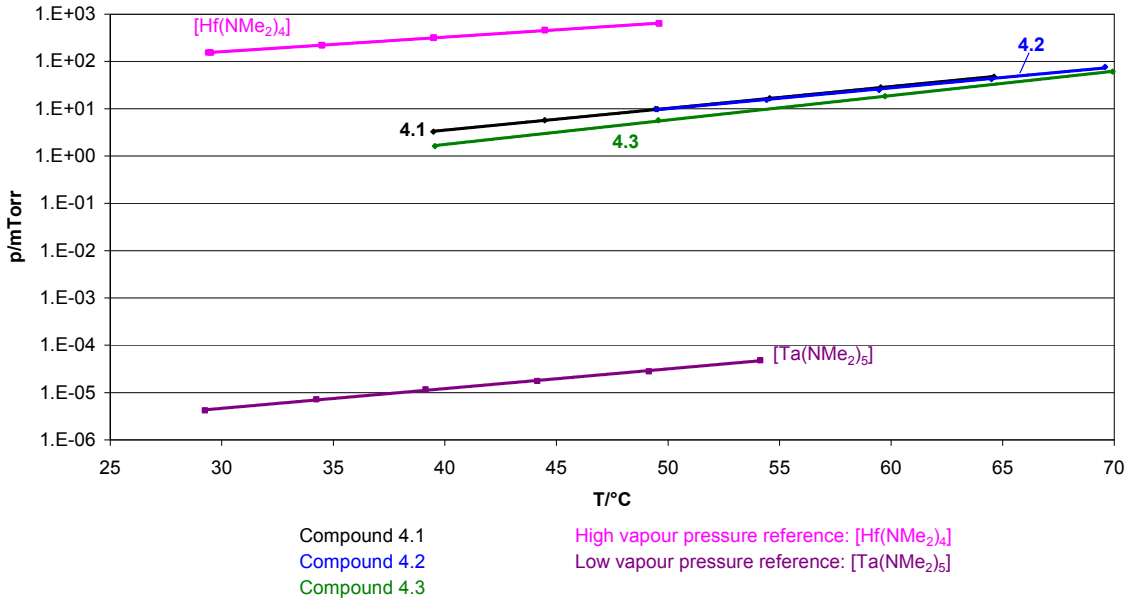

Figure 4.7 Vapour pressure lines for compounds **4.1-4.3** as compared to the high pressure industry standard, [Hf(NMe$_2$)$_4$], and the low pressure industry standard, [Ta(NMe$_2$)$_5$].

The vapour pressure curves for [ZrCp$_2$(NMe$_2$)$_2$] (**4.1**) and [ZrCp$_2$(η^2-MeNCH$_2$CH$_2$NMe)] (**4.2**) are very similar to one another as their vapour pressures are just lower than 10 mTorr at 50 °C. These are comparable to those of [W(μ-

$N^tBu)(N^tBu)Cl_2(H_2N^tBu)]_2$ (**2.1**) and $[W(N^tBu)_2Cl_2(TMEDA)]$ (**2.2**) (see Section 2.3.4.) as they are significantly higher than the vapour pressure of $[Ta(NMe_2)_5]$. More surprising is the vapour pressure of $[ZrCp'_2(NMe_2)_2]$ (**4.1**), which is approximately 6 mTorr at 50 °C. The rationale behind the addition of the methyl group on the cyclopentadiene ring was that it should hopefully increase the volatility of the compound, with respect to its unsubstituted analogue, by reducing the packing efficiency. This may be due to the weight of the two methyl groups, although this is unlikely to be a significant factor.

4.4. Conclusions

$[ZrCp_2(NMe_2)_2]$ (**4.1**), $[ZrCp_2(\eta^2\text{-}MeNCH_2CH_2NMe)]$ (**4.2**), $[ZrCp'_2(NMe_2)_2]$ (**4.3**), $[ZrCp'_2(NEt_2)_2]$ (**4.4**), $[ZrCp'\{\eta^2\text{-}(^i PrN)_2CNMe_2\}_2Cl]$ (**4.5**) and $[ZrCp'_2\{\eta^2\text{-}(^i PrN)_2CNMe_2\}Cl]$ (**4.6**) were all synthesised in good yields. The crystal structures of compounds **4.5** and **4.6** were also obtained from hexane solutions. Compounds **4.1-4.3** all decomposed cleanly with mass losses in close approximation to those expected for the formation of zirconium carbonitride. Compounds **4.4** and **4.5** showed mass losses that were lower than expected, suggesting that full decomposition had not taken place at 590 °C. The mass loss of compound **4.6** was much greater than expected, implying that significant sublimation was taking place before decomposition. The vapour pressures of compounds **4.1-4.3** were all greater than 1 mTorr at 50 °C. The vapour pressures for compounds **4.1** and **4.2** were very similar and that of compound **4.3** was surprisingly lower, but not significantly so. The clean decomposition and volatility of these compounds shows promise for their use as CVD precursors, although significant amounts of carbon may be deposited.

4.5. References

1. M. F. Lappert, G. Chandra, *J. Chem. Soc. A*, 1968, 1940-1945.
2. A. C. Jones, R. O'Kane, J. Gaskell, P. R. Chaulker, K. Black, M. Werner, P. Taechakumput, S. Taylor, P. N. Heys, R. Odedra, *Chem. Vap. Deposition*, 2007, **13**, 609-617.
3. R Kempe, S. Brenner, P. Arndt, *Z. Anorg. Allg. Chem.*, 1995, **621**, 2021-2024.

4. R. G. Bergman, J. Arnold, A. P. Duncan, S. M. Mullins, *Organometallics*, 2001, **20**, 1808-1819.
5. S. R. Stobart, A. Bonny, A. D. McMaster, *Inorg. Chem.*, 1978, **17**, 935-938.
6. J. L. Petersen, S. B. Jones, *Inorg. Chem.*, 1981, **20**, 2889-2894.
7. E. Hey-Hawkins, F. Lindenburg, J. Sieler, *Polyhedron*, 1996, **15**, 1459-1471.
8. G. Erker, M. Albrecht, R. Benn, S. Dehnicke, C. Krüger, R. Mynott, E. Raabe, A. Rufińska, C. Sarter, R. Schlund, *J. Organomet. Chem.*, 1990, **382**, 89-102.
9. R. A. Fischer, A. Baunemann, C. Gemel, Y. Kim, A. Milanov, D. Rische, M. Winter, *Dalton Trans.*, 2005, 3051-3055.
10. D. S. Richeson, P. Bazinet, D. Wood, G. P. A. Yap, *Inorg. Chem.*, 2003, **42**, 6225-6229.
11. R. Fischer, D. Rische, H. Parala, A. Baunemann, T. Thiede, *Surf. Coat. Technol.*, 2007, **201**, 9125-9130.
12. E. Hey-Hawkins, F. Lindenburg, *Z. Naturforsch., B*, 1993, **48**, 951-957.
13. P. J. Bailey, S. Pace, *Coord. Chem. Rev.*, 2001, **214**, 91-141.
14. G. Huttner, V. Bejenke, L. G. Bell, H. H. Brintzinger, P. Friedrich, D. Neugebauer, *J. Organomet. Chem.*, 1978, **145**, 329-333.
15. G. Rossetto, S. Codato, G. Carta, M. Leoni, G. A. Rizzi, P. Scardi, P. Zanella, *Chem. Vap. Deposition*, 1999, **5**, 159-163.
16. M. F. Lappert, P. P. Power, A. R. Sanger, R. C. Srivastava, *Metal and Metalloid Amides: Syntheses, Structures, and Physical and Chemical Properties*. 1980: Ellis Horwood Ltd.

5

Chemical Vapour Deposition of Zirconium Carbonitride

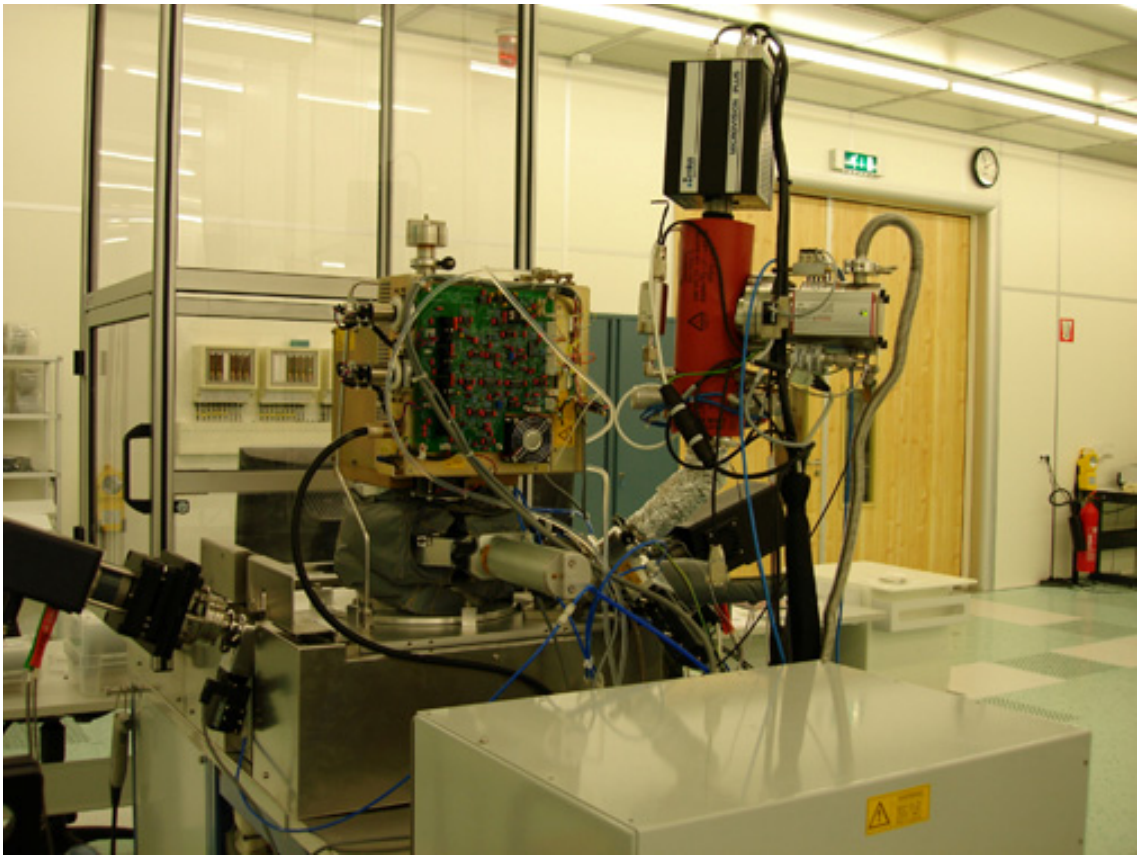

Figure 5.0 Plasma-enhanced ALD reactor at the Eindhoven University of Technology.

5.1. Introduction

This chapter discusses the attempted low pressure (LP)CVD of zirconium carbonitride thin films using $[ZrCp_2(NMe_2)_2]$ (**4.1**), $[ZrCp_2(\eta^2\text{-}MeNCH_2CH_2NMe)]$ (**4.2**), $[ZrCp'_2(NMe_2)_2]$ (**4.3**), $[ZrCp'_2(NEt_2)_2]$ (**4.4**), $[ZrCp'\{\eta^2\text{-}(^i PrN)_2CNMe_2\}_2Cl]$ (**4.5**) and $[ZrCp'_2\{\eta^2\text{-}(^i PrN)_2CNMe_2\}Cl]$ (**4.6**) (Cp = η^5-cyclopentadienyl, Cp' = η^5-methylcyclopentadienyl) as precursors. The attempted plasma-enhanced atomic layer deposition (PEALD) of zirconium carbonitride using compounds **4.1** and **4.2** is also discussed.

5.2. Experimental

5.2.1. Physical Measurements

X-ray diffraction (XRD) was carried out on a Bruker AXS D8 Discover machine using monochromatic Cu-Kα radiation (λ_1 = 1.54 Å). WDX was performed on a Philips XL30ESEM machine. Scanning electron microscope (SEM) images were obtained on a JSM-6301F Scanning Microscope Field Emission machine. UV-Vis spectra were recorded in the range 300-2500 nm using a Helios double beam instrument.

5.2.2. Low Pressure Chemical Vapour Deposition

LPCVD was carried out using the methods described in Section 3.2.3.

5.2.3. Plasma-Enhanced Atomic Layer Deposition

PEALD using $[ZrCp_2(NMe_2)_2]$ (**4.1**) and $[ZrCp_2(\eta^2\text{-}MeNCH_2CH_2NMe)]$ (**4.2**) was carried out in an Oxford Instruments FlexAL reactor (**Figure 5.1**) at the Eindhoven University of Technology. The substrates were p-type Si{100} wafers, which were 20 cm in diameter. These were not cleaned prior to use so it was assumed they were covered in a monolayer of SiO_2. Approximately 20 g of each precursor was loaded into a bubbler, which was subsequently attached to the reactor so that the precursors could be used as required. The bubbler temperature was varied over the range 70-90 °C and the substrate temperature was 200 °C. The base pressure of the system was ~10^{-6} Torr. Hydrogen, nitrogen, ammonia and oxygen (all purity >99.999%) were used to form the

plasmas and argon (purity >99.9999%) was employed as the purge gas and bleed gas. Plasmas used were H_2-N_2, N_2, NH_3 and O_2 at a power of 300 W. The depositions were followed using *in situ* ellipsometry and mass spectroscopy.

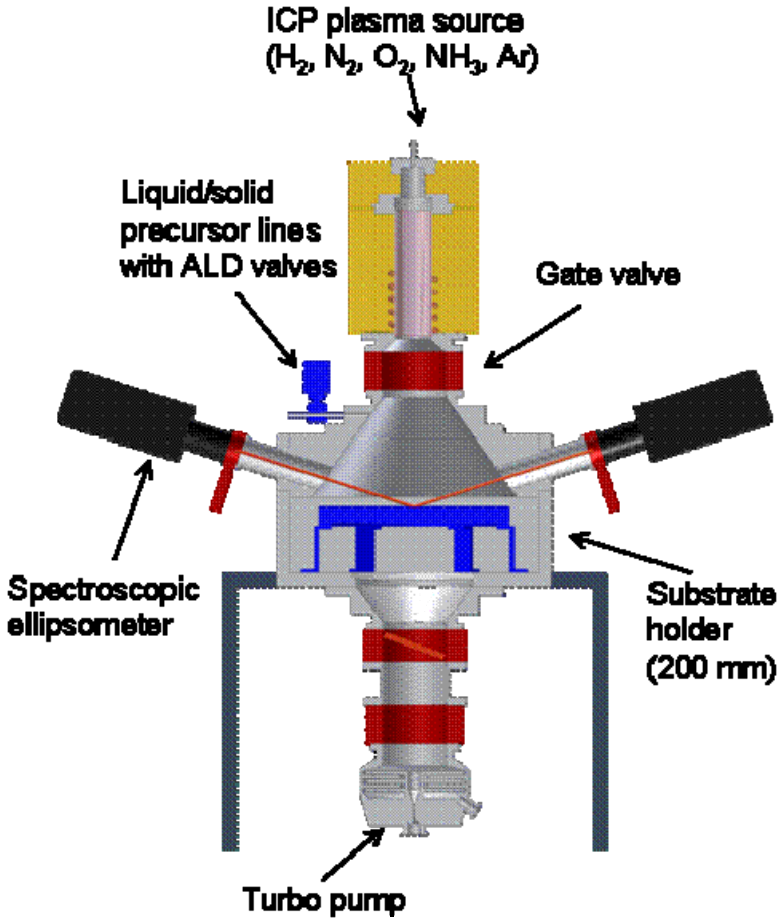

Figure 5.1 Oxford Instruments FlexAL PEALD reactor, reproduced with permission.[1]

A more detailed description of the PEALD apparatus is given in the literature.[1] A typical cycle is shown in **Figure 5.2**. With the gate valve closed, the precursor was pumped into the reaction chamber (6 s), followed by a purge of argon (4 s) to remove unreacted precursor. After a lag time of 3 s the gate valve was opened, followed 2 s later by the introduction of the plasma gas. After another 2 s, the power was applied to

the gas to create the plasma, which lasted for 5 s, after which time the power and gas were shut off, followed by the closure of the gate valve. A further 3 s lag time was allowed for any remaining reaction before a 5 s purge of argon to remove any remaining plasma gas and by-products. Another 3 s lag time was left between each cycle.

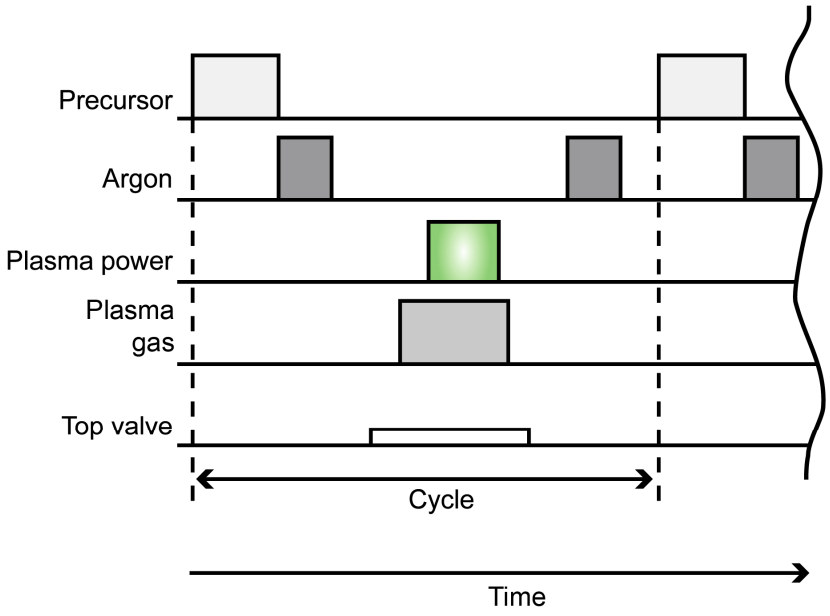

Figure 5.2 A typical ALD cycle, lasting approximately 30 s.

5.3. Results and Discussion

5.3.1. Low-Pressure CVD Using Zirconocene Bis(amido) Compounds

LPCVD of $[ZrCp_2(NMe_2)_2]$ (**4.1**), $[ZrCp_2(\eta^2\text{-}MeNCH_2CH_2NMe)]$ (**4.2**), $[ZrCp'_2(NMe_2)_2]$ (**4.3**), $[ZrCp'_2(NEt_2)_2]$ (**4.4**) under a vapour draw gave shiny brown-grey films on glass substrates. The temperature of the tube furnace was set to 600 °C although the glass substrates were not in direct contact with the heating element, being approximately 50 °C lower. The films were adhesive, as they were not removed by Scotch tape, although black flakes were removed from the thicker films by Scotch tape and tissue. The films were not hard as they were scratched by brass and steel styluses, which is not expected for zirconium nitride or carbide. This suggests that there are

areas of carbon (graphite) in the films, which may be disrupting the crystal lattice and weakening the films.

Prior to the vapour-draw experiments, LPCVD using **4.1** was carried out on the rig with gas bleeds as described in Section 3.2.3.1, giving grey mirror-like films. However, due to a leak in the system, films of polycrystalline zirconium oxide (**Figure 5.3**), amorphous zirconium carbide and graphite were observed. The average composition was $ZrO_{2.1\pm0.10}C_{0.9\pm0.19}$, which did not vary significantly when changing bleed gases. The crystallinity of the ZrO_2 was higher in the films deposited with ammonia, which suggested that in addition to the leak in the system, the ammonia had become wet.

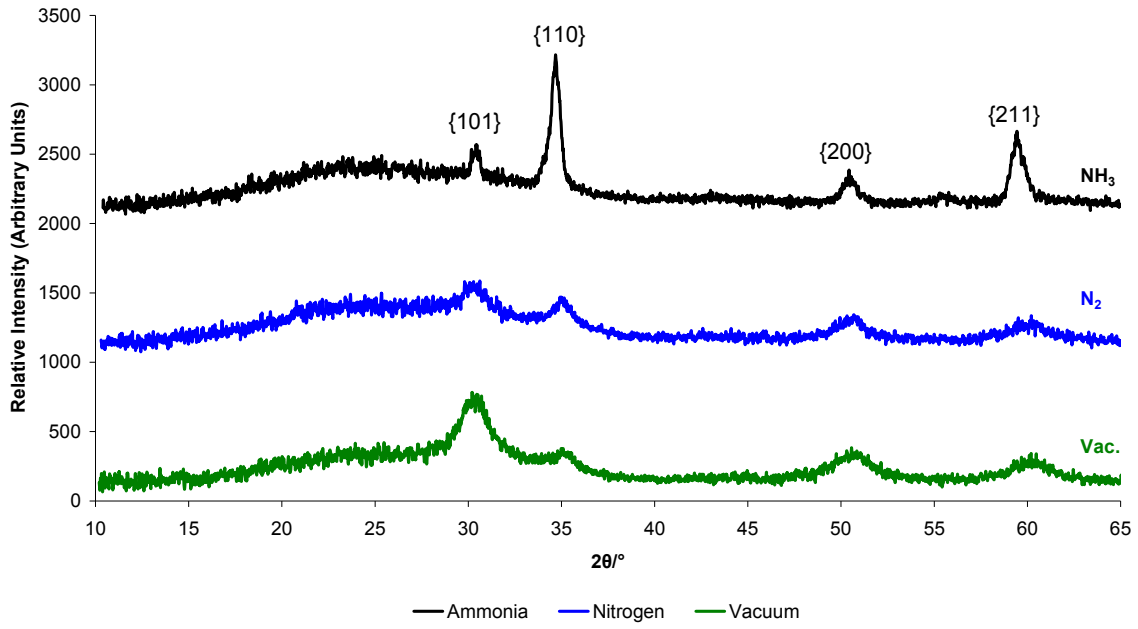

Figure 5.3 XRD patterns from initial LPCVD experiments using $[ZrCp_2(NMe_2)_2]$ (**4.1**), the peaks labelled are for cubic ZrO_2.

In order to overcome this, a more basic vapour-draw apparatus was used, as described in Section 3.2.3.2. It is on this method that the remainder of the chapter is based.

5.3.1.1. Composition of Films

The films were analysed by wavelength dispersive X-ray spectroscopy (WDX), which showed them to be devoid of nitrogen but containing a large amount of carbon. All films were sufficiently conductive with the exception of those deposited by $[ZrCp'_2(NEt_2)_2]$ (**4.4**). It is possible that the volatility of **4.4** was insufficient for this system, which is supported by the large residual mass in the TGA data. Unfortunately, these films required carbon coating for this analysis so the carbon content was falsely high.

Table 5.1 Compositions of the films from compounds **4.1-4.4** as found by WDX. The compositions are the average values for at least three runs.

Compound	Composition
4.1	$ZrC_{9.74\pm1.24}$
4.2	$ZrC_{7.17\pm1.31}$
4.3	$ZrC_{8.27\pm1.09}$
4.4	$Zr(C_{32.48\pm9.11})$

The lack of nitrogen is unsurprising, as the proposed decomposition mechanism for zirconocene amido compounds (shown in **Scheme 4.4**), which is related to the proposed decomposition mechanism for $[ZrCp_2(Me)_2]$ and $[ZrCp'_2(Me)_2]$,[2] suggests the initial loss of the amido groups (**Eq. 5.1**).

$$[Zr(C_5H_4R)_2(NR'_2)_2] \rightarrow [Zr(C_5H_3R)_2] + 2\,HNR'_2 \qquad (R = H, Me) \quad \textbf{(5.1)}$$

This may be due to the strong π-bonding of the cyclopentadienyl ligands to the zirconium centre and the fact that loss of highly volatile amines will drive the reaction to the right hand side. The residual cyclopentadienyl ligands are likely to be insufficiently volatile to leave the molecule and so deposit onto the film. The

mechanism in **Eq. 5.1** is potentially enhanced by substitution of the cyclopentadienyl ring because (a) alkyl groups donate electron density to the π-system, strengthening the M–Cp bonds and (b) the alkyl substituent forms an olefinic component (as shown in **Scheme 4.4** for methylcyclopentadienyl compounds), which can form an agostic interaction with the metal centre. This could have a stabilising effect in the sense that it sterically protects the metal centre from the amine. However, this is not a desirable property for a single-source precursor to a nitride.

As the films were so thin, it is not possible to accurately determine the oxygen content by WDX, due to the oxygen present in the glass. However, to get an approximation, the Si:O ratio of the glass was determined and then subtracted from the oxygen content. The oxygen levels were generally in the range of 3-5 at.%, although one film deposited from **4.1** showed oxygen levels as high as 13 at.%.

5.3.1.2. X-Ray Diffraction Studies

The X-ray diffraction patterns of the films deposited by compounds **4.1-4.4** were largely amorphous. However, where the films were thicker, there were small broad peaks, which could be attributed to polycrystalline ZrC,[3] an example of which is shown in **Figure 5.4**. The results of indexing these patterns was treated with caution as there is a lot of baseline noise and the peaks are so broad, however, the peaks indexed to a = 4.80-4.83 Å. This is higher than the reported a value for ZrC, 4.69 Å,[4] but there is a positive correlation between the carbon content and the unit cell parameter, where the a value increases with increasing carbon content. For example, in the PVD of ZrC_x (x = 0.22-1.50) by Brücker and Mäntylä, the a values were observed in the range 4.58-4.77 Å.[3] In this case, the C/Zr is significantly higher, which would account for the higher lattice parameter but the peaks are also broad, so the a value might be falsely high. However, the increase in lattice parameter is also likely to be due to deposited graphite and, perhaps, incorporation of ZrO_2, although no crystalline ZrO_2 was observed.

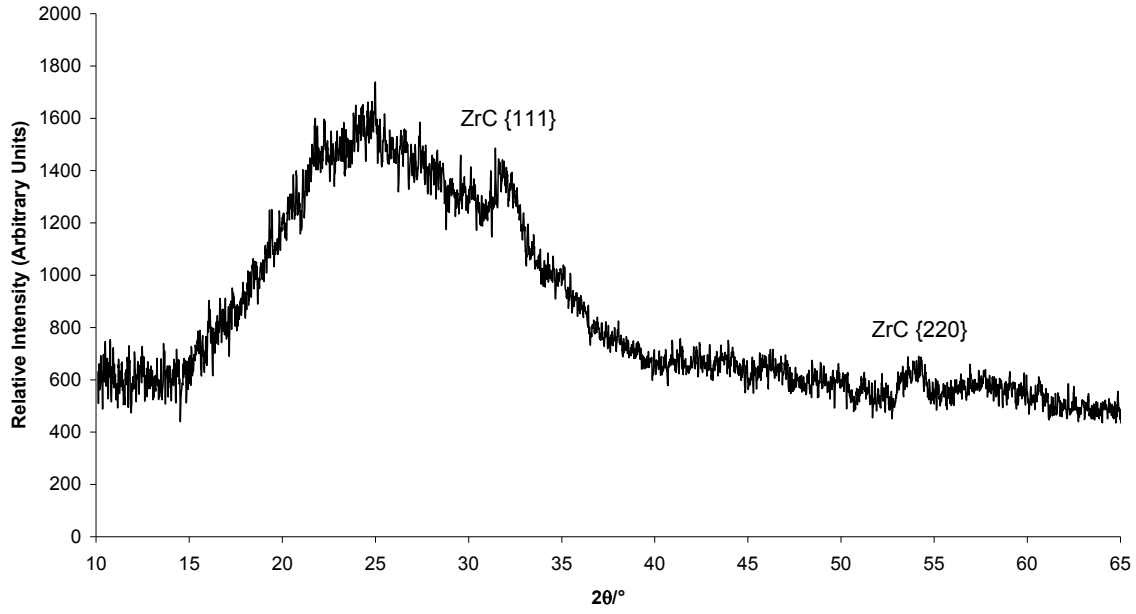

Figure 5.4 XRD pattern of the film deposited from $[ZrCp_2(NMe_2)_2]$ (**4.1**).

5.3.1.3. Optical Properties

The films were generally not highly reflective over the spectrum (**Figure 5.5**), not exceeding 30%. They were marginally more reflective to infra-red light. The films were sufficiently thin to be transmitting at 70-80% in the infra-red, dropping by about 10% with minima at ~400 nm. The transmission spectra of the films were comparable to those reported of titanium nitride.[5]

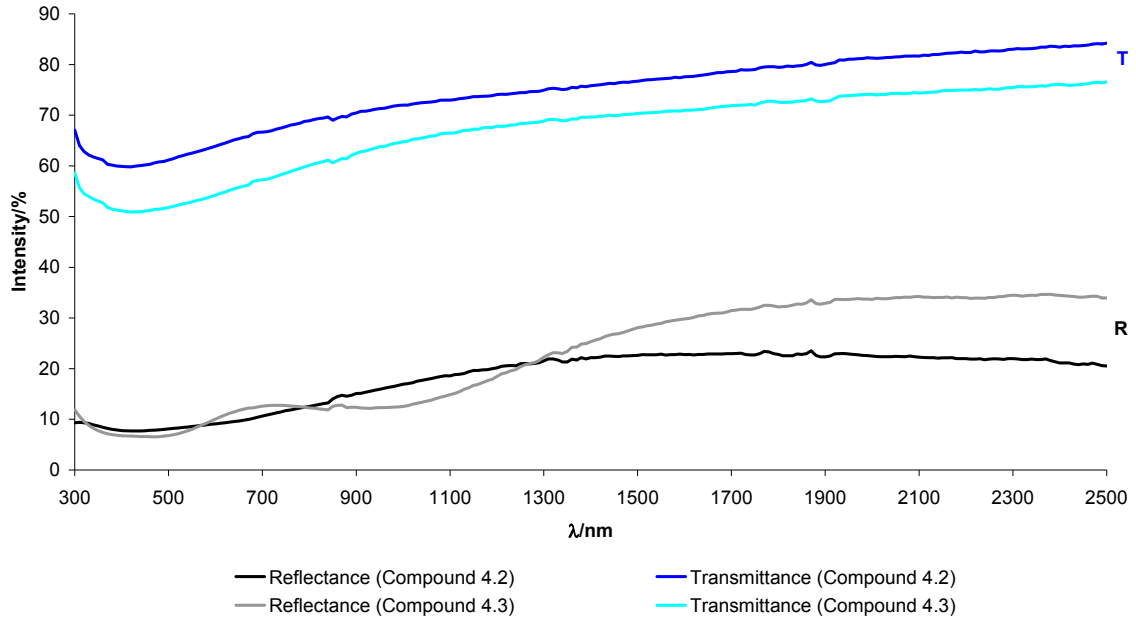

Figure 5.5 Reflectance-transmittance plots for $[ZrCp_2(\eta^2\text{-}MeNCH_2CH_2NMe)]$ (**4.2**) and $[ZrCp'_2(NMe_2)_2]$ (**4.3**).

5.3.1.4. Scanning Electron Microscopy

SEM images of the films showed them to be similar to those of tungsten carbonitride as described in Chapter 3 (**Figure 5.6**). Island-growth was evident and the nodules were approximately 50 nm in diameter. In some cases there were cracks evident in the gold overlayer, although cracks are common in films deposited by the vapour-draw LPCVD method. In most cases the islands of zirconium carbide are visible amongst the cracks, although the thinner the films were, the smaller the nodules were, which made them difficult to see under the scanning electron microscope.

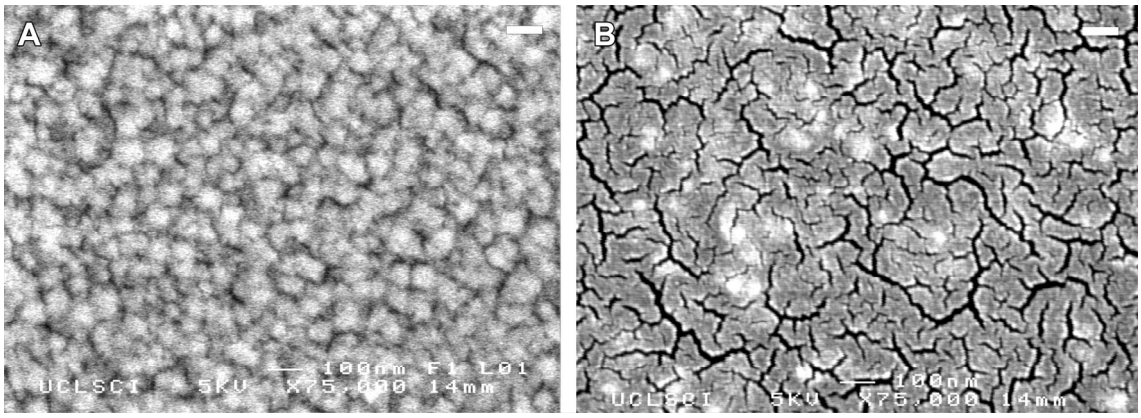

Figure 5.6 SEM images of the films formed from the vapour-draw LPCVD of (A) $[ZrCp'_2(NMe_2)_2]$ (**4.3**) and (B) $[ZrCp'_2(NEt_2)_2]$ (**4.4**). Both images are × 75,000, bars = 100 nm.

Side-on SEM images showed these films to be significantly thinner then those of tungsten carbonitride, ranging from approximately 80-250 nm thick. An example is shown in **Figure 5.7**.

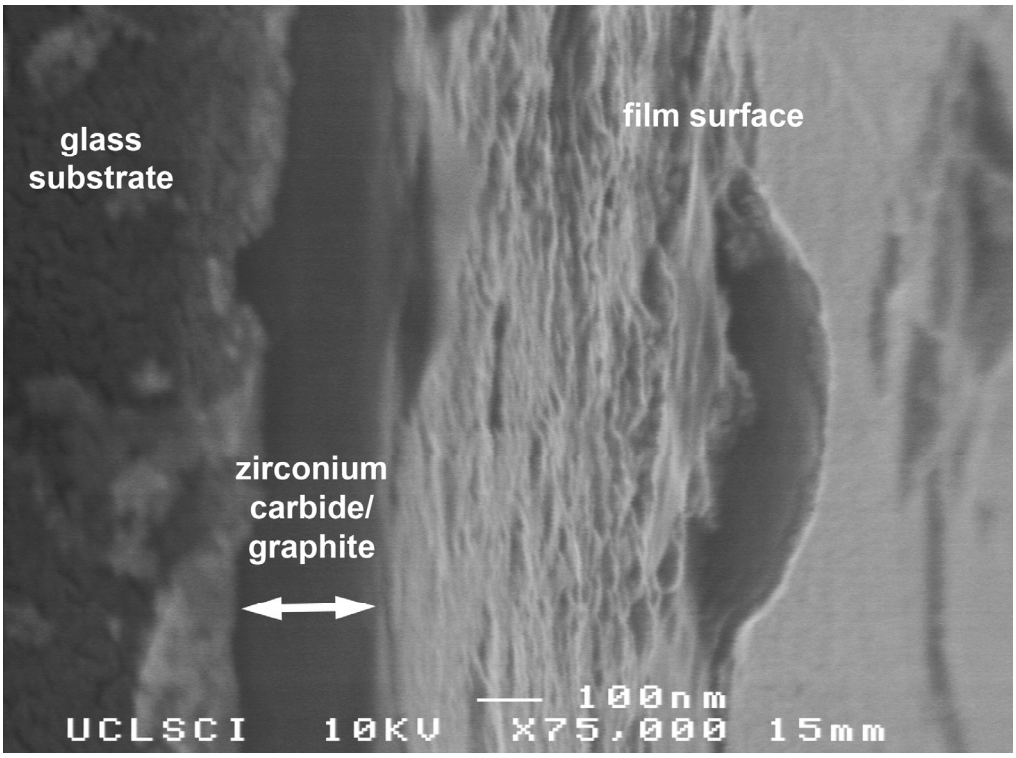

Figure 5.7 Side-on SEM image of a film deposited from $[ZrCp_2(NMe_2)_2]$ (**4.1**).

5.3.2. Low-Pressure CVD Using Zirconium Guanidinate Compounds

[ZrCp'{η^2-(^{i}PrN)$_2$CNMe$_2$}$_2$Cl] (**4.5**) and [ZrCp'$_2${η^2-(^{i}PrN)$_2$CNMe$_2$}Cl] (**4.6**) gave shiny films *via* vapour-draw LPCVD at 600 °C. Those from **4.5** were brown with a metallic lustre, whereas those from **4.6** were metallic grey. Films from both **4.5** and **4.6** were adhesive and could not be removed by Scotch tape. They could not be scratched with brass or steel styluses, showing them to be hard, as expected of zirconium carbonitride.

5.3.2.1. Composition of Films

WDX showed that zirconium carbonitride had been deposited although there was some chlorine contamination present in the films (**Table 5.2**).

Table 5.2 Compositions of the films from compounds **4.5** and **4.6** as found by WDX. The compositions are the average values for at least three runs.

Compound	Composition
4.5	$ZrN_{2.80\pm0.19}C_{1.82\pm0.20}$
4.6	$ZrN_{1.31\pm0.14}C_{2.46\pm0.22}$

The WDX data makes clear the case that more nitrogen in the single-source precursor results in more nitrogen in the film. The film formed from compound **4.5**, containing two guanidinate ligands, contained almost three times as much nitrogen, and twice as much carbon, as zirconium. For compound **4.6** the inverse is the case. Films from both compounds were conducting, which implies that this was either a result of conducting zirconium carbonitride or graphite. If the former is the case, a significant proportion of the nitrogen and carbon cannot form part of the zirconium carbonitride lattice, as only compounds of the formula ZrN_x or ZrC_x where $x \leq 0.5$ are electrically conducting.[6-8] However, it is interesting to note that the Zr:N ratio in the films deposited from **4.6** is almost equal to that of insulating Zr_3N_4.

The films deposited from these compounds showed chlorine contamination, although this was never higher than 3 at.% for **4.5** and 1.5 at.% for **4.6**. These values are significantly higher than the ambient chlorine levels in the glass (which were

typically < 0.1 at.%). It is an interesting comparison to the tungsten carbonitride precursors **2.1-2.4**, as no chlorine was found in those films deposited by LPCVD. It is perhaps a result of the affinity of zirconium carbide for the halogens.[9] The incorporation of chlorine may distort the lattice so replacement of the chloride ligands with a small nitrogen-based moiety, such as NMe_2, would be an improvement. Oxygen levels in the films from **4.5** were remarkably low, not exceeding 2 at.%, which might suggest that this was incorporated after deposition. It was higher in those from **4.6** (no higher than 12 at.%). Compound **4.5** is more sterically crowded so therefore might be less sensitive to oxygen or water than **4.6**, despite efforts to exclude it from the compounds. This might allow compound **4.5** to be used for larger scale CVD operations.

5.3.2.2. X-ray Diffraction Studies

The XRD patterns of the films were similar to those of compounds **4.1-4.4**, suggesting that polycrystalline ZrC is present (**Figure 5.8**).

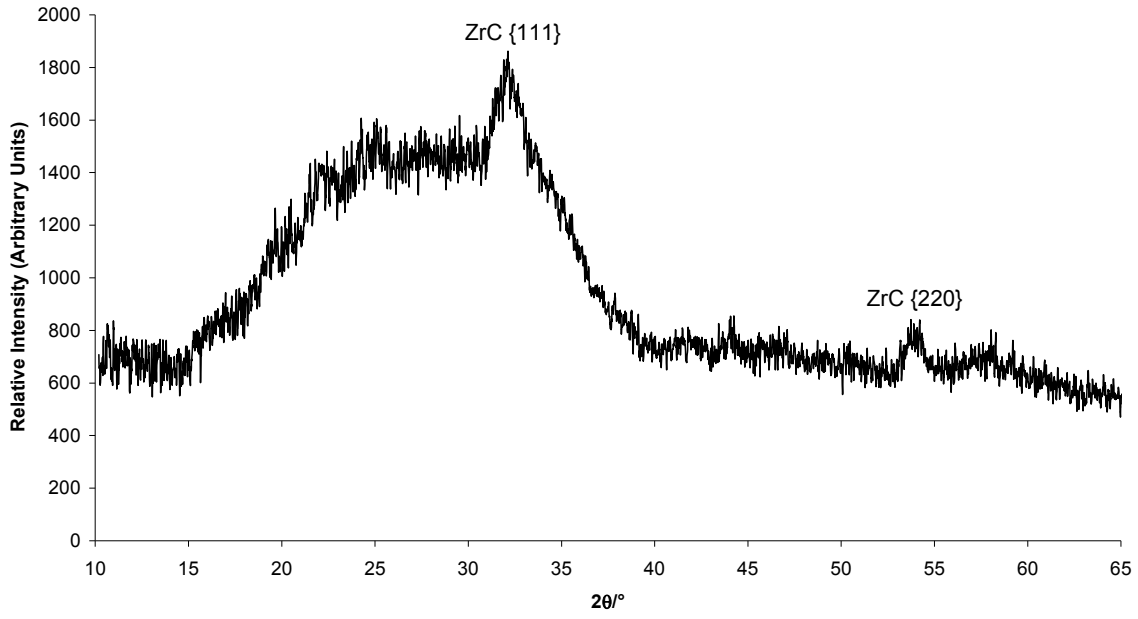

Figure 5.8 XRD pattern of the film deposited from [ZrCp'$\{\eta^2$-(^{i}PrN)$_2$CNMe$_2\}_2$Cl] (**4.5**).

As the substrate is likely to have been closer to 550 °C in temperature, it is unlikely that polycrystalline zirconium nitride would form. In a similar manner to films deposited by compounds **4.1-4.4**, the zirconium carbide peaks could be indexed to 4.73-4.81 Å. The lower values are certainly within the boundaries for ZrC_x (x = 1.1-1.5) suggested Brücker and Mäntylä,[3] which confirms that some of the carbon is incorporated by zirconium carbonitride. However, there is likely to be some amorphous graphite in the films as well.

5.3.2.3. Optical Properties

The reflectance of the films (**Figure 5.9**) was higher in the infra-red for the nitrogen-rich films deposited by compound **4.5**, although for compound **4.6** the reflectance was similar those deposited by **4.1-4.4**, possibly due to the amount of carbon in the films. The films from both compounds were highly transmitting in the infra-red, dropping in transparency over the visible and ultraviolet regions of the spectrum.

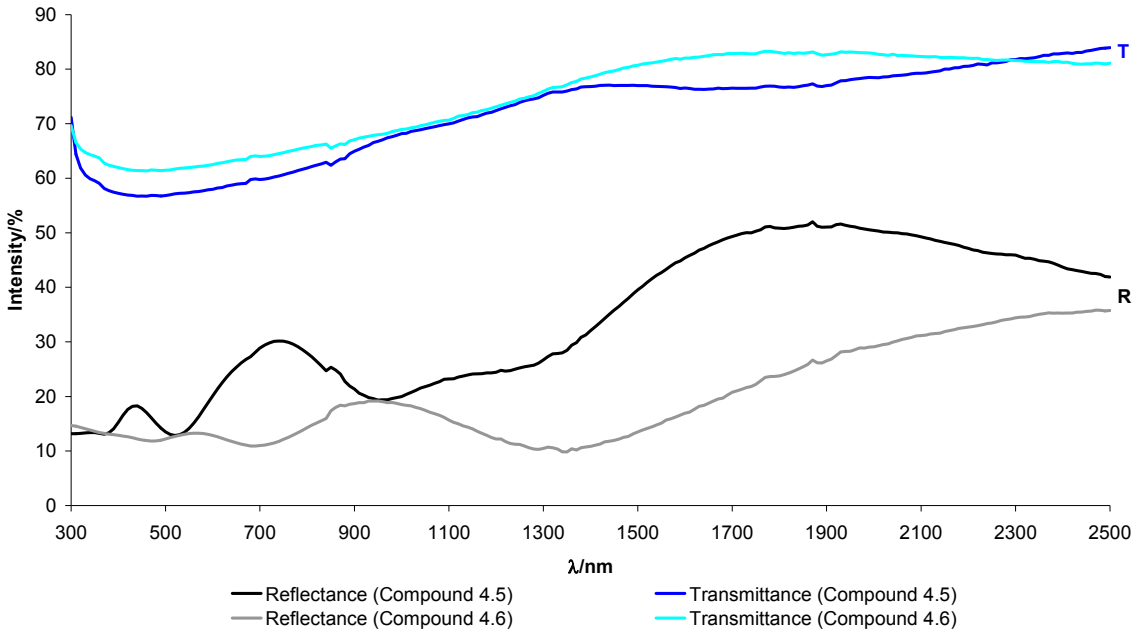

Figure 5.9 Reflectance-transmittance plots for [ZrCp'{η^2-(^{i}PrN)$_2$CNMe$_2$}$_2$Cl] (**4.5**) and [ZrCp'$_2${η^2-(^{i}PrN)$_2$CNMe$_2$}Cl] (**4.6**).

5.3.2.4. Scanning Electron Microscopy

SEM images of the films showed small nodules ~10 nm in diameter, which are similar to those deposited to **4.1-4.4** (**Figure 5.10**).

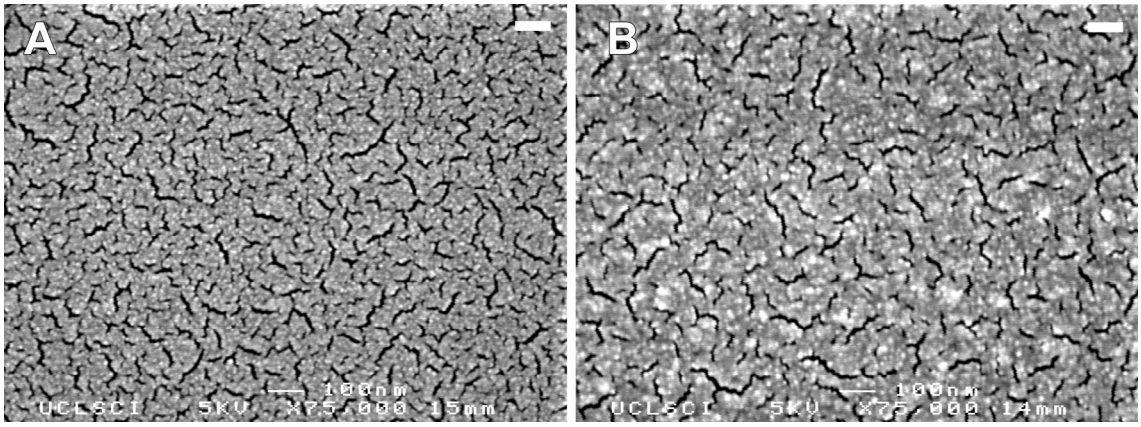

Figure 5.10 SEM images of the films formed from (A) [ZrCp'{η^2-(^{i}PrN)$_2$CNMe$_2$}$_2$Cl] (**4.5**) and (B) [ZrCp'$_2${η^2-(^{i}PrN)$_2$CNMe$_2$}Cl] (**4.6**). Both images × 75,000, bars = 100 nm.

Again there are crevices due to the vapour-draw method, which were accentuated by the gold coating. However, the nodules are still visible. Side-on SEM images (**Figure 5.11**) showed the films to be 50-200 nm thick.

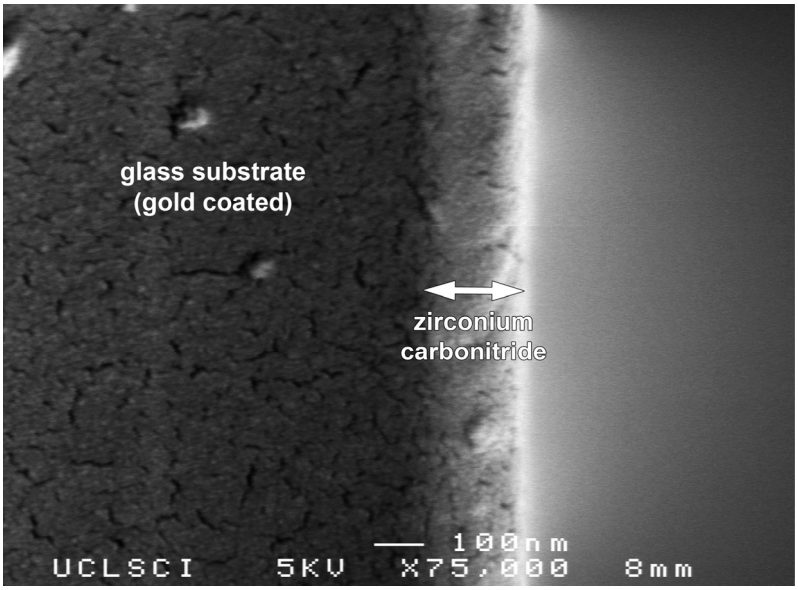

Figure 5.11 Side-on SEM image of a film deposited from [ZrCp'{η^2-(^{i}PrN)$_2$CNMe$_2$}$_2$Cl] (**4.5**).

5.3.3. Plasma-Enhanced Atomic Layer Deposition Using [$ZrCp_2(L)_x$] (4.1 and 4.2)

Plasma-enhanced (PE)ALD was carried out on [$ZrCp_2(NMe_2)_2$] (**4.1**) and [$ZrCp_2(\eta^2$-$MeNCH_2CH_2NMe)$] (**4.2**) using a variety of plasma gases.

5.3.3.1. Initial Experiments

The first ALD runs were attempted using [$ZrCp_2(NMe_2)_2$] (**4.1**) using N_2, H_2-N_2 and NH_3 plasmas, followed initially using *in situ* ellipsometry. There were two main deposition regimes (shown in **Figure 5.12**), the first was apparent up to 70 cycles, with growth rates approximating to 0.02 nm/cycle. This was three orders of magnitude lower than growth rates of ~12 nm/cycle reported for the deposition of Zr_3N_4 from [$Zr(NR_2)_4$] (NR_2 = NMe_2, NEtMe, NEt_2),[10] which was an initial cause for concern. Also, similar cyclopentadienyl compounds [$HfCp'_2(Me)(O^iPr)$] and [$HfCp'_2(Me)(mmp)$] (mmp = 1-methoxy-2-methylpropan-2-olate) showed growth rates of 0.09-0.29 and 0.04-0.06 nm/cycle respectively,[11] albeit liquid injection ALD for oxide films.

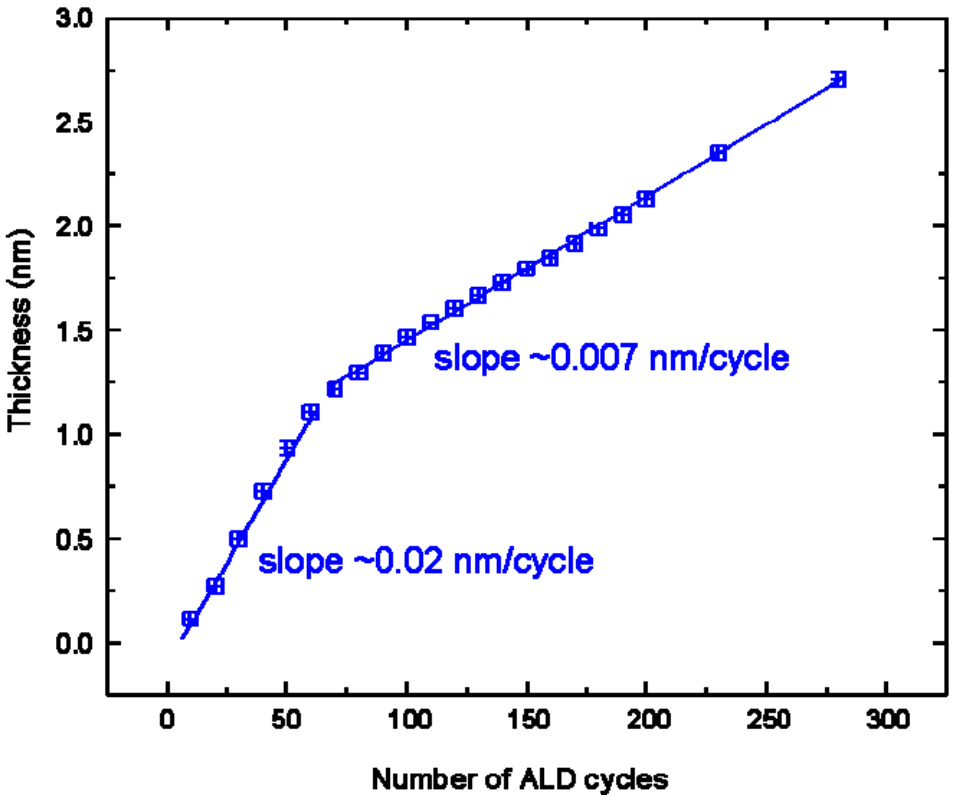

Figure 5.12 Initial ALD growth rates using [$ZrCp_2(NMe_2)_2$] (**4.1**) in an N_2 plasma.

After 70 cycles the growth rate decreased to 0.007 nm/cycle, which was very low for a useful ALD process. Further attempts were made using an O_2 plasma, as compound **4.1** gave films of ZrO_2 by LPCVD (Section 5.3.1). However, the results were the same. This implied that the surface was becoming saturated with the precursor after 70 cycles. To test this, the experiment with an O_2 plasma was repeated. At 70 cycles, no more of the precursor was injected into the system and the deposited film was exposed to the plasma only for the remaining cycles. Still, a growth rate of 0.007 nm/cycle was observed, suggesting that any growth beyond 70 cycles was due to the plasma reacting with the surface and that there was insufficient precursor in the system.

5.3.3.2. *In Situ* Mass Spectrometry

In order to ascertain why there was insufficient precursor in the system, *in situ* mass spectrometry was carried out on **4.1** and **4.2**, to see which fragments were most prominent in the reaction chamber.

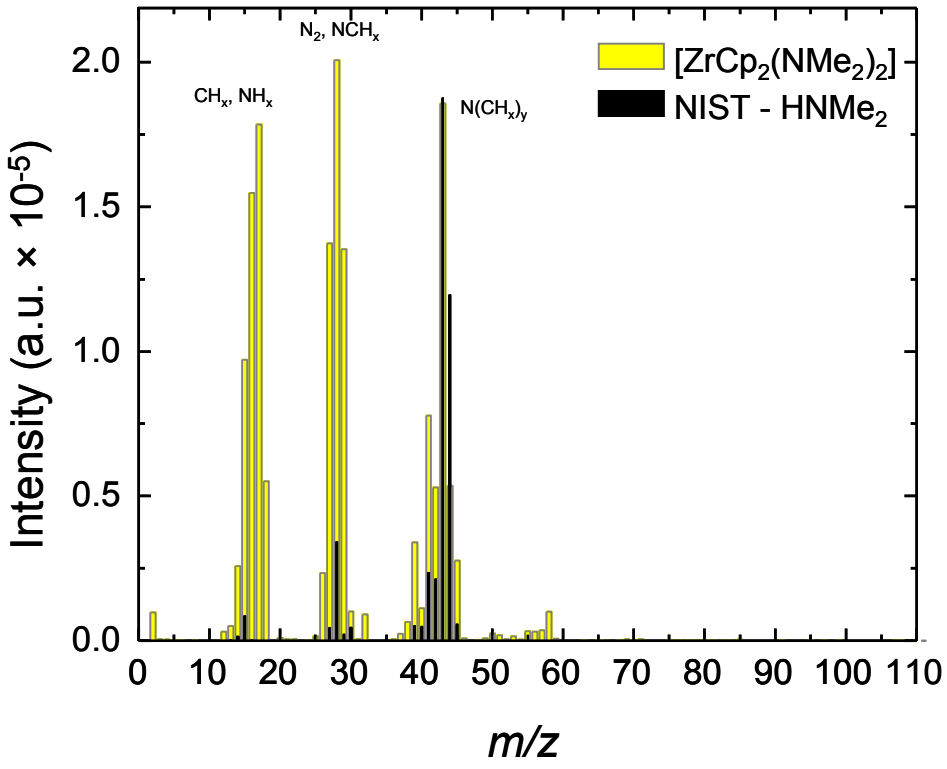

Figure 5.13 *In situ* cracking pattern of $[ZrCp_2(NMe_2)_2]$ (**4.1**).

The cracking pattern of compound **4.1** (**Figure 5.13**) showed that $[NMe_2]^+$ was present, and fragments thereof, but none for cyclopentadiene. This suggested that **4.1** was decomposing into $[Zr(C_5H_4)_2]$ and $HNMe_2$ before reaching the system and that $[Zr(C_5H_4)_2]$ was not sufficiently volatile to be carried into the reaction chamber. This was clear during each cycle as, again, nothing of greater mass than NMe_2 was seen during the ALD process (**Figure 5.14**).

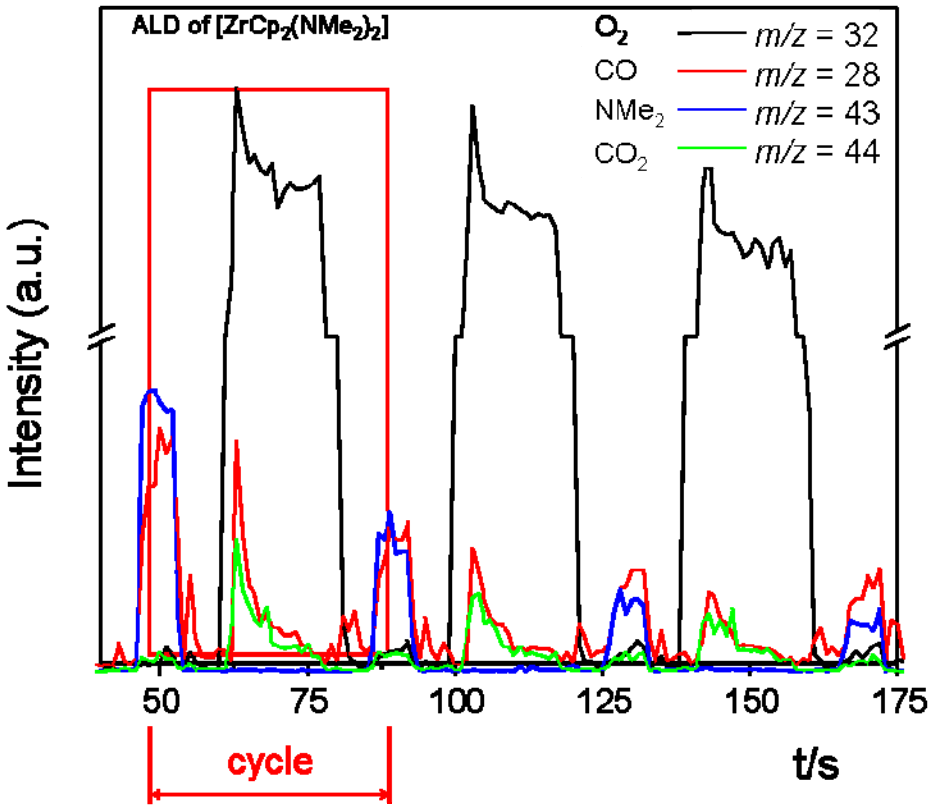

Figure 5.14 Three ALD cycles of $[ZrCp_2(NMe_2)_2]$ (**4.1**) in an O_2 plasma. Argon line (m/z = 40) omitted for clarity.

It was also noted that the concentration of the dimethylamido groups decreased over time, which meant that only a small amount of the precursor was entering the system over the entire process.

For compound **4.2**, the cracking pattern (**Figure 5.15**) showed peaks corresponding to $[Cp]^+$ and $[MeNCH_2CH_2NMe]^+$ and their fragments, suggesting that

the *N,N'*-dimethylethylenediamido ligand was more strongly bound to the zirconium centre than the NMe_2 ligands in **4.1**.

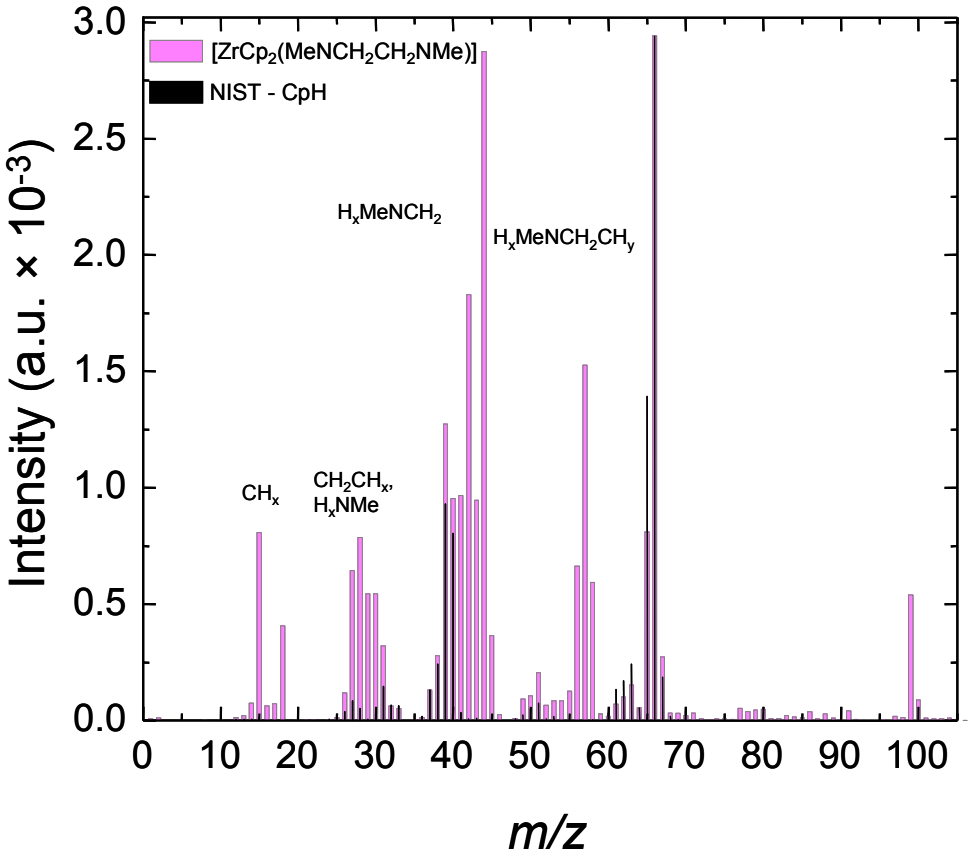

Figure 5.15 *In situ* cracking pattern of $[ZrCp_2(\eta^2\text{-}MeNCH_2CH_2NMe)]$ (**4.2**).

However, a similar pattern emerged, in that, over a period of cycles, the amount of precursor in the reaction chamber decreased rapidly over time. This is shown in **Figure 5.16**, where the amount of cyclopentadiene in the system decreased with each cycle, compared to the constant levels of the O_2 plasma (shown by a red dashed line).

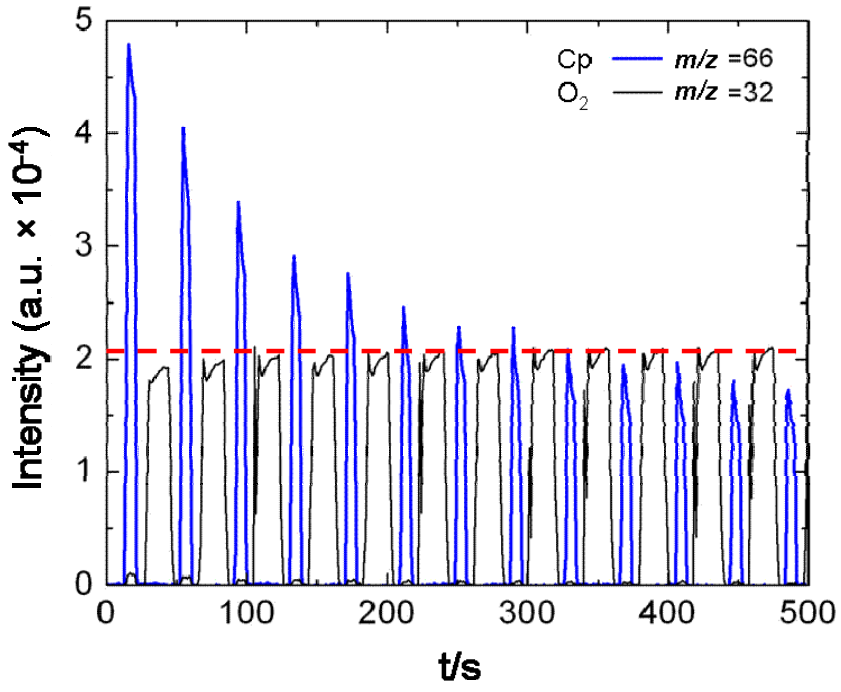

Figure 5.16 ALD cycles of $[ZrCp_2(\eta^2\text{-}MeNCH_2CH_2NMe)]$ (**4.2**) in an O_2 plasma.

It was clear that an insufficient amount of precursor was being transported into the reaction chamber. In an attempt to sublime more of the precursor, further experiments were carried out using **4.2** at bubbler temperatures of 80 and 90 °C, but no change in the amount of precursor entering the system was observed in the mass spectral data (**Figure 5.17**). These results suggest that, despite good initial volatilisation of $[ZrCp_2(NMe_2)_2]$ (**4.1**) and $[ZrCp_2(\eta^2\text{-}MeNCH_2CH_2NMe)]$ (**4.2**), the remaining precursor in the bubbler is becoming involatile. In the case of **4.1** it is likely that it is decomposing *via* the loss of the dimethylamido ligands first, despite the bubbler temperature being below its decomposition temperature according the TGA data (Section 4.3.2, **Figure 4.6**). However, the low pressure in the system overall (~10^{-6} Torr) may reduce the decomposition temperature. Another factor to consider is that some of the precursor may have melted and re-solidified, forming a glassy solid. This was observed during the sublimation of **4.1** at the synthesis stage, and further sublimation would not occur until the material had been ground into a powder. (Subsequent sublimations were run at a lower temperature as a consequence.) Again, the temperature at which this occurs may be much lower under reduced pressure. It is clear that these precursors may be

more suited to a technique where premature precursor decomposition is minimised and volatility is not an issue, such as liquid injection CVD or ALD or AACVD.

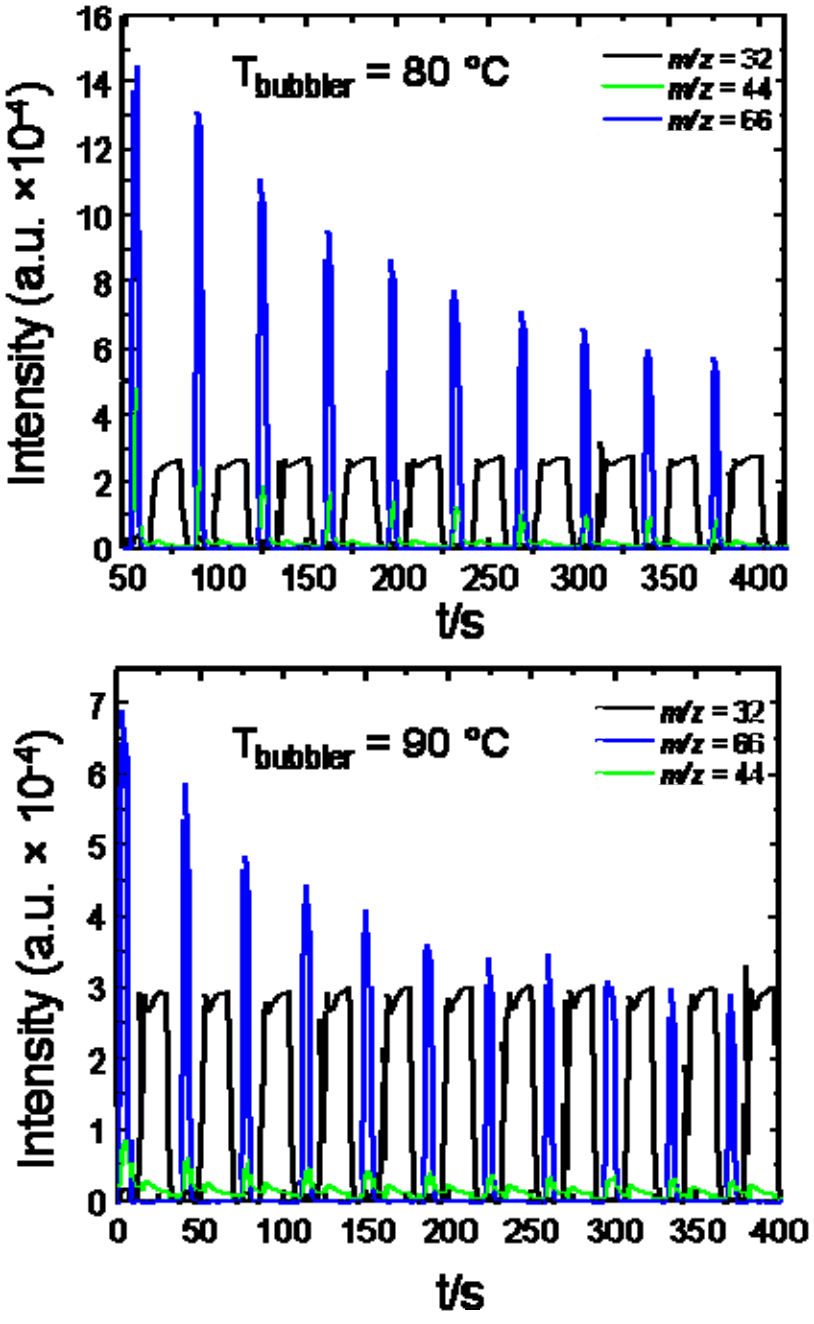

Figure 5.17 ALD cycles of $[ZrCp_2(\eta^2\text{-}MeNCH_2CH_2NMe)]$ (**4.2**) in an O_2 plasma at increased bubbler temperatures.

5.4. Conclusions

LPCVD of compounds **4.1-4.4** gave shiny grey films of zirconium carbide that were heavily contaminated with graphite. Guanidinate compounds **4.5** and **4.6** afforded zirconium carbonitride films of $ZrN_{2.80\pm0.19}C_{1.82\pm0.20}$ and $ZrN_{1.31\pm0.14}C_{2.46\pm0.22}$ respectively, although they were contaminated with chlorine. The films were generally 50-350 nm thick. Attempted PEALD of compounds **4.1** and **4.2** showed them to be insufficiently volatile to grow films greater than 1.25 nm thick at a growth rate of approximately 0.02 nm/cycle. Any subsequent growth was due to the plasma only.

5.5. References

1. W. M. M. Kessels, S. B. S. Heil, C. J. Hodson, J. H. Klootwijk, F. Roozeboom, N. Singh, M. C. M. van de Sanden, J. L. van Hemmen, *J. Vac. Sci. Technol. A*, 2007, **25**, 1357-1366.
2. G. Rossetto, S. Codato, G. Carta, M. Leoni, G. A. Rizzi, P. Scardi, P. Zanella, *Chem. Vap. Deposition*, 1999, **5**, 159-163.
3. J. Brücker, T. Mäntylä, *Surf. Coat. Technol.*, 1993, **59**, 166-170.
4. M. Yashima, K. Nakamura, *Mater. Sci. Eng., B*, 2008, **148**, 69-72.
5. C. J. Carmalt, A. Newport, I. P. Parkin, P. Mountford, A. J. Sealey, S. R. Dubberley, *J. Mater. Chem.*, 2003, **13**, 84-87.
6. H. O. Pierson, *Handbook of Refractory Carbides and Nitrides. 3: Interstitial Carbides: Structure and Composition*. 1996: William Andrew Publishing. 17-54.
7. H. O. Pierson, *Handbook of Refractory Carbides and Nitrides. 10: Interstitial Nitrides: Structure and Composition*. 1996: William Andrew Publishing. 163-180.
8. H. O. Pierson, *Handbook of Refractory Carbides and Nitrides. 11: Interstitial Nitrides: Properties and General Characteristics*. 1996: William Andrew Publishing. 181-208.
9. H. O. Pierson, *Handbook of Refractory Carbides and Nitrides. 4: Carbides of Group IV*. 1996: William Andrew Publishing. 55-80.
10. R. G. Gordon, J. S. Becker, E. Kim, *Chem. Mater.*, 2004, **16**, 3497-3501.

11. A. C. Jones, R. O'Kane, J. Gaskell, P. R. Chaulker, K. Black, M. Werner, P. Taechakumput, S. Taylor, P. N. Heys, R. Odedra, *Chem. Vap. Deposition*, 2007, **13**, 609-617.

6

Conclusions

Figure 6.0 The clean room at the Eindhoven University of Technology.

6.1. Synthesis of Tungsten Carbonitride Precursors

The syntheses of $[W(\mu\text{-}N^tBu)(N^tBu)Cl_2(H_2N^tBu)]_2$ (**2.1**),[1] $[W(N^tBu)_2Cl_2(TMEDA)]$ (**2.2**, TMEDA = *N*,*N*,*N'*,*N'*-tetramethylethylenediamine)[2] and $[W(N^tBu)_2Cl_2(py)_2]$ (**2.3**, py = pyridine),[1,3] were carried out by modified literature procedures. $[W(N^tBu)_2Cl\{N(SiMe_3)_2\}]$ (**2.4**) was synthesised as a dark orange oil *via* the reaction of one equivalent of sodium bis(trimethylsilyl)amide with compound **3**. X-ray quality crystals of **2.4** could not be grown, despite numerous attempts with a variety of solvents, although its mass was confirmed by high resolution CI+ mass spectrometry. The synthesis of $[W(N^tBu)_2Cl\{N(H)NMe_2\}]$ (**2.5**) was complicated due to the reactivity of the NH moiety of the *N*,*N'*-dimethylhydrazido ligand, which resulted in polymerisation, rendering it involatile and unsuitable for chemical vapour deposition (CVD). The synthesis of $[W(N^tBu)_2(\eta^5\text{-Cp'})(\eta^1\text{-Cp'})]$ (**2.6**) (adapted from that of $[W(N^tBu)_2(\eta^5\text{-Cp})(\eta^1\text{-Cp})]$[4]) involved the reaction of compound **2.3** and two equivalents of [NaCp'(THF)] to give a dark yellow oil (Cp = cyclopentadienyl, Cp' = methylcyclopentadienyl, THF = tetrahydrofuran). The methyl-substituted cyclopentadienyl ligand was selected with a view to increasing the volatility of the compound. High resolution mass spectrometry and room temperature NMR confirmed the presence of **2.6** and variable temperature, COSY and NOSEY experiments confirmed that exchange was occurring between the η^5- and η^1-Cp' environments as well as two potential exchange mechanisms within the η^1-Cp' alone. This lead to the conclusion that there were both 2-η^1-Cp' and 3-η^1-Cp' isomers of **2.6**.

Compounds **2.1**-**2.4** and **2.6** decomposed cleanly, as shown by TGA and compounds **2.1**-**2.3** were found to be volatile, their vapour pressures being greater than 1 mTorr at 50 °C. These high vapour pressures and clean decompositions suggest that **2.1**-**2.4** are promising as precursors to tungsten carbonitride.

6.2. Chemical Vapour Deposition of Tungsten Carbonitride

Low pressure CVD (LPCVD) of compounds **2.1**-**2.4** onto glass substrates at 550 °C afforded highly reflective and adhesive films of polycrystalline tungsten carbonitride. The composition of the films, $WN_{1.12\text{-}1.32}C_{0.20\text{-}0.29}$, showed them to be generally nitrogen rich and chlorine was absent from them. The use of ammonia as opposed to nitrogen

did not affect the nitrogen and carbon levels in the films significantly, possibly because there was simply not a sufficient excess of the gas in the system, although it did reduce oxygen levels. The composition and appearance of these films were comparable to those reported in the literature,[5-7] showing compounds **2.1-2.4** to be potentially good precursors for the LPCVD of tungsten carbonitride. Aerosol-assisted CVD (AACVD) of compound **2.1** in toluene gave reflective, amorphous films of average composition $WN_{0.41\pm0.21}C_{0.26\pm0.04}$, with negligible chlorine contamination, although the oxygen content was higher than that observed for LPCVD, which might account for the lower nitrogen content.

LPCVD of compound **2.6** onto glass at 600 °C using a vapour-draw afforded shiny grey non-adhesive films of carbon-rich tungsten carbonitride ($WN_{1.02\pm0.40}C_{2.70\pm0.53}$) and graphite. In all films, the oxygen was low. However, their low adhesion would render them unsuitable for use as a barrier layer in microelectronics, and the excess graphite may well disrupt the tungsten carbonitride lattice, providing diffusion pathways.

6.3. Synthesis of Zirconium Carbonitride Precursors

$[ZrCp_2(NMe_2)_2]$ (**4.1**)[8] and $[ZrCp_2(\eta^2\text{-}MeNCH_2CH_2NMe)]$ (**4.2**) were synthesised *via* the metathesis reaction of zirconocene dichloride and the respective lithium amides, whereas $[ZrCp'_2(NMe_2)_2]$ (**4.3**)[8] and $[ZrCp'_2(NEt_2)_2]$ (**4.4**) were formed from the reaction of $[ZrCl_2(NR_2)_2(THF)_2]$ (R = Me, Et)[9] and two equivalents of [NaCp'(THF)]. Additionally, two guanidinate compounds were synthesised, the ligand being selected for its high nitrogen content. $[ZrCp'\{\eta^2\text{-}(^i PrN)_2CNMe_2\}_2Cl]$ (**4.5**) was formed from the reaction of $[ZrCl_2\{\eta^2\text{-}(^i PrN)_2CNMe_2\}_2]$[10] and one equivalent of [NaCp'(THF)], whereas the reaction of $[ZrCp'_2Cl_2]$ and $[Li\{(^i PrN)_2CNMe_2\}]$ afforded $[ZrCp'_2\{\eta^2\text{-}(^i PrN)_2CNMe_2\}Cl]$ (**4.6**). Compounds **4.2** and **4.4-4.6** are novel, and X-ray quality crystals of compounds **4.5** and **4.6** were grown from hexane and their crystal structures determined. Compounds **4.1-4.6** all decomposed cleanly, although compounds **4.4** and **4.5** showed mass losses that were lower than expected, suggesting that full decomposition had not taken place at 590 °C. The vapour pressures of compounds **4.1-4.3** were all greater than 1 mTorr at 50 °C and comparable to those of compounds **2.1-2.3**. The vapour pressure of **4.3** was lower than **4.1**, which was

unexpected and implies that the addition of a methyl group to the cyclopentadienyl ring reduces the volatility of the compound with respect to its unsubstituted analogue. The clean decomposition and volatility of these compounds shows promise for their use as CVD precursors, although potentially more as carbide precursors rather than nitride.

6.4. Chemical Vapour Deposition of Zirconium Carbonitride

LPCVD of compounds **4.1-4.4** under a vapour-draw, onto glass substrates at 600 °C, afforded highly reflective and adhesive films of zirconium carbide and amorphous carbon. Nitrogen was not present in any of the films, which were of the average composition $ZrC_{8.32\pm2.50}$. Powder XRD indicated that the films were largely amorphous, although small, broad peaks accounting for stoichiometric ZrC were present, suggesting that the remaining carbon was due to amorphous deposits from the cyclopentadienyl ligands. It was apparent that, when heated, the bis(cyclopentadienyl)bis(amido) zirconium compounds lose the amido ligands first when heated, which resulted in films devoid of nitrogen.

LPCVD of compounds **4.5** and **4.6** on glass at 600 °C gave highly reflective, adhesive, amorphous films of zirconium carbonitride. The XRD patterns for films from both precursors showed some polycrystalline ZrC, although the films are assumed to be largely amorphous. Films deposited by **4.5** were nitrogen rich and their average composition was $ZrN_{2.80\pm0.19}C_{1.82\pm0.20}$. Unsurprisingly, films from compound **4.6** contained more carbon respective to nitrogen, their average composition being $ZrN_{1.31\pm0.14}C_{2.46\pm0.22}$. It is interesting to note that the Zr:N ratio is almost equal to that of insulating Zr_3N_4. Chlorine contamination was present (< 3 at.%) and oxygen levels were low. Compounds **4.5** and **4.6** show potential as precursors to zirconium carbonitride although there is clearly a case for incorporating as much nitrogen as possible into the precursor as more nitrogen was present in the films from **4.5**.

Attempted plasma-enhanced atomic layer deposition (PEALD) using compounds **4.1** and **4.2** served only to show that these compounds were not suitable for high-vacuum systems, as the amount of precursor in the reaction chamber decreased over time. Where the precursor was present, the deposition rates were approximately 0.02 nm/cycle, lower than the rates reported for similar compounds.[11,12] However, after approximately 70 cycles, the deposition appeared to be caused by the plasma only. It

would therefore appear that compounds **4.1-4.4** are not suitable precursors for deposition methods requiring gaseous precursors, such as LPCVD or ALD. They may be better suited to AACVD or liquid injection ALD. The inclusion of the ligands is beneficial in that they stabilise the compounds, although the quantity of carbon deposited brings this benefit into question. Therefore, if pure nitrides and carbides are required, cyclopentadienyl ligands are not suitable in the precursors.

6.5. Summary

A range of tungsten imido precursors and cyclopentadienyl zirconium guanidinate precursors have been used successfully to deposit tungsten carbonitride and zirconium carbonitride thin films respectively *via* low pressure CVD. $[W(\mu\text{-}N^tBu)(N^tBu)Cl_2(H_2N^tBu)]_2$ (**2.1**) in toluene has also been successfully employed as a precursor to tungsten carbonitride *via* aerosol-assisted CVD.

6.6. References

1. R. G. Gordon, J. S. Becker, S. Suh, S. Wang, *Chem. Mater.*, 2003, **15**, 2969-2976.
2. A. J. Nielson, *Polyhedron*, 1987, **6**, 1657-1667.
3. R. A. Fischer, A. Baunemann, D. Rische, M. Winter, *Inorg. Chem.*, 2006, **45**, 269-277.
4. J. Sundermeyer, K. Peters, U. Radius, H.-G. von Schnering, *Eur. J. Inorg. Chem.*, 2001, 1617-1623.
5. H. T. Chiu, S. H. Chuang, *J. Mater. Res.*, 1993, **8**, 1353-1360.
6. K.-B. Kim, S.-H. Kim, S. S. Oh, H.-M. Kim, D.-H. Kang, W.-M. Li, S. Haukka, M. Tuominen, *J. Electrochem. Soc.*, 2004, **151**, C272-C282.
7. H. Volders, Z. Tökei, H. Bender, B. Brijs, R. Caluwaerts, L. Carbonell, T. Conard, C. Drijbrooms, A. Franquet, S. Garaud, I. Hoflijk, A. Moussa, F. Sinapi, Y. Travaly, D. Vanhaeren, G. Vereecke, C. Zhao, W.-M. Li, H. Sprey, A. M. Jonas, *Microelectron. Eng.*, 2007, **84**, 2460-2465.
8. M. F. Lappert, G. Chandra, *J. Chem. Soc. A*, 1968, 1940-1945.
9. R Kempe, S. Brenner, P. Arndt, *Z. Anorg. Allg. Chem.*, 1995, **621**, 2021-2024.
10. R. G. Bergman, J. Arnold, A. P. Duncan, S. M. Mullins, *Organometallics*, 2001, **20**, 1808-1819.

11. R. G. Gordon, J. S. Becker, E. Kim, *Chem. Mater.*, 2004, **16**, 3497-3501.
12. A. C. Jones, R. O'Kane, J. Gaskell, P. R. Chaulker, K. Black, M. Werner, P. Taechakumput, S. Taylor, P. N. Heys, R. Odedra, *Chem. Vap. Deposition*, 2007, **13**, 609-617.

Appendices

A.1. Publications

Tungsten imido complexes as precursors to tungsten carbonitride thin films.

S. E. Potts, C. J. Carmalt, C. S. Blackman, T. Leese, H. O. Davies, *Dalton Trans.*, 2008, 5730-5736. This article was illustrated on the inside front cover of the issue that it appeared in.

Toughening up thin films.

S. E. Potts, C. J. Carmalt, C. S. Blackman, T. Leese, H. O. Davies, *Chem. Tech.*, 2008, published as an online article (http://www.rsc.org/Publishing/ChemTech/index.asp) featuring the work described in the paper above.

Reactivity of $ZrCl_4$ and $HfCl_4$ with silylamines and thermal decomposition of the compounds $[MCl_4\{NH(R)(SiR'_3)\}]$ (M = Zr, Hf, R = ^{t}Bu, R' = Me; R = SiR'_3 = $SiMe_3$, $SiMe_2H$).

P. Hasan, S. E. Potts, C. J. Carmalt, R. G. Palgrave, H. O. Davies, *Polyhedron*, 2008, **27**, 1041-1045.

Synthesis of zirconium guanidinate complexes and the formation of zirconium carbonitride *via* low pressure CVD.

S. E. Potts, C. J. Carmalt, C. S. Blackman, F. Abou-Chahine, D. Pugh, H. O. Davies, *Organometallics*, 2009, *submitted*.

Low pressure CVD and plasma-enhanced ALD of bis(cyclopentadienyl) zirconium(IV) amides.

S. E. Potts, C. J. Carmalt, C. S. Blackman, F. Abou-Chahine, N. Leick, W. M. M. Kessels, H. O. Davies, 2009, *in preparation.*

A.2. Crystal Data for [ZrCp'{η^2-(^{i}PrN)$_2$CNMe$_2$}$_2$Cl] (4.5)

Empirical formula	$C_{24}H_{47}N_6ClZr$	
Formula weight	546.35	
Temperature	150(2) K	
Wavelength	0.71073 Å	
Crystal system	Monoclinic	
Space group	$P2_1/n$	
Unit cell dimensions	a = 9.2554(13) Å	$\alpha = 90°$
	b = 18.498(3) Å	$\beta = 97.835(2)°$
	c = 16.649(2) Å	$\gamma = 90°$
Volume	2823.9(7) Å^3	
Z	4	
Density (calculated)	1.285 Mg/m^3	
Absorption coefficient	0.506 mm^{-1}	
F(000)	1160	
Crystal size	0.30 × 0.30 × 0.20 mm^3	
Theta range for data collection	2.20 to 28.26°.	
Index ranges	$-11 \le h \le 12$, $-24 \le k \le 24$, $-21 \le l \le 22$	
Reflections collected	15140	
Independent reflections	5065 [R(int) = 0.0480]	
Completeness to theta = 26.00°	71.5 %	
Absorption correction	Semi-empirical from equivalents	
Max. and min. transmission	0.9056 and 0.8631	
Refinement method	Full-matrix least-squares on F^2	
Data / restraints / parameters	5065 / 0 / 302	
Goodness-of-fit on F^2	1.013	
Final R indices [I>2sigma(I)]	R1 = 0.0470, wR2 = 0.1260	
R indices (all data)	R1 = 0.0557, wR2 = 0.1299	
Largest diff. peak and hole	1.651 and -0.587 e.Å^{-3}	

Atomic coordinates ($\times 10^4$) and equivalent isotropic displacement parameters ($Å^2 \times 10^3$) for compound **4.5**. U(eq) is defined as one third of the trace of the orthogonalised U^{ij} tensor.

	x	y	z	U(eq)
C(1)	3582(4)	1292(2)	3591(2)	29(1)
C(2)	2651(4)	1653(2)	2991(2)	30(1)
C(3)	3026(4)	2392(2)	3031(2)	33(1)
C(4)	4200(5)	2488(2)	3659(2)	32(1)
C(5)	4544(4)	1803(2)	3992(2)	28(1)
C(6)	3442(7)	515(3)	3825(4)	76(2)
C(7)	3418(4)	377(2)	1283(2)	25(1)
C(8)	3164(5)	943(2)	617(2)	38(1)
C(9)	1931(4)	136(2)	1510(2)	35(1)
C(10)	7637(4)	397(2)	3398(2)	28(1)
C(11)	7492(5)	591(2)	4278(2)	40(1)
C(12)	9137(4)	633(2)	3215(3)	35(1)
C(13)	5540(4)	297(2)	2336(2)	21(1)
C(14)	4747(5)	-987(2)	2238(3)	42(1)
C(15)	7047(5)	-635(2)	1807(3)	45(1)
C(16)	3830(4)	3166(2)	1227(2)	26(1)
C(17)	4074(5)	3790(2)	1831(3)	39(1)
C(18)	2213(4)	2992(2)	992(2)	37(1)
C(19)	7755(4)	1401(2)	1223(2)	26(1)
C(20)	9069(4)	1896(2)	1296(3)	37(1)
C(21)	7489(5)	1027(2)	396(3)	46(1)
C(22)	5808(4)	2312(2)	1137(2)	20(1)
C(23)	6973(5)	3382(2)	649(3)	40(1)
C(24)	5460(5)	2598(2)	-324(2)	45(1)
N(1)	4379(3)	657(1)	1983(2)	22(1)

N(2)	6434(3)	707(1)	2839(2)	22(1)
N(3)	5821(3)	-436(2)	2194(2)	32(1)
N(4)	4662(3)	2521(1)	1509(2)	20(1)
N(5)	6434(3)	1730(1)	1453(2)	20(1)
N(6)	6320(3)	2676(2)	480(2)	26(1)
Cl(1)	7394(1)	2407(1)	3167(1)	29(1)
Zr(1)	5180(1)	1741(1)	2536(1)	16(1)

Bond lengths/Å and angles/° for compound **4.5**.

C(1)–C(2)	1.397(5)	C(7)–C(9)	1.541(5)
C(1)–C(5)	1.404(5)	C(7)–H(7)	1.0000
C(1)–C(6)	1.498(6)	C(8)–H(8A)	0.9800
C(1)–Zr(1)	2.583(3)	C(8)–H(8B)	0.9800
C(2)–C(3)	1.409(5)	C(8)–H(8C)	0.9800
C(2)–Zr(1)	2.563(4)	C(9)–H(9A)	0.9800
C(2)–H(2)	0.9500	C(9)–H(9B)	0.9800
C(3)–C(4)	1.413(6)	C(9)–H(9C)	0.9800
C(3)–Zr(1)	2.560(3)	C(10)–N(2)	1.466(4)
C(3)–H(3)	0.9500	C(10)–C(12)	1.525(5)
C(4)–C(5)	1.402(5)	C(10)–C(11)	1.532(5)
C(4)–Zr(1)	2.586(3)	C(10)–H(10)	1.0000
C(4)–H(4)	0.9500	C(11)–H(11A)	0.9800
C(5)–Zr(1)	2.575(3)	C(11)–H(11B)	0.9800
C(5)–H(5)	0.9500	C(11)–H(11C)	0.9800
C(6)–H(6A)	0.9800	C(12)–H(12A)	0.9800
C(6)–H(6B)	0.9800	C(12)–H(12B)	0.9800
C(6)–H(6C)	0.9800	C(12)–H(12C)	0.9800
C(7)–N(1)	1.462(4)	C(13)–N(1)	1.330(4)
C(7)–C(8)	1.520(5)	C(13)–N(2)	1.331(4)

C(13)–N(3)	1.408(4)	C(20)–H(20A)	0.9800
C(13)–Zr(1)	2.718(3)	C(20)–H(20B)	0.9800
C(14)–N(3)	1.432(5)	C(20)–H(20C)	0.9800
C(14)–H(14A)	0.9800	C(21)–H(21A)	0.9800
C(14)–H(14B)	0.9800	C(21)–H(21B)	0.9800
C(14)–H(14C)	0.9800	C(21)–H(21C)	0.9800
C(15)–N(3)	1.428(5)	C(22)–N(5)	1.299(4)
C(15)–H(15A)	0.9800	C(22)–N(4)	1.356(4)
C(15)–H(15B)	0.9800	C(22)–N(6)	1.421(4)
C(15)–H(15C)	0.9800	C(22)–Zr(1)	2.691(3)
C(16)–N(4)	1.463(4)	C(23)–N(6)	1.451(5)
C(16)–C(17)	1.527(5)	C(23)–H(23A)	0.9800
C(16)–C(18)	1.529(5)	C(23)–H(23B)	0.9800
C(16)–H(16)	1.0000	C(23)–H(23C)	0.9800
C(17)–H(17A)	0.9800	C(24)–N(6)	1.467(5)
C(17)–H(17B)	0.9800	C(24)–H(24A)	0.9800
C(17)–H(17C)	0.9800	C(24)–H(24B)	0.9800
C(18)–H(18A)	0.9800	C(24)–H(24C)	0.9800
C(18)–H(18B)	0.9800	N(1)–Zr(1)	2.287(2)
C(18)–H(18C)	0.9800	N(2)–Zr(1)	2.260(3)
C(19)–N(5)	1.463(4)	N(4)–Zr(1)	2.237(3)
C(19)–C(20)	1.514(5)	N(5)–Zr(1)	2.273(3)
C(19)–C(21)	1.531(5)	Cl(1)–Zr(1)	2.4961(9)
C(19)–H(19)	1.0000		

C(2)–C(1)–C(5)	107.9(3)	C(1)–C(2)–C(3)	107.8(3)
C(2)–C(1)–C(6)	125.3(4)	C(1)–C(2)–Zr(1)	75.1(2)
C(5)–C(1)–C(6)	126.4(4)	C(3)–C(2)–Zr(1)	73.9(2)
C(2)–C(1)–Zr(1)	73.43(19)	C(1)–C(2)–H(2)	126.1
C(5)–C(1)–Zr(1)	73.87(19)	C(3)–C(2)–H(2)	126.1
C(6)–C(1)–Zr(1)	124.3(3)	Zr(1)–C(2)–H(2)	117.0

C(2)–C(3)–C(4)	108.4(3)	C(7)–C(8)–H(8B)	109.5
C(2)–C(3)–Zr(1)	74.1(2)	H(8A)–C(8)–H(8B)	109.5
C(4)–C(3)–Zr(1)	75.1(2)	C(7)–C(8)–H(8C)	109.5
C(2)–C(3)–H(3)	125.8	H(8A)–C(8)–H(8C)	109.5
C(4)–C(3)–H(3)	125.8	H(8B)–C(8)–H(8C)	109.5
Zr(1)–C(3)–H(3)	117.0	C(7)–C(9)–H(9A)	109.5
C(5)–C(4)–C(3)	106.9(3)	C(7)–C(9)–H(9B)	109.5
C(5)–C(4)–Zr(1)	73.78(19)	H(9A)–C(9)–H(9B)	109.5
C(3)–C(4)–Zr(1)	73.05(19)	C(7)–C(9)–H(9C)	109.5
C(5)–C(4)–H(4)	126.6	H(9A)–C(9)–H(9C)	109.5
C(3)–C(4)–H(4)	126.6	H(9B)–C(9)–H(9C)	109.5
Zr(1)–C(4)–H(4)	118.6	N(2)–C(10)–C(12)	113.3(3)
C(4)–C(5)–C(1)	108.9(3)	N(2)–C(10)–C(11)	110.9(3)
C(4)–C(5)–Zr(1)	74.69(19)	C(12)–C(10)–C(11)	108.9(3)
C(1)–C(5)–Zr(1)	74.55(19)	N(2)–C(10)–H(10)	107.8
C(4)–C(5)–H(5)	125.5	C(12)–C(10)–H(10)	107.8
C(1)–C(5)–H(5)	125.5	C(11)–C(10)–H(10)	107.8
Zr(1)–C(5)–H(5)	117.2	C(10)–C(11)–H(11A)	109.5
C(1)–C(6)–H(6A)	109.5	C(10)–C(11)–H(11B)	109.5
C(1)–C(6)–H(6B)	109.5	H(11A)–C(11)–H(11B)	109.5
H(6A)–C(6)–H(6B)	109.5	C(10)–C(11)–H(11C)	109.5
C(1)–C(6)–H(6C)	109.5	H(11A)–C(11)–H(11C)	109.5
H(6A)–C(6)–H(6C)	109.5	H(11B)–C(11)–H(11C)	109.5
H(6B)–C(6)–H(6C)	109.5	C(10)–C(12)–H(12A)	109.5
N(1)–C(7)–C(8)	110.7(3)	C(10)–C(12)–H(12B)	109.5
N(1)–C(7)–C(9)	111.9(3)	H(12A)–C(12)–H(12B)	109.5
C(8)–C(7)–C(9)	108.9(3)	C(10)–C(12)–H(12C)	109.5
N(1)–C(7)–H(7)	108.4	H(12A)–C(12)–H(12C)	109.5
C(8)–C(7)–H(7)	108.4	H(12B)–C(12)–H(12C)	109.5
C(9)–C(7)–H(7)	108.4	N(1)–C(13)–N(2)	112.9(3)
C(7)–C(8)–H(8A)	109.5	N(1)–C(13)–N(3)	124.4(3)

N(2)–C(13)–N(3)	122.7(3)	C(16)–C(18)–H(18C)	109.5
N(1)–C(13)–Zr(1)	57.12(15)	H(18A)–C(18)–H(18C)	109.5
N(2)–C(13)–Zr(1)	55.94(16)	H(18B)–C(18)–H(18C)	109.5
N(3)–C(13)–Zr(1)	175.2(2)	N(5)–C(19)–C(20)	114.7(3)
N(3)–C(14)–H(14A)	109.5	N(5)–C(19)–C(21)	112.7(3)
N(3)–C(14)–H(14B)	109.5	C(20)–C(19)–C(21)	112.0(3)
H(14A)–C(14)–H(14B)	109.5	N(5)–C(19)–H(19)	105.5
N(3)–C(14)–H(14C)	109.5	C(20)–C(19)–H(19)	105.5
H(14A)–C(14)–H(14C)	109.5	C(21)–C(19)–H(19)	105.5
H(14B)–C(14)–H(14C)	109.5	C(19)–C(20)–H(20A)	109.5
N(3)–C(15)–H(15A)	109.5	C(19)–C(20)–H(20B)	109.5
N(3)–C(15)–H(15B)	109.5	H(20A)–C(20)–H(20B)	109.5
H(15A)–C(15)–H(15B)	109.5	C(19)–C(20)–H(20C)	109.5
N(3)–C(15)–H(15C)	109.5	H(20A)–C(20)–H(20C)	109.5
H(15A)–C(15)–H(15C)	109.5	H(20B)–C(20)–H(20C)	109.5
H(15B)–C(15)–H(15C)	109.5	C(19)–C(21)–H(21A)	109.5
N(4)–C(16)–C(17)	112.4(3)	C(19)–C(21)–H(21B)	109.5
N(4)–C(16)–C(18)	111.4(3)	H(21A)–C(21)–H(21B)	109.5
C(17)–C(16)–C(18)	112.3(3)	C(19)–C(21)–H(21C)	109.5
N(4)–C(16)–H(16)	106.8	H(21A)–C(21)–H(21C)	109.5
C(17)–C(16)–H(16)	106.8	H(21B)–C(21)–H(21C)	109.5
C(18)–C(16)–H(16)	106.8	N(5)–C(22)–N(4)	112.6(3)
C(16)–C(17)–H(17A)	109.5	N(5)–C(22)–N(6)	121.9(3)
C(16)–C(17)–H(17B)	109.5	N(4)–C(22)–N(6)	125.5(3)
H(17A)–C(17)–H(17B)	109.5	N(5)–C(22)–Zr(1)	57.43(16)
C(16)–C(17)–H(17C)	109.5	N(4)–C(22)–Zr(1)	56.04(15)
H(17A)–C(17)–H(17C)	109.5	N(6)–C(22)–Zr(1)	170.7(2)
H(17B)–C(17)–H(17C)	109.5	N(6)–C(23)–H(23A)	109.5
C(16)–C(18)–H(18A)	109.5	N(6)–C(23)–H(23B)	109.5
C(16)–C(18)–H(18B)	109.5	H(23A)–C(23)–H(23B)	109.5
H(18A)–C(18)–H(18B)	109.5	N(6)–C(23)–H(23C)	109.5

H(23A)–C(23)–H(23C)	109.5	N(5)–Zr(1)–N(1)	81.11(9)
H(23B)–C(23)–H(23C)	109.5	N(4)–Zr(1)–Cl(1)	94.70(8)
N(6)–C(24)–H(24A)	109.5	N(2)–Zr(1)–Cl(1)	87.50(7)
N(6)–C(24)–H(24B)	109.5	N(5)–Zr(1)–Cl(1)	81.93(7)
H(24A)–C(24)–H(24B)	109.5	N(1)–Zr(1)–Cl(1)	143.52(7)
N(6)–C(24)–H(24C)	109.5	N(4)–Zr(1)–C(3)	81.26(11)
H(24A)–C(24)–H(24C)	109.5	N(2)–Zr(1)–C(3)	136.46(11)
H(24B)–C(24)–H(24C)	109.5	N(5)–Zr(1)–C(3)	139.86(10)
C(13)–N(1)–C(7)	122.8(3)	N(1)–Zr(1)–C(3)	108.52(12)
C(13)–N(1)–Zr(1)	93.64(19)	Cl(1)–Zr(1)–C(3)	105.27(10)
C(7)–N(1)–Zr(1)	139.5(2)	N(4)–Zr(1)–C(2)	99.07(11)
C(13)–N(2)–C(10)	122.0(3)	N(2)–Zr(1)–C(2)	110.00(11)
C(13)–N(2)–Zr(1)	94.9(2)	N(5)–Zr(1)–C(2)	145.08(12)
C(10)–N(2)–Zr(1)	142.7(2)	N(1)–Zr(1)–C(2)	78.69(11)
C(13)–N(3)–C(15)	120.0(3)	Cl(1)–Zr(1)–C(2)	129.62(9)
C(13)–N(3)–C(14)	122.1(3)	C(3)–Zr(1)–C(2)	31.94(12)
C(15)–N(3)–C(14)	116.1(3)	N(4)–Zr(1)–C(5)	129.67(10)
C(22)–N(4)–C(16)	119.7(3)	N(2)–Zr(1)–C(5)	90.16(11)
C(22)–N(4)–Zr(1)	93.77(19)	N(5)–Zr(1)–C(5)	162.60(12)
C(16)–N(4)–Zr(1)	145.1(2)	N(1)–Zr(1)–C(5)	108.30(10)
C(22)–N(5)–C(19)	125.5(3)	Cl(1)–Zr(1)–C(5)	82.06(9)
C(22)–N(5)–Zr(1)	93.77(19)	C(3)–Zr(1)–C(5)	52.24(12)
C(19)–N(5)–Zr(1)	138.3(2)	C(2)–Zr(1)–C(5)	52.32(12)
C(22)–N(6)–C(23)	116.8(3)	N(4)–Zr(1)–C(1)	130.08(11)
C(22)–N(6)–C(24)	117.4(3)	N(2)–Zr(1)–C(1)	84.23(11)
C(23)–N(6)–C(24)	115.2(3)	N(5)–Zr(1)–C(1)	159.67(10)
N(4)–Zr(1)–N(2)	140.07(10)	N(1)–Zr(1)–C(1)	78.85(10)
N(4)–Zr(1)–N(5)	58.66(9)	Cl(1)–Zr(1)–C(1)	112.70(9)
N(2)–Zr(1)–N(5)	82.36(9)	C(3)–Zr(1)–C(1)	52.33(11)
N(4)–Zr(1)–N(1)	103.53(10)	C(2)–Zr(1)–C(1)	31.51(12)
N(2)–Zr(1)–N(1)	58.38(10)	C(5)–Zr(1)–C(1)	31.58(11)

N(4)–Zr(1)–C(4)	98.56(11)
N(2)–Zr(1)–C(4)	120.68(11)
N(5)–Zr(1)–C(4)	147.77(10)
N(1)–Zr(1)–C(4)	129.21(11)
Cl(1)–Zr(1)–C(4)	77.36(9)
C(3)–Zr(1)–C(4)	31.86(13)
C(2)–Zr(1)–C(4)	52.80(12)
C(5)–Zr(1)–C(4)	31.53(11)
C(1)–Zr(1)–C(4)	52.43(11)
N(4)–Zr(1)–C(22)	30.19(10)
N(2)–Zr(1)–C(22)	111.13(10)
N(5)–Zr(1)–C(22)	28.80(9)
N(1)–Zr(1)–C(22)	95.29(9)
Cl(1)–Zr(1)–C(22)	84.78(7)
C(3)–Zr(1)–C(22)	111.37(11)
C(2)–Zr(1)–C(22)	126.50(11)
C(5)–Zr(1)–C(22)	154.41(10)
C(1)–Zr(1)–C(22)	157.80(11)
C(4)–Zr(1)–C(22)	123.72(11)
N(4)–Zr(1)–C(13)	123.84(9)
N(2)–Zr(1)–C(13)	29.21(10)
N(5)–Zr(1)–C(13)	79.00(9)
N(1)–Zr(1)–C(13)	29.24(10)
Cl(1)–Zr(1)–C(13)	115.40(8)
C(3)–Zr(1)–C(13)	127.97(11)
C(2)–Zr(1)–C(13)	96.07(11)
C(5)–Zr(1)–C(13)	101.89(10)
C(1)–Zr(1)–C(13)	81.83(10)
C(4)–Zr(1)–C(13)	132.37(10)
C(22)-Zr(1)-C(13)	103.57(9)

Symmetry transformations used to generate equivalent atoms:

Anisotropic displacement parameters ($Å^2 \times 10^3$) for compound **4.5**. The anisotropic displacement factor exponent takes the form: $-2\pi^2[h^2a^{*2}U^{11} + ... + 2\ h\ k\ a^*\ b^*\ U^{12}]$.

	U^{11}	U^{22}	U^{33}	U^{23}	U^{13}	U^{12}
C(1)	34(2)	27(2)	28(2)	1(1)	13(2)	-1(1)
C(2)	24(2)	44(2)	23(2)	-3(1)	9(2)	0(1)
C(3)	39(2)	36(2)	27(2)	3(1)	16(2)	16(2)
C(4)	44(2)	24(2)	31(2)	-9(1)	16(2)	-4(2)
C(5)	32(2)	39(2)	12(2)	-2(1)	5(1)	-2(1)
C(6)	84(4)	70(4)	81(4)	10(3)	40(4)	8(3)
C(7)	30(2)	22(2)	23(2)	-4(1)	3(1)	-3(1)
C(8)	46(2)	37(2)	27(2)	0(2)	-6(2)	-12(2)
C(9)	32(2)	38(2)	35(2)	-1(2)	1(2)	-7(2)
C(10)	31(2)	25(2)	27(2)	5(1)	-3(2)	5(1)
C(11)	44(2)	48(2)	26(2)	6(2)	-3(2)	10(2)
C(12)	26(2)	37(2)	40(2)	3(2)	-4(2)	5(2)
C(13)	25(2)	18(2)	21(2)	2(1)	5(1)	-2(1)
C(14)	44(2)	22(2)	61(3)	2(2)	9(2)	-8(2)
C(15)	52(3)	27(2)	61(3)	-11(2)	25(2)	2(2)
C(16)	27(2)	25(2)	28(2)	9(1)	7(2)	5(1)
C(17)	44(2)	21(2)	53(2)	1(2)	7(2)	1(2)
C(18)	27(2)	48(2)	34(2)	6(2)	-3(2)	11(2)
C(19)	32(2)	24(2)	26(2)	1(1)	12(2)	4(1)
C(20)	24(2)	42(2)	48(2)	2(2)	12(2)	1(2)
C(21)	52(3)	49(2)	40(2)	-15(2)	15(2)	8(2)
C(22)	23(2)	21(2)	16(1)	0(1)	2(1)	-5(1)
C(23)	42(2)	30(2)	50(3)	9(2)	21(2)	-7(2)
C(24)	52(3)	60(3)	21(2)	12(2)	1(2)	1(2)

N(1)	24(1)	18(1)	23(1)	-3(1)	2(1)	-2(1)
N(2)	23(1)	18(1)	24(1)	1(1)	2(1)	1(1)
N(3)	34(2)	16(1)	49(2)	-4(1)	10(2)	1(1)
N(4)	19(1)	23(1)	19(1)	4(1)	0(1)	3(1)
N(5)	22(1)	18(1)	21(1)	1(1)	5(1)	0(1)
N(6)	29(2)	30(1)	19(1)	6(1)	5(1)	-3(1)
Cl(1)	29(1)	24(1)	31(1)	-2(1)	-5(1)	-6(1)
Zr(1)	19(1)	14(1)	15(1)	0(1)	2(1)	0(1)

A.3. Crystal Data for [ZrCp'$_2${η^2-(^{i}PrN)$_2$CNMe$_2$}Cl] (4.6)

Empirical formula	$C_{21}H_{34}N_3ClZr$	
Formula weight	455.18	
Temperature	150(2) K	
Wavelength	0.71073 Å	
Crystal system	Monoclinic	
Space group	$P2_1/n$	
Unit cell dimensions	a = 11.6842(17) Å	$\alpha = 90°$
	b = 14.005(2) Å	$\beta = 105.225(2)°$
	c = 13.931(2) Å	$\gamma = 90°$
Volume	2199.6(5) Å^3	
Z	4	
Density (calculated)	1.375 Mg/m^3	
Absorption coefficient	0.631 mm^{-1}	
F(000)	952	
Crystal size	0.30 × 0.20 × 0.20 mm^3	
Theta range for data collection	2.65 to 28.30°.	
Index ranges	$-14 \le h \le 15$, $-18 \le k \le 18$, $-18 \le l \le 18$	
Reflections collected	18479	
Independent reflections	5250 [R(int) = 0.0780]	
Completeness to theta = 28.30°	96.0 %	
Absorption correction	Semi-empirical from equivalents	
Max. and min. transmission	0.8842 and 0.8333	
Refinement method	Full-matrix least-squares on F^2	
Data / restraints / parameters	5250 / 0 / 243	
Goodness-of-fit on F^2	0.918	
Final R indices [I>2sigma(I)]	R1 = 0.0478, wR2 = 0.0919	
R indices (all data)	R1 = 0.0913, wR2 = 0.1017	
Largest diff. peak and hole	0.606 and -0.638 e.Å^{-3}	

Atomic coordinates ($\times 10^4$) and equivalent isotropic displacement parameters ($Å^2 \times 10^3$) for compound **4.6**. U(eq) is defined as one third of the trace of the orthogonalised U^{ij} tensor.

	x	y	z	U(eq)
C(1)	1370(3)	1373(2)	1106(3)	30(1)
C(2)	2232(3)	1090(3)	617(3)	34(1)
C(3)	2951(3)	1870(3)	559(3)	35(1)
C(4)	2534(3)	2648(3)	1004(3)	35(1)
C(5)	1572(3)	2341(3)	1338(3)	34(1)
C(6)	352(3)	790(3)	1245(3)	51(1)
C(7)	2605(3)	1402(3)	3923(3)	32(1)
C(8)	3811(3)	1148(3)	4237(3)	37(1)
C(9)	4497(3)	1940(3)	4140(3)	40(1)
C(10)	3711(4)	2689(3)	3762(3)	37(1)
C(11)	2571(3)	2361(3)	3644(3)	36(1)
C(12)	1575(4)	793(3)	3988(3)	58(1)
C(13)	5235(3)	3428(2)	2128(3)	28(1)
C(14)	6255(3)	3779(3)	2988(3)	38(1)
C(15)	5441(3)	3706(2)	1129(3)	38(1)
C(16)	5843(3)	-37(2)	2259(3)	29(1)
C(17)	5230(3)	-680(2)	1392(3)	36(1)
C(18)	6012(3)	-532(3)	3259(3)	37(1)
C(19)	5692(3)	1705(2)	2170(2)	24(1)
C(20)	7048(3)	1573(3)	1100(3)	39(1)
C(21)	7835(3)	1663(3)	2908(3)	43(1)
N(1)	4984(2)	2422(2)	2208(2)	23(1)
N(2)	5176(2)	868(2)	2231(2)	25(1)
N(3)	6850(2)	1859(2)	2050(2)	28(1)
Cl(1)	2922(1)	-278(1)	2460(1)	33(1)

Zr(1)	3434(1)	1489(1)	2382(1)	20(1)

Bond lengths/Å and angles/° for compound **4.6**.

C(1)–C(5)	1.399(5)	C(9)–Zr(1)	2.518(3)
C(1)–C(2)	1.411(5)	C(9)–H(9)	0.9500
C(1)–C(6)	1.497(5)	C(10)–C(11)	1.377(5)
C(1)–Zr(1)	2.598(3)	C(10)–Zr(1)	2.510(3)
C(2)–C(3)	1.394(5)	C(10)–H(10)	0.9500
C(2)–Zr(1)	2.552(3)	C(11)–Zr(1)	2.556(3)
C(2)–H(2)	0.9500	C(11)–H(11)	0.9500
C(3)–C(4)	1.402(5)	C(12)–H(12A)	0.9800
C(3)–Zr(1)	2.511(3)	C(12)–H(12B)	0.9800
C(3)–H(3)	0.9500	C(12)–H(12C)	0.9800
C(4)–C(5)	1.393(5)	C(13)–N(1)	1.449(4)
C(4)–Zr(1)	2.523(3)	C(13)–C(15)	1.524(5)
C(4)–H(4)	0.9500	C(13)–C(14)	1.532(5)
C(5)–Zr(1)	2.571(3)	C(13)–H(13)	1.0000
C(5)–H(5)	0.9500	C(14)–H(14A)	0.9800
C(6)–H(6A)	0.9800	C(14)–H(14B)	0.9800
C(6)–H(6B)	0.9800	C(14)–H(14C)	0.9800
C(6)–H(6C)	0.9800	C(15)–H(15A)	0.9800
C(7)–C(11)	1.397(5)	C(15)–H(15B)	0.9800
C(7)–C(8)	1.406(5)	C(15)–H(15C)	0.9800
C(7)–C(12)	1.497(5)	C(16)–N(2)	1.483(4)
C(7)–Zr(1)	2.579(3)	C(16)–C(18)	1.522(5)
C(8)–C(9)	1.395(5)	C(16)–C(17)	1.527(5)
C(8)–Zr(1)	2.550(3)	C(16)–H(16)	1.0000
C(8)–H(8)	0.9500	C(17)–H(17A)	0.9800
C(9)–C(10)	1.403(5)	C(17)–H(17B)	0.9800

C(17)–H(17C)	0.9800	C(20)–H(20B)	0.9800
C(18)–H(18A)	0.9800	C(20)–H(20C)	0.9800
C(18)–H(18B)	0.9800	C(21)–N(3)	1.451(4)
C(18)–H(18C)	0.9800	C(21)–H(21A)	0.9800
C(19)–N(1)	1.311(4)	C(21)–H(21B)	0.9800
C(19)–N(2)	1.331(4)	C(21)–H(21C)	0.9800
C(19)–N(3)	1.422(4)	N(1)–Zr(1)	2.298(3)
C(19)–Zr(1)	2.748(3)	N(2)–Zr(1)	2.274(3)
C(20)–N(3)	1.458(4)	Cl(1)–Zr(1)	2.5542(9)
C(20)–H(20A)	0.9800		

C(5)–C(1)–C(2)	106.6(3)	C(3)–C(4)–Zr(1)	73.4(2)
C(5)–C(1)–C(6)	126.1(3)	C(5)–C(4)–H(4)	125.9
C(2)–C(1)–C(6)	126.9(3)	C(3)–C(4)–H(4)	125.9
C(5)–C(1)–Zr(1)	73.25(19)	Zr(1)–C(4)–H(4)	116.7
C(2)–C(1)–Zr(1)	72.33(19)	C(4)–C(5)–C(1)	108.8(3)
C(6)–C(1)–Zr(1)	124.9(2)	C(4)–C(5)–Zr(1)	72.21(19)
C(3)–C(2)–C(1)	109.0(3)	C(1)–C(5)–Zr(1)	75.34(19)
C(3)–C(2)–Zr(1)	72.4(2)	C(4)–C(5)–H(5)	125.6
C(1)–C(2)–Zr(1)	75.9(2)	C(1)–C(5)–H(5)	125.6
C(3)–C(2)–H(2)	125.5	Zr(1)–C(5)–H(5)	118.7
C(1)–C(2)–H(2)	125.5	C(1)–C(6)–H(6A)	109.5
Zr(1)–C(2)–H(2)	118.1	C(1)–C(6)–H(6B)	109.5
C(2)–C(3)–C(4)	107.3(3)	H(6A)–C(6)–H(6B)	109.5
C(2)–C(3)–Zr(1)	75.7(2)	C(1)–C(6)–H(6C)	109.5
C(4)–C(3)–Zr(1)	74.3(2)	H(6A)–C(6)–H(6C)	109.5
C(2)–C(3)–H(3)	126.3	H(6B)–C(6)–H(6C)	109.5
C(4)–C(3)–H(3)	126.3	C(11)–C(7)–C(8)	106.4(3)
Zr(1)–C(3)–H(3)	115.9	C(11)–C(7)–C(12)	126.8(4)
C(5)–C(4)–C(3)	108.3(3)	C(8)–C(7)–C(12)	126.4(4)
C(5)–C(4)–Zr(1)	76.1(2)	C(11)–C(7)–Zr(1)	73.3(2)

C(8)–C(7)–Zr(1)	73.0(2)	H(12B)–C(12)–H(12C)	109.5
C(12)–C(7)–Zr(1)	124.2(2)	N(1)–C(13)–C(15)	113.7(3)
C(9)–C(8)–C(7)	108.9(3)	N(1)–C(13)–C(14)	112.6(3)
C(9)–C(8)–Zr(1)	72.8(2)	C(15)–C(13)–C(14)	110.8(3)
C(7)–C(8)–Zr(1)	75.2(2)	N(1)–C(13)–H(13)	106.4
C(9)–C(8)–H(8)	125.6	C(15)–C(13)–H(13)	106.4
C(7)–C(8)–H(8)	125.6	C(14)–C(13)–H(13)	106.4
Zr(1)–C(8)–H(8)	118.3	C(13)–C(14)–H(14A)	109.5
C(8)–C(9)–C(10)	107.1(3)	C(13)–C(14)–H(14B)	109.5
C(8)–C(9)–Zr(1)	75.3(2)	H(14A)–C(14)–H(14B)	109.5
C(10)–C(9)–Zr(1)	73.5(2)	C(13)–C(14)–H(14C)	109.5
C(8)–C(9)–H(9)	126.4	H(14A)–C(14)–H(14C)	109.5
C(10)–C(9)–H(9)	126.4	H(14B)–C(14)–H(14C)	109.5
Zr(1)–C(9)–H(9)	117.0	C(13)–C(15)–H(15A)	109.5
C(11)–C(10)–C(9)	108.2(3)	C(13)–C(15)–H(15B)	109.5
C(11)–C(10)–Zr(1)	76.1(2)	H(15A)–C(15)–H(15B)	109.5
C(9)–C(10)–Zr(1)	74.1(2)	C(13)–C(15)–H(15C)	109.5
C(11)–C(10)–H(10)	125.9	H(15A)–C(15)–H(15C)	109.5
C(9)–C(10)–H(10)	125.9	H(15B)–C(15)–H(15C)	109.5
Zr(1)–C(10)–H(10)	116.0	N(2)–C(16)–C(18)	110.7(3)
C(10)–C(11)–C(7)	109.4(3)	N(2)–C(16)–C(17)	110.5(3)
C(10)–C(11)–Zr(1)	72.4(2)	C(18)–C(16)–C(17)	112.1(3)
C(7)–C(11)–Zr(1)	75.1(2)	N(2)–C(16)–H(16)	107.8
C(10)–C(11)–H(11)	125.3	C(18)–C(16)–H(16)	107.8
C(7)–C(11)–H(11)	125.3	C(17)–C(16)–H(16)	107.8
Zr(1)–C(11)–H(11)	118.9	C(16)–C(17)–H(17A)	109.5
C(7)–C(12)–H(12A)	109.5	C(16)–C(17)–H(17B)	109.5
C(7)–C(12)–H(12B)	109.5	H(17A)–C(17)–H(17B)	109.5
H(12A)–C(12)–H(12B)	109.5	C(16)–C(17)–H(17C)	109.5
C(7)–C(12)–H(12C)	109.5	H(17A)–C(17)–H(17C)	109.5
H(12A)–C(12)–H(12C)	109.5	H(17B)–C(17)–H(17C)	109.5

C(16)–C(18)–H(18A)	109.5	C(19)–N(3)–C(20)	116.6(3)
C(16)–C(18)–H(18B)	109.5	C(21)–N(3)–C(20)	114.5(3)
H(18A)–C(18)–H(18B)	109.5	N(2)–Zr(1)–N(1)	57.17(9)
C(16)–C(18)–H(18C)	109.5	N(2)–Zr(1)–C(10)	112.86(11)
H(18A)–C(18)–H(18C)	109.5	N(1)–Zr(1)–C(10)	75.71(11)
H(18B)–C(18)–H(18C)	109.5	N(2)–Zr(1)–C(3)	87.49(11)
N(1)–C(19)–N(2)	111.7(3)	N(1)–Zr(1)–C(3)	75.28(11)
N(1)–C(19)–N(3)	121.3(3)	C(10)–Zr(1)–C(3)	125.59(13)
N(2)–C(19)–N(3)	127.0(3)	N(2)–Zr(1)–C(9)	87.76(11)
N(1)–C(19)–Zr(1)	56.36(17)	N(1)–Zr(1)–C(9)	76.04(11)
N(2)–C(19)–Zr(1)	55.40(16)	C(10)–Zr(1)–C(9)	32.40(12)
N(3)–C(19)–Zr(1)	177.6(2)	C(3)–Zr(1)–C(9)	148.52(13)
N(3)–C(20)–H(20A)	109.5	N(2)–Zr(1)–C(4)	112.32(11)
N(3)–C(20)–H(20B)	109.5	N(1)–Zr(1)–C(4)	74.70(11)
H(20A)–C(20)–H(20B)	109.5	C(10)–Zr(1)–C(4)	95.51(13)
N(3)–C(20)–H(20C)	109.5	C(3)–Zr(1)–C(4)	32.35(12)
H(20A)–C(20)–H(20C)	109.5	C(9)–Zr(1)–C(4)	125.38(13)
H(20B)–C(20)–H(20C)	109.5	N(2)–Zr(1)–C(8)	95.83(11)
N(3)–C(21)–H(21A)	109.5	N(1)–Zr(1)–C(8)	106.39(11)
N(3)–C(21)–H(21B)	109.5	C(10)–Zr(1)–C(8)	52.83(12)
H(21A)–C(21)–H(21B)	109.5	C(3)–Zr(1)–C(8)	176.67(12)
N(3)–C(21)–H(21C)	109.5	C(9)–Zr(1)–C(8)	31.95(12)
H(21A)–C(21)–H(21C)	109.5	C(4)–Zr(1)–C(8)	144.90(12)
H(21B)–C(21)–H(21C)	109.5	N(2)–Zr(1)–C(2)	96.14(11)
C(19)–N(1)–C(13)	126.8(3)	N(1)–Zr(1)–C(2)	105.81(11)
C(19)–N(1)–Zr(1)	95.3(2)	C(10)–Zr(1)–C(2)	144.28(13)
C(13)–N(1)–Zr(1)	137.9(2)	C(3)–Zr(1)–C(2)	31.96(12)
C(19)–N(2)–C(16)	120.7(3)	C(9)–Zr(1)–C(2)	176.09(12)
C(19)–N(2)–Zr(1)	95.79(19)	C(4)–Zr(1)–C(2)	52.70(12)
C(16)–N(2)–Zr(1)	143.3(2)	C(8)–Zr(1)–C(2)	147.16(13)
C(19)–N(3)–C(21)	116.6(3)	N(2)–Zr(1)–Cl(1)	81.88(7)

N(1)–Zr(1)–Cl(1)	139.05(7)	C(4)-Zr(1)-C(7)	119.44(12)
C(10)–Zr(1)–Cl(1)	126.93(9)	C(8)-Zr(1)-C(7)	31.83(11)
C(3)–Zr(1)–Cl(1)	104.83(9)	C(2)-Zr(1)-C(7)	124.01(12)
C(9)–Zr(1)–Cl(1)	105.25(10)	Cl(1)-Zr(1)-C(7)	77.04(8)
C(4)–Zr(1)–Cl(1)	126.87(9)	C(11)-Zr(1)-C(7)	31.56(11)
C(8)–Zr(1)–Cl(1)	75.89(9)	C(5)-Zr(1)-C(7)	92.64(12)
C(2)–Zr(1)–Cl(1)	75.70(9)		
N(2)–Zr(1)–C(11)	140.44(11)		
N(1)–Zr(1)–C(11)	105.37(11)		
C(10)–Zr(1)–C(11)	31.53(11)		
C(3)–Zr(1)–C(11)	124.76(12)		
C(9)–Zr(1)–C(11)	52.69(12)		
C(4)–Zr(1)–C(11)	93.17(12)		
C(8)–Zr(1)–C(11)	52.16(12)		
C(2)–Zr(1)–C(11)	123.41(12)		
Cl(1)–Zr(1)–C(11)	107.15(9)		
N(2)–Zr(1)–C(5)	140.38(11)		
N(1)–Zr(1)–C(5)	104.46(11)		
C(10)–Zr(1)–C(5)	92.41(13)		
C(3)–Zr(1)–C(5)	52.93(12)		
C(9)–Zr(1)–C(5)	124.17(13)		
C(4)–Zr(1)–C(5)	31.73(11)		
C(8)–Zr(1)–C(5)	123.74(12)		
C(2)–Zr(1)–C(5)	52.19(12)		
Cl(1)–Zr(1)–C(5)	107.51(9)		
C(11)–Zr(1)–C(5)	74.89(12)		
N(2)–Zr(1)–C(7)	126.86(11)		
N(1)–Zr(1)–C(7)	126.41(10)		
C(10)–Zr(1)–C(7)	52.80(12)		
C(3)–Zr(1)–C(7)	144.94(12)		
C(9)–Zr(1)–C(7)	53.10(12)		

Symmetry transformations used to generate equivalent atoms:

Anisotropic displacement parameters ($Å^2 \times 10^3$) for compound **4.6**. The anisotropic displacement factor exponent takes the form: $-2\pi^2[h^2a^{*2}U^{11} + ... + 2\ h\ k\ a^*\ b^*\ U^{12}\ ]$.

	U^{11}	U^{22}	U^{33}	U^{23}	U^{13}	U^{12}
C(1)	22(2)	36(2)	28(2)	4(2)	2(2)	1(2)
C(2)	34(2)	36(2)	27(2)	-9(2)	-4(2)	0(2)
C(3)	26(2)	56(3)	20(2)	6(2)	0(2)	-3(2)
C(4)	33(2)	31(2)	33(2)	7(2)	-8(2)	-4(2)
C(5)	25(2)	38(2)	32(2)	2(2)	-3(2)	10(2)
C(6)	29(2)	58(3)	62(3)	8(2)	4(2)	-9(2)
C(7)	37(2)	39(2)	23(2)	-4(2)	14(2)	-3(2)
C(8)	51(3)	39(2)	18(2)	7(2)	7(2)	7(2)
C(9)	29(2)	63(3)	23(2)	-10(2)	0(2)	-9(2)
C(10)	53(3)	33(2)	29(2)	-12(2)	17(2)	-10(2)
C(11)	39(2)	44(2)	27(2)	-6(2)	10(2)	11(2)
C(12)	62(3)	68(3)	58(3)	-13(2)	39(2)	-25(2)
C(13)	21(2)	26(2)	38(2)	3(2)	8(2)	1(2)
C(14)	34(2)	31(2)	48(3)	-8(2)	9(2)	-7(2)
C(15)	39(2)	32(2)	47(2)	9(2)	19(2)	2(2)
C(16)	27(2)	26(2)	35(2)	1(2)	9(2)	8(2)
C(17)	38(2)	29(2)	44(2)	1(2)	15(2)	5(2)
C(18)	37(2)	35(2)	40(2)	13(2)	11(2)	10(2)
C(19)	21(2)	29(2)	21(2)	-2(1)	3(1)	1(1)
C(20)	38(2)	40(2)	46(2)	3(2)	24(2)	0(2)
C(21)	23(2)	48(3)	55(3)	-7(2)	6(2)	-1(2)
N(1)	21(1)	21(2)	26(2)	-1(1)	4(1)	-2(1)
N(2)	25(2)	17(1)	35(2)	2(1)	10(1)	4(1)
N(3)	15(1)	33(2)	36(2)	0(1)	11(1)	1(1)
Cl(1)	32(1)	23(1)	47(1)	1(1)	16(1)	-2(1)

Zr(1)	18(1)	21(1)	21(1)	0(1)	4(1)	0(1)